WATER RESEARCH LABORATORY

THE UNIVERSITY OF NEW SOUTH WALES

NON-DARCY FLOW OF GROUNDWATER

by

C.R.Dudgeon

Part 1. Theoretical, experimental and numerical studies

Report No. 162

1985

BIBLIOGRAPHIC DATA SHEET	1. REPORT No. 162	2. I.S.B.N. 0/85824/123/4

3. TITLE AND SUBTITLE

NON-DARCY FLOW OF GROUNDWATER.
PART 1. THEORETICAL, EXPERIMENTAL AND NUMERICAL STUDIES.

4. REPORT DATE

1985

5. AUTHOR (S)

C.R. DUDGEON

6. SPONSORING ORGANISATION

7. SUPPLEMENTARY NOTES

This report is a slightly amended version of the text of a Ph.D. thesis submitted to The University of New South Wales in 1984. Report No. 163 contains a set of tables and graphs presented in Volume 2 of the thesis.

8. ABSTRACT

This report describes research into non-Darcy flow of groundwater and some implications in groundwater engineering. Both low shear rate flows and high Reynolds number flows are covered.

Experiments designed to examine the possibility of non-Newtonian flow of water occurring at low shear rates in a tube were carried out under carefully controlled conditions. The tube chosen for the work had a diameter of 0.29mm which was considered large enough for the layer of water affected by surface forces near the boundary to have negligible effect on the flow. Pure water was found to behave as a Newtonian fluid down to shear rates as low as 10^{-8} sec^{-1}. However, water containing dissolved air behaved as a thixotropic non-Newtonian fluid at shear rates below 10^{-4} sec^{-1}.

The investigation of non-Darcy flow at high Reynolds numbers comprised a numerical investigation of unconfined non-Darcy flow to large diameter wells and pits and a series of large scale physical experiments to verify the numerical work. The finite element method was used for the numerical analysis. The results are presented as a series of tables and dimensionless graphs. Some applications in mine de-watering and extraction of groundwater supplies are discussed.

9. DISTRIBUTION STATEMENT

For general distribution.

10. DESCRIPTORS Groundwater Movement ; Nonnewtonian Flow ; Wells ; Mine Drainage ; Finite Element Method

11. IDENTIFIERS

12. CLASSIFICATION	13. NUMBER OF PAGES	14. PRICE

SUMMARY

This report describes and presents the results of research into non-Darcy flow of groundwater and some of its implications in groundwater engineering.

The work covers both low shear rate flows and high Reynolds number flows. In the former case non-Darcy flow effects are attributed to the molecular structure of water while in the latter case they are attributed to energy losses caused by inertia and turbulence.

The investigation of low shear rate flow of water included an extensive literature survey and an experimental investigation of low velocity flow in a long capillary tube. The experiments were designed to examine the possibility of non-Newtonian flow of water occurring at low shear rates in conduits with diameters large enough for the layer of water affected by surface forces at the boundary to have negligible effect on the flow. The conclusion drawn from the results was that pure water behaves as a Newtonian fluid down to shear rates as low as 10^{-8} sec^{-1} but that water containing dissolved air acts as a thixotropic non-Newtonian fluid at shear rates below 10^{-4} sec^{-1}. It was found that the viscosity could be altered by the input of energy resulting from shock or vibration. The effects observed were attributed to changes in the molecular structure of the water.

The investigation of non-Darcy flow of groundwater at high flow rates consisted of a survey of existing knowledge of non-Darcy flow in porous media at high Reynolds numbers, a numerical investigation of unconfined non-Darcy flow into large diameter wells and pits and a series of large scale experiments to verify the numerical work. The

finite element method was used to explore the relationships between geometric and flow variables for a range of conditions likely to be encountered in groundwater engineering practice. Unconfined flow to fully penetrating pits with unrestricted side entry, to partially penetrating pits with both bottom and side entry and to partially penetrating pits with only bottom entry were all investigated. An extensive set of tables and graphs is provided in Water Research Laboratory Report No. 163 to allow non-Darcy flow effects to be assessed for the range of well and pit geometries and aquifer properties likely to be encountered. Applications in mine de-watering and extraction of groundwater supplies are discussed and examples are given of the use of the results in actual investigations.

ACKNOWLEDGEMENTS

The assistance of many past and present members of the staff of the University of New South Wales Water Research Laboratory in the pursuit of the research described in this report is gratefully acknowledged. Particular thanks are due to Mrs. P. Auld for her untiring effort and meticulous work in drafting the large number of figures, to Mrs. P. Decent for her patience and skill in typing many tables and to Mrs. C. Sherris for carefully typing the text and making many alterations and additions without complaint.

The experimental work on flow into large diameter pits was carried out in facilities funded to a large extent by the Australian Water Resources Council. The financial contribution from this organisation is gratefully acknowledged.

Thanks are also due to the staff of the Computing Services Unit of the University of New South Wales for assistance and careful handling of computer output.

LIST OF SYMBOLS

Symbols are defined within the text following their first use and again when some particular purpose is served by doing so. The main symbols are listed below to allow easy reference.

a	coefficient in Forchheimer equation $i = aV + bV^2$
b	coefficient in Forchheimer equation $i = aV + bV^2$
c	coefficient in equation $i = cV^n$
d	diameter of particle; or internal diameter of tube
d_{10}	sieve opening through which 10 per cent by weight of a granular material passes
d_{50}	sieve opening through which 50 per cent by weight of a granular material passes
d'	effective hydraulic radius of flow channels in a granular porous medium
e	pore dimension in granular porous medium
f_o	Darcy-Weisbach pipe friction factor in Equation 2.6
f_e	Darcy-Weisbach pipe friction factor in Equation 2.6

g	gravitational acceleration
h	height of piezometric surface above base of aquifer; or head
h_b	height of bottom of well or pit above base of aquifer
h_f	height of free water surface at well or pit above base of aquifer
h_o	height of piezometric surface at radius of influence above base of aquifer
h_w	height of water surface in well or pit above base of aquifer
i	hydraulic gradient, $\frac{dh}{d\ell}$
ℓ	distance in direction of flow
m	aquifer thickness; or porosity in Equations 2.5 and 2.6
n	exponent in Equation $i = cV^n$
q	macroscopic flow velocity in Equations 2.5 and 2.6
r	radial distance from centre of well or pit
r_o	radius of influence

r_w radius to well or pit boundary

s drawdown of piezometric surface below level at radius of influence: $s = h_o - h$

s_f drawdown of free water surface at well or pit below level at radius of influence: $s_f = h_o - h_f$

s_w drawdown of water level in well or pit below level at radius of influence

t time

x_i cartesian co-ordinates x_1, x_2, x_3

$\overline{A}$ area

A coefficient in equation $s_w = AQ + BQ^2$

B coefficient in equation $s_w = AQ + BQ^2$

H_e Hedstrom number for non-Newtonian flow

K coefficient in Darcy equation $Q = KiA$

P porosity

Q volumetric flow rate (discharge)

R'_e	Reynolds number
S	storage coefficient
S_s	specific storage coefficient
T	transmissivity of aquifer: T = mK
V	macroscopic flow velocity
$\overline{V}$	volume
X	length characterising flow geometry
ρ	density
μ	viscosity
ν	kinematic viscosity
τ	shear stress

TABLE OF CONTENTS

Table of Contents (Cont'd)

Table of Contents (Cont'd)

Table of Contents (Cont'd)

LIST OF FIGURES

LIST OF FIGURES (Cont'd)

LIST OF FIGURES (Cont'd)

LIST OF FIGURES (Cont'd)

LIST OF FIGURES (Cont'd)

LIST OF TABLES

LIST OF TABLES (Cont'd)

LIST OF PHOTOGRAPHS

1. INTRODUCTION

The flow of fluids through porous media has been subjected to extensive study since Darcy (1856) published the results of tests on the rate of filtration of water through sand. The porous media have included naturally occurring unconsolidated sands and gravels, artificial filter media used in industry, soils, clays and consolidated rocks. Fluids have ranged from gases through liquids such as water to manufactured materials of complex rheology. The results have provided a general framework of knowledge of flow through porous media in which the more specific subject of groundwater flow should be examined.

In this introductory chapter the terms "groundwater" and "non-Darcy flow" are defined and non-Darcy flow of groundwater is related to the general field of flow through porous media. The conditions which may give rise to non-Darcy flow of groundwater are outlined and the possible effects of non-Darcy flow in groundwater engineering are briefly referred to. Finally, the scope of work covered by the report is set out.

1.1 Groundwater

Groundwater is defined as water which occurs in the saturated zone beneath the earth's surface in an inter-connected system of voids through which the water may flow. It is normal to exclude from the definition, and to treat separately, water in the overlying unsaturated zone.

The unsaturated zone may be subdivided into a soil water zone at the top, an intermediate or vadose zone and a capillary fringe. The latter is an extension of the saturated zone and contains water held up against gravity by surface forces at the water-air and water-solid interfaces. Its thickness is of the order of millimetres in materials with large pores such as open gravels and of the order of metres in fine-grained materials such as clays. The degree of saturation varies from a minimum at the top, where only the smallest pores are saturated and vertical connection of the water is discontinuous to 100 per cent where the fringe joins the saturated zone.

Whether or not flow in the capillary fringe can be neglected without introducing appreciable error depends on the type of problem under consideration. It may, for instance, be a major component of both horizontal and vertical flow in the drainage of soils and other fine-grained unconfined materials. However, in cases of substantial lateral flows to excavations such as wells, mine shafts and open-cut mines considered later in this report the contribution of the capillary fringe can safely be neglected.

The cases examined subsequently are those for which inflows are large enough to be useful as water supplies or to present de-watering problems. Porosities and permeabilities will be relatively high and the capillary fringe thickness will be small in comparison with that of the aquifer. Unconfined aquifers with transmissivities low enough for the fringe to contribute significantly to the lateral flow are unlikely to be significant sources of water for exploitation. Nor are they likely to present serious problems of water inflow to civil or mining engineering excavations.

Groundwater is not pure water. Since it comes into contact with soluble materials both before and after entering the ground it may contain a wide variety of types and concentrations of dissolved substances.

Both ionic and non-ionic solutes may affect the physical properties of water, particularly near solid boundaries. Since groundwater flows in close proximity to very large areas of solid surface there is considerable scope for molecular interaction between the flowing groundwater and the boundaries. This interaction may have the effect of reducing or even preventing flow within some distance from boundaries.

The chemical composition of the groundwater may also have an appreciable effect on the bulk flow (i.e. remote from boundaries on a molecular scale) since it may affect forces acting between water molecules. It may also affect the response to externally applied forces such as those imposed by electric and magnetic fields. The well known electrokinetic effect is an example.

The boundary and bulk flow effects described may be important for flows at low hydraulic gradients. These may occur in groundwater flowing naturally in aquifers where flow paths are long and head differences are small or near the radius of influence of a pumped well, mine or other excavation.

1.2 Groundwater Flow

Groundwater flow occurs mainly in aquifers, which have relatively large pores, and to a lesser extent in aquicludes and aquitards which have pores so small that there is little or no flow. Flow of groundwater is a particularly complex example of flow through porous media. It

occurs through an irregular network of channels bounded by the particles or blocks of which the aquifer is composed. This contrasts with flow through manufactured porous materials or beds which are normally much more homogeneous.

The interconnected porosity of unconsolidated or consolidated rocks through which groundwater flows may be distributed more or less randomly or be repeated cyclically throughout the flow region. For example, unconsolidated aquifers composed of sands and gravels frequently have randomly located strings of coarse open gravel which act as preferred flow channels through a less permeable matrix. An even more complex distribution of flow channels would be that of a porous limestone with small scale random porosity between particles of limestone, larger scale porosity of a regular fracture system and an irregular network of large solution tunnels and caves which act as main flow arteries fed by water flowing from the other pore systems.

Because of this lack of homogeneity it may be necessary to view groundwater flow on one or more of several scales. The scale of the pore or fracture is often referred to as the "microscopic" scale whereas the scale at which the aquifer can be treated as a continuum is referred to as the "macroscopic" scale. These definitions will be adhered to in this report. If a flow field extending over part or all of an aquifer is analysed using equations valid only for flow on the macroscopic scale it is to be assumed that the scale of the porosity is microscopically small relative to the flow region considered.

Engineers and hydrogeologists concerned with the exploitation or drainage of groundwater are not normally interested in details of flow at the microscopic scale. Equations for use in practice should thus,

wherever possible, apply on the macroscopic scale. However, the derivation of these equations and investigation of the limits of their validity require an understanding of the physical and chemical behaviour of static and flowing groundwater on the microscopic scale. Subsequent discussion of the basic relationships applicable to groundwater flow will thus be concerned mainly with the microscopic scale whereas application of the equations to the solution of flow problems of practical importance in groundwater hydrology and engineering will be discussed on the macroscopic scale. An exception is where flow converges to a well or other excavation in a fractured rock aquifer and is concentrated into a small number of fractures at the inflow face. Under such conditions it is necessary to treat the flow on the microscopic scale at the inflow face and the macroscopic scale at more remote points.

Groundwater flow occurs over a very wide range of velocities and hydraulic gradients with a large proportion of cases of hydrologic and engineering interest involving moderately low flow velocities. For these velocities a linear relationship between the macroscopic flow velocity V and hydraulic gradient $\frac{dh}{d\ell}$ has been found to apply.

This relationship,

$$V = \frac{Q}{A} = K \frac{dh}{d\ell} \qquad (1.1)$$

is known as Darcy's law. The macroscopic flow velocity V is calculated as the volumetric flow rate Q divided by the gross cross-sectional area of the flow $\bar{A}$. The coefficient of proportionality K is known as the transmission constant, coefficient of permeability or hydraulic conductivity.

Deviations from Darcy's law have been reported for both high and low flow rates for porous media for which the law has been found to hold at intermediate flow rates. However, the limits of validity of Darcy's law have not been clearly defined.

Flow which does not obey Darcy's law is referred to as non-Darcy or non-linear flow. The former term will be adopted in this report.

1.3 Non-Darcy Flow of Groundwater

Non-Darcy flow is defined as flow for which the macroscopic flow velocity V is not linearly proportional to the hydraulic gradient $\frac{dh}{d\ell}$.

Non-Darcy flow at high flow rates has been reported from many laboratory permeameter tests and well-flow simulation experiments since Darcy's experiments on flow through sand were carried out.

Flow behaviour attributable to non-Darcy flow of groundwater has also been observed on numerous occasions near pumped boreholes and other points of flow concentration. Head losses near these points of relatively high velocity have been found to be much higher than those predicted by equations based on Darcy's law. However, in the absence of piezometric measurements in the aquifer just outside the inflow face it has been found difficult to distinguish between high head losses caused by non-Darcy flow in the aquifer and head losses caused by screens, drilling mud intrusion or other construction effects.

Non-Darcy flow near pumped boreholes may have great practical significance. It may, for instance, severely limit the inflow to boreholes used for de-watering aquifers or extracting water supplies. It may also

be responsible for maintaining groundwater levels around boreholes much higher than would be the case if flow near the inflow face obeyed Darcy's law. The conditions under which non-Darcy flow near boreholes has a significant effect on flow rates and water levels have been outlined by Dudgeon and Cox (1977).

Neglect of non-Darcy flow effects when predicting inflows to, or water levels in and around boreholes may result in the introduction of an unacceptable degree of error under some conditions. Although the region in which non-Darcy flow occurs may be a small part of the overall flow field it may have a disproportionately large effect on the flow because of the relatively high head losses involved. The effect on water levels and velocities extends into the rest of the flow field.

The occurrence and effects of non-Darcy flow near excavations such as mine shafts, open cut mines and other large open pits has not, to the author's knowledge, been the subject of published research. A literature search failed to reveal any information on the subject. The lack of information is attributed partly to the common belief that non-Darcy flow will occur only near holes of relatively small diameter and partly to the analytical and experimental problems associated with an investigation of unconfined non-Darcy flow to large diameter partially penetrating pits. Because of the economic importance of mine dewatering and of large dug wells in some parts of the world, an investigation of unconfined non-Darcy flow to large pits was chosen as part of the research described in this report.

Non-Darcy flow at low velocities has also been observed during laboratory experiments. However, to the author's knowledge, no conclusive demonstration of non-Darcy flow of groundwater at low velocities

has been made in the field. The potential importance of the occurrence of such flow in aquifers and of the possible immobilisation of water in regions of low hydraulic gradient warrants investigation of possible causes and consequences. Although velocities associated with such flows may be very small, the flows may occur over very large cross-sectional areas and involve high volumetric flow rates of economic importance. A typical example would be recharge flows at low hydraulic gradients into extensive artesian groundwater basins such as Australia's Great Artesian Basin. Hydraulic gradients associated with flows through these basins are often very low because of the large flow distances between recharge and discharge areas. Flow through such a basin and the amount of water which can be extracted without "mining" the resource could be seriously over-estimated if the extrapolation of Darcy's law to very low flow rates were invalid.

Although a substantial number of investigations into non-Darcy flow at low velocities through porous media have been reported, little of the information is of direct relevance to flow in aquifers. Most of the work relates to drainage of clays under relatively high hydraulic gradients. Much of the experimental evidence is conflicting and important variables were not always controlled. There is little quantitative evidence available in published literature on the occurrence of non-Darcy flow at low velocities in porous media with pore sizes of the order of those associated with aquifers.

As a contribution to the scant knowledge of non-Darcy flow in aquifers at low velocities, an investigation of the low shear-rate flow characteristics of water was undertaken as part of the research desribed in this report. The aim was to determine whether non-Newtonian flow could occur in pores of the relatively large size found in aquifers and

whether this could cause the deviations from Darcy's law observed at low macroscopic flow velocities.

1.4 Scope of Report

The scope of the research covered by this report and aims which the work was intended to satisfy are summarised below:

1. Evidence for the occurrence of non-Darcy flow of groundwater and factors affecting its occurrence at both high and low velocities is evaluated.

2. Existing explanations for the occurrence of non-Darcy flow at high velocities in porous media are discussed and related to groundwater flow conditions.

3. An hyporeport that the occurrence of non-Darcy flow at low velocities in porous media may be due to non-Newtonian flow properties of bulk water at low shear rates is proposed and evaluated.

4. The results of laboratory experiments designed to investigate the occurrence of non-Newtonian flow of water in capillaries are presented. The relevance of the results to low velocity groundwater flow is discussed.

5. The implications of non-Darcy flow at high velocities in groundwater engineering are examined. The results of numerical and experimental investigations are used to demonstrate that non-Darcy flow can have a major effect on groundwater inflows to, and water levels around, large diameter open pits in unconfined aquifers. The

results are relevant to the design and management of open-cut mines, mine shafts, civil engineering excavations and large diameter wells in highly permeable aquifers.

6. A set of dimensionless curves derived from the results of numerical analysis and aimed at facilitating the prediction of inflows to, and water levels at, open pits in unconfined aquifers is presented. The curves cover the full range of aquifer thickness, pit diameter, radius of influence, degree of penetration of the aquifer and permeabilities likely to be met in practice. They should enable many well-flow and excavation problems to be solved without the use of a large computer and should allow reasonable preliminary estimates to be made for problems with more complex boundary conditions. These estimates can then be used as initial trial values for particular computer solutions.

7. The results of field investigations of water level changes caused by test pumping at proposed sites of open cut mines and actual dewatering of mines are included to support the results of the numerical and experimental studies. Examples of the prediction of inflows to these mines and to water supply wells in a gravel aquifer are also given.

2. NON-DARCY FLOW REGIMES

In Chapter 1, reference was made to Darcy flow and to non-Darcy flow at both high and low velocities. It is relevant at this stage to define these flow regimes more precisely, examine known and possible causes of deviation from Darcy's law and discuss appropriate criteria for defining the limits of the Darcy flow regime. Only those aspects relevant to the prediction of groundwater flows in aquifers are discussed. The reader is referred to a review by Hannoura and Barends (1981) for a broader picture of non-Darcy flow in porous media.

2.1 Evidence for Darcy and Non-Darcy Flow Regimes

Experimental permeameter investigations which have covered a sufficiently wide range of porous media and flow rates (Slepicka (1961), Dudgeon (1964), Kazemipour (1974)) have demonstrated that the flow can be divided into a number of regimes. For one of these, the Darcy flow regime, the linear relationship between macroscopic flow velocity and hydraulic gradient expressed by Equation (1.1) has been found valid within the limits of experimental accuracy. For high velocities, the relationship between velocity and hydraulic gradient becomes non-linear with the gradient increasing with velocity at a higher rate than predicted by Darcy's law. The permeameter test results provide some, but not conclusive, evidence that a non-linear relationship may also apply to very low velocity flows. However, the great difficulty of making accurate measurements of low velocities and gradients has resulted in very few data sets being available for analysis.

A plot of a carefully taken set of permeameter results (Dudgeon (1964)) is reproduced in Figure 2.1. Table 2.1 shows the data from which the graphs were plotted. The non-linearity of the data is clearly evident at high velocities. The data for two of the materials also show definite deviations from Darcy's law at low velocities.

The scatter of points and small range of velocity and gradient covered by many other sets of published data make it difficult to determine the exact nature of the flow relationship. In Figure 2.1 the same problem arises in the lower part of the velocity range. Had it been possible to make more accurate and lower gradient measurements, the existence of a low velocity non-Darcy flow regime could have been established as clearly as has been done for the high velocity non-Darcy regime.

Although it has been argued theoretically (Stark and Volker (1967)) that there should be one continuous relationship between flow rate and hydraulic gradient, the experimental evidence available justifies the division of the flow range into distinct pre-linear, linear (Darcy) and post-linear regimes.

The theoretical arguments of Stark and Volker were based on solutions of the Navier-Stokes equations for flow through ordered arrays of regularly shaped particles. They do not allow for the possibility of re-adjustment of flow paths through real porous media as the hydraulic gradient alters. Separation of flow at expanding channel cross-sections and the disproportionate increase in head loss in the higher velocity flow filaments could play a significant part in causing observed deviations from a continuous macroscopic velocity-hydraulic gradient relationship covering the linear and post linear regimes. Nor does the

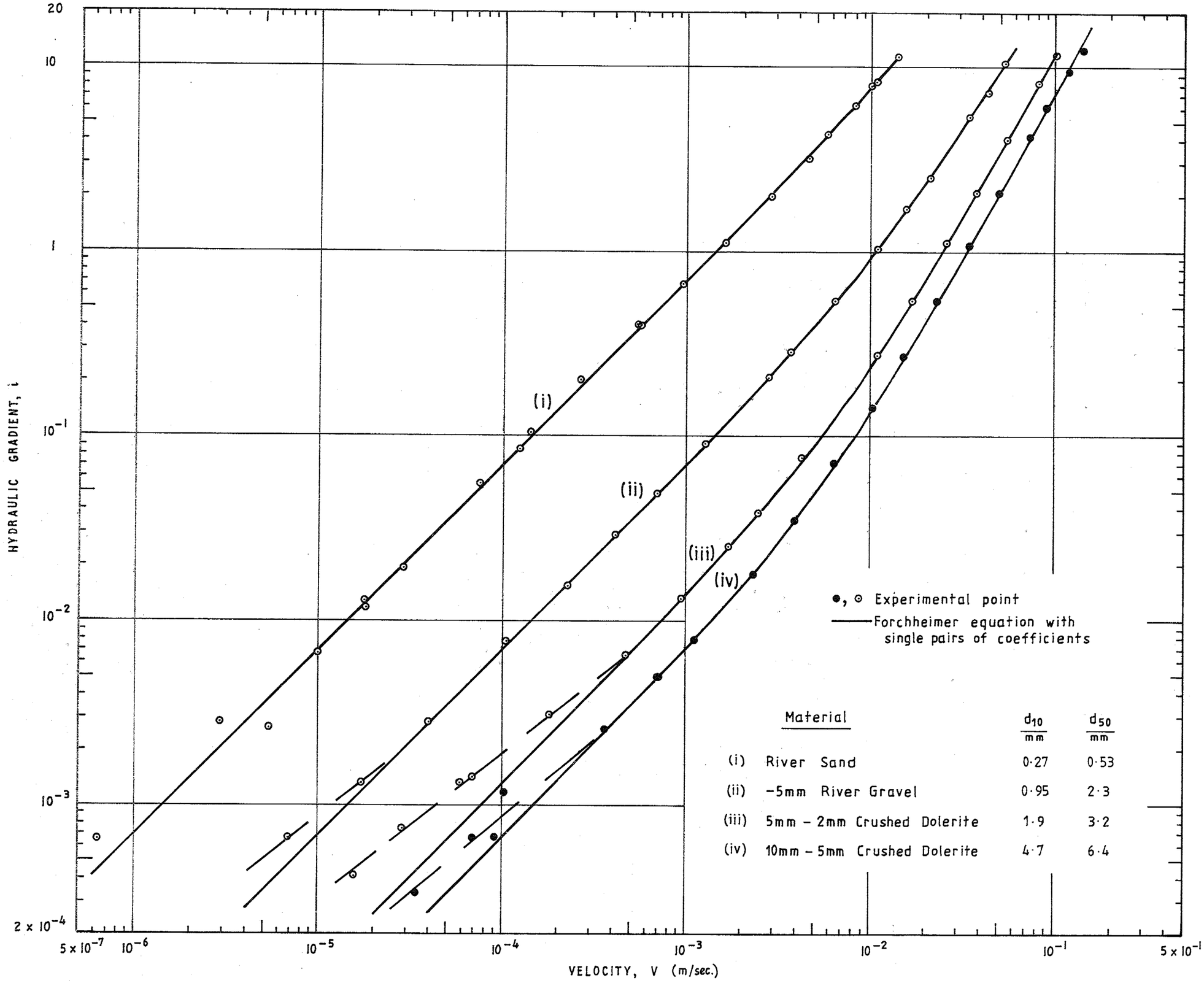

PERMEAMETER TEST RESULTS (Dudgeon (1964))

FIGURE 2·1

Table 2.1: Permeameter Test Results (Dudgeon (1964)) Plotted In Figure 1.1

(i) River Sand		(ii) 0 - 5mm River Gravel		(iii) 2 - 5mm Crushed Dolerite		(iv) 5 - 10mm Crushed Dolerite	
V (m/s)	i	V (m/s)	i	V (m/s)	i	V (m/s)	i
1.38×10^{-2}	11.30	5.33×10^{-2}	10.50	1.00×10^{-1}	11.70	1.41×10^{-1}	12.40
1.34×10^{-2}	11.00	4.30×10^{-2}	7.37	8.05×10^{-2}	8.04	1.18×10^{-1}	9.37
1.06×10^{-2}	8.06	3.44×10^{-2}	5.31	5.52×10^{-2}	3.98	8.96×10^{-2}	5.89
9.91×10^{-3}	7.75	2.10×10^{-2}	2.55	3.78×10^{-2}	2.06	7.38×10^{-2}	4.10
8.11×10^{-3}	6.15	1.55×10^{-2}	1.68	2.60×10^{-2}	1.10	5.03×10^{-2}	2.04
5.73×10^{-3}	4.24	1.08×10^{-2}	1.03	1.68×10^{-2}	0.537	3.47×10^{-2}	1.06
4.57×10^{-3}	3.13	6.37×10^{-3}	0.532	1.08×10^{-2}	0.273	2.34×10^{-2}	0.541
2.90×10^{-3}	1.96	3.72×10^{-3}	0.283	4.30×10^{-3}	7.53×10^{-2}	1.54×10^{-2}	0.268
1.63×10^{-3}	1.12	2.83×10^{-3}	0.208	2.46×10^{-3}	3.80×10^{-2}	1.03×10^{-2}	0.140
9.54×10^{-4}	0.659	1.29×10^{-3}	9.01×10^{-2}	1.71×10^{-3}	2.50×10^{-2}	6.43×10^{-3}	7.08×10^{-2}
5.73×10^{-4}	0.387	6.95×10^{-3}	4.81×10^{-2}	9.42×10^{-4}	1.31×10^{-2}	3.90×10^{-3}	3.47×10^{-2}
5.49×10^{-4}	0.400	4.11×10^{-4}	2.89×10^{-2}	4.69×10^{-4}	6.45×10^{-3}	2.35×10^{-3}	1.78×10^{-2}
2.66×10^{-4}	0.198	2.27×10^{-4}	1.54×10^{-2}	1.80×10^{-4}	3.30×10^{-3}	1.12×10^{-3}	7.79×10^{-3}
1.42×10^{-4}	0.103	1.05×10^{-4}	7.7×10^{-3}	6.86×10^{-5}	1.4×10^{-3}	3.66×10^{-4}	2.54×10^{-3}
1.24×10^{-4}	8.42×10^{-2}	3.96×10^{-5}	2.8×10^{-3}	3.85×10^{-5}	1.3×10^{-3}	1.03×10^{-4}	1.15×10^{-3}
7.44×10^{-5}	5.48×10^{-2}	1.71×10^{-5}	1.3×10^{-3}	2.87×10^{-5}	7.4×10^{-4}	9.27×10^{-5}	6.56×10^{-4}
2.86×10^{-5}	1.92×10^{-2}	6.98×10^{-6}	6.6×10^{-4}	1.58×10^{-5}	4.1×10^{-4}	6.95×10^{-5}	6.56×10^{-4}
1.80×10^{-5}	1.15×10^{-2}					3.41×10^{-5}	3.28×10^{-4}
1.78×10^{-5}	1.27×10^{-2}					7.19×10^{-4}	4.84×10^{-3}
1.00×10^{-5}	6.6×10^{-3}					7.04×10^{-4}	4.84×10^{-3}
5.36×10^{-6}	2.6×10^{-3}						
2.88×10^{-6}	2.8×10^{-3}						
6.40×10^{-7}	6.5×10^{-4}						

theoretical analysis allow for the possibility of non-Newtonian flow effects at low shear rates. In the pre-linear regime, reduction in effective flow channel cross-sections as a result of surface forces immobilising water near boundaries may occur. At very low flow rates an increase in effective viscosity may also result in reduced microscopic flow rates in zones which are remote, in terms of molecular size, from boundaries. These microscopic flow effects would have a marked effect on the macroscopic flow relationship at low flow rates.

2.2 Relationship Between Velocity and Hydraulic Gradient for Darcy and Non-Darcy Flow

The two forms of equation which have been proposed most frequently to cover the complete range of flow through porous media are:

$$i = cV^n \tag{2.1}$$

where c and n are numerical constants for a particular flow regime, and

$$i = aV + bV^2 \tag{2.2}$$

where a and b are numerical coefficients. Equation (2.2) is attributed to Forchheimer (1901). The equation will be referred to as the Forchheimer equation and the coefficients a and b as the linear and non-linear Forchheimer coefficients throughout the remainder of this report.

The best fit to accurate permeameter data which covers a wide range of the variables V and i is obtained by fitting different pairs of the coefficients a and b to parts of the data representing different flow regimes. However, a single pair of Forchheimer coefficients can be

fitted to linear and post-linear flow regime data such as that plotted in Figure 2.1 without the deviations exceeding the possible experimental error. This level of accuracy is more than adequate for most groundwater flow analysis involving moderate macroscopic velocities when other uncertainties are taken into account.

The smooth curves plotted in Figure 2.1 were calculated using Forchheimer coefficients obtained by first selecting a value of the coefficient a to match the Darcy flow section for a set of data and then selecting a value of the coefficient b to fit the high velocity data. The coefficients are listed in Table 2.2. The good fit is apparent from the plot.

Table 2.2: Forchheimer Coefficients Fitted to Data in Table 2.1

Material					Forchheimer Coefficients	
Type		d_{10} (mm)	d_{50} (mm)	porosity (per cent)	a (s/m)	b (s^2/m^2)
(i)	river sand	0.27	0.53	38.7	700	9700
(ii)	0 mm-5 mm gravel	0.95	2.3	41.8	70	2400
(iii)	2 mm-5 mm dolerite	1.9	3.2	41.7	13	1100
(iv)	5 mm-10 mm dolerite	4.7	6.4	45.8	6.5	700

Equation (1.1) which expresses Darcy's law, can be re-arranged to give:

$$i = \frac{1}{K} V \qquad (2.3)$$

For all practical purposes the coefficient a in the Forchheimer equation can be equated to $\frac{1}{K}$ over the Darcy flow range since the term bV^2 is very small.

If Equation (2.1) is adopted instead of the Forchheimer equation, $c = \frac{1}{K}$ for the Darcy flow regime and n = 1.

It will be observed from Figure 2.1 that the experimental data points for low velocities do not fit the Forchheimer equation curves. As the velocity approaches zero the curves fall below the experimental points. When examining the fit it should be kept in mind that the accuracy of the lowest points is doubtful because of the difficulty of maintaining a steady flow and measuring the very small flow rates and head differences.

If the trend of the low velocity measurements were to continue to zero flow, the actual curve relating the velocity V and gradient i would intersect the i axis at a finite gradient. This would indicate the existence of a "starting" gradient which must be overcome before flow commences and confirm that the water had non-Newtonian flow properties at low shear rates.

2.3 Upper Limit of Darcy Flow Regime

Turbulence measurements by Dudgeon (1964) and Wright (1968) and visual observations by Schneebeli (1955), Chauveteau and Thirriot (1967) and Kyle and Perrine (1971) in flow through granular media have demonstrated that the upper limit of the Darcy flow regime occurs before turbulence commences in the flow. This confirms the theoretical analysis of Stark and Volker (1967) that inertial effects cause a significant deviation from a linear relationship between the macroscopic flow velocity and hydraulic gradient before turbulence occurs. The continual acceleration and deceleration of the flow on a microscopic scale induces a head loss additional to that which is proportional to the macroscopic flow velocity.

The stability of the flow in individual channels depends on the shear rate and the lateral dimensions of the flow. For a given geometry of the flow passages the shear rate will depend on the volumetric flow rate Q and thus on the macroscopic velocity V. The criterion for the upper limit of laminar flow should thus be a Reynolds number $\frac{VX\rho}{\mu}$ where X is a dimension representing the cross-sectional size of flow channels and ρ and μ are respectively the fluid density and viscosity. For flow in circular pipes, all of which have geometrically similar cross-sections, the diameter is an appropriate choice for X. A relatively constant value of Reynolds number is found to define the upper limit of laminar flow in pipes. Unfortunately, porous media do not, in general, have geometrically similar microscopic flow cross-sections even if the particle shapes are geometrically similar. For this reason, no single value of Reynolds number has been found to define either the upper limit of laminar flow or the upper limit of the Darcy flow regime. Despite this difficulty, Reynolds number is the only valid indicator of the

upper limit of laminar flow or of the Darcy flow regime for similar porous media.

Although it is difficult to predict accurately, for a given porous medium, the velocity, hydraulic gradient or Reynolds number above which significant deviations from Darcy's law will occur, the reasons for the deviations have been well established by the theoretical and experimental investigations previously referred to. Once thought to be the result of turbulence alone, it is now known that the deviation commences with the occurrence of significant inertial effects in the microscopic flow channels and that it is only at considerably higher flow velocities and hydraulic gradients that a transition to turbulent flow occurs. The linear and post-linear flow range may thus be sub-divided into linear laminar (Darcy), non-linear laminar, transition turbulent and turbulent regimes. In practice it is not always necessary or practical to distinguish between the last three.

In groundwater flow it is probable that fully turbulent flow rarely develops since sufficiently high Reynolds numbers are only likely to occur at points of extreme flow concentration. However, the velocities at which significant deviations from Darcy's law have been observed in very permeable aquifer materials are well inside the range which may occur near high yielding boreholes and wells and deep excavations below the water table.

2.4 Lower Limit of Darcy Flow Regime

Although the change from linear to post-linear regime flow may be defined by a Reynolds number based on the microscopic flow velocity, this parameter may not be sufficient or even a valid parameter to

characterize the lower limit of the linear laminar flow regime.

The upper limits of the linear laminar and non-linear laminar regimes are affected only by the viscosity of the flowing fluid, local velocity gradients and pore dimensions since the deformation of streamlines resulting from inertial effects and the development and growth of turbulent eddies depends on these variables alone. Local velocity gradients are governed by pore dimensions and flow rates through the individual pore channels. These flow rates depend in turn on the macroscopic flow velocity so it is valid to use a Reynolds number based on pore dimensions and macroscopic flow velocity to distinguish between the linear, inertial and turbulent regimes.

The Reynolds number incorporates a single variable, the viscosity, μ, to define the relationship between shear stress and shear rate throughout the flow. It should be noted that shear rate and velocity gradient are identical for laminar shear. The use of a single viscosity term is sufficient if the fluid behaves as a Newtonian fluid at all points since μ, which is equal to the ratio of shear stress to velocity gradient, will remain constant throughout the flow even if microscopic velocities approach zero.

If the fluid is non-Newtonian a single variable is not sufficient to define the relationship between shear stress and shear rate at all points in the fluid. Reynolds number will thus not be sufficient to characterize pre-linear non-Darcy flow or define the change to linear flow.

The simplest reason which can be cited for the occurrence of a lower limit to the validity of Darcy's law and the existence of a pre-linear flow regime when water flows through a porous medium is that water can display non-Newtonian flow characteristics at low shear rates. Since this report is concerned with groundwater, and both groundwater and the water flowing in laboratory permeameter experiments may contain a variety of types and concentrations of impurities which may affect their physical properties, the term water used in this discussion does not refer to pure water unless otherwise stated.

Although it has been conclusively established that, within the accuracy of measurement, water behaves as a Newtonian fluid at normal shear rates, this does not preclude the possibility of either pure water or water containing dissolved substances from deviating from this behaviour at low shear rates. Water could exhibit several types of non-Newtonian behaviour at low shear rates without this being evident at higher shear rates.

Figure 2.2(a) shows the relation between shear stress and velocity gradient for a Newtonian fluid, and three non-Newtonian materials exhibiting initial shear strengths which must be overcome before flow occurs. These materials are described as plasto-inelastic. They include Bingham materials which have the additional characteristic of a linear relationship between shear rate and the difference between shear stress and initial shear strength. Many materials have more complex properties, including that of thixotropy (shear thinning).

It is necessary to introduce time as a separate variable to describe the behaviour of thixotropic materials or other materials with time-dependent relationships between shear stress and shear rate or

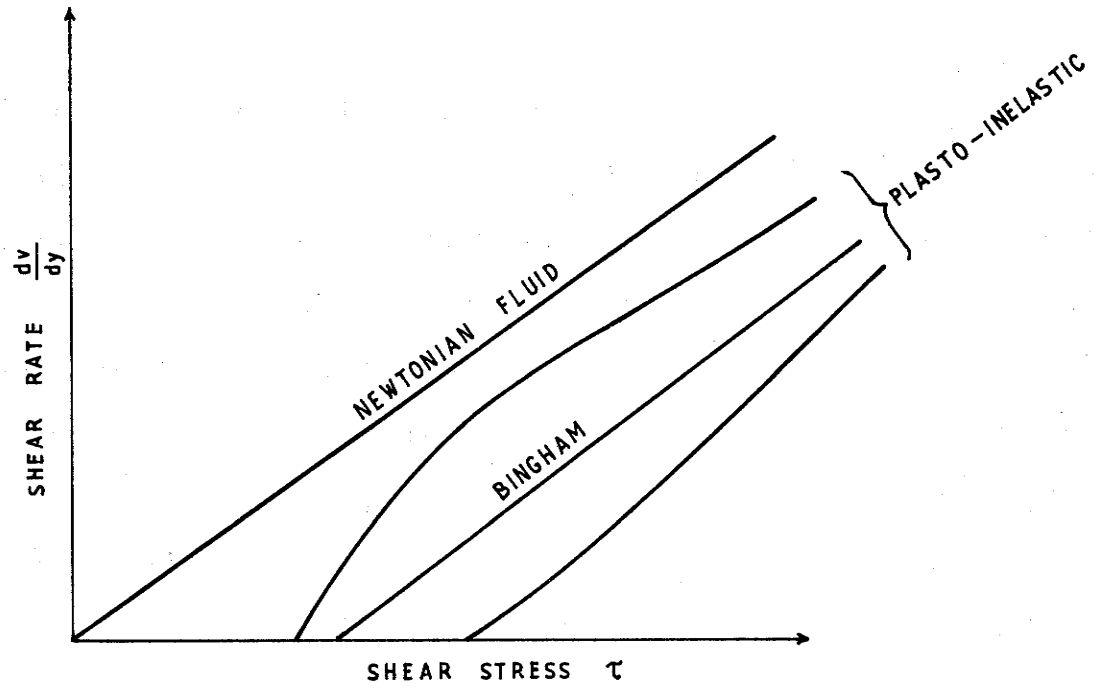

FIGURE 2·2 (a): TIME-INDEPENDENT RELATIONSHIPS BETWEEN SHEAR STRESS AND SHEAR RATE

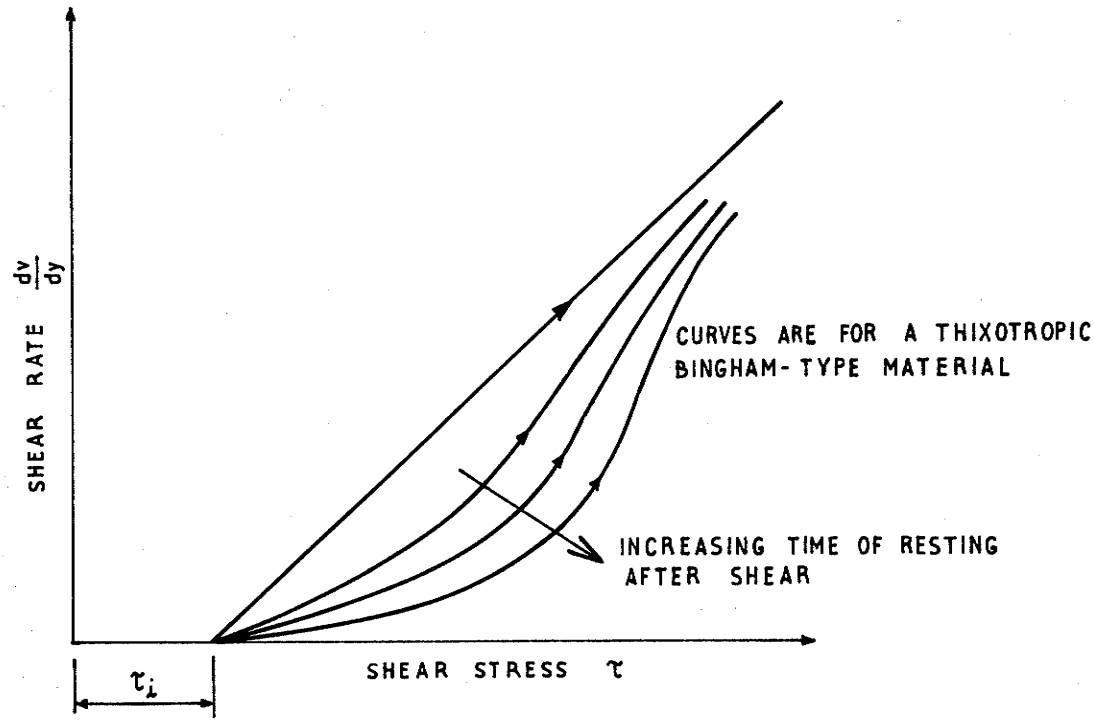

FIGURE 2·2(b): TIME-DEPENDENT RELATIONSHIPS BETWEEN SHEAR STRESS AND SHEAR RATE

velocity gradient. Figure 2.2(b) shows the types of curves required to describe the flow characteristics of a thixotropic material. The characteristics of such a material are dependent on the previous history of shearing.

Relationships such as those shown in Figure 2.2 could apply to water at low shear rates. In view of the many anomalous properties of water compared with otherwise similar liquids this would not be too surprising.

Surface forces are usually postulated to explain the occurrence of a pre-linear flow regime in clays and other fine-grained materials. It is argued that interaction between the electromagnetic fields of water molecules near the boundary and the molecules of the boundary reduces the mobility of water molecules in a layer close to the boundary. This layer is believed to be of the order of 0.1 μm thick (Drost-Hansen (1976)). Swartzendruber (1966) reviewed the experiments and reasons given for non-linear flow behaviour in soils and like materials. Since the experiments referred to by Swartzendruber were carried out using materials with pore sizes in the range zero to 1 μm the explanation that surface forces affect the flow may be correct. However, this explanation is unlikely to be valid for pore dimensions up to several millimetres present in the relatively coarse granular materials for which pre-linear flow regimes are indicated in Figure 2.1.

Aquifer materials may have pore sizes in the range zero to some millimetres. Both surface effects and bulk flow effects should thus be taken into account when the possibility of a pre-linear regime occurring in groundwater is being investigated. However, since most of the flow will take place in the larger pore spaces the non-Newtonian behaviour of

the water in these channels would have more pronounced effects on the flow than the occurrence of non-Newtonian flow in the narrower channels. It might be possible for the overall flow, and thus the macroscopic flow velocity, to be only slightly reduced if flow in the smaller pores were to cease completely because of surface effects.

The first step required in a full investigation of pre-linear regime non-Darcy flow of groundwater is to determine conclusively whether non-Newtonian flow effects can occur outside the layer of "vicinal water" affected by surface forces at the pore boundaries. To allow this possibility to be investigated for the simplest pore geometry it was decided to carry out experiments to examine the relationship between velocity and hydraulic gradient in capillary tubes for shear rates as low as could be measured. The results of these experiments are given in Chapter 3.

If, as is postulated, the lower limit of Darcy's law is reached when a significant part of the flow is affected by non-Newtonian behaviour of the water, more than one variable defining the relationship between shear stress and shear rate must be present in any parameter(s) used to define the limit. The minimum number would be two, as would be the case if water were a time-independent Bingham material with a small initial shear strength. The latter would need to be small enough to be masked by errors of measurement at higher shear rates if water were in fact to behave in this way. Since some plastics are Bingham materials, considerable study has been made of Bingham flow. A dimensionless number involving the initial shear strength is required in addition to a Reynolds number to define the flow resistance relationship. If water had an initial shear strength and then a linear relationship between shear stress and shear rate, as does a Bingham plastic, it would be

expected that the additional dimensionless parameter and Reynolds number would be sufficient to define this limit for a given geometrically similar group of porous media.

The additional number, $H_e = \frac{\tau_i X^2}{\mu_p^2}$

where τ_i = initial shear strength

= density

X = characteristic cross-sectional dimension of flow channels

$$\mu_p = \frac{\tau - \tau_i}{\frac{dv}{dy}}$$

has been named the Hedstrom number after Hedstrom (1952).

If the low shear-rate behaviour of water were more complex than that of a Bingham material the definition of the lower limit of Darcy's law would be even more difficult because further variables would have to be introduced to allow for the more complex relationship linking shear stress and shear rate.

2.5 Dimensionless Equations for Predicting Head Losses for Darcy and Non-Darcy Flow

The most comprehensive recently published attempt to rationalise the prediction of both Darcy and non-Darcy head losses for flow through granular porous media is that of McCorquodale, Hannoura and Nasser

(1978). The study adds to earlier work in this field by Ward (1964), Dudgeon (1964), Ahmed and Sunada (1969), Kovacs (1969) and others.

A dimensionless plot produced by McCorquodale et al. after an extensive analysis of published experimental results is reproduced in Figure 2.3.

The plot is effectively a modified form of friction factor versus Reynolds number graph similar to that used for flow in circular pipes.

The equations suggested as giving the best fit to the experimental data are:

For low Reynolds numbers, $R_e' < 500$

$$\frac{igmd'^2}{\nu q} = 4.6 + 0.79 \left(\frac{d'qm}{\nu}\right)^{1/2} \qquad (2.5)$$

For high Reynolds numbers, $R_e' > 500$

$$\frac{igmd'^2}{\nu q} = 79.0 + 0.54 \left(0.5 + 0.5 \frac{f_\varepsilon}{f_o}\right) \left(\frac{d'qm}{\nu}\right)^{1/2} \qquad (2.6)$$

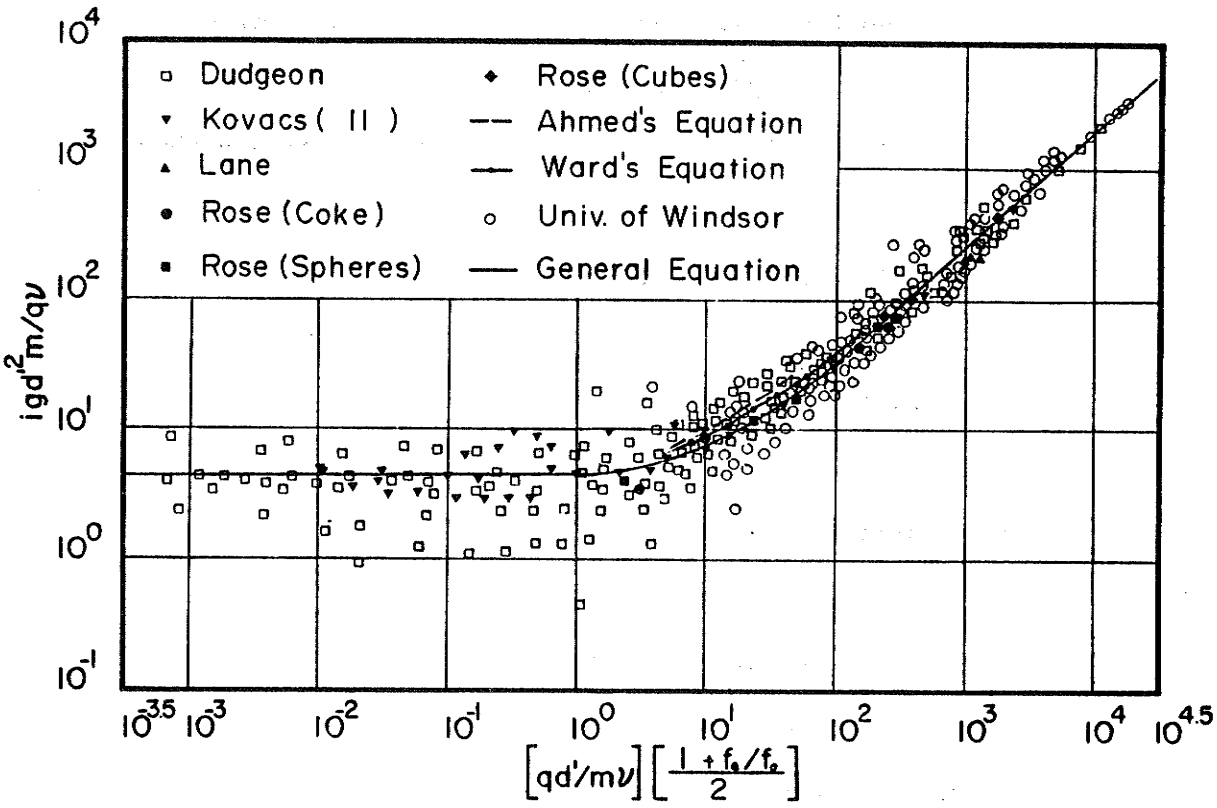

FIGURE 2·3: FRICTION FACTOR PLOT FOR GRANULAR MATERIALS

(from McCorquodale et al. (1978))

where d' = effective hydraulic radius

$$= \frac{\text{volume of voids carrying flow}}{\text{surface area of voids carrying flow}}$$

f_α, f_o = Darcy-Weisbach pipe friction factors for a surface with the roughness of the particles and an hydraulically smooth surface, respectively, for the pertinent Reynolds number

g = gravitational acceleration

i = hydraulic gradient

m = porosity

q = macroscopic flow velocity

$R_e' = \frac{qd'}{m\nu}$ = pore Reynolds number

ν = kinematic viscosity

The scatter of the experimental results around the line of best fit indicates that the error in predicting an actual measured permeameter gradient for a given granular medium and flow rate would very frequently be 100 per cent and quite commonly 200 per cent or more, particularly at lower values of the Reynolds number term. The errors cannot be attributed to errors in the experimental data analysed since errors for carefully made measurements of flow rate and hydraulic gradient are less than 5 per cent except for very low hydraulic gradients.

The only conclusion which can be drawn from the results of the analysis quoted and the earlier studies referred to is that it is impractical to derive a single relationship between a friction factor and Reynolds number for porous media. Measurement of porosity and grain size is clearly insufficient to allow classification of porous media into geometrically similar groups for which a single relationship could be expected to hold. Measurement of a sufficient number of geometric variables to allow classification into geometrically similar groups has proved impractical to date even for media composed of particles of simple shape. The only reliable procedure for determining the hydraulic characteristics of granular porous media is to carry out flow tests which allow the relationship between hydraulic gradient and macroscopic flow velocity to be determined for at least part of the flow range of interest. It may then be possible to make more extensive predictions from these basic data. The use by Ward (1964) of the experimentally determined Darcy coefficient K as a length parameter for use in calculating Reynolds numbers and friction factors is an implicit acceptance of this fact, although this was not apparently recognised by Ward or later workers.

For the class of porous media represented by in-situ aquifer materials, the problem of determining the relationship between hydraulic gradient and macroscopic flow velocity is even more difficult. It is difficult to obtain samples for permeameter testing without disturbing the porosity. In addition, the general lack of homogeneity of aquifers would require tests to be performed on a large number of samples even if they could be taken satisfactorily. In-situ testing to determine the hydraulic characteristics of aquifers is essential. Properly designed and executed pumping tests will provide data on both Darcy and non-Darcy flow behaviour.

A practical method for predicting post-linear non-Darcy flow characteristics for granular media such as sands, gravels and angular rock particles has been proposed by Cox (1977). The method allows the prediction of the Forchheimer coefficient ratio $\frac{b}{a^2}$ from the Darcy permeability coefficient K. Unfortunately, no data are yet available to extend the method to other types of aquifer material such as fractured rocks.

3. INVESTIGATION OF LOW SHEAR RATE FLOW OF WATER

It has been argued in the previous chapter that non-Newtonian flow of bulk water at low shear rates may be the principal cause of deviations from Darcy's law observed at low flow rates in some porous media. Since the materials of interest in this report are those which are permeable enough to be described as aquifers, the discussion in this chapter will be concentrated on flow through pore and fracture channels of a size which will allow a substantial contribution to the flow.

Channels with cross-sectional dimensions from zero to several millimetres occur in most types of aquifer while channel widths up to several metres are met occasionally in limestone and lava aquifers.

Since the very large channels occur infrequently and are unlikely to provide the steady, low shear-rate flow conditions which would be required for non-Newtonian flow to occur, they will not be considered.

The channels at the bottom end of the size distribution are incapable of carrying more than a small proportion of the flow. The small channel widths may also enable surface effects at the solid-water boundaries to be felt over a large part of the flow cross-section. These effects will reduce even further the potential of the small channels for carrying flow. Since the effects of surface forces are more relevant to a study of aquicludes and aquitards in which flow rates are very small, flow through pores with dimensions less than 100 μm will be discussed only briefly.

The cross-sectional dimensions of channels which are unlikely to be significantly affected by surface forces and which occur frequently enough to carry most of the flow are of the order of 10^{-1} to 1 mm. The aim of the investigation reported in the remainder of this chapter was to examine the possibility of non-Newtonian flow of water occurring in channels with dimensions in this range.

3.1 Theoretical Aspects

The hyporeport of a non-Newtonian relationship between shear stress and shear rate for water at low shear rates requires investigation at a fundamental level. The first step is to review the state of knowledge of the structural properties of water.

3.1.1 Molecular Structure of Water

A large number of chemists and physicists have been investigating the structure and related properties of water and dilute solutions for many years. It was hoped that by the time the investigation being reported was complete a firm consensus on water structure and its effect on the flow of water at low shear rates would be available. Unfortunately, this is not so. In the absence of a firm theoretical basis for predicting the flow behaviour of water at low shear rates, it has been necessary to proceed on an empirical basis, guided by the little firmly established relevant fundamental knowledge which is available.

Water behaves in a completely anomalous fashion in relation to other substances with similar chemical formulae. This is the result of "hydrogen bonding" which has a dominant effect on the physical properties of water and ice.

With two hydrogen atoms on one side of the oxygen atom, the water molecule is electrically polarised and allows bonding by forces of electrical attraction between adjacent hydrogen and oxygen atoms of different molecules. This makes possible the formation of groups or clusters of molecules in the liquid state and the formation of a regular lattice of molecules in the common form of ice.

Research into the structure of ice has provided a clearer picture than that available for water. The permanent structure of ice has made it relatively easy to investigate by spectroscopic methods. It is now known that a number of forms of ice occur varying from an amorphous form to the common form which has a regular hexagonal crystalline structure. The type depends on such factors as the rate of freezing and the environment in which the ice is formed.

For water, the problem of identification of the degree of structuring and its permanence has proved more difficult. A large number of research papers has provided, and continues to provide, conflicting evidence and theories. However, improvements in spectroscopic techniques and computer simulations of water structure give promise of better data on which theory can be based. The review by Stillinger (1980) provides a recent survey of the more positive aspects of the state of knowledge.

The view which appears to have the widest acceptance is that liquid water at ordinary temperatures and pressures is a mixture of groups of bonded molecules and free molecules. The degree of permanence of residence of molecules in any one state has not been firmly established but it appears that the interchange is relatively free at normal temperatures.

The picture may be complicated by the presence of non-polar and/or ionic solutes which either enhance or detract from the basic structure. There is a considerable amount of published information on the structure "making" and "breaking" properties of various solutes. Many ions, and possibly non-polar gases, are present in groundwater and can be expected to influence its molecular structure. Results of interactions between water molecules and some solutes which affect molecular structure are often grouped under the heading "hydrophobic effects". These effects are the subject of a recent text by Ben-Naim (1980).

The aspects of structure formation in water which are of particular interest to flow at low shear rates are:

i. Is the structure sufficiently extensive to have an effect on viscosity?

ii. Does the occurrence of present or past shearing have an effect on the nature of the structure and thus possibly on the viscosity at low shear rates?

iii. Does the ultimate degree of structuring depend on the time for which a particular rate of shear is imposed?

Answers to these questions are important in the study of groundwater flow at low velocities since shear rates may be very small and stable for long periods. Any non-linearity or time dependence of the relationship between flow rate and hydraulic gradient caused by increase or decrease in structuring with time could have a significant effect on volumetric flow rates through aquifers.

3.1.2 Evidence For Time And Shear Dependence Of The Structure Of Water And Dilute Solutions

An extensive search of the literature on the chemistry and physics of water has provided no evidence at a fundamental level of the long term time-dependence of water structure. This is not surprising when the lack of definite conclusions on the general nature of the structure of water is considered. Added to this is the difficulty of maintaining a constant low shear rate in the types of apparatus in which basic studies of water structure are performed.

Without direct experimental evidence on the effect of shear rate and time on structure it is necessary to depend on indirect evidence. Only four examples can be cited. Klassen (1969) refers to a gradual change of the density of distilled water with time after distillation and attributes the phenomenon to a gradual strengthening of the water structure with time. Gurney (1908(b)) found time dependent effects in the "surface rigidity" of water during his low shear rate viscometer experiments. Duff (1905) observed an apparent increase in viscosity of water with time of resting but attributed it to solution of glass from his capillary tube. Griffiths and Knowles (1912) found that flow in a capillary tube decreased by one-third with time but decided this must be due to growth of a fungus.

3.2 Previous Reports Of Non-Linear Flow At Low Flow Rates

Almost all of the experimental evidence available on non-linear flow in capillaries and between closely spaced plates is relevant only to the study of the effect of surface forces on the flow relationship. These forces are potentially important in flow through fine grained

materials, particularly clays in which surface charges and the location of adsorbed water molecules have a profound effect on the physical properties of the matrix and its permeability to water. The paper by Swartzendruber (1966) provides an account and interpretation of the early work on flow through clays and material containing clay. Apart from work by Kutilek (1969) and Kovacs (1969(a)) there appears to have been little further progress reported in this field. The complexity of the variables involved makes a quantitative treatment very difficult.

There have been few reports of experiments on flow at low shear rates through porous media or capillaries with flow cross-sections of the size of importance in aquifers. This is probably because of the difficulty of measuring the low gradients and flow rates. These are much lower than those at which low shear rate non-linear flow can be induced in very small diameter capillaries or porous media consisting of, or containing clay.

The experiments of Poiseuille (1840, 1841) provided the basis for the linear equation relating velocity and hydraulic gradient for laminar flow in circular tubes:

$$\frac{\Delta h}{\Delta \ell} = \frac{32\ \mu V}{\rho\ g\ d^2} \qquad (3.1)$$

where $\frac{\Delta h}{\Delta \ell}$ = hydraulic gradient along tube

V = mean velocity

ρ = fluid density

d = internal diameter of tube

Laminar flow was obtained by Poiseuille by using small diameter capillary tubes. These had diameters in the range 0.01 mm to 1 mm, but lengths were short and hydraulic gradients, velocities and shear rates were relatively high. The lowest shear rate was of the order of 5×10^3 sec^{-1}. No non-linear flow effects were reported.

Duff (1905) checked the validity of Poiseuille's equation for the flow of water down to shear rates of 5 sec^{-1}. He concluded that glass dissolved from the walls of his drawn tubes, which had diameters of approximately 3.3 mm, caused measured viscosities to be up to 10 per cent greater than Poiseuille's values. When the tubes were silvered, the viscosities measured agreed with Poiseuille's values. An interesting statement made by Duff was that ...."These results seemed to show that the difference between the viscosity of water at low rates of shear and those at high rates was greater the longer the liquid had been at rest".

Gurney (1980) attempted unsuccessfully to use a co-axial viscometer to measure the viscosity of water at shear rates lower than 5 sec^{-1}. Convection currents in the water caused trouble. The time to establish steady conditions was extremely great, indicating, perhaps, that he also had trouble with time-dependent alteration of water properties. The mention by Gurney of "surface rigidity" after the water had been left standing in the viscometer suggests possible changes in water structure at the surface in contact with the air. To check Duff's conclusion that glass dissolved from tube walls was the cause of observed anomalies in viscosity, Gurney stood water in a container with crushed glass for one week to provide conditions favourable to solution of the glass. He could find no effect on viscosities measured at and above 5 sec^{-1}.

Griffiths and Knowles (1912) also carried out flow tests in tubes. They found that the flow rate dropped by as much as one third with time. They assumed that fungoid growths had caused the decrease in flow and added copper nitrate to the water to act as a fungicide. The effect of decreasing flow rate disappeared so they concluded that water did obey Poiseuille's equation at low shear rates. A factor they did not consider was that the addition of a strongly ionised substance like copper nitrate could have a pronounced effect on the molecular structure of water. At that time the effects of solutes on water structure were unknown. Interesting observations made during the tests were that prior stirring of the water affected the results and that there were other changes of flow with time which could not be explained.

Griffiths and Griffiths (1921) pursued the matter further at shear rates from 0.0017 to 0.0233 sec^{-1} in tubes with diameters between 1.5 and 2.0 mm. They found no discrepancies between measured flow rates and those predicted by Poiseuille's law. However, they added uranine dye to part of the water in the tube to cause a density difference to drive the flow and allow movement to be observed. This also could have affected the molecular structure of the water. However, a more significant difference between this set of tests and those reported by Griffiths and Knowles is that the later experiments were carried out using air free water in a closed loop which eliminated contact between the water and the atmosphere.

Several more recent experiments have produced conflicting evidence on the validity of Poiseuille's equation for flow in tubes and Darcy's law for flow in granular media. In all cases, tube and pore dimensions were in the range relevant to flow in aquifers.

Skawinski and Lasowska (1974) described experiments in which dilute solutions of calcium chloride and sodium chloride were passed through crushed quartz glass with pore dimensions between 0.5 and 5 mm and through bundles of quartz capillary tubes with diameters in the range 0.5 to 0.75 mm. In both cases the hydraulic conductivity was dependent on the hydraulic gradient. This indicates shear rate dependence of the viscosity of the solutions.

Bondarenko and Nerpin (1965) and Bondarenko (1968) have also described experiments with water and water-alcohol mixtures which indicated non-linearity of the relationship between velocity and hydraulic gradient at low velocities. They reported a threshold gradient below which no flow occurred. The non-linearity was attributed by Bondarenko to hydrogen bonding in the liquids.

Childs and Tzimas (1971) on the other hand detected no non-linearity down to one-tenth of the hydraulic gradient at which Bondarenko reported cessation of flow. They deduced that Darcy's law was valid to zero hydraulic gradient.

"Polywater"

During the course of the low shear rate flow tests reported in this chapter, research workers in the U.S.S.R. reported the preparation of a form of water with properties different from normal water. Large anomalies were reported in density, viscosity and other properties in relation to accepted values for normal water. This modification of water has commonly been called "anomalous water" or "polywater". The latter term was adopted because of the supposed polymer structure of the modified water.

After a great deal of international experimental and theoretical research and debate during which "polywater" was made and tested in several countries it was concluded that the anomalous water properties were the result of impurities dissolved in the water during its preparation by condensation in quartz capillary tubes. The debate about the possibility of occurrence of a different structural form of water aroused strong feelings. Some of these would appear to have been based on grounds of nationalism and personal rivalry. Some western research workers criticised the research techniques and the early conclusions drawn.

Despite the criticisms, the interest generated was sufficient to justify the writing by Franks (1981) of a book on the subject. The bibliography covers nearly one hundred of the several hundred papers published on the topic, many by workers eminent in the fields of the chemistry and physics of water.

As soon as the evidence became available from spectroscopic studies that impurities were the cause of the anomalous water behaviour, research workers interested in the fundamental behaviour of pure water lost interest in the subject, losing sight of the potential implications in the study of the flow of impure water such as groundwater.

The results of the research described are considered to have particular significance in the study of low shear rate flow of groundwater, despite the current lack of interest by those people concerned with the properties of pure water. If small concentrations of solutes in water condensed in quartz capillaries in the laboratory can have such a large effect on the viscosity of water as that reported during the course of the "polywater" research it is possible that similar effects can occur

in groundwater flowing at low shear rates. Groundwater has prolonged contact with quartz and other siliceous materials and is known to carry small concentrations of silica and silicates in solution.

3.3 Experimental Investigation

The evidence cited for the existence of a pre-linear laminar flow regime in capillary tubes and porous media with flow channel cross-section dimensions of the order of those of the main flow channels in aquifers is scant and conflicting.

When carefully performed experiments give conflicting results it is usually caused by the failure to take into account some important variable. Because of this, it was decided that the first step in a systematic investigation of the occurrence of a non-linear laminar flow regime should be a carefully performed and controlled series of flow tests in a capillary tube of circular cross-section. The tube should be inert and should be long enough to give measurable head differences at very low hydraulic gradients. The diameter should be large enough to restrict surface effects to a small proportion of the flow cross-section and yet small enough to give low shear rates. If conclusive evidence for the occurrence of a non-linear flow relationship could be obtained it would then be necessary to investigate the cause so that the evidence from previous experiments could be reconciled. Only then would it be profitable to proceed to low shear rate tests in porous media. The prospects of determining whether any non-linearity observed in flow through aquifer material was caused solely by the water property or by an interaction between the water and the porous medium would be poor unless the simpler problem of understanding the behaviour of water flowing in a capillary tube could be solved first.

The remainder of this chapter is devoted to a description of a series of flow tests in a capillary tube. The tests were carried out to provide a basis for the logical design of a complementary series of tests on flow through porous media. A better understanding of the factors which affect the viscosity of water at low shear rates would allow the occurrence of, and reasons for, pre-linear non-Darcy groundwater flow to be examined systematically.

3.3.1 Experimental Equipment

Initial Apparatus

Figure 3.1(a) shows the initial set of experimental apparatus. It consisted of a 46.3 metre length of 0.29 mm internal diameter stainless steel tubing, an upstream container to supply water to the tube and a downstream container to collect the discharge. Flow rates could be measured by weighing the container on a precision balance to determine mass inflows and by timing flow durations. Head differences could be measured by micrometer point gauges or millimetre rules, depending on the magnitude of the head difference.

The upstream end of the tube entered the upstream reservoir container below the water surface through a brass union cemented with epoxy resin into the glass wall. The downstream end of the tube entered the downstream collecting and weighing container through a loose rubber plug in the lid. The end of the tube was held below the water surface to eliminate surface tension effects.

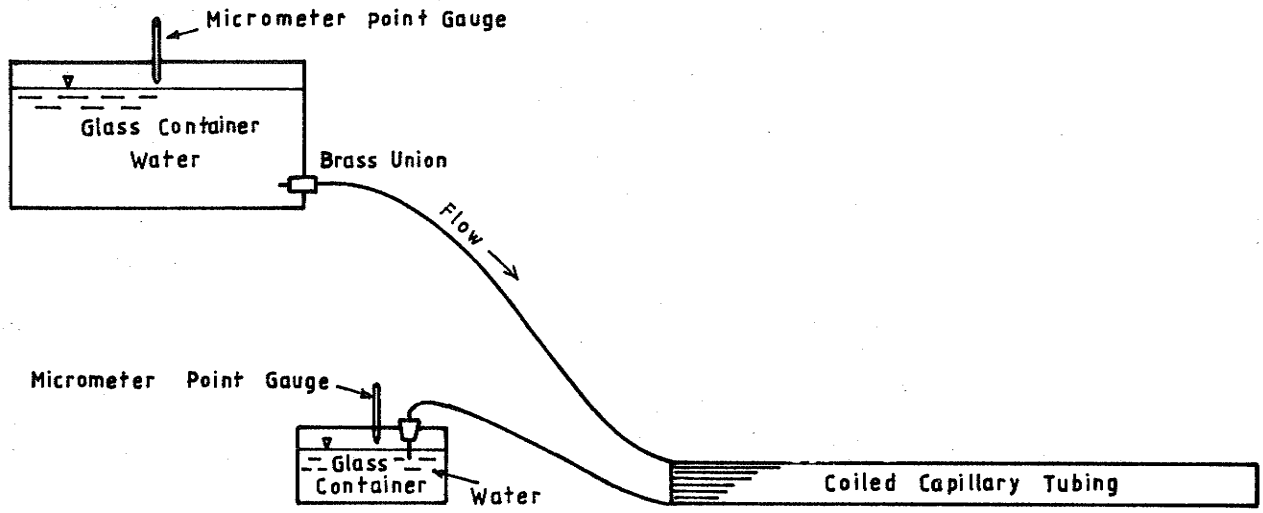

a) DIAGRAM OF ORIGINAL APPARATUS

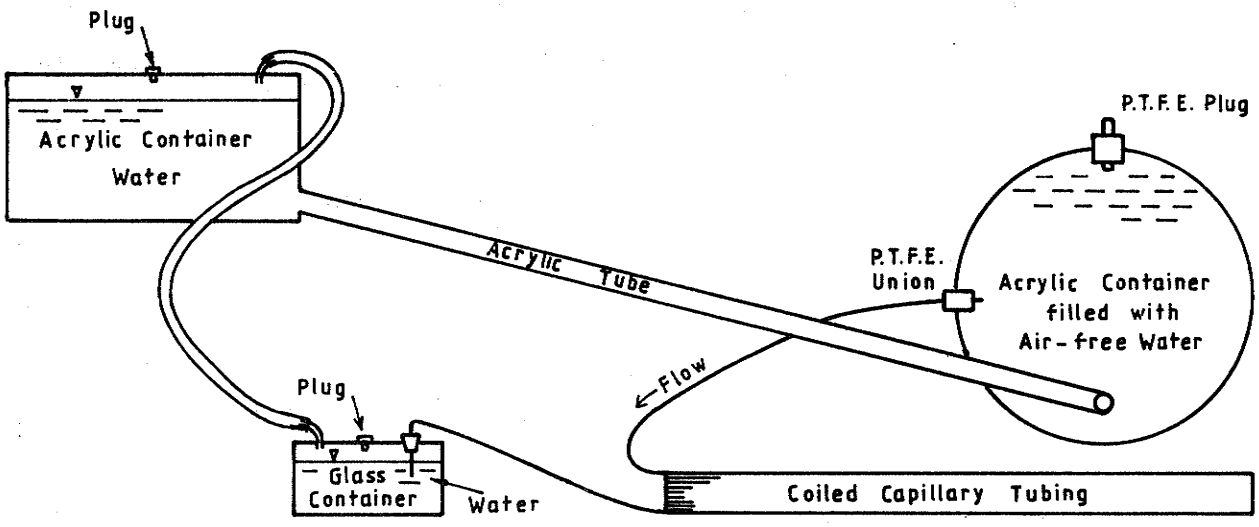

b) DIAGRAM OF MODIFIED APPARATUS

Not to Scale

FIGURE 3·1: APPARATUS USED FOR LOW SHEAR RATE FLOW TESTS IN CAPILLARY TUBE

A resting container similar to the weighing container was positioned near the latter to accommodate the tube while weighings were carried out. The water in the resting container was maintained approximately at the same level as that in the weighing container.

Small diameter central holes in the lids of all the containers allowed access for the 3 mm diameter micrometer gauge points. Holes not in use were kept plugged. The small gap between the gauge points and access holes ensured that both the upstream and downstream water surfaces were subjected to atmospheric pressure during flow tests.

Both the upstream and downstream containers were made from "Pyrex" glass dishes with glass lids cemented on with epoxy resin. The diameters of the containers and thus of the upstream and downstream free water surfaces (150 mm and 65 mm respectively) were made as large as practicable to reduce the effect on head difference of water flowing from one container to the other. The maximum size of the downstream container was set by the pan size and maximum weight limitations of balances which would weigh to 0.0001 g.

Modified Apparatus

After several series of tests had been completed using the apparatus shown in Figure 3.1(a) it was decided to use more chemically inert material for the upstream container and eliminate the air surface from the upstream container into which the stainless steel tube was connected. The modified apparatus is shown in Figure 3.1(b). Only clear "Perspex" (acrylic) and "Teflon" (P.T.F.E.) were in contact with the water in the upstream reservoir system. An additional container was added to the system and connected by a 1.2 m length of acrylic tube to

the upstream head container which enclosed the free water surface. The purpose was to provide a long air diffusion path between the upstream water surface and the entrance to the stainless steel tubing. The complete apparatus and a close-up of the weighing container and equipment for measuring small head differences are shown in Photographs 3.1(a) and 3.1(b). In Photograph 3.1(b) the downstream end of the tube is in the resting container while the weighing container is under the point gauge.

3.3.2 Constant Temperature Room

Preliminary tests on flow through a length of polyethylene capillary tubing at uncontrolled room temperature demonstrated the futility of attempting to make precise measurements of low flow rates under these conditions. Expansion and contraction of the tube and its contents could completely mask the flow being measured.

To overcome the problems caused by varying temperatures, a well insulated constant temperature room was constructed in the basement of a building. Since very fine control of temperature was required, an over-cool and re-heat system was adopted for adjusting the temperature. A commercial air conditioner was fitted into an interior wall of an enclosed area under a concrete staircase which adjoined the constant temperature room. The heat exchanger of the air conditioner was in the thermally stable sheltered space under the floor of the building. The air conditioner was used to cool air to a temperature lower than the $20^{o}C$ at which the constant temperature room was to operate. A domestic fan heater fitted into a door between the air conditioned space and the constant temperature room was used to re-heat the air to maintain a constant temperature in the room. An extractor fan and ceiling duct was used to return air from the remote end of the room. The wiring of the

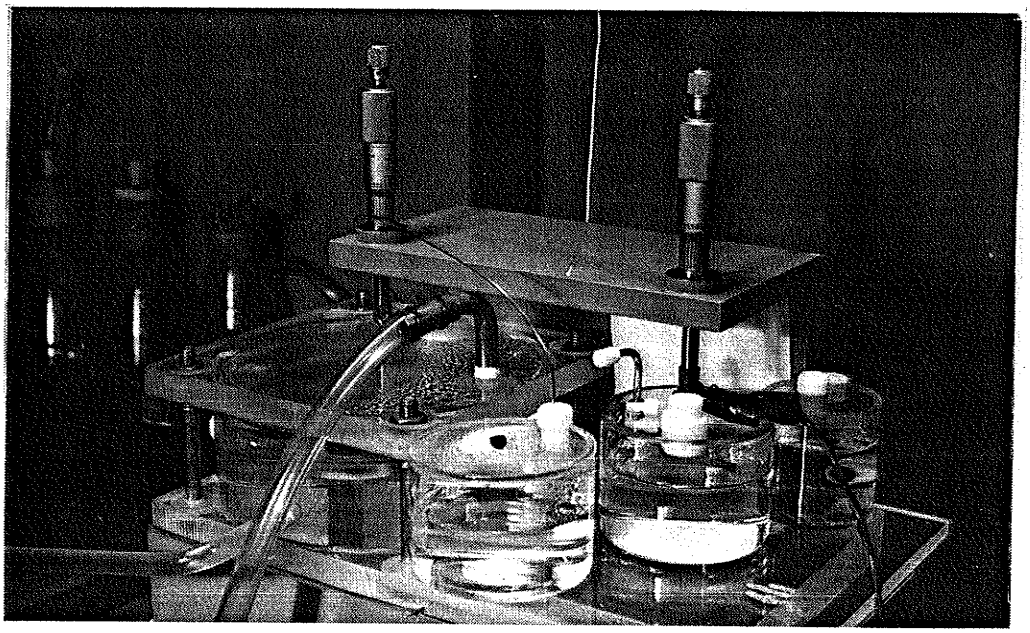

Photograph 3.1 (b) Head Measuring Equipment for Capillary Flow Tests.

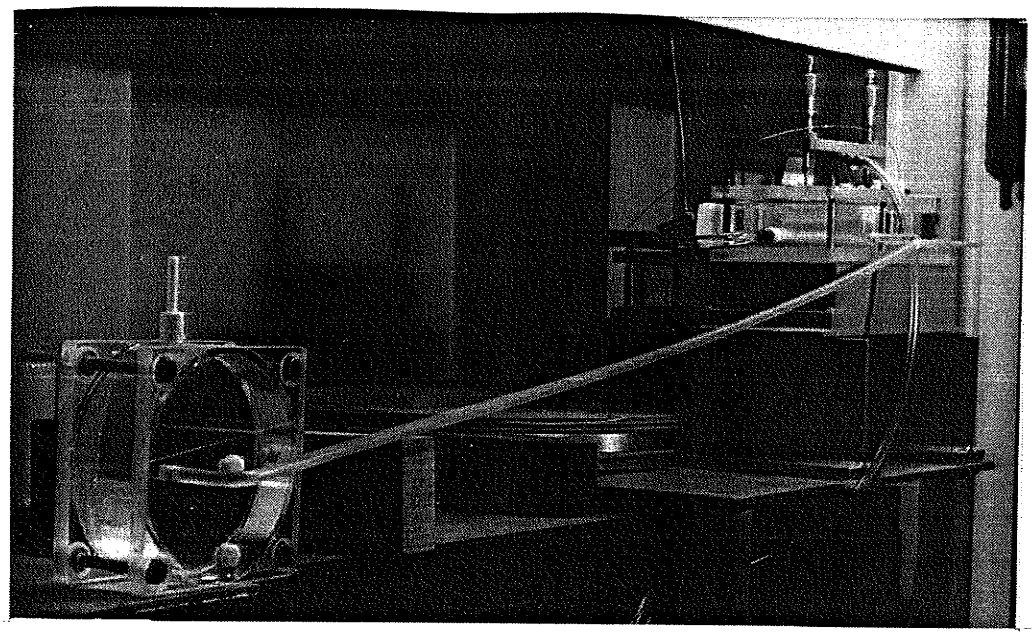

Photograph 3.1 (a) Capillary Tube Flow Apparatus

heater was altered to allow the fan to run continuously with the heating elements switched by a relay operated by a sensitive mercury contact thermometer. The thermometer was adjustable to allow switching at temperatures in the range 0 - 50°C. It was located in a sheltered position near the experimental apparatus.

During the course of the experiments it was decided that humidity control would improve the accuracy of the test results. Since the air conditioner extracted water by condensation on the cooling coils and re-heating lowered the relative humidity it was necessary to add water to the re-circulated air. This was done by spraying high pressure water from a hypodermic needle against a small plate fixed in front of the fan heater. The needle was fitted to an adaptor screwed to a high pressure water line from ion-exchange units. It was found necessary to de-ionise the water to prevent blockage of the needle and the dispersal of salt crystals throughout the room. The flow of water to the jet was controlled by a solenoid operated valve activated by a relay connected to a second mercury contact thermometer. The second thermometer was positioned near the one which controlled the re-heating. Its bulb was inserted into a cotton mesh sleeve which drew water by capillary action from a shallow 1 litre container. The thermometer measured the "wet bulb temperature" which depends on relative humidity. The humidity at which the room operated could be adjusted independently of the temperature.

A recording thermo-hygrograph and accurate wet and dry bulb thermometers located near the control thermometers were used to monitor the temperature and humidity. It was found that if the room was closed with the lights off, both wet and dry bulb temperatures could be maintained within $\pm 0.1^{\circ}C$. Normal dry and wet bulb settings were $20^{\circ}C$ and $16^{\circ}C$

respectively.

The heat from lights and one person working in the room could upset the balance by up to $+0.2^{o}C$. However, the thermal lag ensured that the temperature of the apparatus and water was not fully subjected to the temperature fluctuations caused by working in the room for short periods.

3.3.3 Experimental Procedure

Before the tests were commenced the containers were cleaned and dried. The apparatus was then assembled and distilled water was added to the upstream container. No attempt was made to prevent air from dissolving in the water prior to and during its addition to the apparatus. A difference in level of approximately 1 metre between the water level in the upstream container and the downstream end of the tube failed to cause the tube to fill as rapidly as desired so a vacuum of approximately 50 kPa was applied at the downstream end of the tube in addition to the level difference to accelerate the progress. Flow was observed at the outlet after approximately 6.5 hours. Water was then added to the downstream container, the downstream end of the tube was inserted and the apparatus was allowed to stabilise for 20 minutes before tests were commenced.

During the tests, water was allowed to flow under the influence of gravity from the upstream to the downstream container. The quantity of water which flowed from the tube during a measured time interval was determined by successive weighings of the downstream container on a single pan balance reading to 0.0001 g. Great care was taken to avoid losses when the downstream end of the tube was transferred to the

similar container in which it remained while weighings were being made.

The difference in water levels in the upstream and downstream containers was measured by a steel rule, if large, and by micrometer point gauges if small. The containers were mounted on a rigid steel frame under the point gauges. The point gauges were zeroed by measuring the water levels in two containers connected by a short length of 6 mm diameter PVC tubing. In the later set of apparatus a zeroing container was connected permanently to the reservoir container furthest upstream to allow the zero readings to be checked without disturbing the apparatus. The polyethylene connecting tube was fitted with a "Teflon" (P.T.F.E.) plug valve. The accuracy of level difference measurements was estimated as ± 0.02 mm for head differences up to 40 mm. For larger level differences measured by sighting meniscus levels against the scale on a steel rule, the accuracy was estimated as ± 0.3 mm up to 300 mm and ± 0.5 mm up to 1 m.

Although the procedure described above appears to be simple, it was very difficult to maintain a level of accuracy that allowed small flows into the downstream container to be detected. The main problems encountered were:

i. In the absence of humidity control in the early experiments, moisture adsorbed onto surfaces and absorbed into the epoxy glue line under the lid of the downstream container could exceed small inflows from the tube.

ii. The balance accuracy was affected by humidity variations. To overcome this, a standard balance weight or a "Teflon" (P.T.F.E.) plug was weighed at the time of each flow measurement and an adjustment

was made to the measured mass of the downstream container.

iii. Because the downstream container displaced a relatively large volume of air in comparison with that displaced by the balance weights, changes in the density of the atmosphere affected the weighings. For small flow rates it was found necessary to make accurate allowance for the difference between the buoyancy forces exerted by the atmosphere on the container and on the balance weights. Until humidity control was established, it was necessary to estimate the relative humidity for use in the adjustment calculations.

For early tests, the barometric pressure was estimated from readings at the Sydney Observatory adjusted for height difference. Since the barometric pressure is important in the buoyancy adjustment, a mercury barometer was subsequently installed. Comparisons with estimates from the observatory readings showed good agreement.

iv. Uncontrolled external factors such as vibrations were found to affect the test results. It took a considerable length of time to isolate the cause of the problem. The effect of accidental and deliberate vibration is discussed fully in the following section.

3.3.4 Test Details, Results And Discussion

The experimental equipment and procedures were designed to provide corresponding values of flow rate and hydraulic gradient for steady flow conditions over a wide range of gradients. It was thought that if the structure of water had a significant effect on the stress-strain relationship, a deviation from linear flow (Poiseuille's Law) would show up

as the flow rate was reduced. Eventually flow would be observed to cease if water had a shear strength greater than the lowest boundary shear stress which could be measured in the apparatus (approximately 10^{-6} Pascals).

The flow behaviour and factors affecting it proved to be much more complex than anticipated. In the remainder of this section the problems that arose, steps that were taken to avoid them and the results of the flow tests are described and discussed in chronological order. Data used to plot the graphs in the figures included in the remainder of this chapter are listed in Appendix A.

Preliminary Tests

A preliminary series of tests was commenced soon after the apparatus had been filled with water. Nine flow rates were measured for head differences between 23.8 mm and 1707 mm. The results are given in Table 3.1.

The plot of flow rate versus hydraulic gradient shown in Figure 3.2 has an unexpected scatter of results that can not be attributed to measurement errors. The plotted points also fall well below the line which represents Poiseuille's equation.

Test Series 1(a)

To allow the problem encountered in the preliminary tests to be resolved, a series of flow measurements was made at a constant head of 252 mm. Parts of the flow history are shown in Figure 3.3. It was found that there was a continuous decline in flow rate with small random

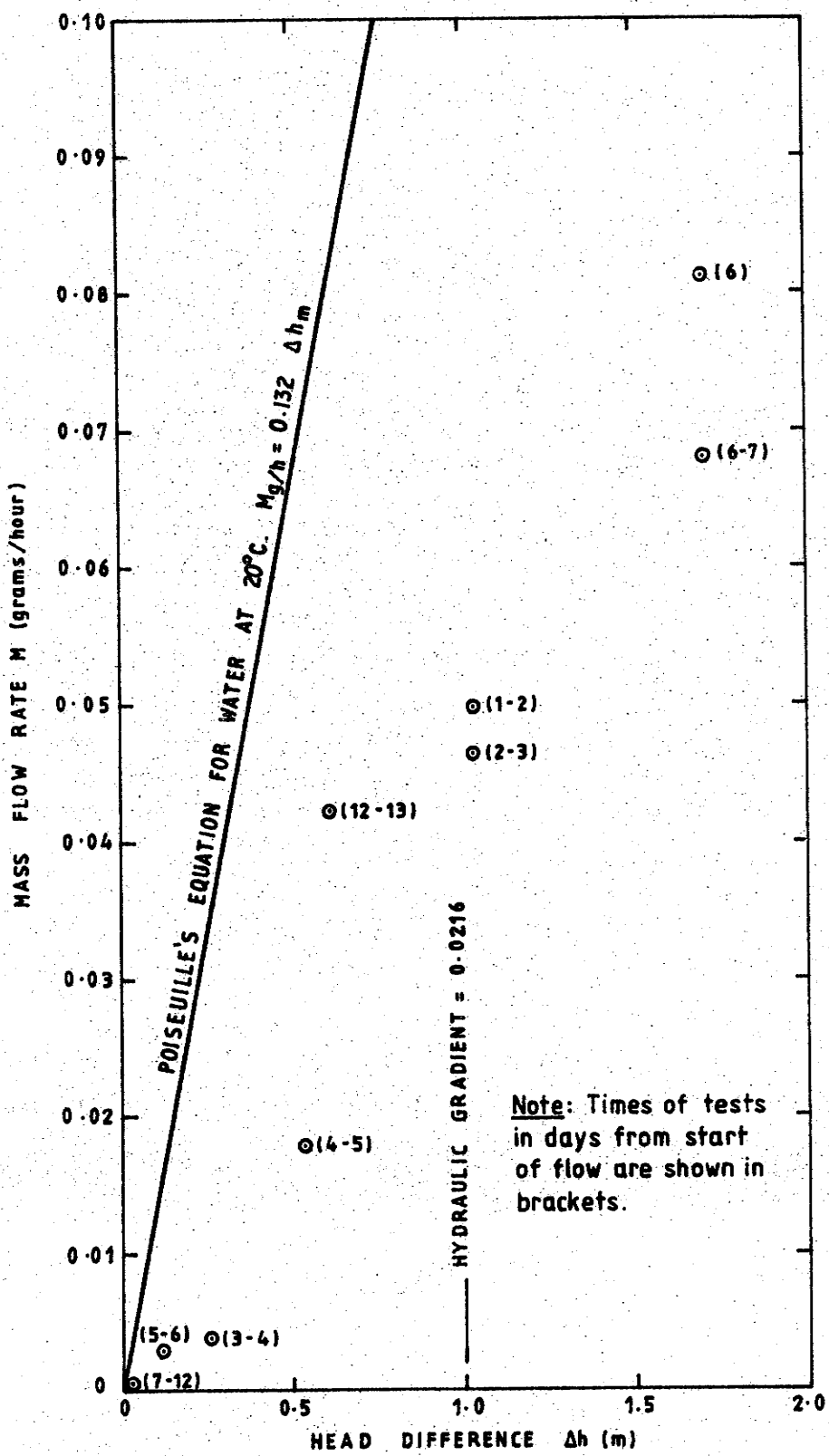

FIGURE 3.2: FLOW IN CAPILLARY TUBE - RESULTS OF PRELIMINARY TESTS

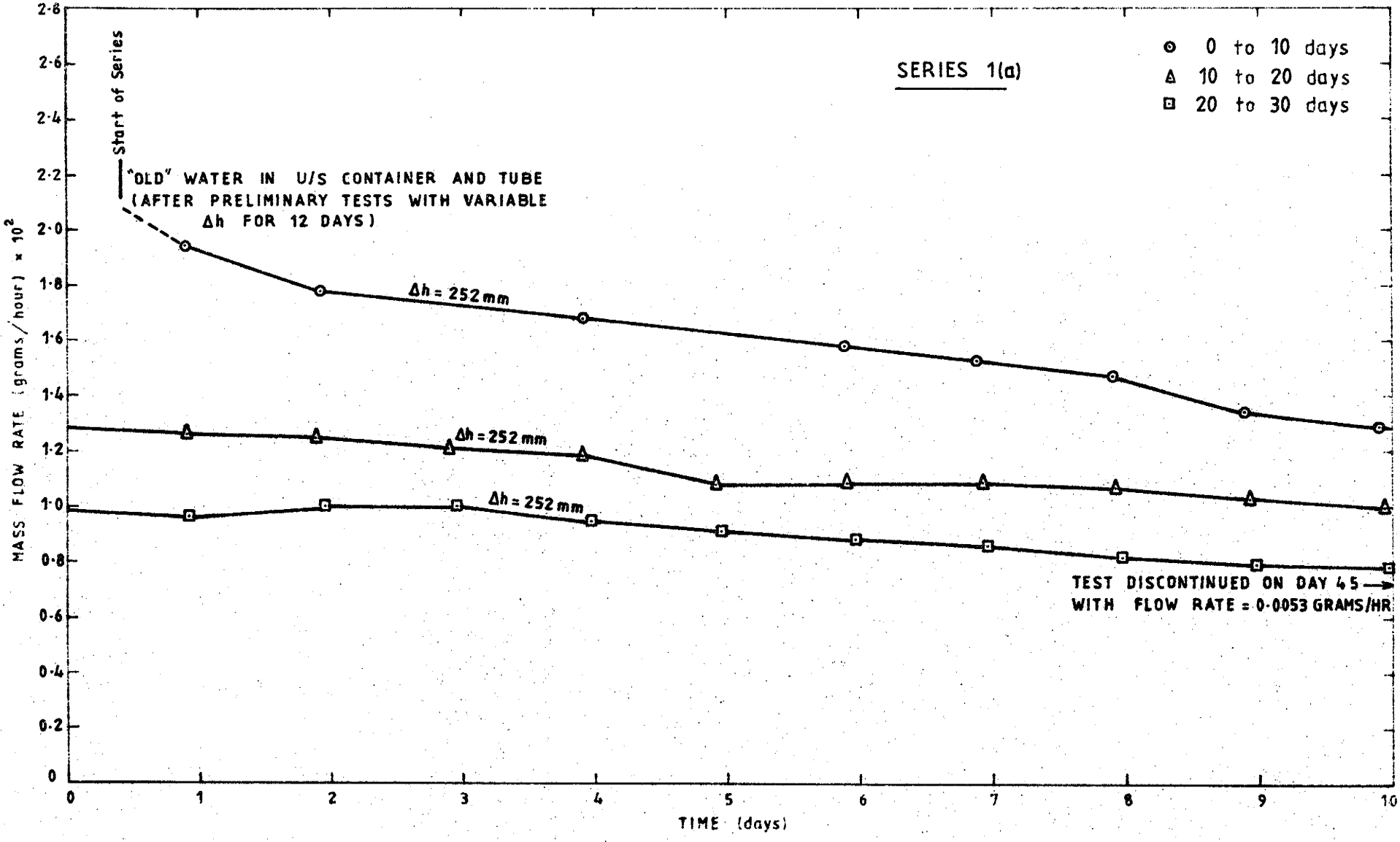

FIGURE 3.3 : FLOW HISTORY IN CAPILLARY TUBE

Table 3.1: Results of Preliminary Flow Tests In Capillary Tube

Day	Head Difference (mm)	Mass Flow Rate (grams/hour)	
		Measured	Predicted By Poiseuille's Equation for d = 0.29 mm
1-2	1029	0.0497	0.1358
2-3	1029	0.0464	0.1358
3-4	257	0.0039	0.0339
4-5	526	0.0178	0.0694
5-6	117	0.0028	0.0154
6	1707	0.0811	0.2253
6-7	1707	0.0679	0.2253
7-12	23.8	0.0009	0.0031
12-13	608	0.0422	0.0803

superimposed fluctuations. The latter were initially attributed to weighing errors. However, during the course of the tests a suspicion arose that accidental impacts and vibrations from both inside and outside the constant temperature room were affecting the results.

Test Series 1(b)

A new series of tests was commenced using the same "old" water in the upstream container and the tube but with the downstream container level lowered to give a head difference of 1343 mm. The apparatus was also subjected to impact and vibration by bumping both it and the bench

on which it rested. The results of the tests are shown in Figure 3.4. The rapid decline in flow rate after the disturbance at the start of the test can be seen. An unexplained increase in flow also occurred at one point. It is assumed that there was some alteration to the apparatus or procedure which was not considered relevant and was thus not noted.

A length of approximately 25 mm was cut from each end of the tube to allow microscopic inspection for entry or exit blockage. None was observed.

At this stage the possible effects of dissolved air or air bubbles in the tube came under scrutiny. The results of the tests carried out so far and some anomalies reported in literature surveyed in Section 3.1.2. led to the belief that the uncontrolled dissolved air content could be a significant factor in the effects observed and shown in Figures 3.1 to 3.4.

Test Series 2

Another series of tests was commenced with a head difference of 250 mm after the tubing had been cleaned with dilute A.R. grade nitric acid, passivated with concentrated A.R. grade nitric acid and flushed thoroughly with distilled water. The acid and water were drawn through the tube by applying a vacuum of approximately 40 kPa at the outlet. The upstream and downstream containers were re-filled with de-aired distilled water and the whole apparatus subjected to shock and vibration by bumping it and the bench prior to the commencement of flow readings.

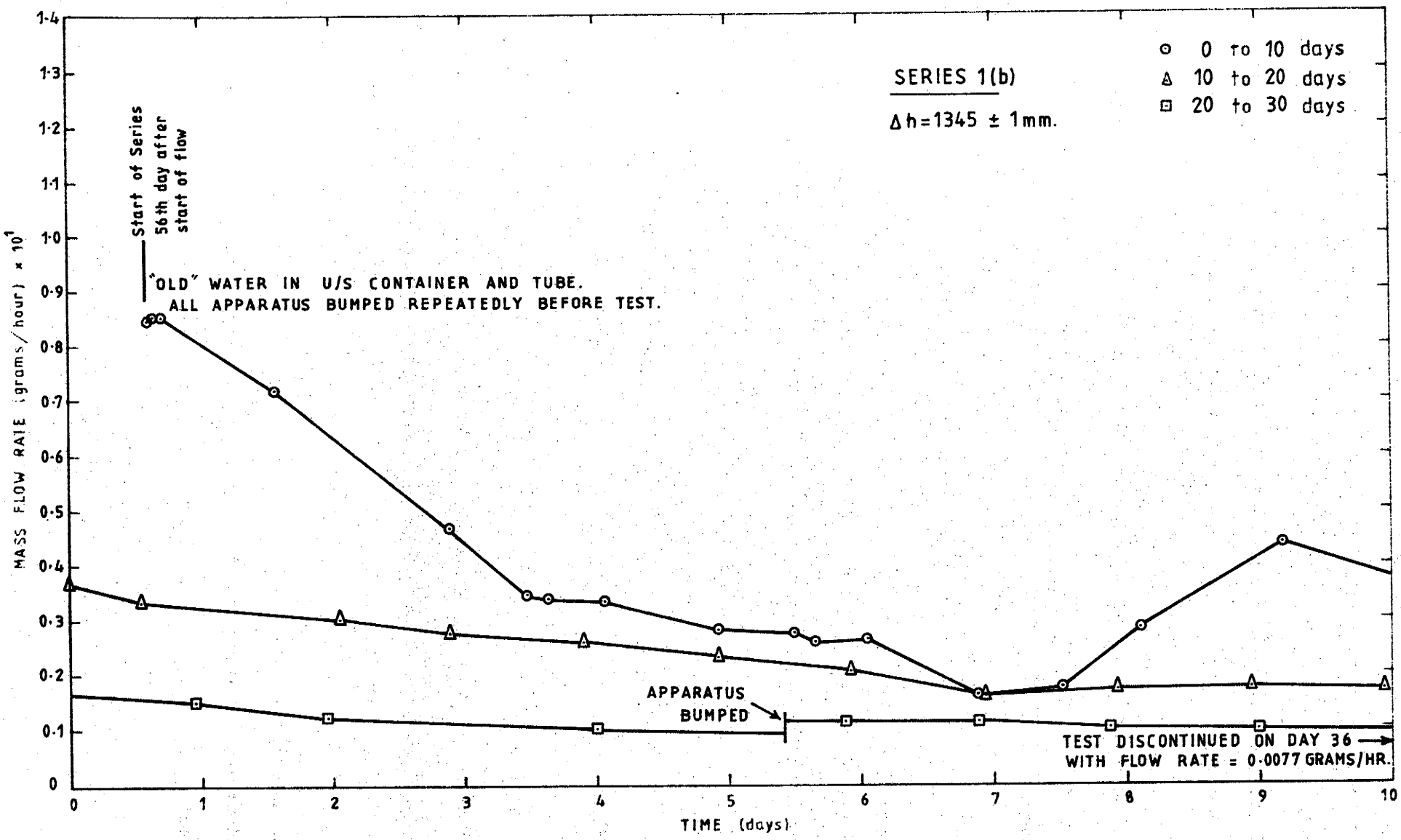

FIGURE 3.4 : FLOW HISTORY IN CAPILLARY TUBE

The results of this series of tests are shown in Figure 3.5. The flow initially increased after the vibration and then commenced to decline as in the previous series. The relatively slow rise after the vibration at the start of the series was unexpected. The only explanation which could be provided was that the tube contained "relatively old" water with some dissolved air following the cleaning and flushing operation but that the water entering the tube from the upstream container was "new" and had little time to absorb air through its surface. The initial rise in flow rate was attributed to replacement of "old" water by "new" water of lower effective viscosity. Since the average concentration of dissolved air in the tube would initially decrease but subsequently increase slowly as air was absorbed into the upstream reservoir, the flow rate would be expected to reach a peak and then decline as the effect of increased time of resting of water in the tube, possibly aided by absorption of air in the upstream container, began to out-weigh the effect of the purging of the "old" water from the tube.

Another point requiring explanation concerning Figure 3.5 is the relatively steady flow and slow decline towards the end of the test after shock and vibration treatment had caused a dramatic increase in the flow rate. At this stage 10 grams of water had flowed from the tube since the start of the series. Since the total volume of water held in the tube was 3.06 grams there had been ample opportunity to flush a large part of the "old" water from the tube leaving it full of water with a low air concentration. If the theory that dissolved air significantly affected the decline in the flow rate were true, the subsequent decline should be slow since the low rate of diffusion of air in the upstream container under the very stable temperature conditions would maintain a low level of dissolved air at the entrance to the tube for a considerable period. The effect of shock and vibration on the flow rate

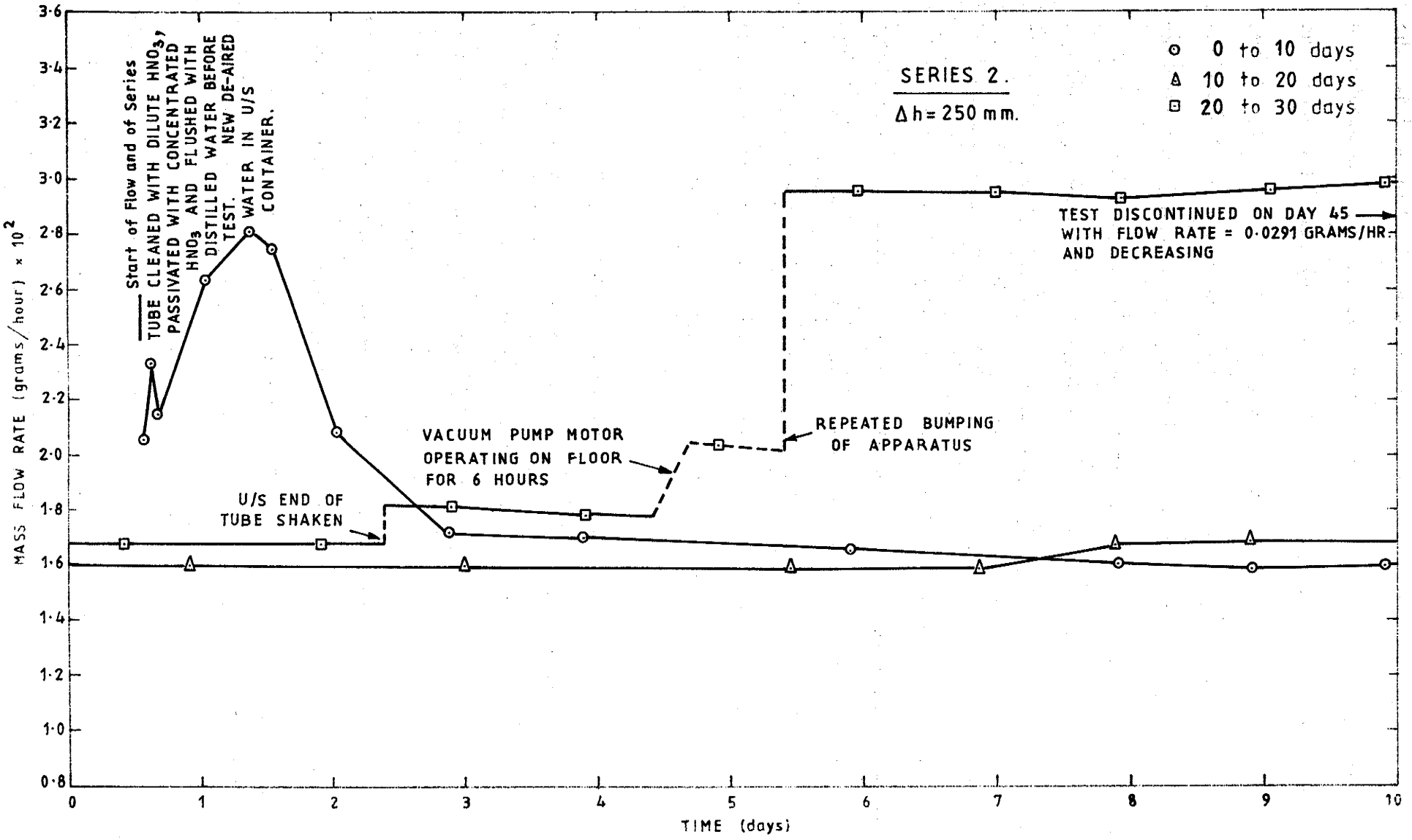

FIGURE 3.5 : FLOW HISTORY IN CAPILLARY TUBE

is clearly demonstrated by the flow behaviour shown in Figure 3.5.

It should be noted also that the maximum flow rate measured during the period of relatively steady flow was 0.0288 grams/hour, 87 per cent of the 0.0330 grams per hour predicted by Poiseuille's equation for normal water viscosity. This occurred after a short period of vigorous bumping of the whole apparatus.

Test Series 3

A final series of tests using the apparatus of Figure 3.1(a) was designed to examine in more detail the effect of change of hydraulic gradient and shock and vibration on the flow rate.

The head difference was increased to 1343 mm as in Series 1(b) by lowering the downstream container. The "old" water was left in the containers and tube and no shock or vibration was deliberately imposed. Care was taken to disturb the tube as little as possible when the downstream container was lowered.

The results of the subsequent flow measurements are plotted in Figures 3.6 to 3.9.

If the flow rate in the tube were linearly proportional to the hydraulic gradient the increase in head difference from 250 mm to 1343 mm should have increased the flow rate from the value of 0.0291 grams/hour which was measured at the end of the previous series (1 hour before the start of the first Series 3 test) to 0.156 grams/hour. The actual flow rate measured over the first hour of flow was 0.159 grams/hour. The flow rate predicted by Poiseuille's

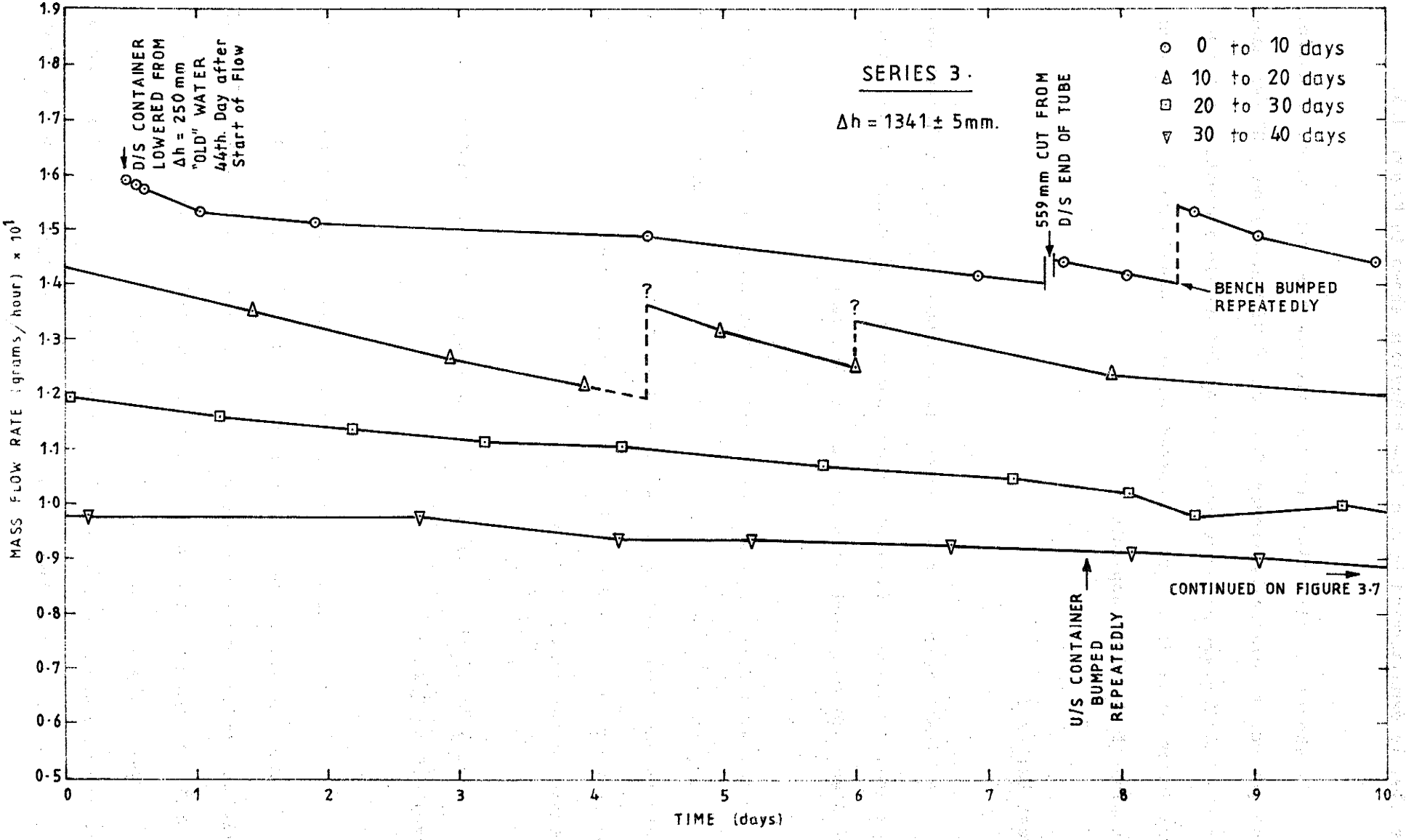

FIGURE 3.6 : FLOW HISTORY IN CAPILLARY TUBE

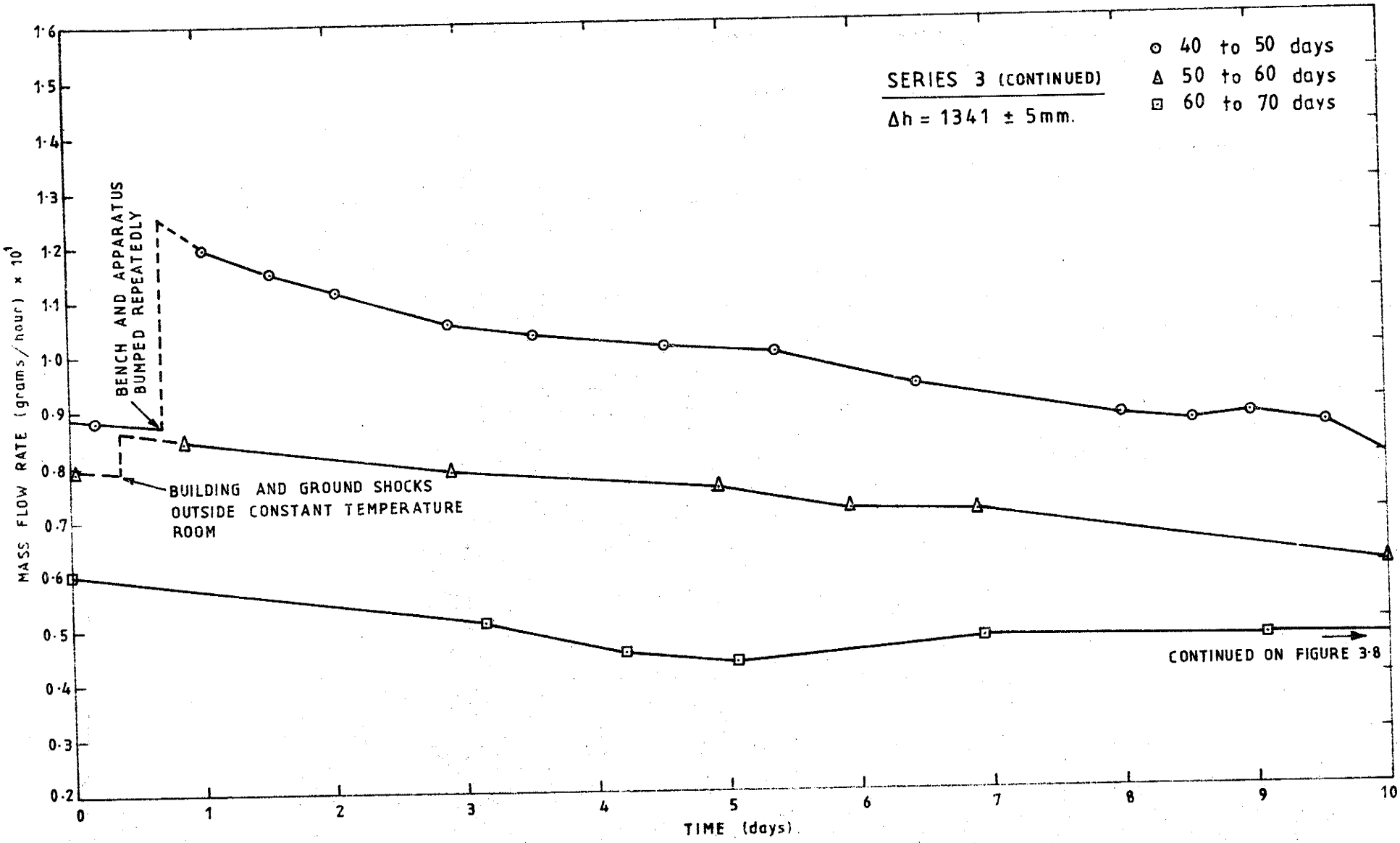

FIGURE 3.7 : FLOW HISTORY IN CAPILLARY TUBE

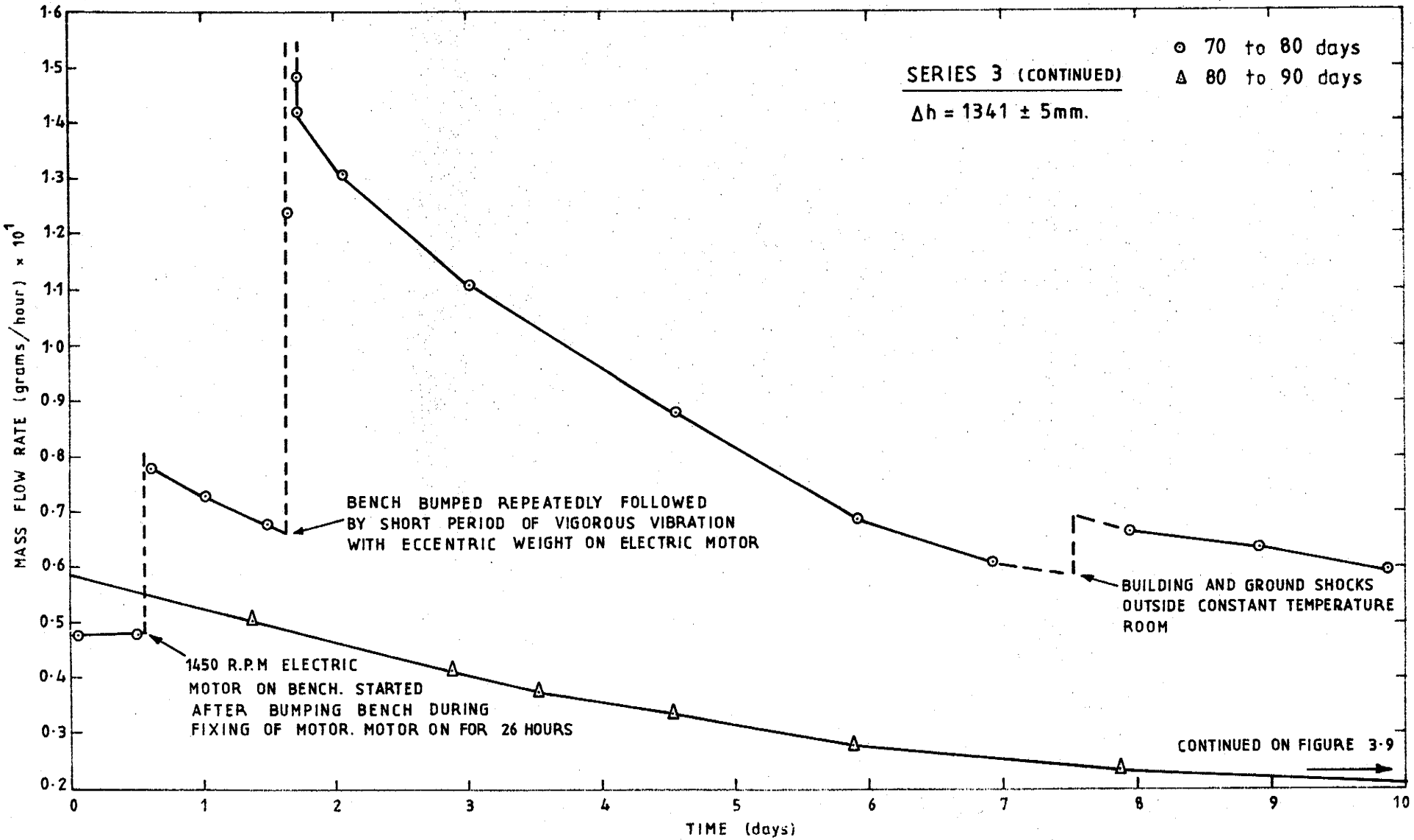

FIGURE 3.8 : FLOW HISTORY IN CAPILLARY TUBE

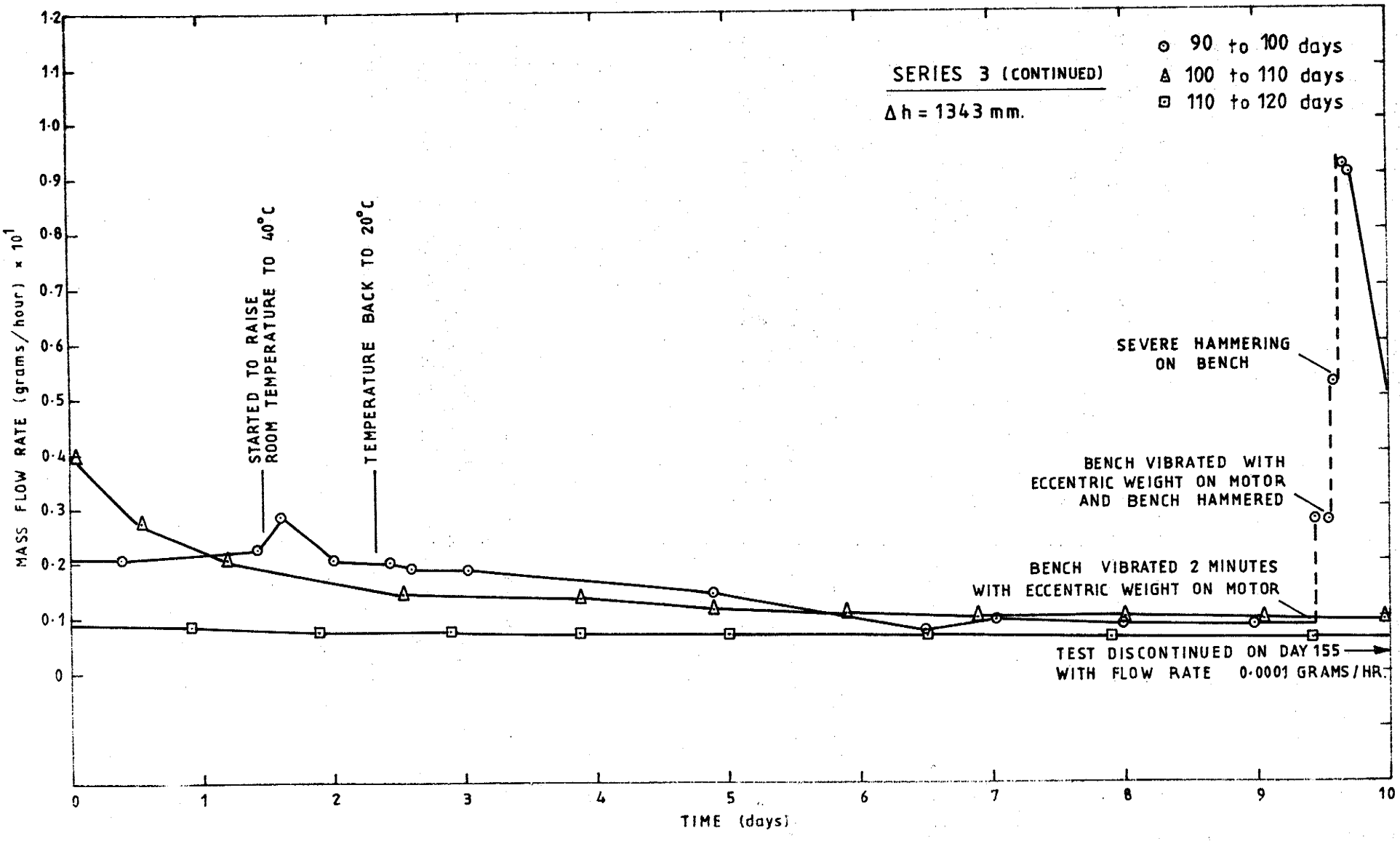

FIGURE 3.9 : FLOW HISTORY IN CAPILLARY TUBE

equation for water at 20°C is 0.177 grams/hour. Thus, although the indicated viscosity of water in the tube was 10 per cent higher than the normal high shear rate value the flow rate was proportional to the impressed gradient. The 2 per cent increase between the proportional and measured flow rates can be attributed to slight disturbance of the downstream end of the tube when the downstream container was lowered. The flow history portrayed in Figures 3.6 to 3.9 again demonstrates the decline in flow rate and sensitivity of the flow rate to deliberate and accidental shock and vibration. An additional point of interest is that the longer the period of decline the more rapidly the flow rate declined towards that which prevailed prior to an increase caused by shock.

Eventually the test series was discontinued when the flow rate had fallen to 0.0001 grams/hour, the limit of measurement with the system in operation. By this time the water had been in the system 199 days and had ample opportunity to become saturated with air.

Air Flow Tests

After the discontinuation of Series 3 tests, air flow tests were carried out to check that the flow of air through the tube was in approximate agreement with Poiseuille's law. No attempt was made to carry out precise measurements since the aim was to check only for gross blockage of the tube. No blockage which could resist the air pressure was discovered. The results are discussed in detail later.

Tests With Modified Apparatus

The modified apparatus shown in Figure 3.1(b) was asssembled with scrupulous attention to cleanliness. The upstream reservoirs were then filled under vacuum with de-aired distilled water. A head equivalent to 22.7 m of water was applied by means of air pressure on the water surface in the uppermost reservoir to initiate the flow. Water appeared at the downstream end of the tube within 5 minutes and commenced to drip into a container at the rate of 4 drops (each 0.026 grams) per second. A preliminary test gave a measured flow rate of 3.2 grams/hour. This compares with 3.00 grams/hour predicted by Poiseuille's equation for a tube diameter of 0.29 mm.

The upstream reservoirs were drained and re-filled under vacuum with de-aired distilled water before starting the next series of tests.

Test Series 4

A series of flows was measured with head differences ranging from 1352 mm down to 0.07 mm to check whether flow obeyed Poiseuille's law when the water was as free from dissolved air as possible with the apparatus and method described. Part of the flow history from the commencement of use of the modified apparatus is shown in Figure 3.10.

With a head difference of approximately 1350 mm, no noticeable decline in the flow rate was observed for seven days. Unfortunately, a breakdown of the air-conditioner occurred just after the tests started and a temperature rise of 2.5°C has complicated the record by causing a temporary increase in the flow rate.

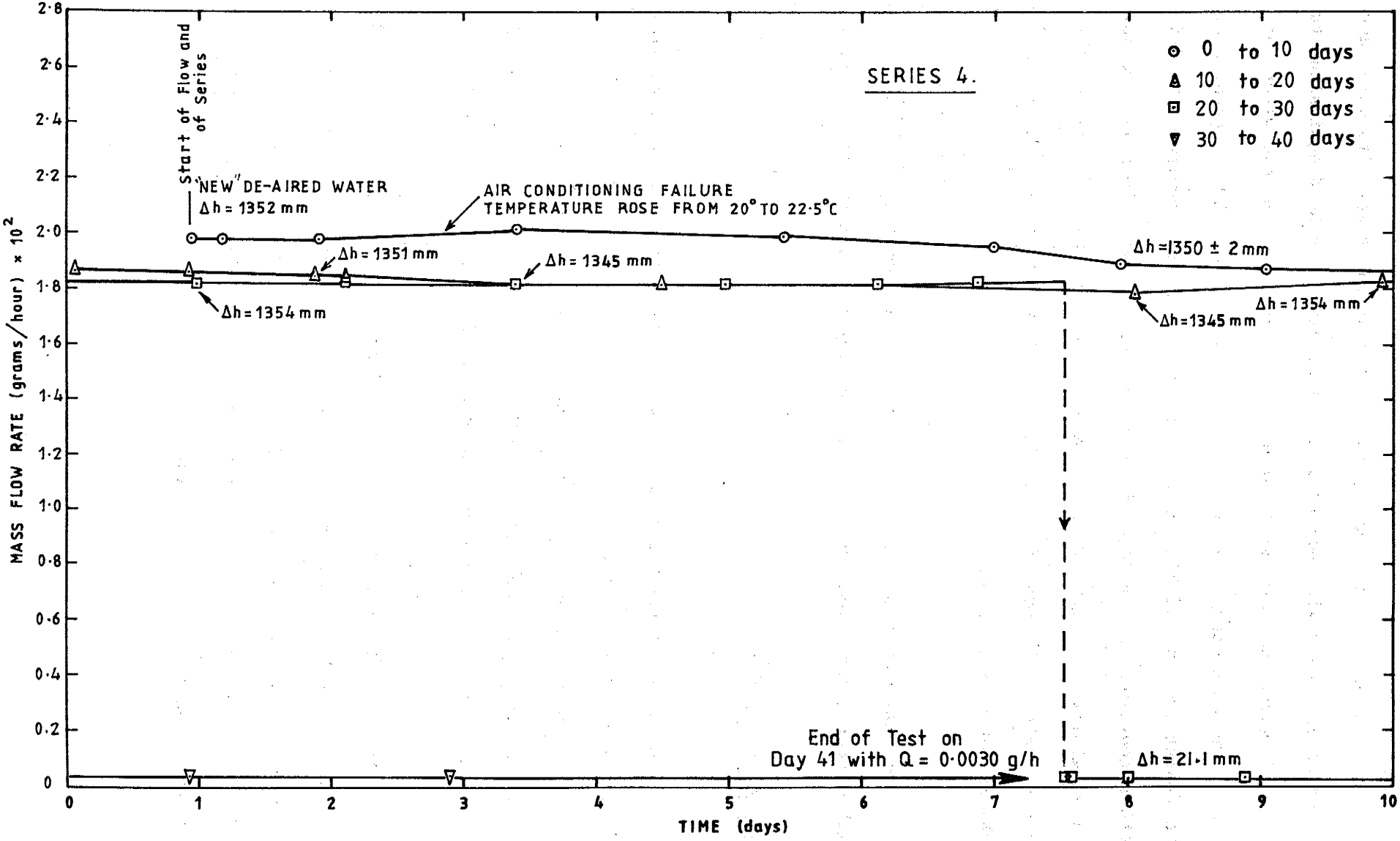

FIGURE 3.10 : FLOW HISTORY IN CAPILLARY TUBE

The mean velocity of flow in the 6 mm I.D. "Perspex" tube connecting the upper and lower upstream reservoirs for a mass flow rate of 0.198 g/h is 1.95×10^{-5} m/s. For laminar flow of a Newtonian fluid the maximum velocity is twice the mean velocity, i.e. 3.9×10^{-5}m/s. Since the connecting tube was 1.2 m in length it would have taken 3.6 days for water to travel at this velocity along the centreline from the upper to the lower reservoir. From that time onwards a low, but gradually increasing, concentration of dissolved air would have been present in the lower reservoir and thus able to diffuse to the entrance of the stainless steel tube.

After the temperature rise caused by the air-conditioner failure had been corrected, the flow rate declined slowly for 7 days but then remained relatively steady for the remainder of the period up to the 27th day when the head difference was reduced. The initial slow 8 per cent reduction in flow rate from 0.198 grams/hour to 0.183 grams/hour and the subsequent steady rate can be compared with the immediate and rapid decline which reduced the flow rate by nearly 100 per cent in 40 days during the earlier tests which did not initially exclude dissolved air.

After 27 days the head difference was reduced to 21.1 mm to check whether the change in flow rate would be proportional to the change in head. This was found to be so. The head and flow rate remained constant for 13 days before the flow measurements were discontinued.

Test Series 5

The flow tests in Series 4 were followed by a series of evaporation rate checks on various downstream containers with the aim of selecting a container with a low and constant evaporation loss rate. In previous tests the accuracy of measurement of low flow rates had been adversely affected by variable evaporation losses.

The next series of flow tests was commenced 28 days after the end of Series 4. Over the intervening period the unmeasured flow rate into the resting container would have been approximately 0.002 grams/hour. This would have produced a total flow of approximately 1.3 grams of water. This flow could not have caused a large increase in air content in the container from which the stainless steel tube drew water since it stored approximately 780 grams of water.

Measurements of flow rates at various heads interspersed with evaporation checks were carried out over a period of 1,133 days to monitor the effective viscosity of the water flowing through the stainless steel tube.

Figure 3.11 is a plot of some of the corresponding head differences and flow rates measured over the duration of Series 4 and 5. The conformity of the early test results to Poiseuille's equation differs completely from the early results for the tests with the apparatus and procedure which did not delay the entry into the tube of water containing dissolved air. Flow rates measured after the arrival of dissolved air in the reservoir into which the tube was connected are all less than those predicted by Poiseuille's law. The difference increased with increasing time during which dissolved air could diffuse and be convected to the tube and with the "age" of water in the tube.

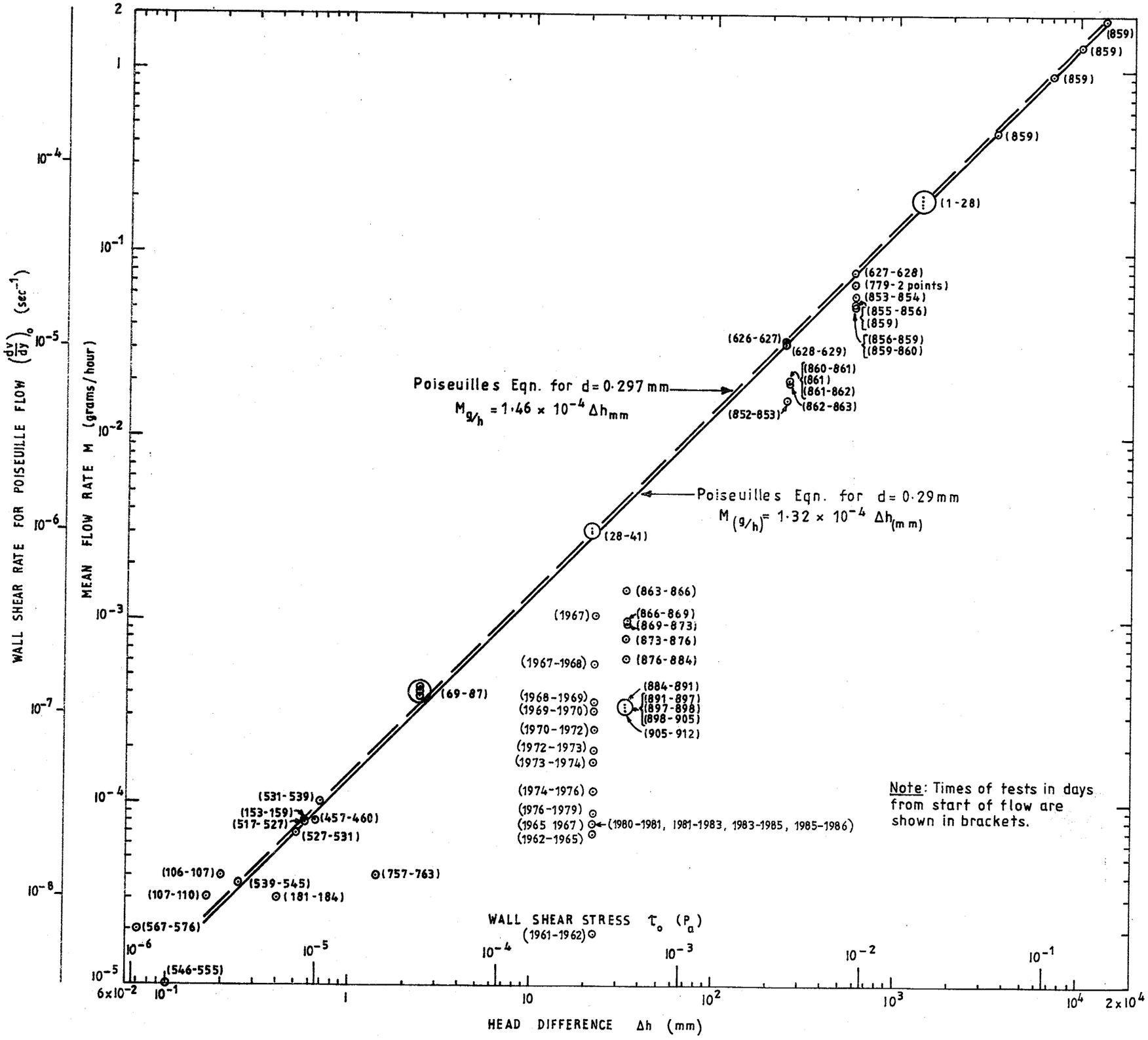

FIGURE 3.11

FLOW IN CAPILLARY TUBE WITH DELAYED AIR ENTRY

Figure 3.12 shows the relative stability of the flow with time for a given head difference compared with previous and subsequent plots even after 859 days from the start of flow. Figures 3.13 to 3.15 show how flow rates decreased and became very sensitive to both accidentally and deliberately imposed shock and vibration as time went on and the concentration of air entering the tube increased. During the period covered by Figures 3.12 to 3.15 the rate of transport of dissolved air to the stainless steel tube was increased by first bubbling air through and then causing an air pocket to form at the top of the lower of the upstream reservoirs. The imposed vibration would also have had the effect of stirring the water in the reservoirs and increasing the rate of transport of air. The times of allowing air to enter the reservoir and of vibration are shown in the figures.

Long Duration Test

During a lengthy absence of the author the flow was allowed to continue undisturbed for 414 days with little disturbance apart from low level background shock and vibration. Natural earth movements, traffic vibrations from an adjacent access road and building vibrations would all have contributed to the pressure fluctuations induced in the water in the apparatus. Pressure changes in the water caused by atmospheric changes would have been relatively slow and small because the air inside the apparatus was isolated from the atmosphere and the reservoir and tube system was relatively rigid.

Over the 414 day period the head difference fell from 25.4 mm to 23.0 mm because of the transfer of 3.27 grams of water from the upstream to the downstream container. An average head difference of 24.2 mm was adopted. The measured average flow rate was 0.00036 grams/hour. This

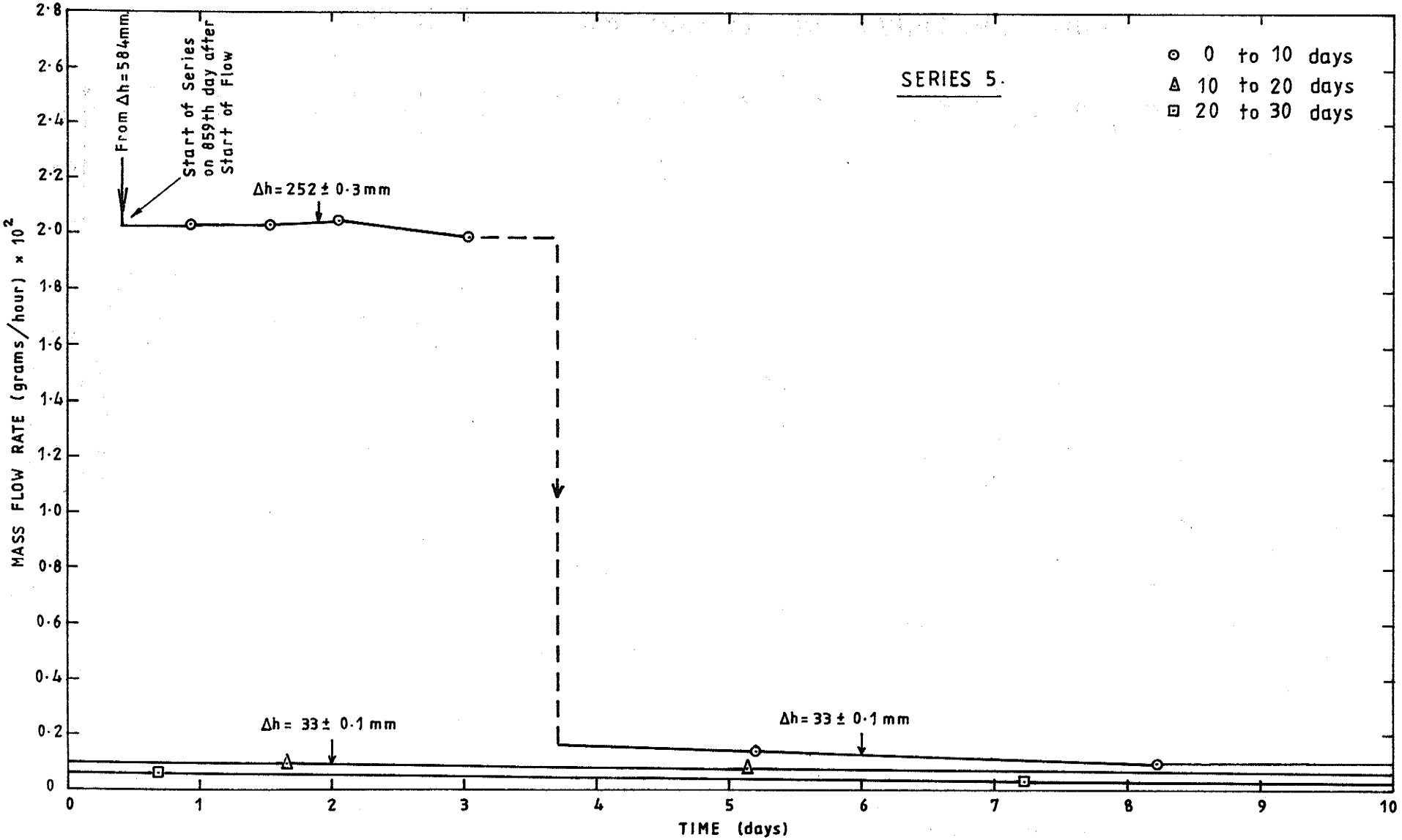

FIGURE 3.12: FLOW HISTORY IN CAPILLARY TUBE

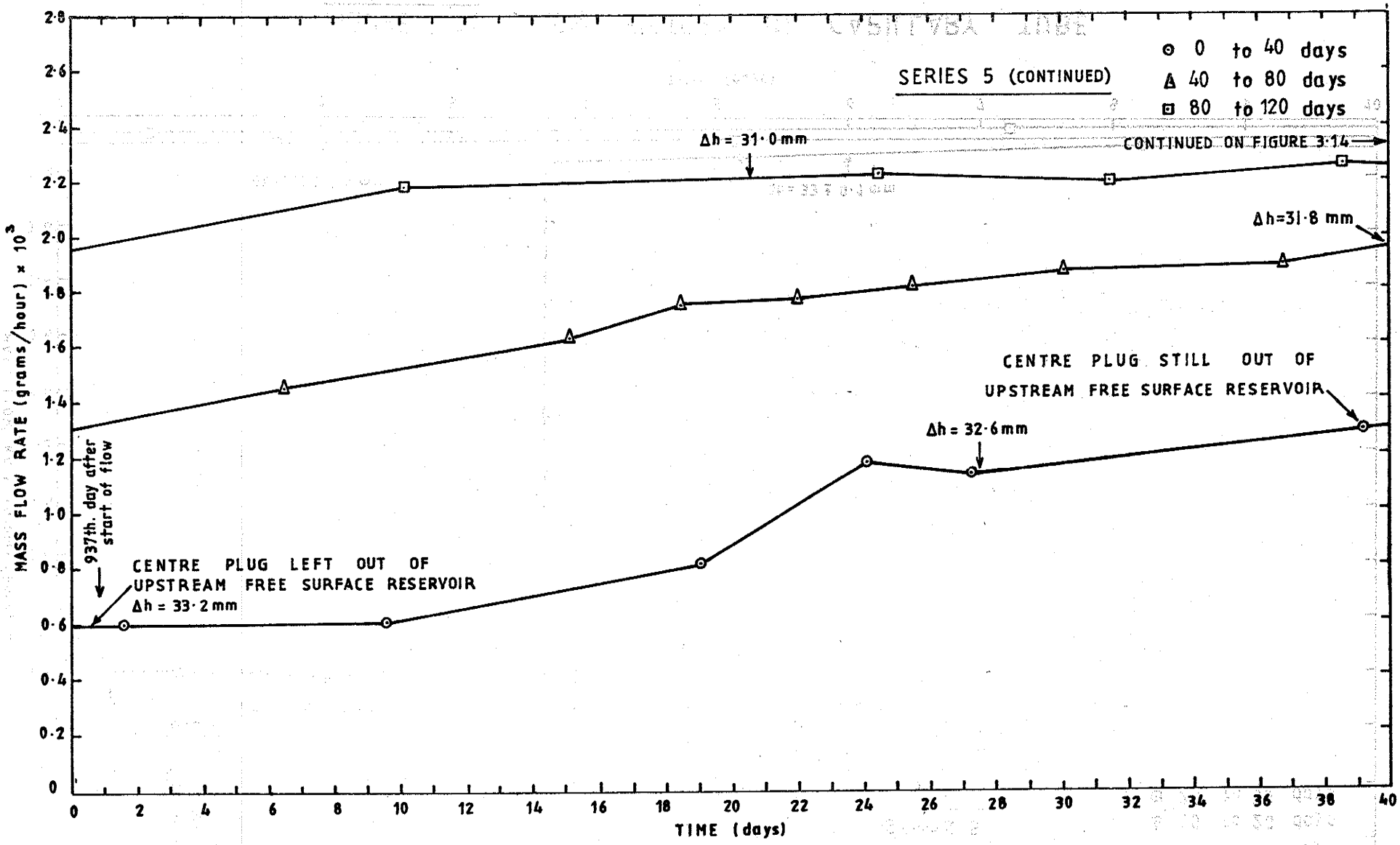

FIGURE 3.13: FLOW HISTORY IN CAPILLARY TUBE

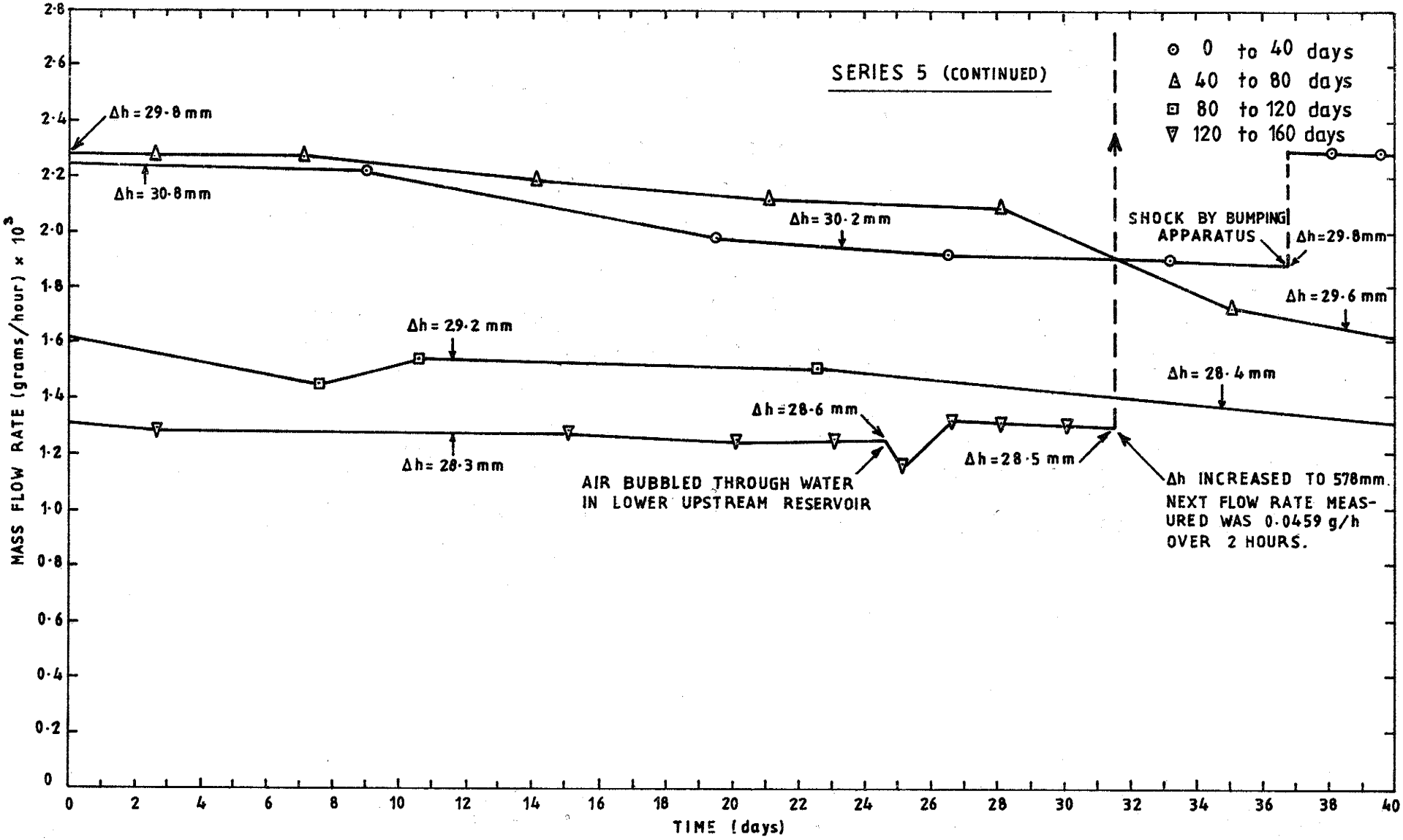

FIGURE 3.14: FLOW HISTORY IN CAPILLARY TUBE

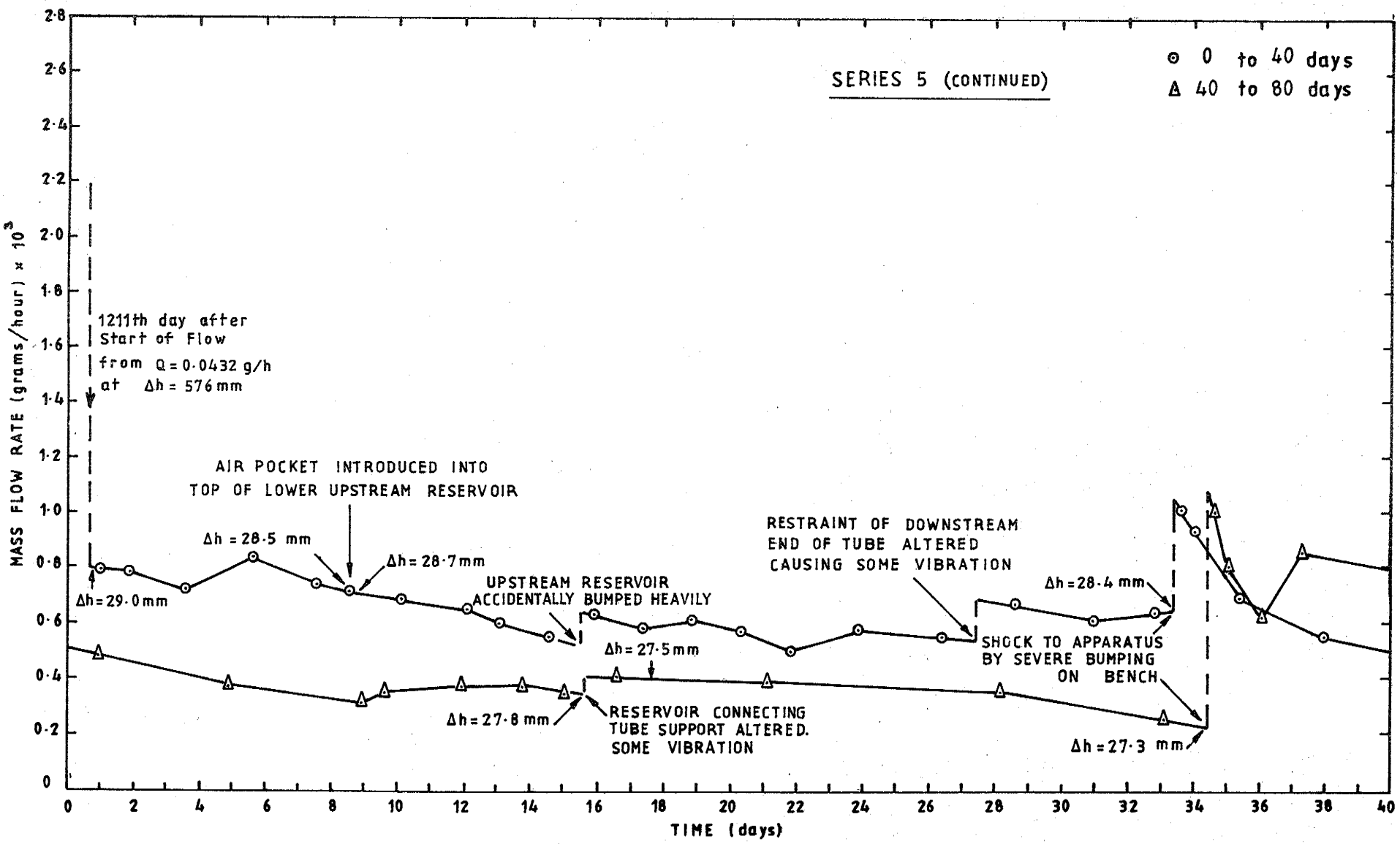

FIGURE 3.15: FLOW HISTORY IN CAPILLARY TUBE

compares with values between 0.00085 and 0.00079 grams/hour measured on four occasions during an interval of 26 days immediately prior to the long term test. The flow rate predicted by Poiseuille's equation for normal water viscosity, a tube diameter of 0.29 mm and a head difference of 24.2 mm is 0.0032 grams/hour. Thus the average effective viscosity of water in the tube over the 414 day test period was approximately four times that of water at high shear rates.

Test Series 6

After completion of the long term test another series of tests was performed to examine the effect of changes in head difference and shock and vibration. Figures 3.16 to 3.20 show parts of the flow history which include both significant changes and periods of relatively stable flow. It can be seen that the behaviour pattern now more clearly resembles that found when using the original apparatus in which water containing dissolved air was given immediate access to the tube.

3.3.5 General Discussion of Results

When the capillary tube flow tests were commenced, the intention was to quantify the relationship between shear stress and shear rate at low shear rates. Previously published experimental results had indicated that, as the hydraulic gradient was reduced, a point would be reached where the flow rate for a given hydraulic gradient would become less than that predicted by Poiseuille's law. The evidence suggested that the deviation would then increase with decreasing gradient. The flow would cease when the applied shear stress fell below the shear strength of the water.

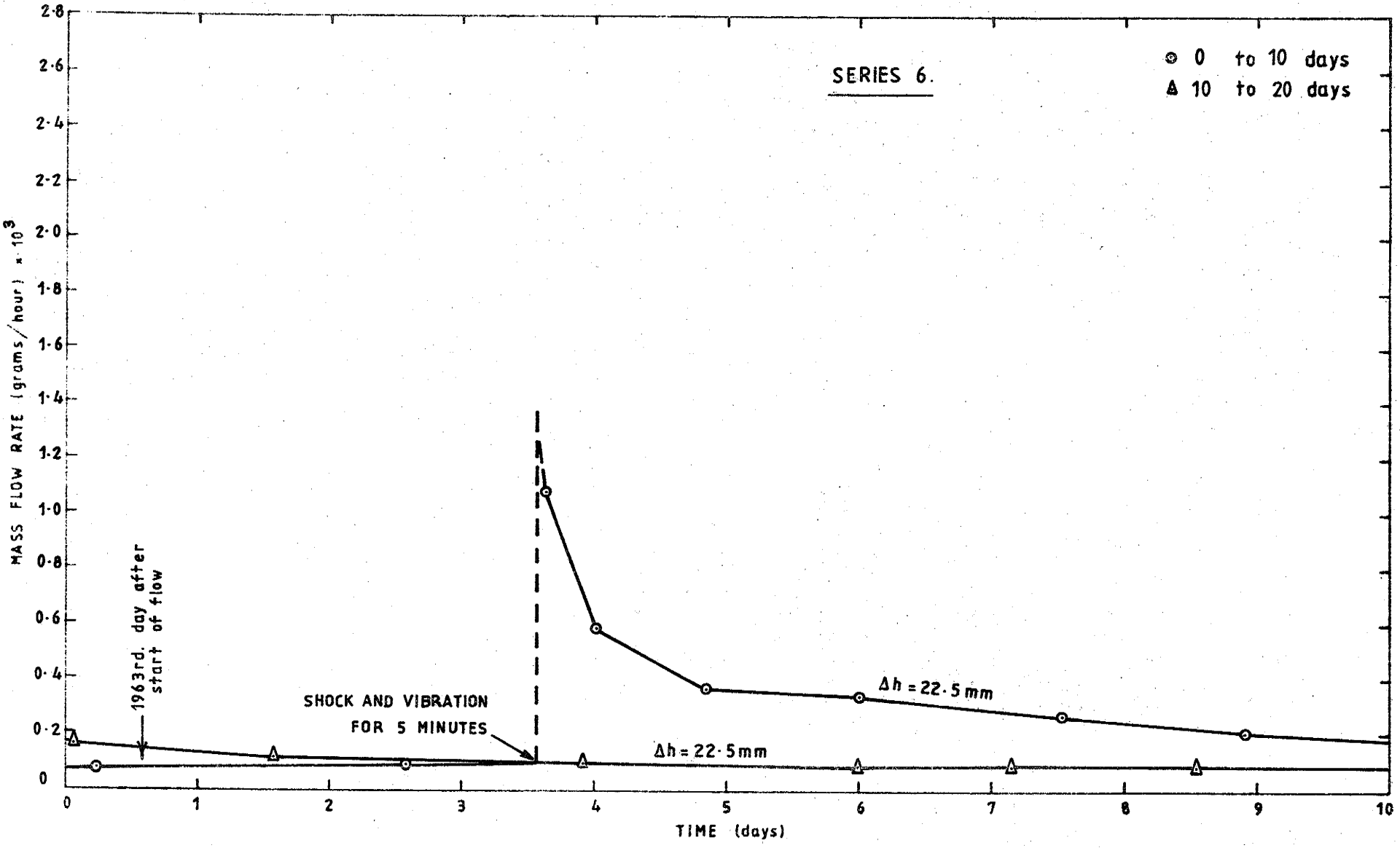

FIGURE 3.16 : FLOW HISTORY IN CAPILLARY TUBE

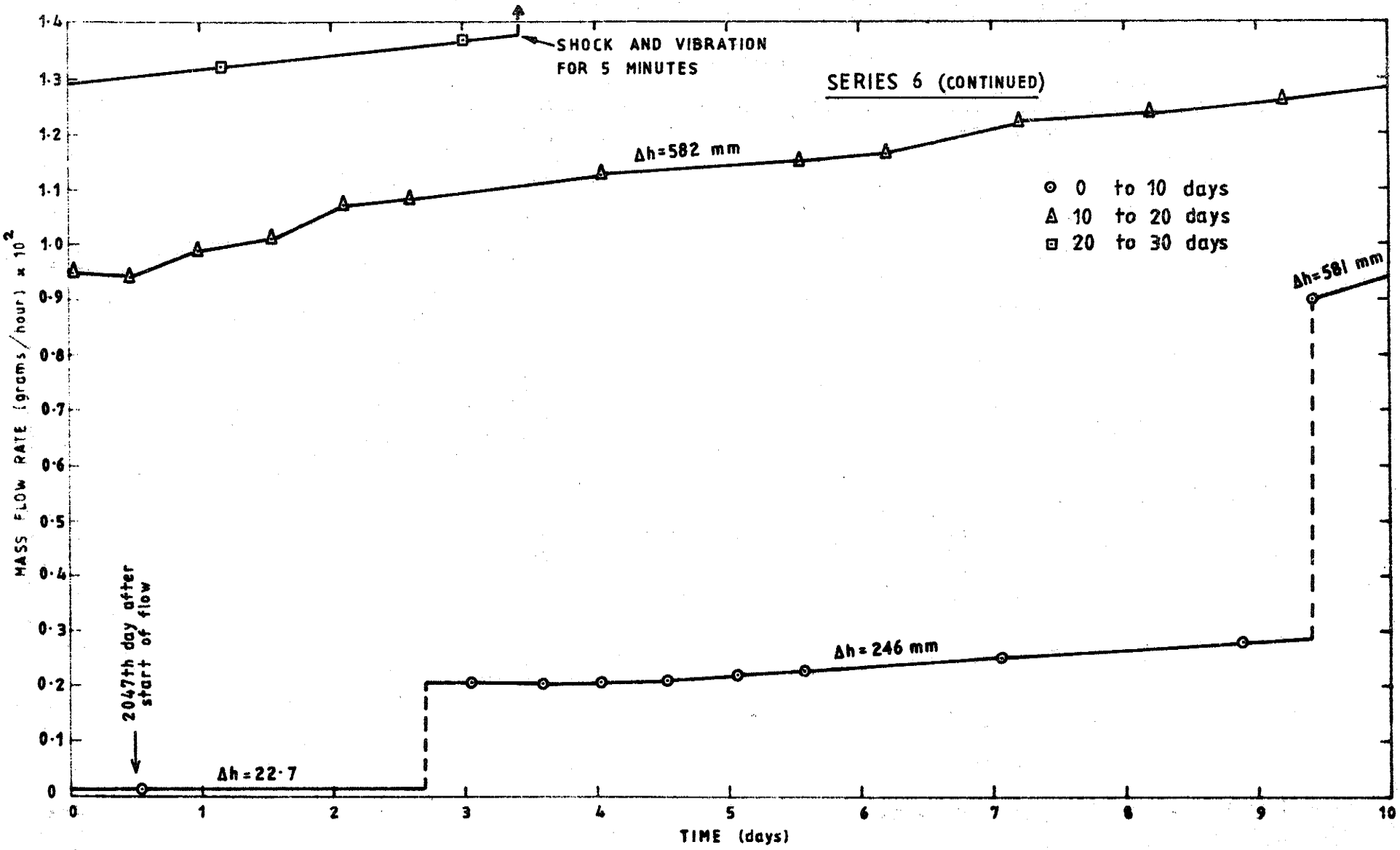

FIGURE 3.17 : FLOW HISTORY IN CAPILLARY TUBE

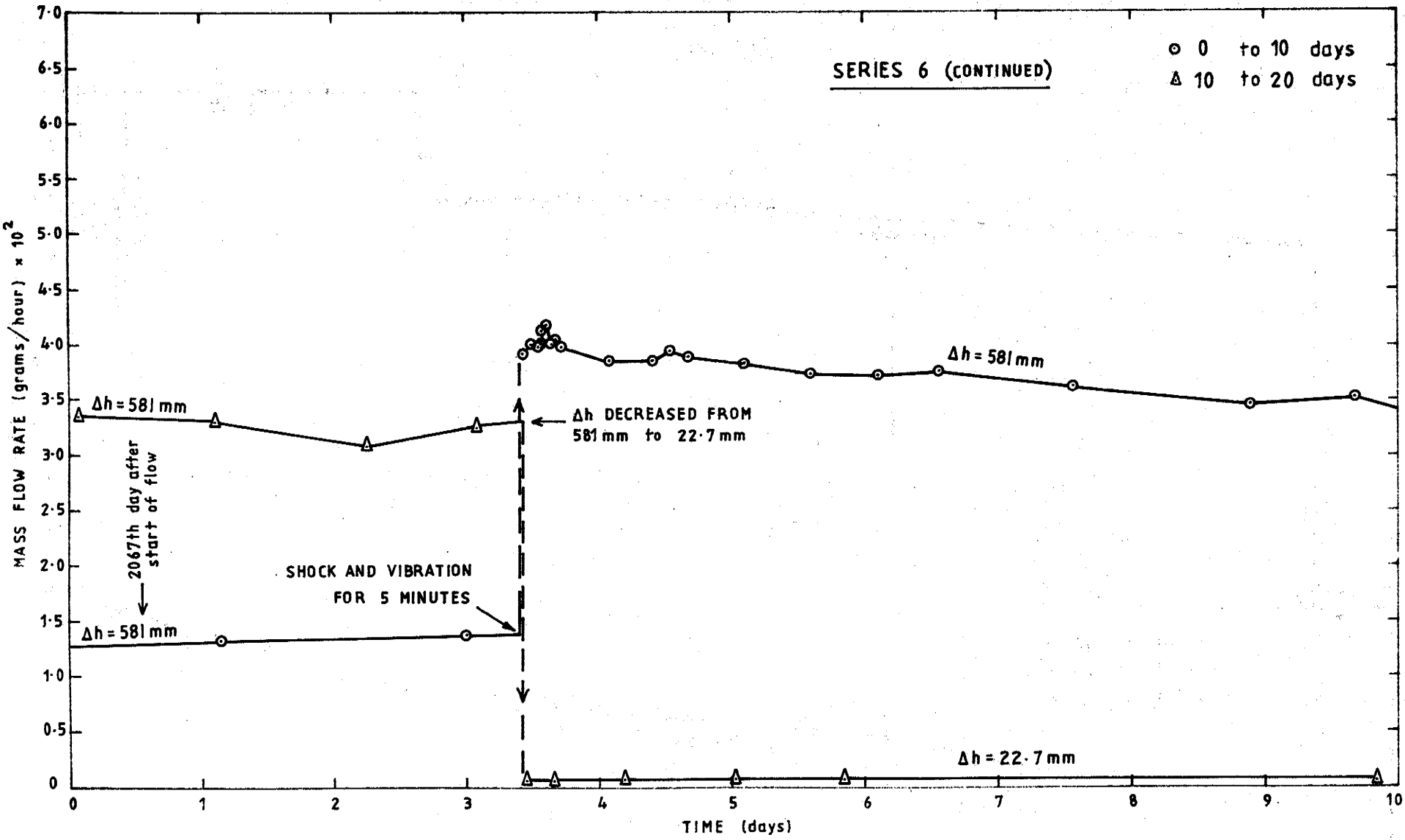

FIGURE 3.18 : FLOW HISTORY IN CAPILLARY TUBE

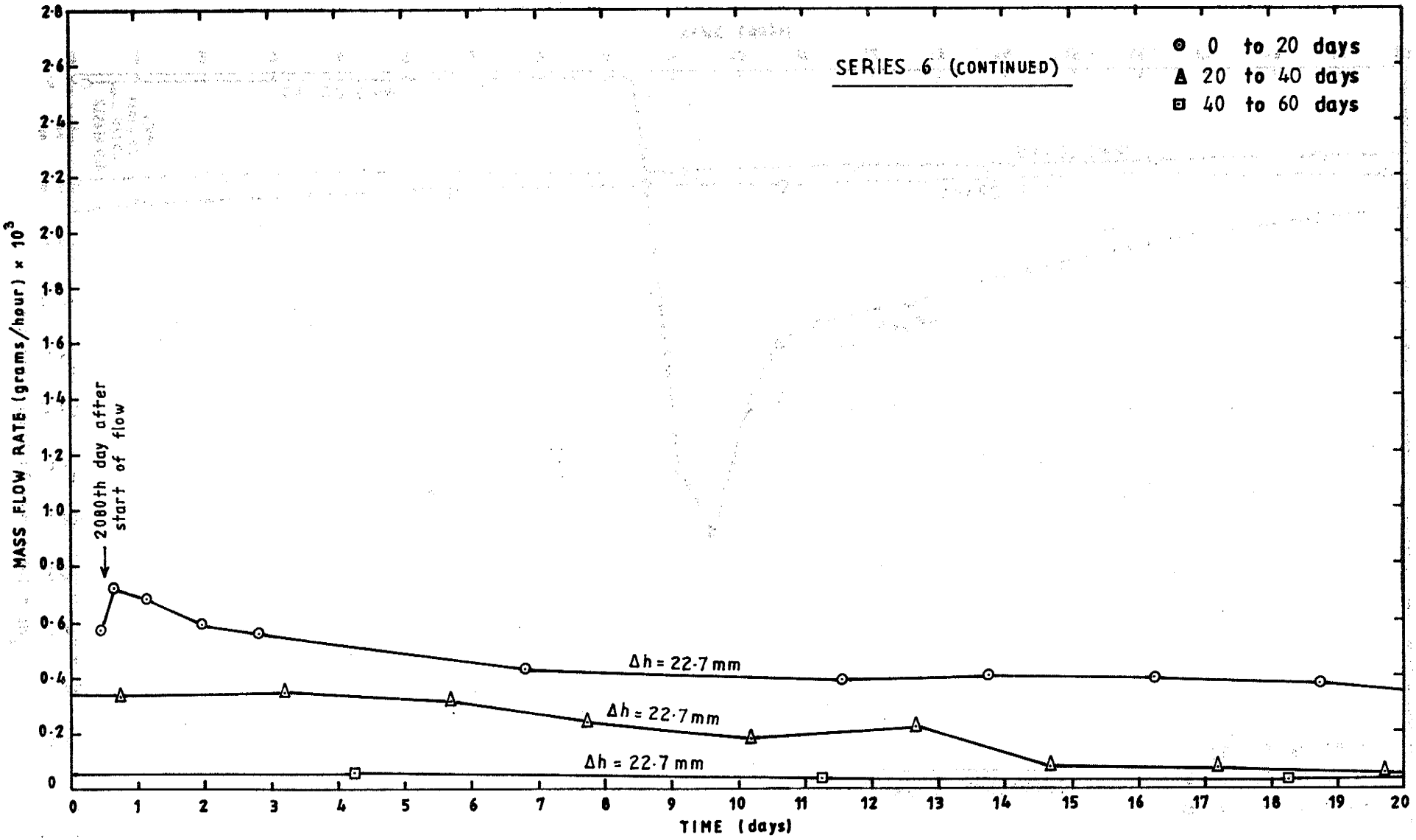

FIGURE 3.19: FLOW HISTORY IN CAPILLARY TUBE

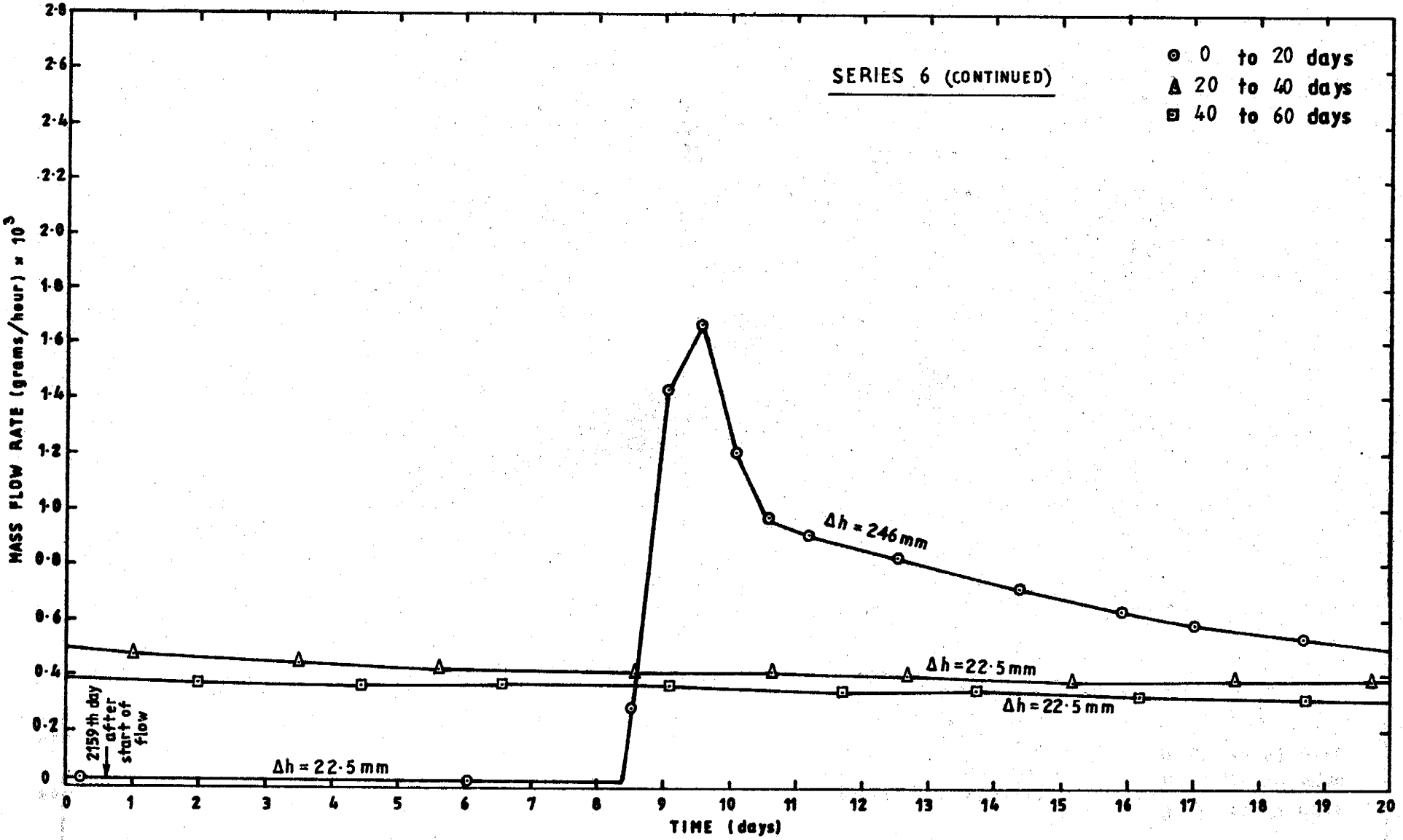

FIGURE 3.20: FLOW HISTORY IN CAPILLARY TUBE

Values claimed to be this initial shear which it was found necessary to exceed before flow occurred have been discovered since the experiments described in this chapter were started. Bondarenko (1965) reported a value between 10^{0} and 10^{-3} Pa for water while Skawinski and Lasowska (1974) reported 1.6×10^{-3} Pa and 4.8×10^{-3} Pa respectively for dilute solutions of calcium chloride and sodium chloride in water (10^{-3} gram-equivalent per litre).

During the course of the first series of flow measurements in the apparatus described in Section 3.3.1 it became apparent that the relationship between shear stress and shear rate was not as simple as first thought. Despite the care taken in setting up the experiment, reproducible results could not be obtained. It was clear that some variable was not being accounted for. Time-dependence of the flow emerged as the main reason for the scatter of the plotted points and the task then became one of seeking the cause of the somewhat erratic decrease in flow with time.

Search For Cause of Time-Dependence of Flow

The more plausible hypotheses investigated and rejected were:

(i) Growth Of Algae In The Water

This was rejected on the grounds that great care had been taken to maintain cleanliness and that the apparatus was located in a windowless basement room in which there was no light except for brief periods during weighings. The conditions were considered unlikely to allow the growth of algae.

(ii) Electro-kinetic And Magneto-hydrodynamic Effects

Since the electrically conductive stainless steel tube connected the water in the reservoirs, the chance of a build-up of electrical potential which would resist the flow of water was small. No potential difference could be detected between the ends of the tube when measurement was attempted. Flow velocities were also so low that the possibility of resistance to flow caused by the local magnetic field could be discounted.

(iii) Corrosion And Blockage Of The Tube

The annealed 316 grade stainless steel tube was chosen since it could be expected to have high corrosion resistance. To improve the surface protection it was cleaned with dilute nitric acid and then re-passivated with concentrated A.R. grade nitric acid which was drawn under vacuum through the tube.

As a check on the freedom of flow through the tube after the water flow had effectively ceased during the experiments, air was forced through the tube under pressure and an approximate check of the air flow was carried out. The air pressure was applied from a cylinder connected to a mercury manometer. Air passing through the tube was collected under water in an inverted burette. To overcome the problem of surface tension at the air-water interface at the small diameter outlet from the tube, the air was discharged into air trapped in a short length of plastic tube which was sealed at one end and inverted under the burette. The large bubbles which periodically rose into the burette were much less affected by surface tension than would have been the case with small bubbles growing at the end of the tubing held in water.

It can be shown from Equation (3.1) that the ratio of the air flow to the water flow should be:

$$\frac{Q_{air}}{Q_{water}} = \frac{(\mu\rho\Delta h)_{air}}{(\mu\rho\Delta h)_{water}} \qquad (3.2)$$

where Δh = head difference applied over the length of the tube.

For Δh_{air} = 1333 mm of mercury at 20°C

Δh_{water} = 1342 mm of water at 20°C

$$\frac{Q_{air}}{Q_{water}} = 766$$

The value of Q_{water} predicted by Equation (3.1) for Δh = 1342 mm of water and actually measured for a short period before the flow rate declined is 0.178 mL/hour. The value of Q_{air} predicted by Equation 3.2 is 136 mL/hour. This compares with a measured value of 145 mL/hour determined from an average time of 1239 seconds taken to collect 50 mL of air.

It is apparent from the results of the air flow test that the diameter of the tube had not been reduced by corrosion.

Erratic Fluctuations in Measured Flow Rates

The search for the cause of the time-dependence of the flow could not be positively identified until the source of the erratic fluctuations superimposed on the steady decline in flow rate could be located.

During the course of the early experiments the recording of apparently unimportant details of the test procedure provided clues that led to the belief that shock and vibration were causing the major erratic fluctuations in flow that could not be accounted for in any other way. Subsequent deliberate input of energy by shock confirmed the hyporeport. Other unaccounted for increases in the flow rate could have resulted from accidental disturbances generated both inside and outside the constant temperature room.

The effect of shock and vibration of the apparatus causing an increase in flow was documented by noting each occurrence of accidental and intentional disturbance and comparing the times with the times of increase in the flow rate. The experiment acted as a seismograph, recording such diverse incidents as a pneumatic pick excavating nearby, shocks caused by unloading heavy equipment onto the ground and, on one occasion, an unusually large natural earth tremor. The systematic vibration of the tube and contents described earlier was imposed to allow the effect of a much higher level of energy input to be observed.

Weighing Adjustments

Not all of the minor fluctuations in the measured flow rate could be explained by vibration so a careful assessment of errors incurred in weighing the downstream container and its contents was carried out. Initially, the humidity in the constant temperature room was not controlled so checks were carried out to determine the effects of moisture adsorption on the container being weighed. Absorption into epoxy resin glue used in the construction of the container was also checked. Repeated weight checks were carried out over lengthy periods for a sealed weighing container, "Teflon" (P.T.F.E.) plugs and a piece of

epoxy resin glue. Two precision balances were also compared at an early stage of the checks and the one which gave the best repeatability was chosen for the remainder of the weighing and flow tests.

It became apparent from the results of the weighing checks that control of the humidity of the air in the constant temperature room was required to reduce weight fluctuations. Further weighing checks were carried out when humidity control was introduced.

The results of the checks are given in Table 3.2.

Table 3.2: Weight Fluctuation Checks

Object	Balance Readings		Number of Weighings	Duration of Checks
	Mean Mass	Variation		
	(g)	(g)		(days)
Without Humidity Control				
"Teflon" (P.T.F.E.) plug	5.9734	± 0.0001	18	65
"Araldite" (epoxy glue)	3.0782	+ 0.0107 - 0.0151	18	65
With Humidity Control				
"Teflon" (P.T.F.E.) plug	88.9973	+ 0.0005 - 0.0001	31	137
All glass moulded downstream container (sealed)	99.8573	+ 0.0006 - 0.0004	24	137

Positive fluctuations of up to 0.0005 g in the indicated mass of the larger of the two "Teflon" plugs occurred during periods of abnormally low atmospheric pressure. It was clear that the low density of this plug caused significant atmospheric buoyancy force differences between the plug and the weights built into the balance. Since the downstream container and contents also had a low average density it was decided to calculate buoyancy corrections to allow indicated masses to

be adjusted.

Variations in the balance zero and other unexplained variations in the performance of the balance were allowed for by weighing a balance weight from a standardised set each time the downstream container was weighed. The weight was selected to have a mass close to that of the downstream container and contents so that the balance mechanism would be loaded to approximately the same extent for all weighings. Since the density of the weights built into the balance and that from the standardised set were approximately equal no significant differential buoyancy effects were present in the weighings of the standard weight.

A computer programme was developed to calculate the density of air in the constant temperature room from measurements of pressure and wet and dry bulb temperatures. The programme used the air density and masses and densities of the downstream container and contents to compute a mass correction. This was calculated and applied to each measured apparent mass of the container and contents after the balance correction obtained by weighing the standard weight had been applied. The programme listing and a sample set of data is given in Appendix A.

The final step taken to remove sources of weight fluctuation was to manufacture downstream containers from only glass, "Teflon" and 316 grade stainless steel with a minimum use of epoxy glue to join the lid to the base. The thin glue line was shaved and the container was baked to set the epoxy. In this way variations in the mass of water absorbed in the epoxy were kept to a minimum.

The result of all the checks and adjustments was a set of data devoid from significant variations in the derived mass of the container and contents except those caused by inflow of water from the tube.

3.4 Conclusions

It is concluded from the results of the experiments that water of the purity that can be obtained by distillation in a glass still (total dissolved salts < 1mg/L) and which is free from dissolved air behaves as a Newtonian fluid even at shear rates as low as $10^{-8}\,sec^{-1}$. This rate is below the limit of interest in groundwater flow. For shear rates as low as this to occur in an aquifer with flow channel widths in the range 0.1 to 1 mm, the piezometric surface gradient would need to be less than 1 metre per 100 kilometres.

On the other hand, distilled water containing dissolved air behaves as a thixotropic non-Newtonian fluid at shear rates as high as $10^{-4}sec^{-1}$. For this rate to occur in an aquifer with pore channels in the range 0.1 to 1 mm the piezometric surface gradient would be of the order of 1 per cent.

Reports of plasto-inelastic type relationships between shear stress and shear rate for water (Bondarenko (1968)), Skawinski and Lasowska (1974)) in capillary tubes and porous media are attributed to the presence of dissolved air in the water and the relatively short times over which the experiments were carried out. The data plotted in Figure 3.11 indicates that if a series of relatively short duration tests were carried out after the effect of dissolved air had become significant, the plot of shear stress versus shear rate would first follow the Poiseuille line and then diverge downwards to cut the line representing the limit

of measurement of shear rate at some positive shear stress. The time-dependent nature of the flow would not become evident unless tests were repeated over a long period.

Evidence from the literature reviewed indicates that other non-polar and ionic solutes are likely to affect the relationship between shear stress and shear rate for flow of groundwater. Much additional experimentation is required to examine the effects of individual solutes and combinations.

Flow of distilled water does not occur in the ground but it has been used in many laboratory experiments intended to simulate groundwater flow. The research reported in this chapter should lead to a more cautious interpretation of the results of previously published results. It also demonstrates the need for careful control and monitoring of solutes present in water used for future tests.

The next phase in the experimental study of low shear rate flow of groundwater should be a series of tests in a capillary tube and a sensitive co-axial viscometer to determine whether water containing ions in concentrations found in normal groundwater behaves as a non-Newtonian fluid at low shear rates. Both water containing and free from dissolved air should be studied. The low flow measurement techniques reported in this chapter should allow experiments in capillary tubes to proceed without further problems. A sensitive co-axial cylinder viscometer designed to extend the work has been constructed but not yet operated. It is expected that the difficulties involved in obtaining accurate measurements from this viscometer at very low shear rates will be great but not insurmountable.

4. OCCURRENCE AND IMPLICATIONS OF PRE-LINEAR NON-DARCY FLOW OF GROUNDWATER

Although there appears to be no documented evidence of groundwater measurements which prove the occurrence of pre-linear non-Darcy flow in aquifers, it is relevant to consider the type of evidence which might be sought. The practical implications of non-Darcy flow at low shear rates in the fields of groundwater hydrology and hydraulics also merits consideration.

4.1 Conditions For Occurrence

The conclusions drawn from the experimental work described in the previous chapter and from a critical appraisal of the results of earlier experiments is that water of the purity which can be produced by high quality distillation will obey Darcy's law at vanishingly small microscopic velocities if no dissolved air is present. If air is present, thixotropic non-Newtonian flow at the microscopic scale occurs at low shear rates. At the macroscopic scale this would cause lower velocities than those predicted by Darcy's law.

The effect of other solutes such as non-polar gases (e.g. hydrocarbons such as methane) and ionic materials which can dissolve in groundwater during its flow through aquifers is unknown. However, it is probable that the effect of the strong electric fields associated with ions will rotate water molecules out of orientations that can bond readily with surrounding molecules (Stillinger (1980)). This would reduce the level of hydrogen bonding which is assumed to be the cause of observed non-Newtonian flow in capillaries. The presence of dissolved non-polar gases would probably lead to enhanced molecular structure

through the "hydrophobic" effect discussed in the previous chapter.

A search for field evidence of the occurrence of pre-linear non-Darcy flow should be directed towards situations in which air or non-polar solutes are present in groundwater but the concentration of strong ions is low. An obvious starting point is where rainwater percolates to the water table through clean inert sand and then flows under the influence of small hydraulic gradients through a clean sand aquifer. The search could then be widened to aerated flows within the zone of saturation of other types of aquifer material. The unsaturated recharge zones of inert sands would also be a likely site for non-Newtonian water viscosity to exert its effect. Unfortunately the difficulty of separating bulk water effects and strong surface effects at the water-air and water-solid boundaries might prove insurmountable in this case. The surface effects might also completely out-weigh any non-Newtonian characteristics of the bulk water.

The problem of independently measuring a range of flow rates and hydraulic gradients in aquifers with low hydraulic gradients is daunting. Groundwater flow rates can be measured accurately only in the case of artificially induced flows near water extraction or injection facilities in near-stationary groundwater bodies. Except in the case of an abnormally homogeneous aquifer with a precisely known level or gently sloping piezometric surface the macroscopic velocity and gradient would not even then be known accurately enough to distinguish between Darcy and non-Darcy flow in regions of low shear.

Because of the difficulties described it is clear that more laboratory work in viscometers and permeameters designed for low shear rate measurements is desirable before even controlled experiments at ideal

field sites should be contemplated. As reported in the previous chapter, the construction of a co-axial viscometer for this purpose has been completed but no further experiments have yet been set in motion. A long permeameter divided into sections connected in series has also been completed. Its use awaits the results of further capillary tube experiments and viscometer studies with water containing ionic solutes.

4.2 Naturally Occurring Shear Rates

The range of naturally occurring shear rates depends on the range of hydraulic gradients and flow channel cross-sections.

Gradients may range from infinite for vertical cascades through coarse broken rock or vertical fissures above the water table down to zero for stationary bodies of water.

Factors which may have a significant effect on local macroscopic gradients or microscopic gradients are thermal effects and earth movements. The former may induce pressure gradients through density differences. Because of the thermally insulating nature of most of the earth's crust, thermally induced hydraulic gradients will be relatively constant except in geothermally active locations.

On the other hand, earth movements caused by atmospheric pressure variations, earth tremors and earth and ocean tides may cause relatively rapid pressure changes and flow adjustments in aquifers. The phenomenon of groundwater movement in boreholes as a result of atmospheric pressure variations is well known. An early account of observed fluctuations was presented by Nilssen (1966). A recent paper by Van der Kamp and Gale (1983) has analysed the effect of earth tides in aquifers with

deformable grains. It also provides an up-to-date list of relevant references.

The vibrations and shear rates associated with flows induced by these naturally occurring pressure fluctuations may maintain the fluidity of groundwater even though the average shear rate may be very low. It is of interest to note that an earth tremor that occurred in Sydney on 9th March, 1973 while the experiments described in the previous chapter were in progress caused a 20% increase in flow rate in the capillary tube at a time when the flow rate had been gradually decreasing.

The magnitude of the influence that can be exerted by barometric pressure effects and earth tides compared with the effects of pumping can be seen from Figures 4.1 and 4.2. The data plotted has been extracted from the records of water levels in an aquifer being pump tested during a mine de-watering investigation discussed in Chapter 9. It can be seen that the naturally induced fluctuations are large in comparison with the rate of change of drawdown caused by pumping.

It is evident that short period vibrations and longer term earth movements could have pronounced influences on both the molecular structure and viscosity of groundwater if the water exhibits thixotropic behaviour as did the water flowing in the capillary tube tests previously described. If the effect were insufficient to maintain the viscosity at the normal value found at higher shear rates it would be a complicating factor. If, however, it were suffficient to prevent non-Newtonian flow from developing in aquifers it would eliminate the need to consider pre-linear non-Darcy flow. Clearly, further research is required into this matter.

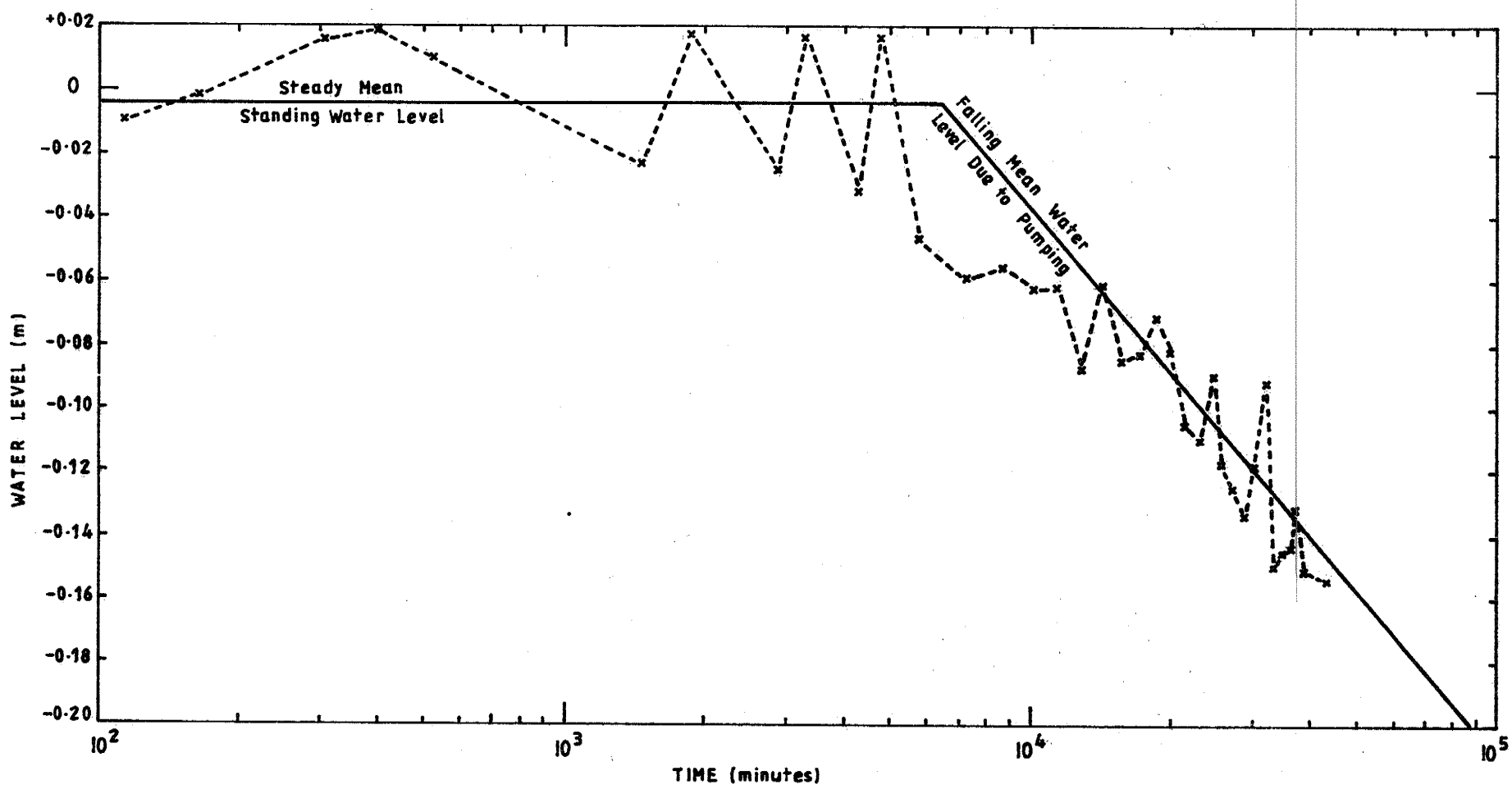

FIGURE 4·1: NATURALLY OCCURRING FLUCTUATIONS IN THE PIEZOMETRIC SURFACE IN A DOLOMITE AQUIFER

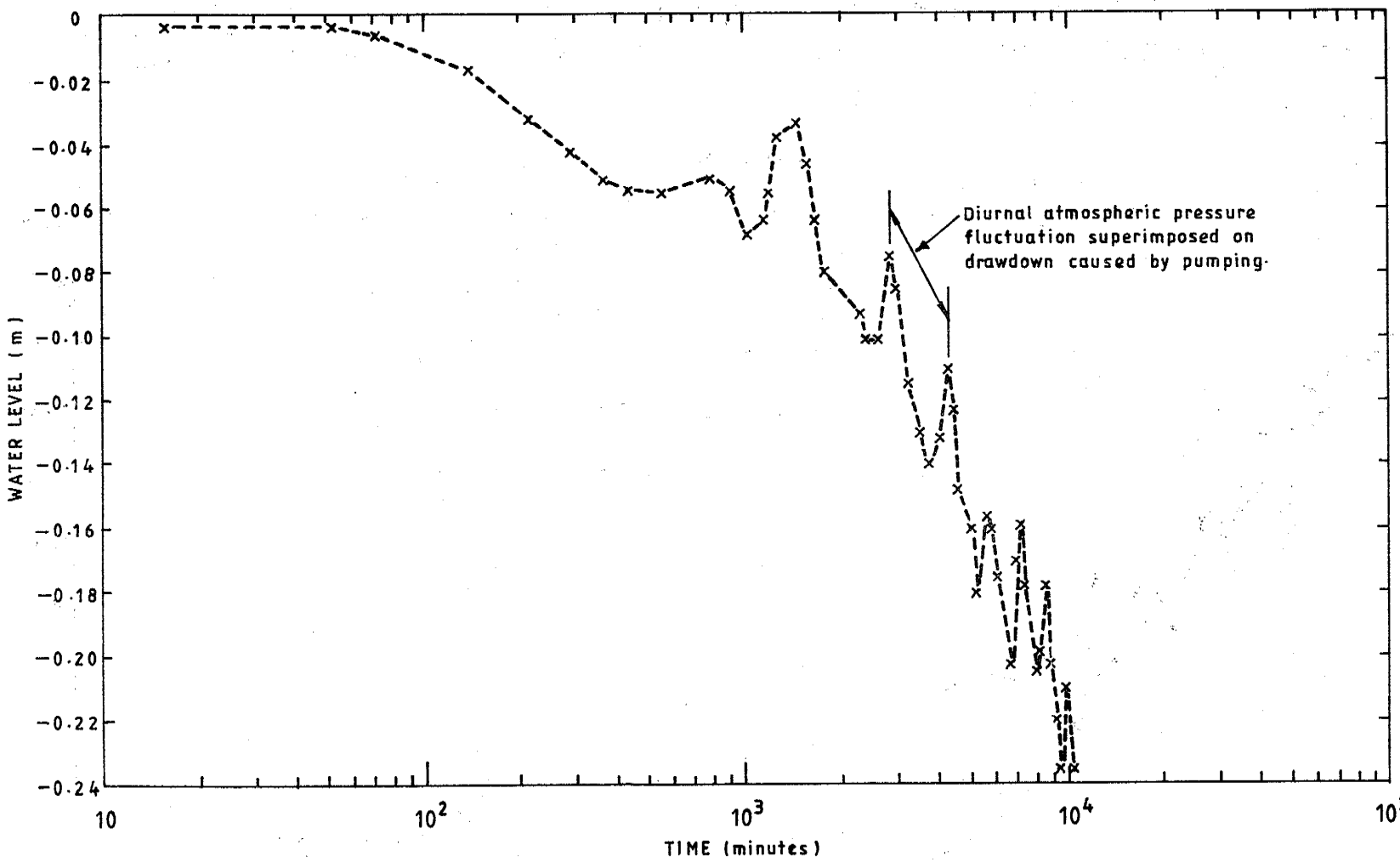

FIGURE 4·2: NATURALLY OCCURING FLUCTUATIONS IN THE PIEZOMETRIC SURFACE IN A FRACTURED CONSOLIDATED SEDIMENTARY AQUIFER

4.3 Implications in Groundwater Hydrology And Hydraulics

In a three sentence discussion of a lower limit to the validity of Darcy's law, Bear (1979) dismissed the occurrence of pre-linear non-Darcy flow as "of no significance in aquifer flows of practical interests". This statement sets a low value on the importance of understanding the relationships governing the movement of groundwater under low hydraulic gradients through extensive aquifers. In large groundwater basins such as Australia's Great Artesian Basin, water may travel great distances under relatively small driving heads. The large cross-sectional areas of flow allow the movement of economically important quantities of water, even though the velocities may be of the order of metres per year or less. If non-Newtonian flow behaviour reduced velocities below those predicted by Darcy's law to the extent observed in some laboratory experiments, large errors could occur in estimated flows.

The use of transmissivities determined from piezometric data obtained at high flow rates such as those induced by pumping or tapping artesian aquifers could lead to gross over-estimates of flow rates induced by low hydraulic gradients. Transmissivity values determined from pumping or artesian pressure release test analyses assume that Darcy's law is valid. These transmissivity values are then frequently divided by the aquifer thickness to yield values of the coefficient of permeability. Use of these permeability values to calculate flow rates in parts of the aquifer where low hydraulic gradients exist will not be valid if a non-linear relationship between shear stress and shear rate causes the Darcy K value to vary with flow rate. Some of the difficulty found in calibrating regional numerical groundwater flow models by inserting K values obtained from pumping tests could be caused by pre-

linear non-Darcy flow effects. A critical evaluation of these problems could be another source of evidence for or against the occurrence of deviations from Darcy's law for flow through aquifers at low shear rates.

5. FIELD EQUATIONS FOR GROUNDWATER FLOW

Groundwater flow is governed by continuity, energy and boundary conditions. Solutions of groundwater flow problems can be obtained by solving a general field equation with pertinent boundary conditions to yield values of velocity V and head h at various points in the flow field. The field equation is obtained by combining a continuity equation, which expresses the law of conservation of matter, and an energy dissipation equation which relates head loss to flow rate.

Specific equations relating head and velocity have been derived for some groundwater flows with relatively simple boundary conditions. Approximate equations have also been developed for more complex boundary conditions. However, the development of numerical techniques and digital computers able to provide more accurate solutions from the general field equation has made the use of approximate equations less necessary.

In the following sections a review is given of equations which are available for solving non-Darcy flow problems. A brief outline of equations and methods used to solve Darcy flow problems is given first to allow comparisons to be drawn.

5.1 Equations for Darcy Flow

The field equation which applies for the general case of unsteady three-dimensional Darcy flow in a system of cartesian co-ordinates (x_1, x_2, x_3) is a differential equation of second order. It may be written in tensor notation (Huyakorn (1973), Cox (1977)) as:

$$K \frac{\partial^2 h}{\partial x_i \partial x_i} = S_s \frac{\partial h}{\partial t} \qquad (5.1)$$

Where S_s, the specific storage of the aquifer material, is the volume of water released from storage per unit volume of aquifer material per unit decrease in pressure head.

No general solution to Equation (5.1) is available. There are, however, particular analytical solutions for some relatively simple flow configurations of interest in groundwater extraction and drainage work. Such solutions are listed in standard texts (De Wiest (1965), Walton (1971), Bouwer (1978) and Bear (1979)). They include the well known Thiem equation for steady flow to a fully penetrating and screened small diameter borehole in a homogeneous, confined aquifer of infinite extent.

$$Q = \frac{2\pi Km\ (h_o - h)}{\ell n\ (r/r_o)} \qquad (5.2)$$

Where K is the hydraulic conductivity from Darcy's equation. The other symbols are defined in Figure 5.1(a).

The Theis equation for unsteady flow to a fully penetrating and screened small diameter borehole in a homogeneous, confined aquifer of infinite extent:

$$s = h_o - h = \frac{Q}{4\pi mK} \int_u^\infty \frac{e^{-u}}{u}\, du \qquad (5.3)$$

$$\text{where } u = \frac{r^2 S_s}{4mKt}$$

is also a specific solution of Equation (5.1).

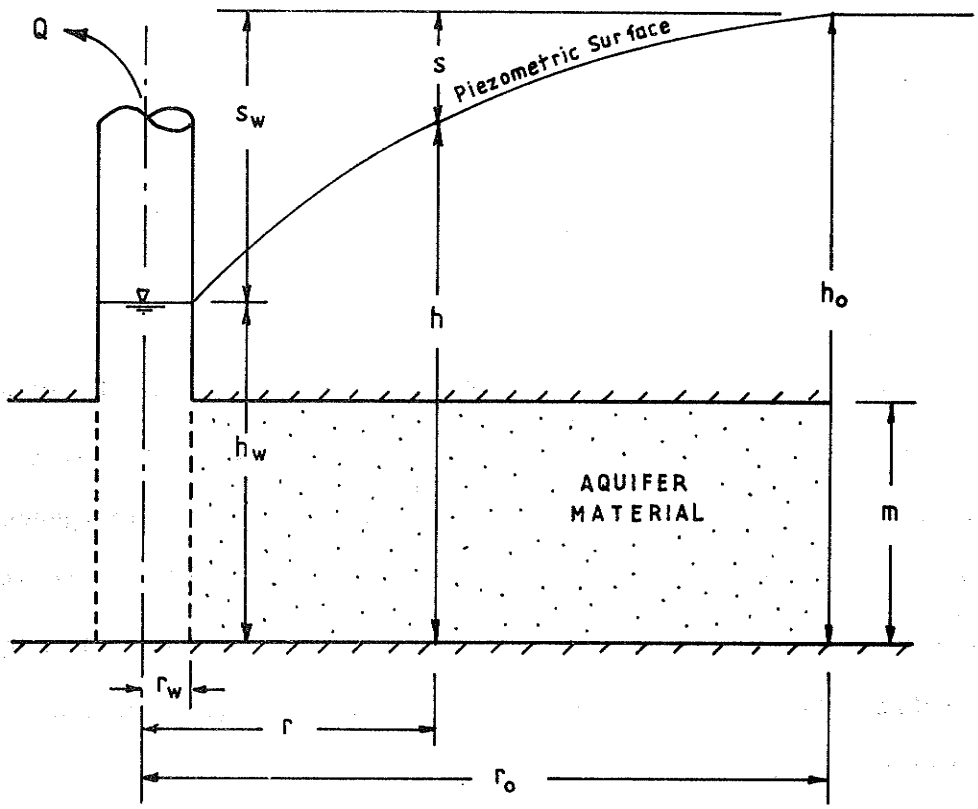

FIGURE 5.1(a): FLOW TO A FULLY SCREENED BOREHOLE IN A CONFINED AQUIFER

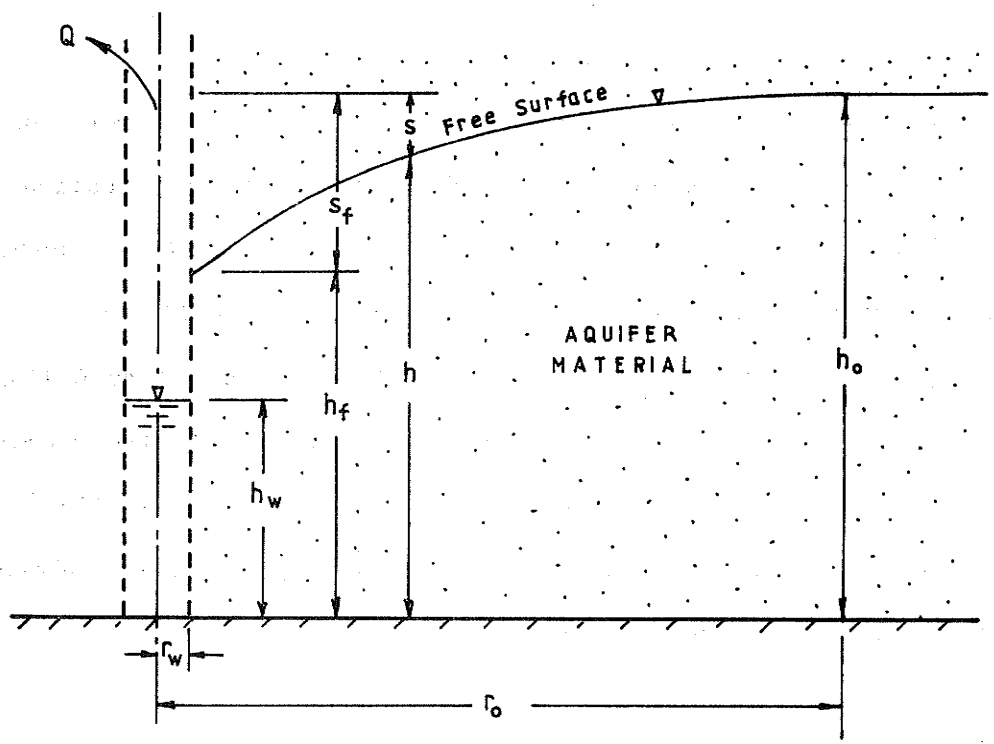

FIGURE 5.1 (b): FLOW TO A FULLY SCREENED BOREHOLE IN AN UNCONFINED AQUIFER

The Dupuit equation:

$$Q = \frac{\pi K (h_o^2 - h^2)}{\ell n (r_o/r)} \qquad (5.4)$$

for steady flow to a fully screened small diameter borehole in an unconfined aquifer of infinite extent, as shown in Figure 5.1(b), is an approximate solution of Equation (5.1). It neglects convergence of flow in a vertical plane and does not satisfactorily predict the water surface profile for $r < 1.5\ h_o$ (Boulton (1951)). However, when r_w and h_w are substituted for r and h, the equation does give an exact solution for the inflow Q.

Equations (5.2) to (5.4) are quoted because they are referred to in discussion in later chapters. Other approximate solutions are to be found in the texts listed.

More complex problems can be solved by finite difference or finite element methods. A recent text which describes the application of finite difference techniques to groundwater flow is that by Rushton and Redshaw (1979). The text by Huyakorn and Pinder (1983) and the conference series on Finite Elements in Fluids (Vol. 1 edited by Gallagher et al (1975) et seq.) contain information specific to finite elements and groundwater flow. Application by Huyakorn (1973) and Cox (1977) of the finite element method to the solution of axi-symmetric groundwater flow problems is of particular relevance.

5.2 Equations for Post-Linear Regime Non-Darcy Flow

Volker (1969) derived field equations applicable to two-dimensional flow fields using both the Forchheimer equation (Equation (2.2)) and the exponential equation $i = \frac{dh}{d\ell} = cV^n$ (Equation (2.1)) to express the rate of energy dissipation with velocity. Using tensor notation to abbreviate their equation, Huyakorn (1973) and Cox (1977) showed that if the Forchheimer equation is used, the equation for three-dimensional non-Darcy flow can be written as:

$$\frac{\partial}{\partial x_i} \left(C \frac{\partial h}{\partial x_i}\right) = S_s \frac{\partial h}{\partial t} \tag{5.5}$$

where $C = \dfrac{1}{\left(\frac{a}{2} + \sqrt{\left(\frac{a^2}{4} + b\left|\frac{\partial h}{\partial s}\right|\right)}\right)}$

Solution of Equation (5.5) for various cases of axi-symmetric flow of groundwater towards boreholes and wells has been investigated by Huyakorn (1973) and Cox (1977).

The only analytical solution available for post-linear regime non-Darcy flow is that derived by Engelund (1953) for flow to a fully penetrating and screened borehole in a confined aquifer with a non-Darcy flow region near the hole. If the Forchheimer equation is applied over the entire flow field, the equation for the piezometric surface profile takes the form:

$$s = h_o - h = \frac{aQ}{2\pi m} \ln\left(\frac{r_o}{r}\right) + b\left(\frac{Q}{2\pi m}\right)^2 \left(\frac{1}{r} - \frac{1}{r_o}\right) \tag{5.6}$$

The symbols are defined in Figure 5.1(a).

It was demonstrated in Chapter 2 that the fit of one Forchheimer curve with a single pair of a and b coefficients over the linear (Darcy) and post-linear flow regimes is sufficiently accurate for predictions of post-linear regime non-Darcy effects in groundwater flow. The alternative procedure of adopting a non-Darcy flow zone near any point of flow concentration and a Darcy flow zone beyond this requires the introduction of an additional variable, a critical velocity or Reynolds number, to define the upper limit of Darcy flow. This complicates the production of dimensionless discharge and drawdown curves without adding significantly to the accuracy of predicted discharges and water levels for real flow conditions. There is normally insufficient field data on aquifer geometry and hydraulic characteristics to justify the separate regime approach.

In practice an empirical approach is often adopted to allow for head losses attributable to non-Darcy flow. If the Darcy permeability coefficient K is taken to be equal to 1/a, where a is the coefficient of the linear term in the Forchheimer equation, the bV term in the Forchheimer equation causes head losses additional to those which would occur if the flow obeyed Darcy's law over the entire flow field. In the absence of field data and analytical methods which allow the distribution of these losses to be determined, the total additional loss is lumped together with the entry loss and considered to occur at the inlet face. It is assumed to be proportional to Q^2. This procedure has proved acceptable for the interpretation of step-discharge pumping tests on many boreholes. It is easily demonstrated that for a limited range of conditions the equation used to analyse such tests:

$$s_w = AQ + BQ^2 \qquad (5.7)$$

where $s_w = h_o - h_w$ is the drawdown at the borehole and A and B are constants, is in accord with the analytical solution for flow to a fully penetrating and screened borehole in a confined aquifer with a non-Darcy flow zone adjacent to the borehole.

However, it has not been demonstrated that the equation is valid for confined or unconfined non-Darcy flow to a partially penetrating borehole, well or pit. Nor is it possible by using the method described to separate the non-linear loss obtained from step-discharge test results into the entry (screen) loss and non-Darcy loss in the aquifer material.

The numerical solution procedure described in Chapter 6 allows the validity of Equation (5.7) to be checked for partially and fully penetrating circular pits if inflow rates are calculated for a range of pit water levels.

Comparisons between measured head losses near boreholes and wells and those predicted from the numerical solutions should also provide an indication of the relative magnitudes of entry losses through screens, gravel packs and zones affected by drilling.

5.3 Effect Of Viscosity Of Water On Field Equations For Darcy And Post-Linear Regime Non-Darcy Flows

The linear permeability coefficients K and a and the non-linear coefficient b include the effect of viscosity. A separate allowance could be made only by using an equation in terms of friction factor and

Reynolds number for the relationship between macroscopic velocity and hydraulic gradient. In Chapter 2 it was indicated that it is impractical to obtain a general relationship of this type. For this reason the more specific Darcy and Forchheimer equations are used in the development of the field equations. Since groundwater temperatures in a given aquifer cover a relatively small range and permeability coefficients are derived from field measurements of flow in the aquifer, viscosity variations can normally be neglected in comparison with other uncertainties related to measurement accuracy, boundaries and homogeneity. For deep artesian groundwater or water in geothermal areas high temperatures may occur. It may be necessary to adjust linear and non-linear permeability coefficients for temperature when comparisons are being made with data from cooler aquifers since the kinematic viscosity of water at $20^{o}C$ is approximately twice that at $60^{o}C$ and three times that at $90^{o}C$.

5.4 Equations for Pre-Linear Regime Non-Darcy Flow

The currently available data relating to pre-linear non-Darcy flow through porous media is insufficient to allow more than hypothetical discussion of equations which might serve to predict flow rates or hydraulic gradients below the limit of validity of Darcy's law.

5.4.1 Field Equation for Exponential Flow Relationship

If the equation $i = cV^{n}$ (Equation (2.1)) were valid for the pre-linear regime, as suggested by the data of Figure 1.1, a field equation equivalent to that developed by Volker (1969) for steady two-dimensional flow would be applicable. Values of the exponent n would be less than one.

Using tensor notation as in Equations (5.1) and (5.5), the relevant equation may be developed in the following manner.

For three-dimensional flow in an isotropic aquifer, the exponential energy dissipation equation, given in one-dimensional form in Equation (2.1), may be written:

$$\frac{\partial h}{\partial x_i} = -c \mid V \mid^{n-1} v_i \tag{5.8}$$

The continuity equation is:

$$\frac{\partial v_i}{\partial x_i} = -S_s \frac{\partial h}{\partial t} \tag{5.9}$$

Combination of Equations (5.8) and (5.9) gives the field equation:

$$\frac{\partial}{\partial x_i} \left(\frac{\mid V \mid^{1-n}}{c} \frac{\partial h}{\partial x_i} \right) = S_s \frac{\partial h}{\partial t} \tag{5.10}$$

Elimination of the velocity terms from Equations (5.8) and (5.9) allows the formulation of a field equation in terms of head, geometric variables and aquifer properties c and n.

Contracting subscript i, Equation (5.8) gives:

$$\frac{\partial h}{\partial x_i} \frac{\partial h}{\partial x_i} = (c \mid V \mid^{n-1})^2 v_i v_i \tag{5.11}$$

The absolute hydraulic gradient is defined as:

$$\left|\frac{dh}{d\ell}\right| = \sqrt{\left(\frac{\partial h}{\partial x_i}\frac{\partial h}{\partial x_i}\right)} \tag{5.12}$$

Then $$\frac{\partial h}{\partial x_i}\frac{\partial h}{\partial x_i} = \left|\frac{\partial h}{\partial \ell}\right|^2 \tag{5.13}$$

and $$v_i v_i = |V|^2 \tag{5.14}$$

Equation (5.11) can be re-written as:

$$\left|\frac{\partial h}{\partial \ell}\right|^2 = (c\,|V|^{n-1})^2\,|V|^2 \tag{5.15}$$

Then $$|V| = \left(\frac{\left|\frac{\partial h}{\partial \ell}\right|}{c}\right)^{1/n} \tag{5.16}$$

From Equation (5.8)

$$v_i = -\frac{\partial h}{\partial x_i}\frac{|V|^{1-n}}{c} \tag{5.17}$$

Substituting for $|V|$ from Equation (5.16)

$$v_i = -\frac{\partial h}{\partial x_i}\frac{\left|\frac{\partial h}{\partial \ell}\right|^{\frac{1}{n}-1}}{c^{1+\frac{1}{n}}} \tag{5.18}$$

Combining this form of the energy dissipation equation and the continuity equation, Equation (5.9) gives the field equation for an exponential relationship:

$$\frac{\partial}{\partial x_i}\left(\frac{\partial h}{\partial x_i}\frac{\left|\frac{\partial h}{\partial \ell}\right|^{\frac{1}{n}-1}}{c^{1/n}}\right) = S_s\frac{\partial h}{\partial t} \tag{5.19}$$

5.4.2 Field Equation for Time-Dependent Flow Relationship

The experiments described in Chapter 3 cast some doubt on the validity of the very low flow rate results plotted in Figure 1.1. At the time the permeameter experiments were carried out it was noted that the very low flow rates being measured tended to decrease with time. The effect was attributed to accumulation of microscopic particles in the control valve. Since the measurements were not considered to be particularly important, as the main interest lay in the transition from linear to post-linear flow, the low flow measurements were averaged over the period necessary to collect a measurable quantity of water. No attempt was made to further investigate the possibility of time dependence of the flow or the effect of the dissolved air or solids content of the water.

If a time-dependent relationship does in fact apply to groundwater flowing under low hydraulic gradients in the zone of aeration, the relationship between flow rate and velocity gradient will be more complex than Equation (2.1). It might be possible to allow for a time-dependent relationship between shear stress and shear rate by making c and n functions of time. Alternatively, other more complex methods developed by rheologists for dealing with materials which have time-dependent relationships between shear-stress and shear rate may be required.

If ionic solutes in groundwater or continual naturally induced pressure fluctuations cause groundwater to behave as a Newtonian fluid down to vanishingly small hydraulic gradients, Equation 5.1 will be valid to the lowest gradients of interest in groundwater studies.

The subject requires further research when more data on the shear stress-shear rate relationship for water at low shear rates becomes available.

5.4.3 Effect Of Density Change On Field Equation

The storage coefficient S_s includes the effect of change of fluid density with pressure. A change in molecular structure of water containing solutes which give rise to non-Newtonian flow must affect the density as well as the viscosity. Change in density could have had some effect on the variation of measured mass flow rates in the capillary tube discussed in Chapter 3. The effect cannot be great or it would have been observed in the many density tests which have been reported for water and solutions. The only reference found to a slight change in density with time, attributed to change of the water structure with resting but possibly caused by the entry of air into solution and consequent change in the molecular structure, is that by Klassen (1969).

6. NUMERICAL INVESTIGATION OF UNCONFINED NON-DARCY FLOW TO LARGE DIAMETER WELLS AND OPEN PITS

No analytical solution of the general case of unconfined Darcy flow to large diameter wells and open pits has been published to date. Nor is this likely in the near future because of the difficulty of dealing with the partial penetration and phreatic surface boundary conditions. The problem becomes even more difficult for non-Darcy flow because of the non-linearity of the field equation.

Papadopulos (1967), Papadopulos and Cooper (1967) and Boulton and Streltsova (1975) have published approximate solutions for Darcy flow to large diameter wells. Cox (1977) used the finite element method to produce the limited amount of data pertinent to non-Darcy flow near bottom entry wells published by Dudgeon and Cox (1977) in a book of design data. Rushton and Holt (1981), Herbert and Kitching (1982) and Rushton and Singh (1983) have used the finite difference method to assist the analysis of pumping test data for wells with significant storage volumes.

The complexity of the field equation for post-linear non-Darcy flow and of the boundary conditions for partially penetrating wells makes the development of even approximate analytical solutions most unlikely. Numerical solution of the equation offers the only practical means of producing a generally applicable set of solutions for flow to large diameter wells and excavations such as open-cut mines. The development of such a set of solutions for both Darcy and non-Darcy flow is described in this chapter. The Darcy flow solutions are needed to provide a datum from which non-Darcy effects can be measured. They are also useful in their own right because they have not previously been

available to solve problems of wholly Darcy flow.

An investigation of the practical range of the pertinent variables and the solution techniques required to handle the extreme values was carried out prior to the computation of a full set of dimensionless relationships. These cover the range of diameter, depth of penetration and aquifer properties likely to be encountered in practice. A complete set of dimensionless graphs which allow solutions for unconfined flow to wells and pits to be obtained without recourse to a computer are given in Water Research Laboratory Report No. 163.

A series of large scale laboratory experiments carried out to verify the numerical work is described in Chapter 7.

Application of the results of the numerical study in mine dewatering and groundwater supply investigations is described in Chapters 8 and 9 to demonstrate the value of the solutions in groundwater engineering practice.

6.1 Dimensional Analysis

Consider the general case of flow to a circular open pit in an unconfined aquifer. The geometric variables involved are shown in Figure 6.1.

For any given entry condition (e.g. full penetration, side entry; partial penetration, bottom and side entry; partial penetration, bottom entry) and the pit de-watered, the following relationships will apply if the Forchheimer equation is used to relate the macroscopic flow velocity to the hydraulic gradient.

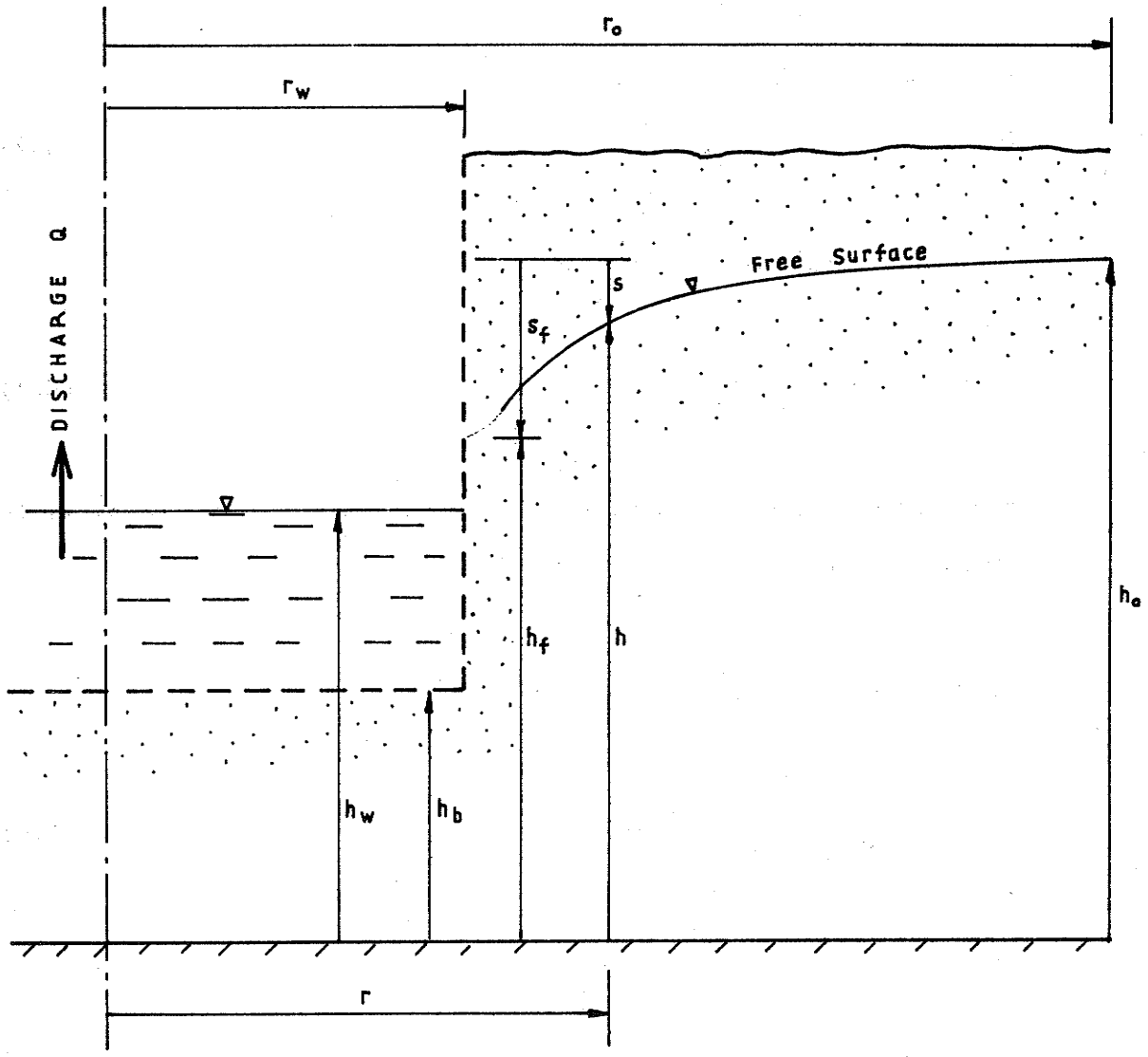

FIGURE 6·1: UNCONFINED FLOW TO OPEN PIT

Height h of the free surface at any radius r is:

$$h = \phi_1 (r, h_o, r_o, r_w, h_b, b, a) \quad (6.1)$$

Discharge Q into the pit is given by:

$$Q = \phi_2 (h_o, r_o, r_w, h_b, b, a) \quad (6.2)$$

Volume $\overline{V}$ in the de-watered drawdown cone is given by:

$$\overline{V} = \phi_3 (h_o, r_o, r_w, h_b, b, a) \quad (6.3)$$

Applying dimensional analysis and using h_o and a as repeating variables when applying Buckingham's π theorem,

From Equation (6.1)

$$\phi_{1a} \left(\frac{h_o}{h}, \frac{h_o}{r}, \frac{h_o}{r_o}, \frac{h_o}{r_w}, \frac{h_o}{h_b}, \frac{a^2}{b}\right) = 0 \quad (6.4)$$

As a special case, for $h = h_f$ and $r = r_w$,

$$\frac{h_o}{h} = \frac{h_o}{h_f} \text{ and } \frac{h_o}{r} = \frac{h_o}{r_w}$$

$$\therefore \phi_{1b} \left(\frac{h_o}{h_f}, \frac{h_o}{r_o}, \frac{h_o}{r_w}, \frac{h_o}{h_b}, \frac{a^2}{b}\right) = 0 \quad (6.5)$$

From Equation (6.2)

$$\phi 2a \left(\frac{h_o^2}{aQ}, \frac{h_o}{r_o}, \frac{h_o}{r_w}, \frac{h_o}{h_b}, \frac{a^2}{b}\right) = 0 \quad (6.6)$$

From Equation (6.3)

$$\phi 3a \left(\frac{h_o^3}{V}, \frac{h_o}{r_o}, \frac{h_o}{r_w}, \frac{h_o}{h_b}, \frac{a^2}{b}\right) = 0 \qquad (6.7)$$

Re-arranging Equations (6.4) to (6.7) into a form more suitable for practical application:

$$\frac{h}{h_o} = \phi_{1c} \left(\frac{r}{h_o}, \frac{r_o}{h_o}, \frac{r_w}{h_o}, \frac{h_b}{h_o}, \frac{b}{a^2}\right) \qquad (6.8)$$

$$\frac{h_f}{h_o} = \phi_{1d} \left(\frac{r_o}{h_o}, \frac{r_w}{h_o}, \frac{h_b}{h_o}, \frac{b}{a^2}\right) \qquad (6.9)$$

$$\frac{aQ}{h_o^2} = \phi_{2b} \left(\frac{r_o}{h_o}, \frac{r_w}{h_o}, \frac{h_b}{h_o}, \frac{b}{a^2}\right) \qquad (6.10)$$

$$\frac{\overline{V}}{h_o^3} = \phi_{3b} \left(\frac{r_o}{h_o}, \frac{r_w}{h_o}, \frac{h_b}{h_o}, \frac{b}{a^2}\right) \qquad (6.11)$$

Various alternative arrangements of Equation (6.7) may be obtained by combination of terms within the function brackets.

Two such arrangements are:

$$\phi_{3c} \left(\frac{\overline{V}}{h_o^3} \times \frac{h_o^2}{r_o^2}, \frac{r_o}{h_o}, \frac{r_w}{h_o}, \frac{h_b}{h_o}, \frac{b}{a^2}\right) = 0 \qquad (6.12)$$

$$\text{and} \quad \phi_{3d}\left(\frac{\overline{V}}{h_o^3} \times \left(\frac{1}{\frac{r_o^2}{h_o^2} - \frac{r_w^2}{h_o^2}}\right), \frac{r_o}{h_o}, \frac{r_w}{h_o}, \frac{h_b}{h_o}, \frac{b}{a^2}\right) = 0 \qquad (6.13)$$

Simplifying and introducing a constant multiplier gives:

$$\frac{\overline{V}}{\pi h_o r_o^2} = \phi_{3e}\left(\frac{r_o}{h_o}, \frac{r_w}{h_o}, \frac{h_b}{h_o}, \frac{b}{a^2}\right) \qquad (6.14)$$

$$\text{and} \quad \frac{\overline{V}}{\pi h_o (r_o^2 - r_w^2)} = \phi_{3f}\left(\frac{r_o}{h_o}, \frac{r_w}{h_o}, \frac{h_b}{h_o}, \frac{b}{a^2}\right) \qquad (6.15)$$

A third form of dimensionless drawdown cone volume parameter can be obtained by combining Equations (6.9) and (6.15). From Equation (6.9)

$$\frac{h_o}{h_o - h_f} = \phi_{1e}\left(\frac{r_o}{h_o}, \frac{r_w}{h_o}, \frac{h_b}{h_o}, \frac{b}{a^2}\right) \qquad (6.16)$$

Since Equations (6.16) and (6.15) have identical dimensionless groups within the function brackets, they may be multiplied to give:

$$\frac{\overline{V}}{s_f (r_o^2 - r_w^2)} = \phi_4\left(\frac{r_o}{h_o}, \frac{r_w}{h_o}, \frac{h_b}{h_o}, \frac{b}{a^2}\right) \qquad (6.17)$$

where $s_f = h_o - h_f$ is the drawdown at the pit boundary.

The two alternative parameters defined in Equations (6.14) and (6.15) are measures of the proportions the de-watered cone volume is of the originally saturated aquifer volumes within the radius of influence and between the pit radius and the radius of influence respectively.

They have the advantage that they range over fewer decimal log cycles than $\frac{\overline{V}}{h_o^3}$ and are thus more easily graphed for the range of values likely to be encountered in groundwater engineering practice. However, they suffer the disadvantage of less simple conversion to actual drawdown cone volumes.

The third alternative parameter defined in Equation (6.17) measures the proportion the de-watered cone volume is of the originally saturated aquifer volume between the pit radius and the radius of influence above the level of the water surface at the well. It may be useful in making comparisons of the steepness of the drawdown cone. A small value will indicate a steep cone whereas small values of the other parameters may simply reflect a small value of drawdown at the well.

Since Equations (6.8) to (6.11), (6.14), (6.15) and (6.17) include all the variables known to control unconfined flow into open pits they provide a suitable basis for numerical analysis and subsequent plotting of relationships for water level, discharge and de-watered drawdown cone volume. Numerical determination of the relationships by means of the finite element method is described in the following section.

6.2 Numerical Analysis

6.2.1 Solution Method and Computer Programme

The finite element methods for non-Darcy flow analysis developed by Volker (1969), McCorquodale (1970), Huyakorn (1973), Barends (1976) and Cox (1977) provide a suitable starting point for the solution of flow problems involving post-linear non-Darcy flow.

The FORTRAN computer programme previously used by Cox to solve axi-symmetric flow problems was developed further to allow solutions of the required accuracy to be obtained for Darcy and non-Darcy flow to large diameter circular pits. A wide range of pit geometries, aquifer properties and inflow conditions could then be handled by this single computer programme by selecting different options.

The range of inflow conditions covered by the programme includes:

i. Full aquifer penetration with unrestricted side entry;

ii. partial aquifer penetration with both side and bottom entry;

iii. partial aquifer penetration with bottom entry only.

The entry conditions are depicted in Figure 6.2.

Five b/a^2 values from 0 (Darcy flow) to 100 were chosen to cover the range which might be met in groundwater engineering. Although values up to 6,000 have been measured in permeameter tests on river boulders between 150 mm and 75 mm in size (Dudgeon (1964)), it is unlikely that these conditions will be met in groundwater extraction or de-watering projects.

The programme was used to compute, for each inflow option, inflow rates, water surface levels and de-watered drawdown cone volumes for the selected range of pit and aquifer geometries, aquifer properties and boundary water levels.

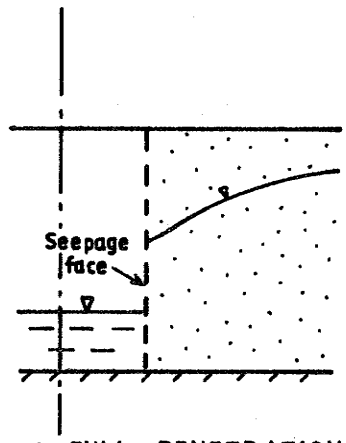

a) FULL PENETRATION, SIDE ENTRY

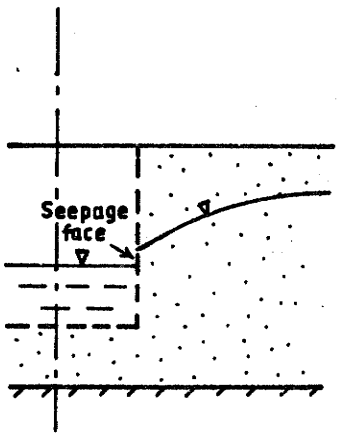

b) PARTIAL PENETRATION, BOTTOM AND SIDE ENTRY

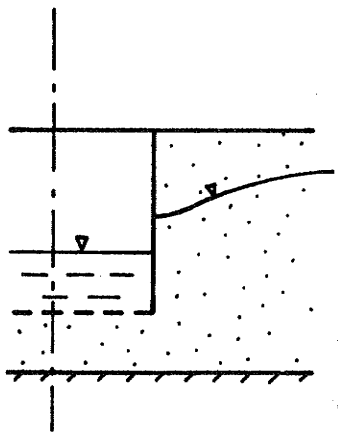

c) PARTIAL PENETRATION, BOTTOM ENTRY ONLY

FIGURE 6·2: ENTRY CONDITIONS FOR A PIT IN AN UNCONFINED AQUIFER

The current version of the computer programme has the following features:

i. Minimum input of data for each flow case to reduce the effort involved in obtaining the large number of solutions necessary to produce the desired range of dimensionless relationships.

ii. Automatic discretization of the flow field to a variable node spacing using triangular ring elements. Rapid expansion of element size away from the zone of flow concentration at the pit allows extended flow regions to be analysed in limited computer memory. The incorporation of new empirical equations into the programme to generate trial free surfaces allows suitable trial surfaces to be selected for large diameter partially penetrating pits.

iii. Iteration to satisfy the head condition following each adjustment of the free surface. When the number of nodes requiring either position or head adjustment is reduced to zero the solution is complete. The tolerance on both head and free surface position is adjustable.

iv. Print-out of positions and heads for all nodes for the final solution and a listing of the final free surface position.

v. Computation and print-out of the inflow rate and the distribution of inflow through the pit boundaries.

vi. Computation and print-out of the volume of material de-watered in the drawdown cone and the distribution of this volume with distance from the pit.

The matrix formulation and Gauss elimination routines used to set up and solve the finite element equations originated from a programme used for structural engineering applications and had been well tested.

New discretization routines were developed to allow an extended range of values of pit radius, degree of penetration and radius of influence to be accommodated. It was found particularly difficult to achieve satisfactory solution accuracy for extreme partial penetration cases such as those requiring maximum pit radius, maximum radius of influence and maximum degree of penetration. Problems of this type demanded a fine mesh under and adjacent to the pit without exceeding the limits of approximately 600 nodes and 900 elements dictated by the 200 K (octal) word central memory allocation within which the programme was required to run on a Cyber 171. Since the computer programme consists of nearly 2,000 statements and has not been documented sufficiently for general use, a listing is not included in this report. It will be available in report form from the University of New South Wales Water Research Laboratory after it has been fully documented.

6.2.2 Programme Verification

The original programme of Cox (1977) was verified by comparing output for non-Darcy flow to a small diameter fully penetrating borehole in a confined aquifer with the analytical solution given by Engelund (1953). Other comparisons with the results of laboratory experiments confirmed the validity of the computational method.

The new discretization routines referred to in the previous section were tested by comparing solutions obtained using old and new routines for problems with dimensions that could be handled by both routines.

This procedure was carried out every time a new modification was introduced to the programme.

6.2.3 Solution Accuracy

Effect of Node Spacing

Trials were carried out to determine the effect on computed discharges and water levels of refining the finite element mesh.

It was found that, provided elements near the well did not become seriously distorted by adjustment of the free surface, solutions for a given problem converged towards a constant discharge and water level at the well as the number of nodes along the well boundary increased.

The solution always over-estimated the discharge and under-estimated the free surface height at the pit if serious mesh distortion did not occur. Over the range of solutions developed, no universally applicable relationship between spacing of nodes at the boundary and discharge or free surface height was detected. Perusal of the data given in Report No. 163, Tables B1 to B14, for cases in which several trial spacings of nodes on the vertical at the well radius were used will give a general picture of the effect of mesh refinement.

Cases least sensitive to node spacing were those in which the well fully penetrated the aquifer. Partial penetration cases with a high degree of penetration and only bottom entry were the most sensitive. The height of the free surface at the pit was found to be more sensitive to node spacing than was the discharge or drawdown cone volume.

The spacing of nodes away from the pit boundary was found to be of secondary importance. The effect on the solution accuracy of rapid expansion of the element size away from the zone of flow concentration at the pit was found to be small compared with the effect of node spacing at the pit boundaries.

Because of the rapid decrease with decreasing radius of the discharge flux through the bottom of a partially penetrating large diameter pit, expansion of the mesh under the pit from the pit radius towards the centreline was found to be acceptable. No significant decrease in solution accuracy was observed provided the pit radius exceeded half the distance between the bottom of the pit and the base of the aquifer. The expansion of the element size afforded a large reduction in the number of nodes and elements in some cases.

A finite element mesh typical of those found to have a suitable rate of expansion of element sizes is shown in Figure 6.3.

The final mesh generation routine used in the computation of data for the dimensionless flow relationships allows rapid expansion of the element sizes both radially inwards and outwards from the vertical at the pit radius. This is achieved by using transitions which either halve the number of intervals between nodes in a vertical or reduce it by one according to whether the number is even or odd. Typical transitions are shown in Figure 6.3.

The overall fineness of the mesh is controlled by adjusting the spacing of nodes in the vertical at the pit radius. This is done by specifying the number of intervals into which the trial free surface height at the pit is to be divided. Each of the vertical distances from

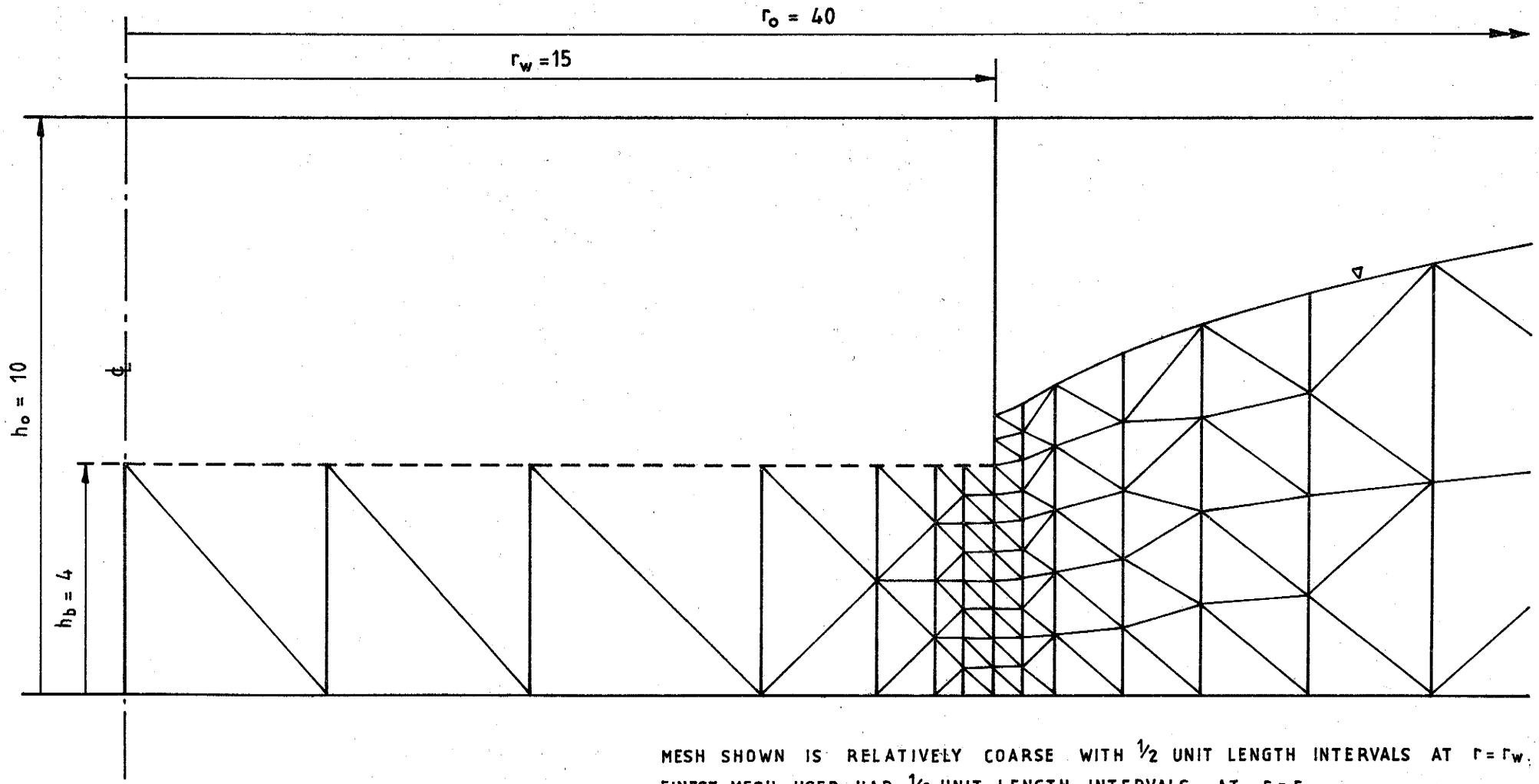

FIGURE 6.3: FINITE ELEMENT MESH FOR FLOW TO LARGE DIAMETER PIT

the bottom of the pit to the free surface and from the bottom of the pit to the base of the aquifer is divided into equal intervals with one node fixed at the bottom corner of the pit. The intervals above and below this node are made as nearly equal to each other as possible. Appropriate choice of values for the depth of penetration, trial free surface height and total number of intervals into which the latter is to be divided will cause initial inter-node spacings to be equal over the full trial free surface height at the pit.

The first vertical mesh line on each side of the vertical at the pit radius is subdivided without the number of nodes being reduced. The mesh is then expanded automatically to larger and smaller radii.

Effect of Mesh Distortion

During the course of the iterative solution, the free surface position is shifted vertically from its initial trial position. It was found that the fixed node at the bottom corner of the pit causes serious distortion of the mesh when a poor choice of trial free surface height at the pit results in a large adjustment to the final position. The solution was generally found to be insufficiently accurate if the difference between the trial and final free surface heights was more than 5 per cent of the saturated thickness. With the fixed node at the bottom corner of the pit, all the vertical adjustment must be absorbed by the nodes above this point. However, equal adjustment of all nodes in the next vertical line of greater radius is necessary to maintain the system of vertically aligned, approximately equilateral triangular elements on which the automatic generation scheme is founded. If the free surface adjustment is large, some elements become very distorted.

Unfortunately, the ill-conditioned elements which result near the bottom corner of the pit occur in a region of flow concentration where they have a disproportionate effect on the accuracy of the solution. The worst conditions are met when only bottom entry is allowed into the pit since the flow concentration is greatest for this type of inflow.

It was found that poorly chosen trial free surface heights at partially penetrating pits yielded solutions within the prescribed tolerance and iteration limits. However, the value of final free surface height differed from the value to which closer trial values converged. The discharge and drawdown cone results were in error to a lesser extent. The error in free surface height differed from that caused by too coarse a mesh in that it was not always negative.

An alternative procedure that was evaluated to overcome the problem was to increase or reduce the number of nodes at the well boundary automatically when the required free surface adjustment exceeded a preset limit. This would have required the generation of a new mesh between the pit and the radius of influence each time a node was added to or eliminated from the vertical at the pit radius. Since the implementation of this procedure would have required a programming effort disproportionate to the potential benefits, it was not adopted. Instead, unsatisfactory solutions were repeated after insertion into the data of adjusted values for the trial free surface height at the pit. It was reasoned that although several trials might be required to obtain solutions for extreme values of the input variables, careful selection of trial free surface heights for intermediate values would allow solutions of the desired accuracy to be obtained at the first attempt. This proved to be the case as data provided in Report No. 163 demonstrates. The results of all the solutions carried out are listed in Report No.

163 Tables B.1 to B.14.

Effect of Free Surface and Head Iteration Tolerances

Iteration for both the free surface position and heads at nodes was continued until either all changes fell within a certain tolerance or the limit set for the number of iterations was exceeded.

The effect of setting the tolerance at 1%, 0.2% and 0.1% of the initial saturated thickness was checked by carrying out trial runs. It was found that a tolerance of 0.2% resulted in the solutions for discharge and free surface height at the pit converging to the required accuracy without unduly extending the number of iterations. The tolerance had a relatively small effect on the final solution compared with the node spacing at the pit boundaries.

Effect of Initial Trial Surface Profile

The shape of profile produced by the equation selected for the initial trial free surface position affected the number of iterations required for the solution to converge to the set tolerances. However, unless the shape was so poorly matched to the final surface close to the pit that serious mesh distortion occurred, it did not have any significant effect on the final solution. If the match near the pit were very poor, the mesh distortion effect described previously was encountered.

Effect Of Velocity Head At Exit

The boundary condition imposed along the part of the pit boundary through which water enters the pit neglects velocity head of water at exit from the aquifer. In an extremely permeable aquifer, such as one composed of boulders, and for a small radius of influence which might be used in laboratory experiments, the velocity head could form a significant part of the total loss of head in the flow. It would not be recovered as pressure head in the pit as it would be lost in turbulence generated by the jets of water leaving the pores in the face of the aquifer.

For a microscopic entry velocity of 1 m/s the velocity head would be 0.05 m and for 0.1 m/s it would be 0.0005 m. For normal field conditions it is obvious that velocity head can be neglected in relation to the total head driving the flow. Only in cases of flow through extremely permeable artificial porous beds is it likely to have any significant effect on the flow rate or distribution.

6.3 Results of Numerical Analysis

A complete set of results of the numerical analysis is given in Tables B.1 to B.14, C.1 to C.13 and D.1 to D.13 in Report No. 163.

All the finite element solutions were carried out with constant values of $h_o = 10.0$ and $a = 0.1$. The values of the other variables r_w, r_o, h_b and b were chosen to produce the values of the dimensionless ratios selected to cover the range of interest in groundwater engineering. Any consistent set of units can be applied to the variables. However, it should be kept in mind that if a set of units is applied to the raw, dimensioned results of computation tabulated in Report No. 163 and results in $\frac{V^2}{2g}$ values which are a significant proportion of the total

head loss from the radius of influence to the water surface in the pit, the assumption that velocity heads can be neglected will be invalidated. The solution will then be incorrect. The problem is unlikely to arise in real flow cases.

Trial values of the height of the free surface at the pit h_f and the number of intervals into which it was divided are included in Tables B.1 to B.14 of Report No. 163. The trial and computed values of h_f and the height of the bottom of the pit h_b allow the degree of distortion of the elements at the pit boundary to be judged. The number of intervals into which h_f was divided gives an indication of the fineness of the mesh at the pit. Solutions which did not achieve the desired accuracy are included to allow comparisons to be made.

The large number of variables involved made it impractical to plot graphs of all the combinations which might be useful in solving different types of problem. The raw data provided will allow other variable groupings to be plotted if necessary without the need to scale off the graphs included in Report No. 163.

The relationships which have been plotted are those which:

i. Allow discharges and water levels to be found easily for various inflow conditions, degrees of aquifer penetration and values of radius of influence, pit or well radius and aquifer non-linearity parameter b/a^2.

ii. Allow drawdown cone volumes to be determined from the simplest of the parameters tabulated.

iii. Best demonstrate the lack of gross errors in the water level data.

The relationships described above are shown in Figures B.1 to B.105, C.1 to C.40 and D.1 to D.38 in Report No. 163.

Points showing the actual numerical results are plotted only on $\overline{V}''$ versus r_w graphs which form the last set described since these were found to be most sensitive to errors caused by distortion of the finite element mesh. All other curves are drawn through the calculated values. During the plotting, points which did not fit a smooth curve were re-calculated with a finer mesh or better trial free surface height until the desired accuracy was obtained.

Some features of the relationships between the variables for the different entry conditions treated are discussed in the following sections.

6.3.1 Effect Of Non-Darcy Flow On Inflow Rate

Figures 6.4 to 6.15 show a selection from the computed dimensionless flow rate results provided in Report No. 163. The computed points used to draw the curves have been added to allow the accuracy of the fit to be assessed.

It will be observed that non-Darcy flow near the pit has a large effect on the inflow rate under all conditions. However, the effect is clearly greatest when inflow is restricted to the bottom of the pit, particularly for small values of the ratios $\frac{r_w}{h_o}$ and $\frac{h_b}{h_o}$. For a given aquifer thickness for both inflow conditions examined the effect of

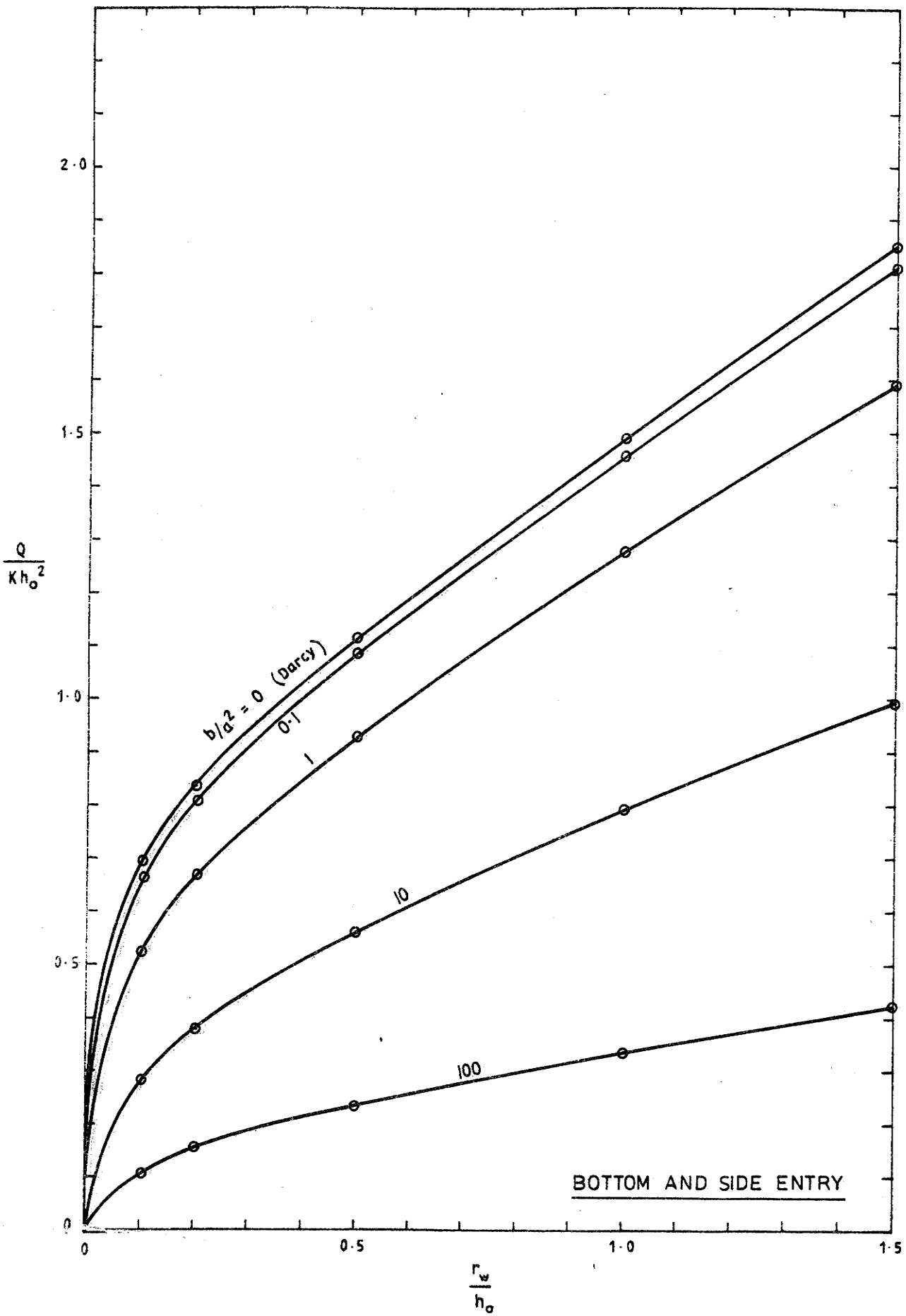

FIGURE 6·4: FLOW INTO DE-WATERED CIRCULAR PIT IN UNCONFINED AQUIFER. $\frac{r_o}{h_o} = 8$ $\frac{h_b}{h_o} = 0{\cdot}1$

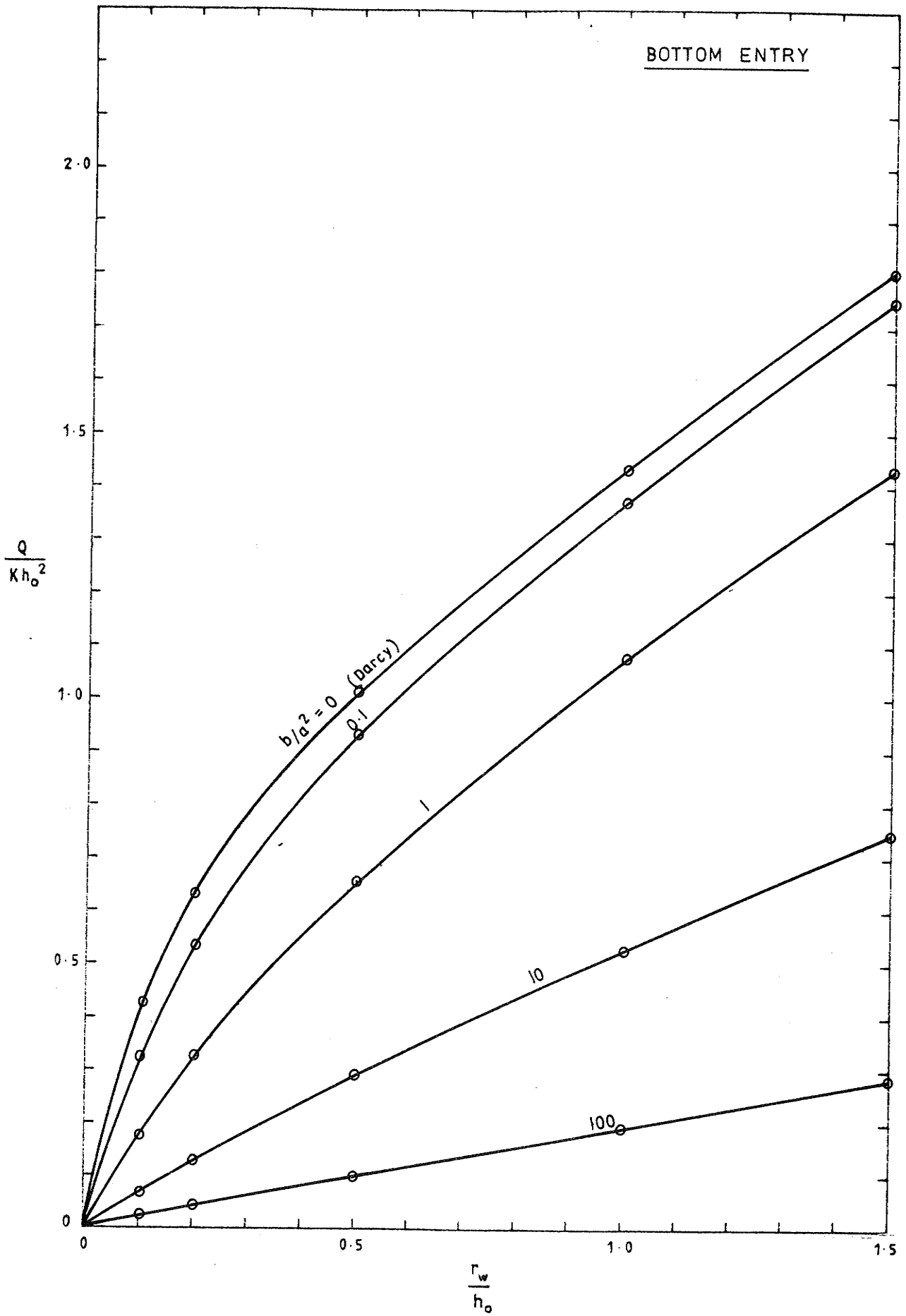

FIGURE 6·5: FLOW INTO DE-WATERED CIRCULAR PIT IN UNCONFINED AQUIFER. $\frac{r_o}{h_o} = 8$ $\frac{h_b}{h_o} = 0{\cdot}1$

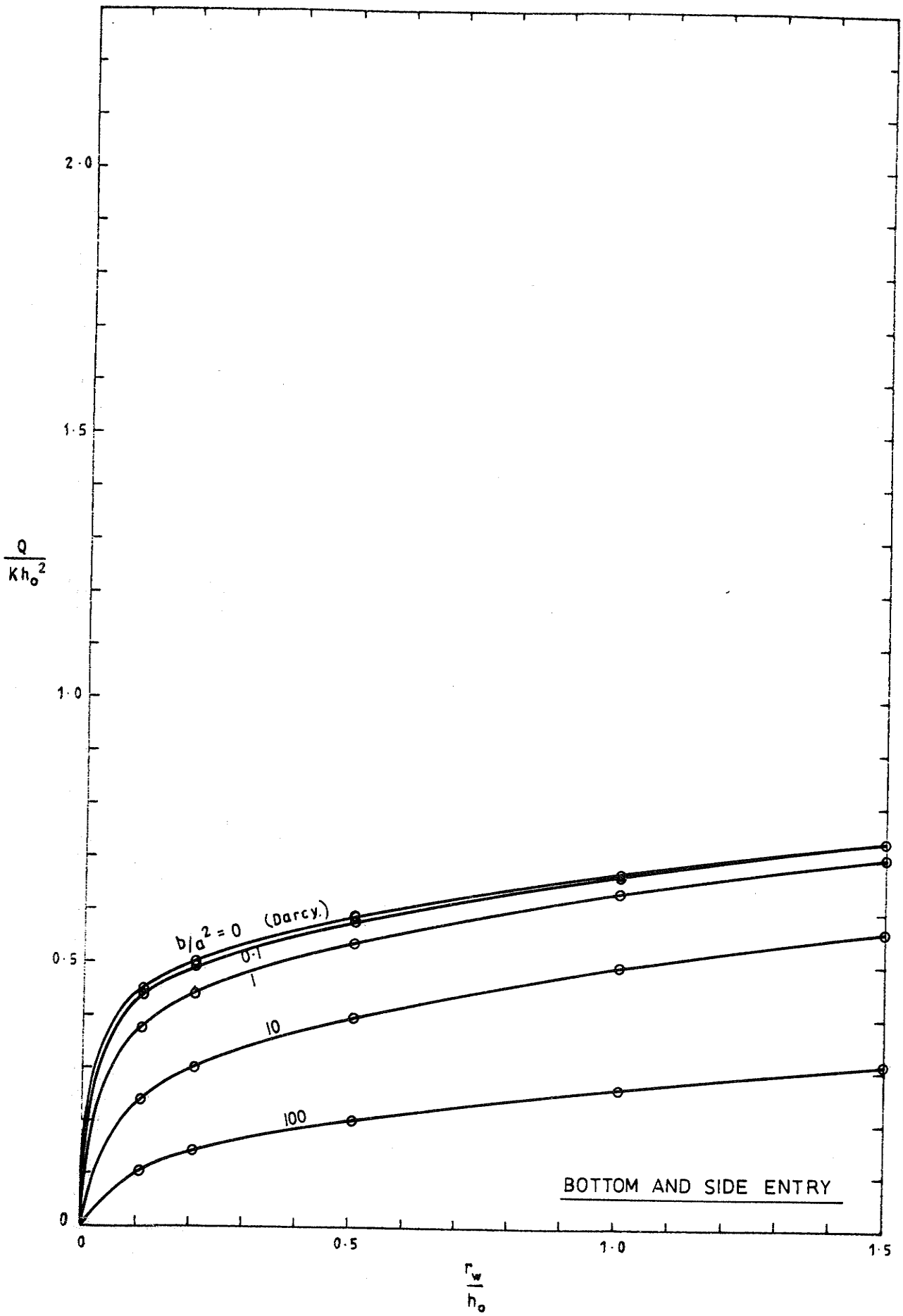

FIGURE 6·6: FLOW INTO DE-WATERED CIRCULAR PIT IN UNCONFINED AQUIFER. $\frac{r_o}{h_o} = 100$ $\frac{h_b}{h_o} = 0{\cdot}1$

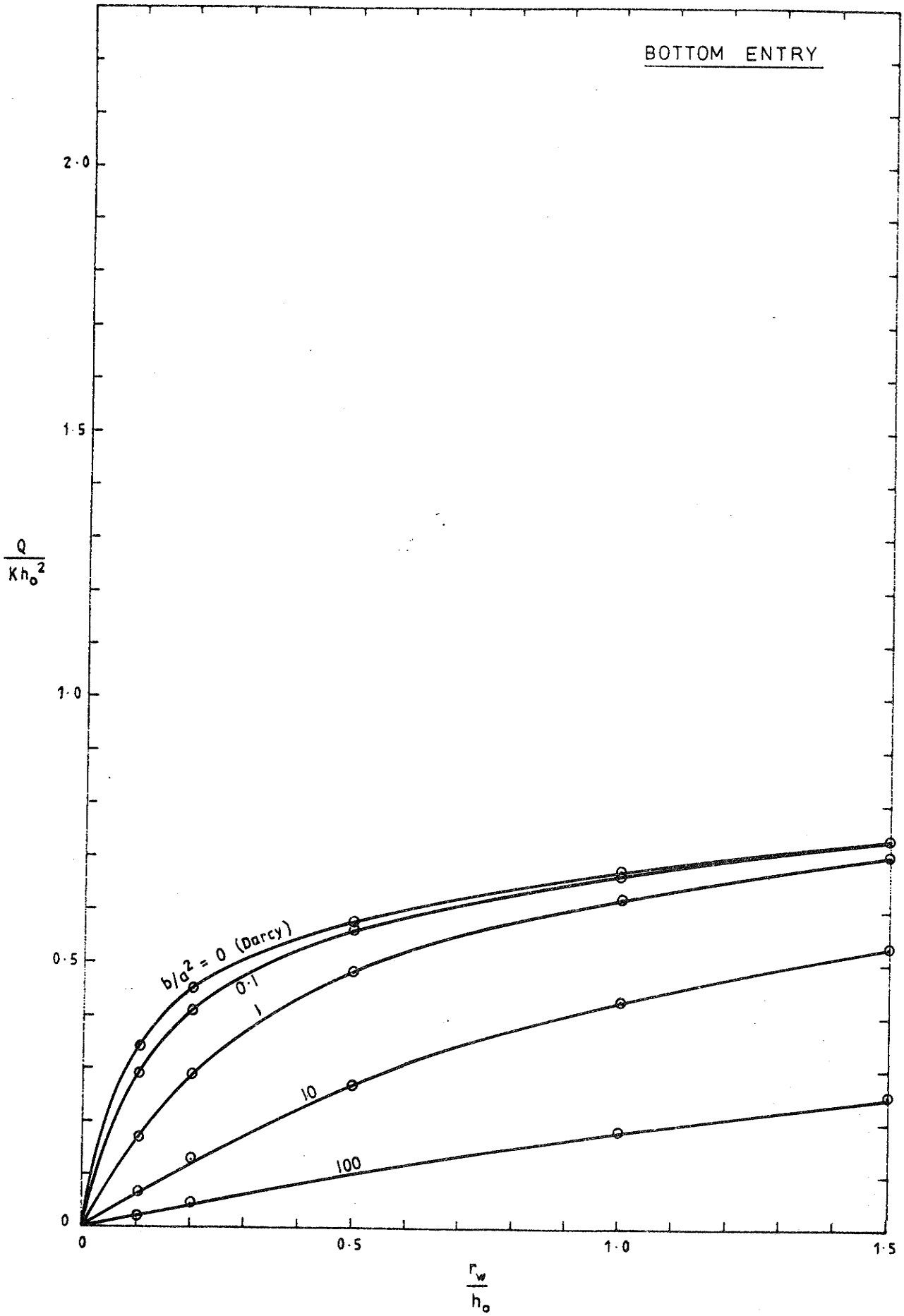

FIGURE 6·7: FLOW INTO DE-WATERED CIRCULAR PIT IN UNCONFINED AQUIFER. $\frac{r_o}{h_o} = 100$ $\frac{h_b}{h_o} = 0{\cdot}1$

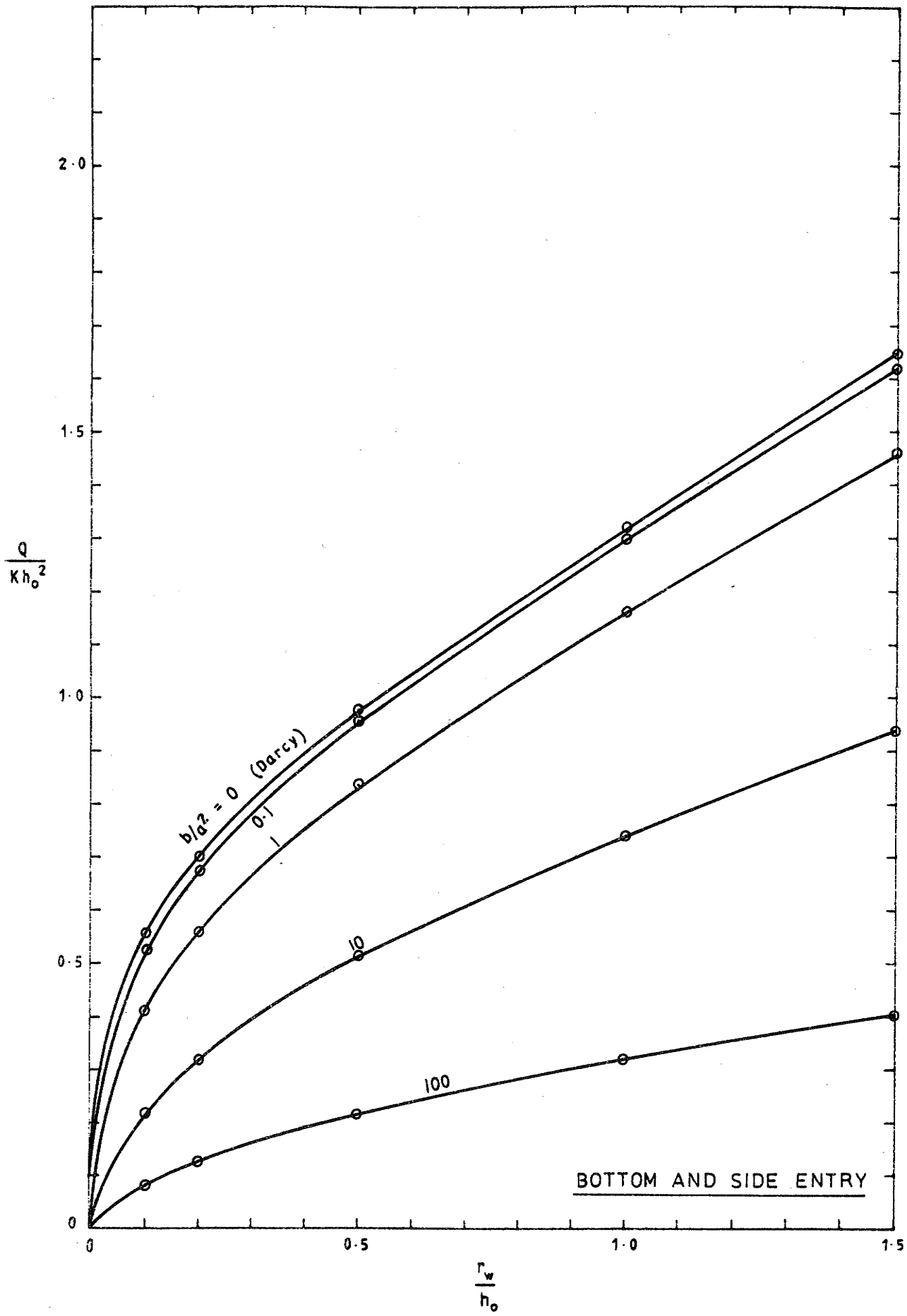

FIGURE 6·8: FLOW INTO DE-WATERED CIRCULAR PIT IN UNCONFINED AQUIFER. $\frac{r_o}{h_o} = 8$ $\frac{h_b}{h_o} = 0{\cdot}3$

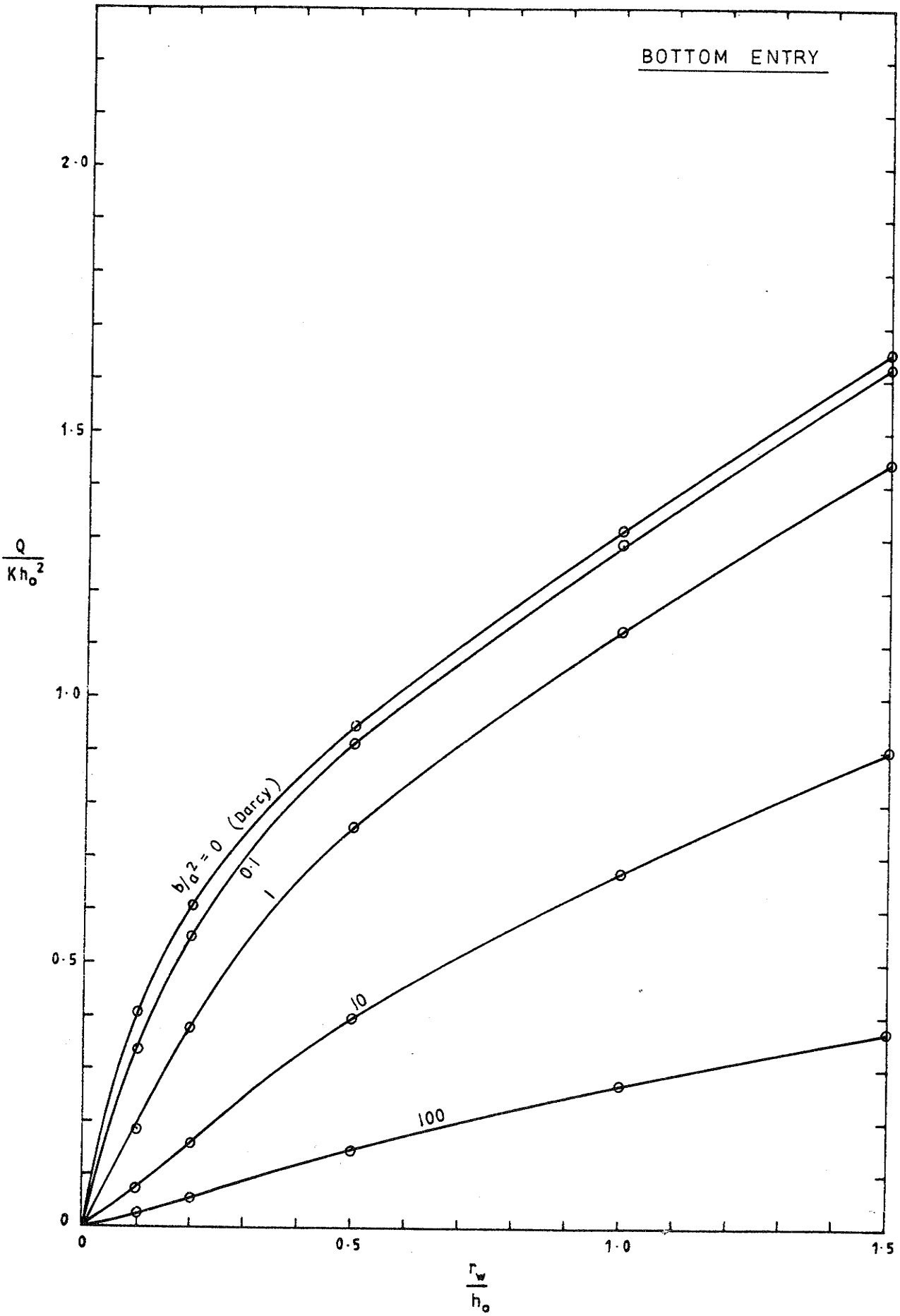

FIGURE 6·9: FLOW INTO DE-WATERED CIRCULAR PIT IN UNCONFINED AQUIFER. $\frac{r_o}{h_o} = 8$ $\frac{h_b}{h_o} = 0{\cdot}3$

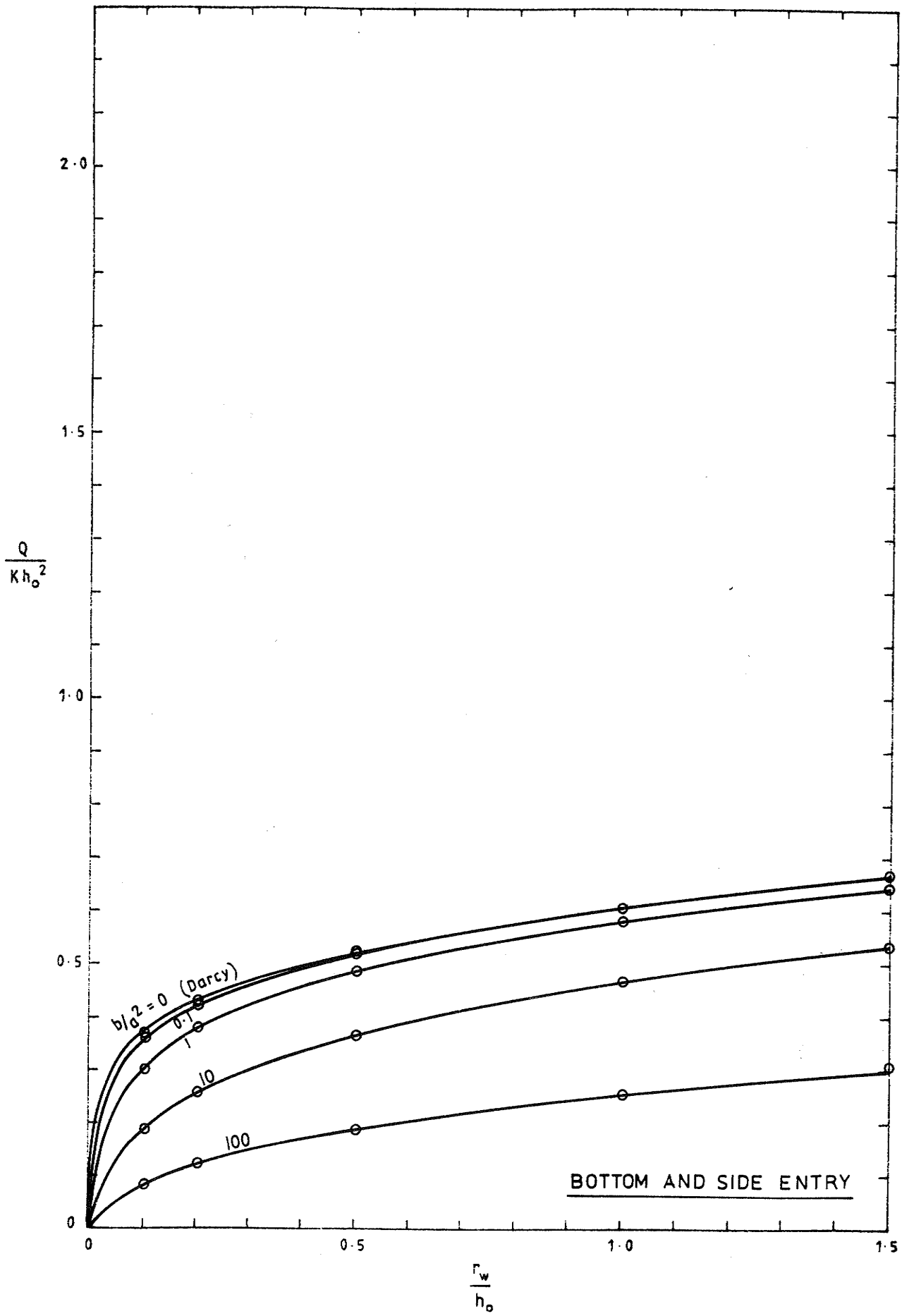

FIGURE 6·10: FLOW INTO DE-WATERED CIRCULAR PIT IN UNCONFINED AQUIFER. $\frac{r_o}{h_o} = 100$ $\frac{h_b}{h_o} = 0{\cdot}3$

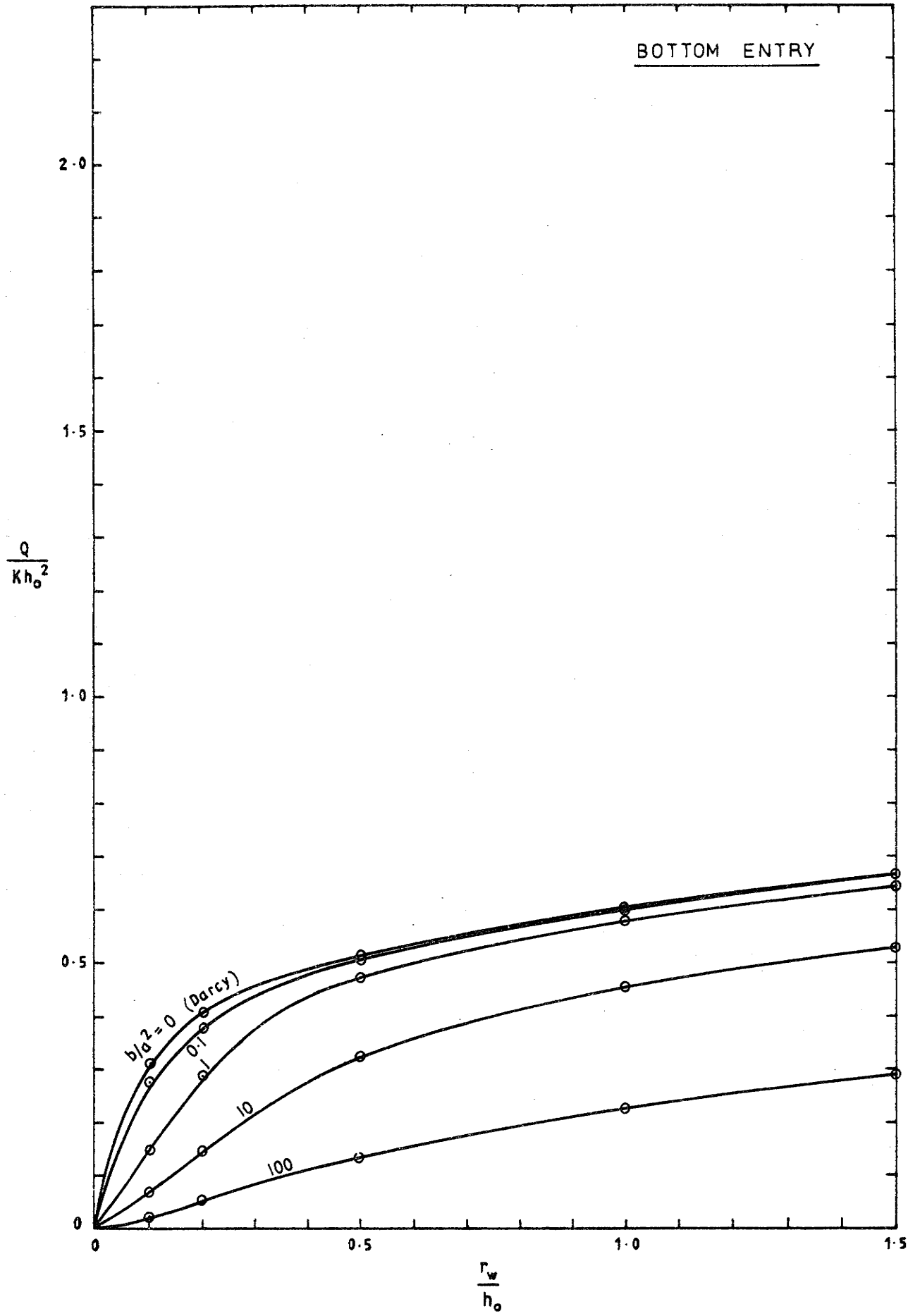

FIGURE 6·11: FLOW INTO DE-WATERED CIRCULAR PIT IN UNCONFINED AQUIFER. $\frac{r_o}{h_o} = 100$ $\frac{h_b}{h_o} = 0.3$

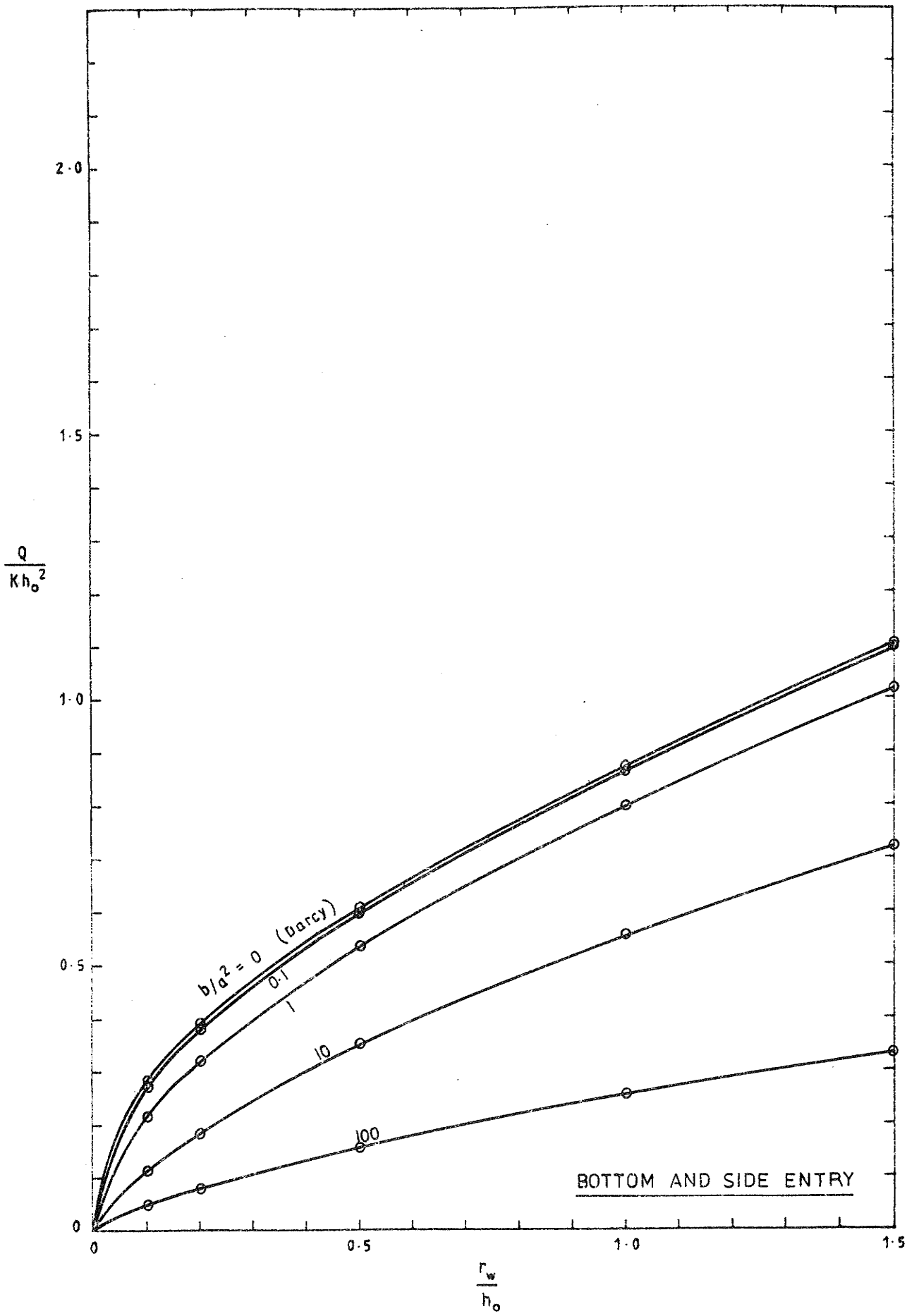

FIGURE 6·12: FLOW INTO DE-WATERED CIRCULAR PIT IN UNCONFINED AQUIFER. $\frac{r_o}{h_o} = 8$ $\frac{h_b}{h_o} = 0·6$

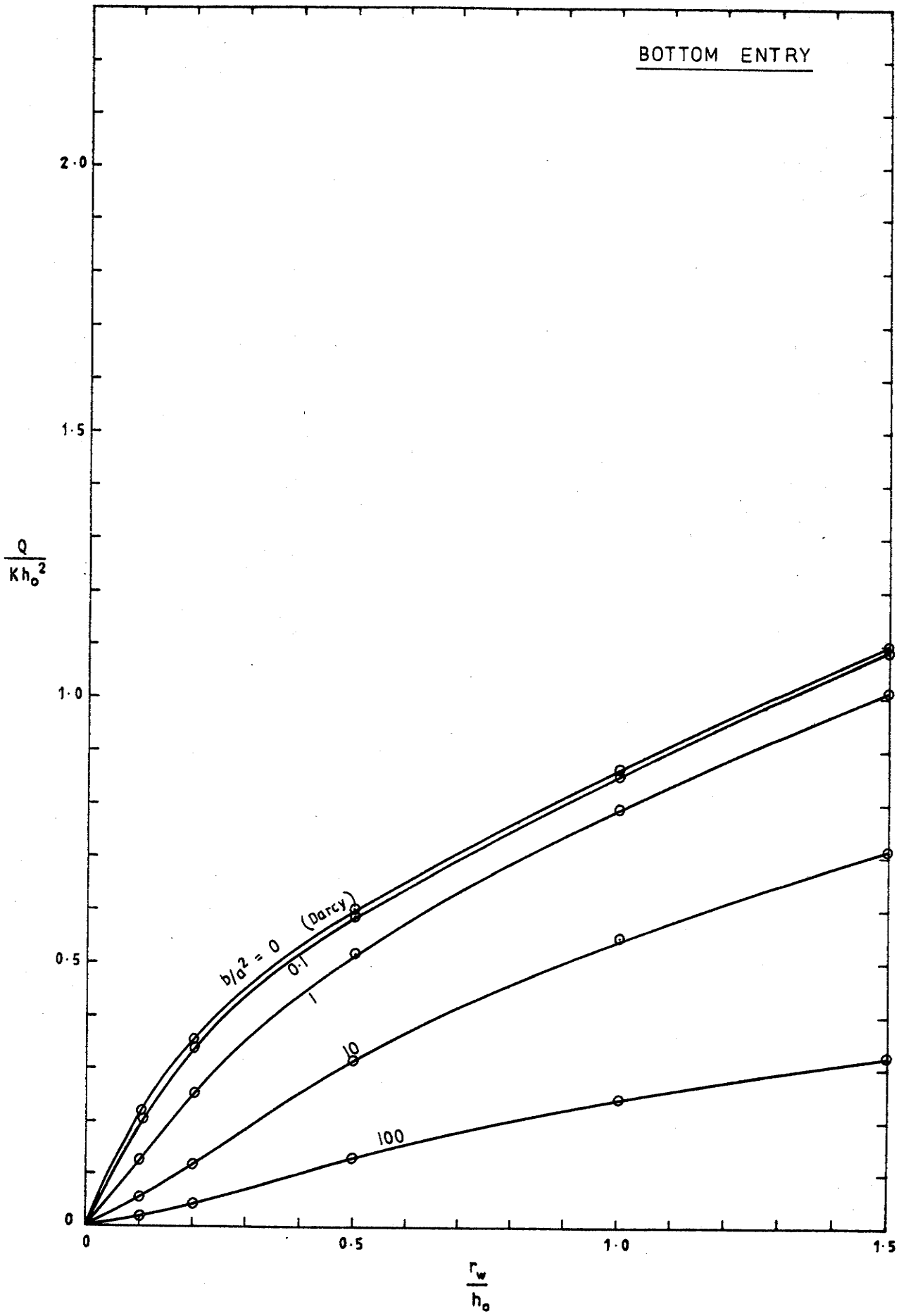

FIGURE 6·13: FLOW INTO DE-WATERED CIRCULAR PIT IN UNCONFINED AQUIFER. $\frac{r_o}{h_o} = 8$ $\frac{h_b}{h_o} = 0{\cdot}6$

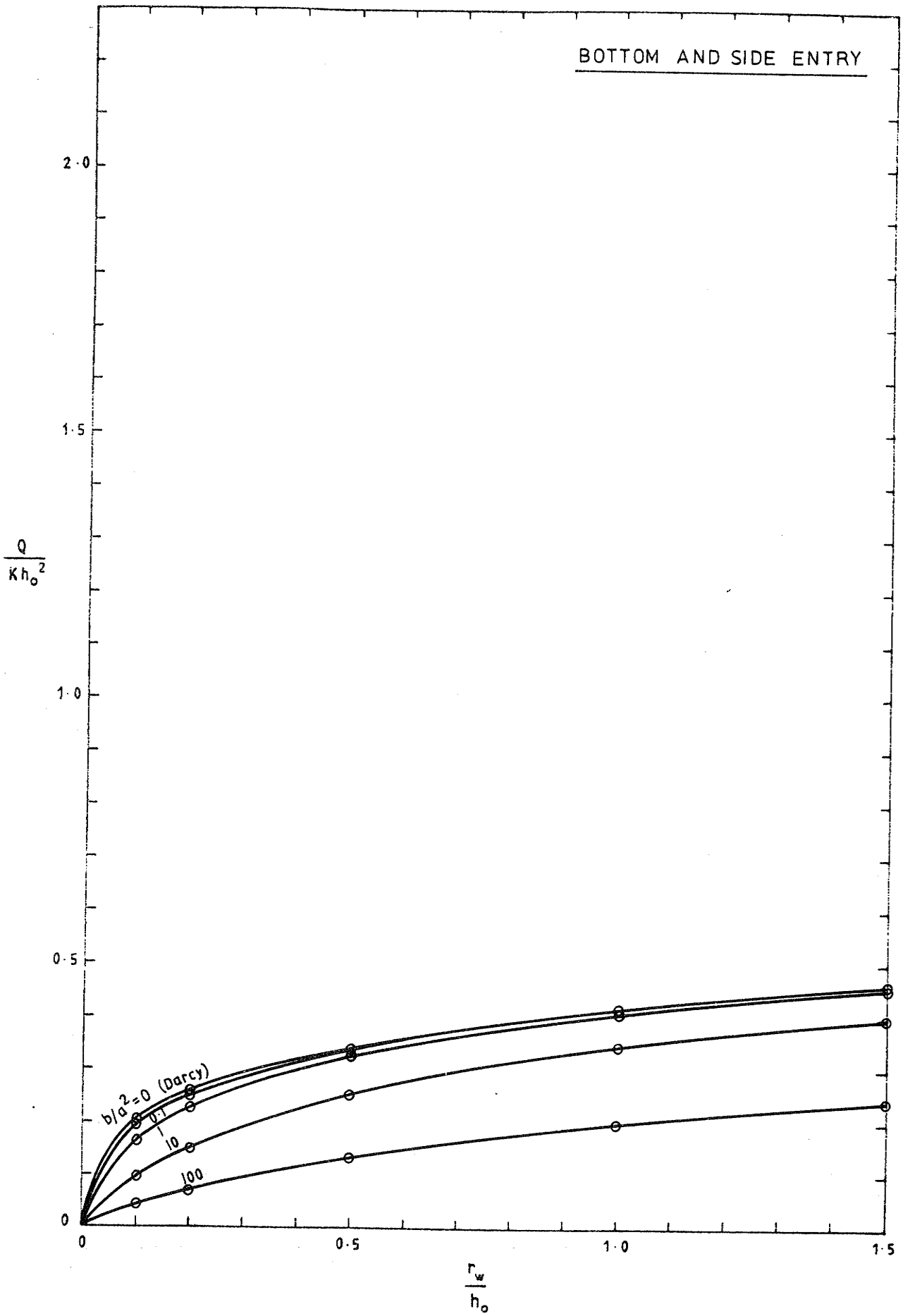

FIGURE 6·14: FLOW INTO DE-WATERED CIRCULAR PIT IN UNCONFINED AQUIFER. $\frac{r_o}{h_o} = 100$ $\frac{h_b}{h_o} = 0{\cdot}6$

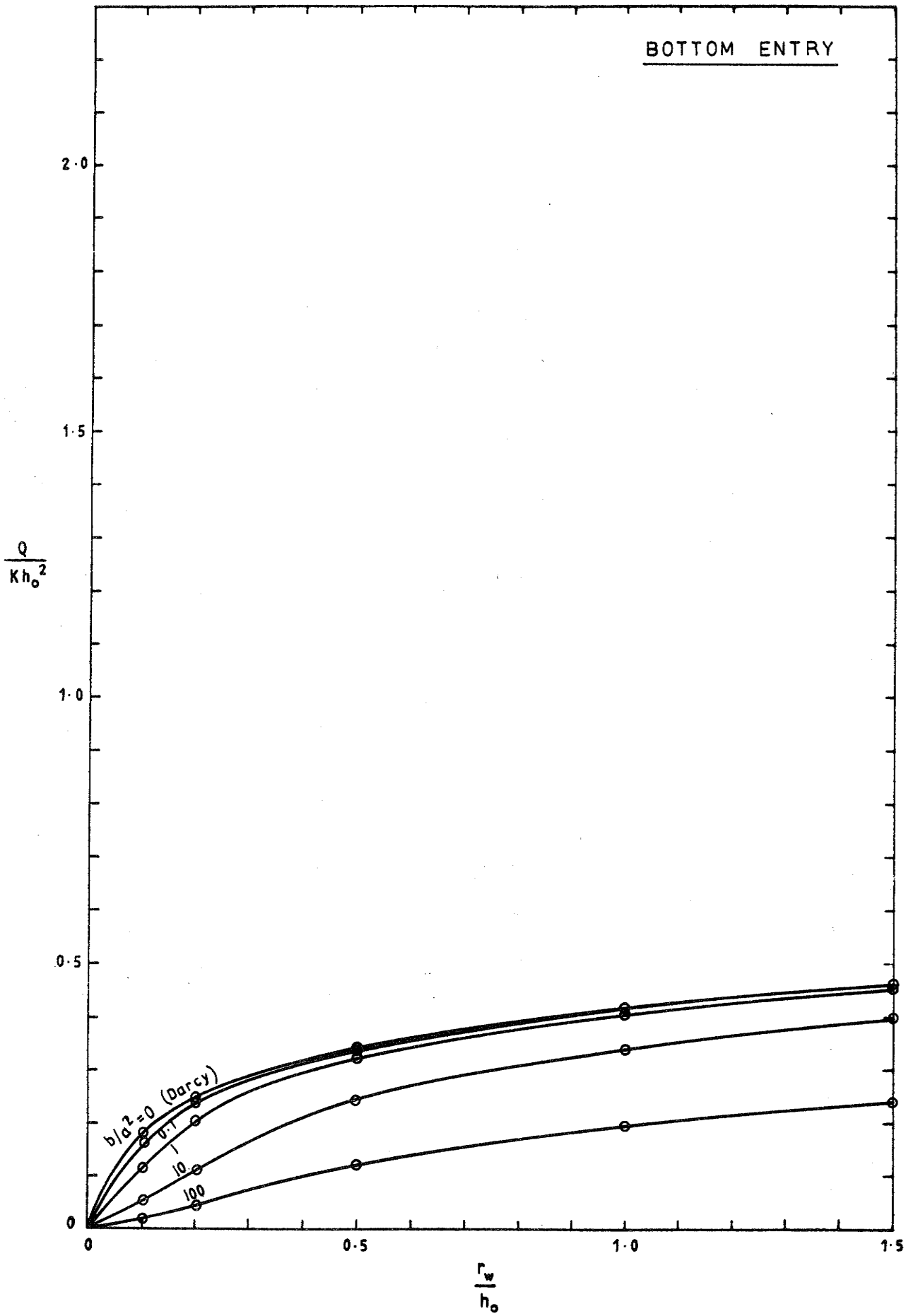

FIGURE 6·15: FLOW INTO DE-WATERED CIRCULAR PIT IN UNCONFINED AQUIFER. $\frac{r_o}{h_o} = 100$ $\frac{h_b}{h_o} = 0{\cdot}6$

non-Darcy flow decreases as the pit radius increases, the depth of penetration decreases and the radius of influence increases.

The strong influence of non-Darcy flow for a small radius of influence is of particular significance in the analysis of the results of pump testing large diameter wells. In the early stages of the test the radius affected by the pumping will be small and conditions will be favourable for the occurrence of highly non-Darcy flow if the water level in the well is drawn down rapidly. Recent papers by Rushton and Holt (1984), Herbert and Kitching (1982) and Rushton and Singh (1983) on pump testing of large diameter wells have avoided the problem of non-Darcy flow. The analyses presented are not applicable to large diameter wells in highly permeable coarse sand and gravel aquifers. The data presented in Report No. 163 can be used as a guide to whether non-Darcy effects are likely to be significant in particular cases.

6.3.2 Effect of Non-Darcy Flow On the Water Level At the Pit

Figures 6.16 to 6.21 show the results of computation of water levels at the pit for the same cases as those for which inflow data are given in Figures 6.4 to 6.15. The computed points have again been added to the graphs reproduced from the full set given in Report No. 163.

The limit on the available computer memory has caused some minor distortions in the water level curves for small values of the ratio $\frac{r_w}{h_o}$. However, the results of the trials listed in Tables B.1 to B.14 in Report No. 163 indicate that these errors, which result from too coarse a finite element mesh, do not exceed and are generally considerably less than 5 per cent.

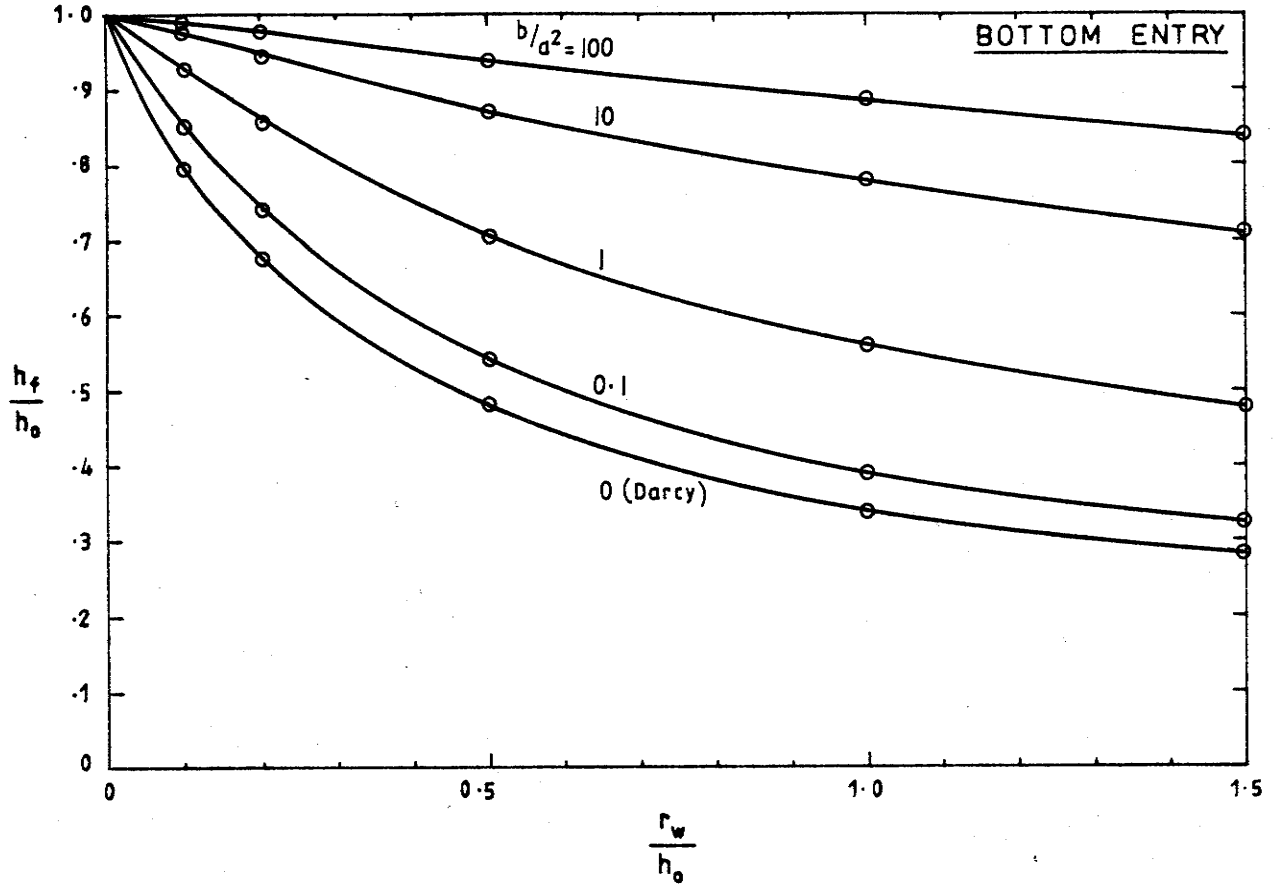

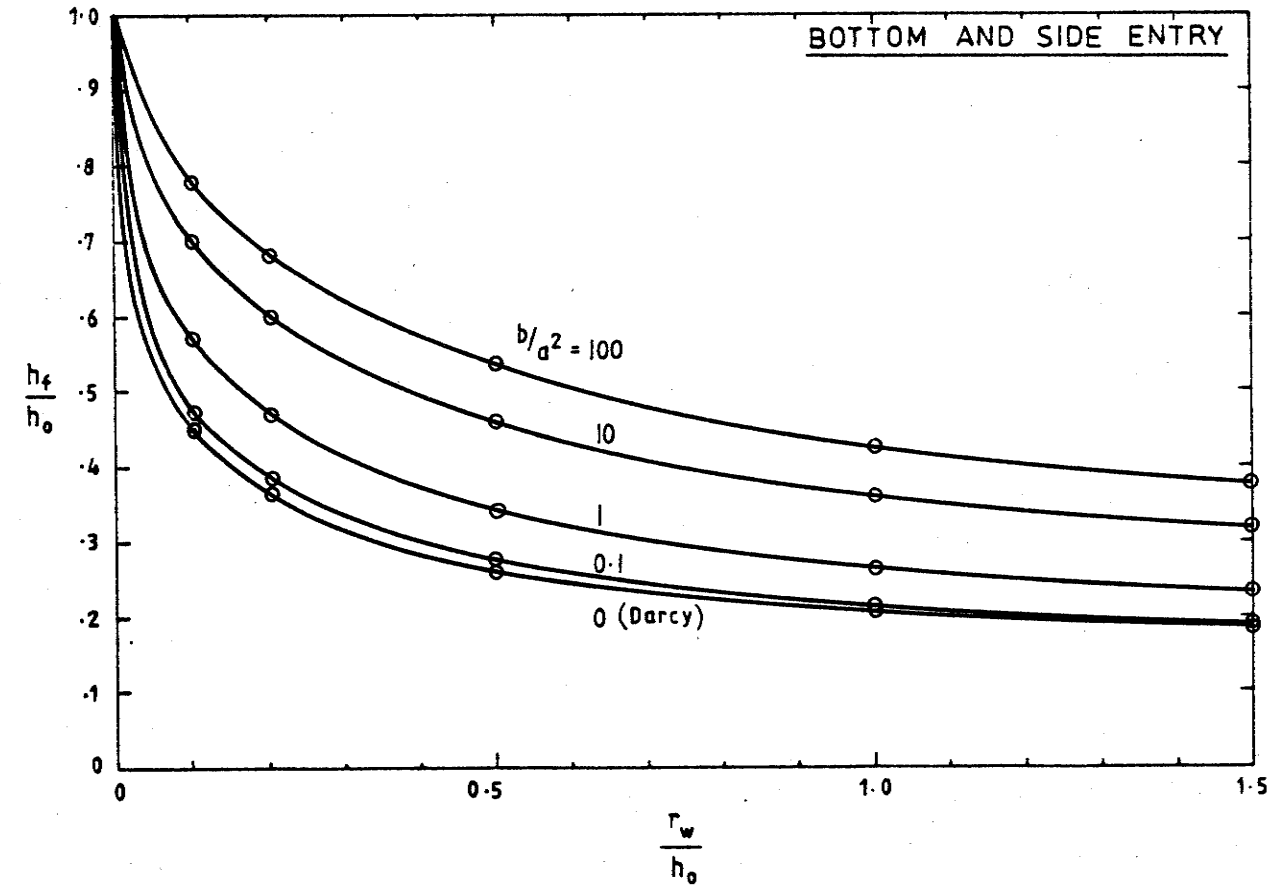

FIGURE 6·16: WATER LEVEL AT DE-WATERED CIRCULAR PIT IN UNCONFINED AQUIFER. $\frac{r_o}{h_o} = 8$ $\frac{h_b}{h_o} = 0{\cdot}1$

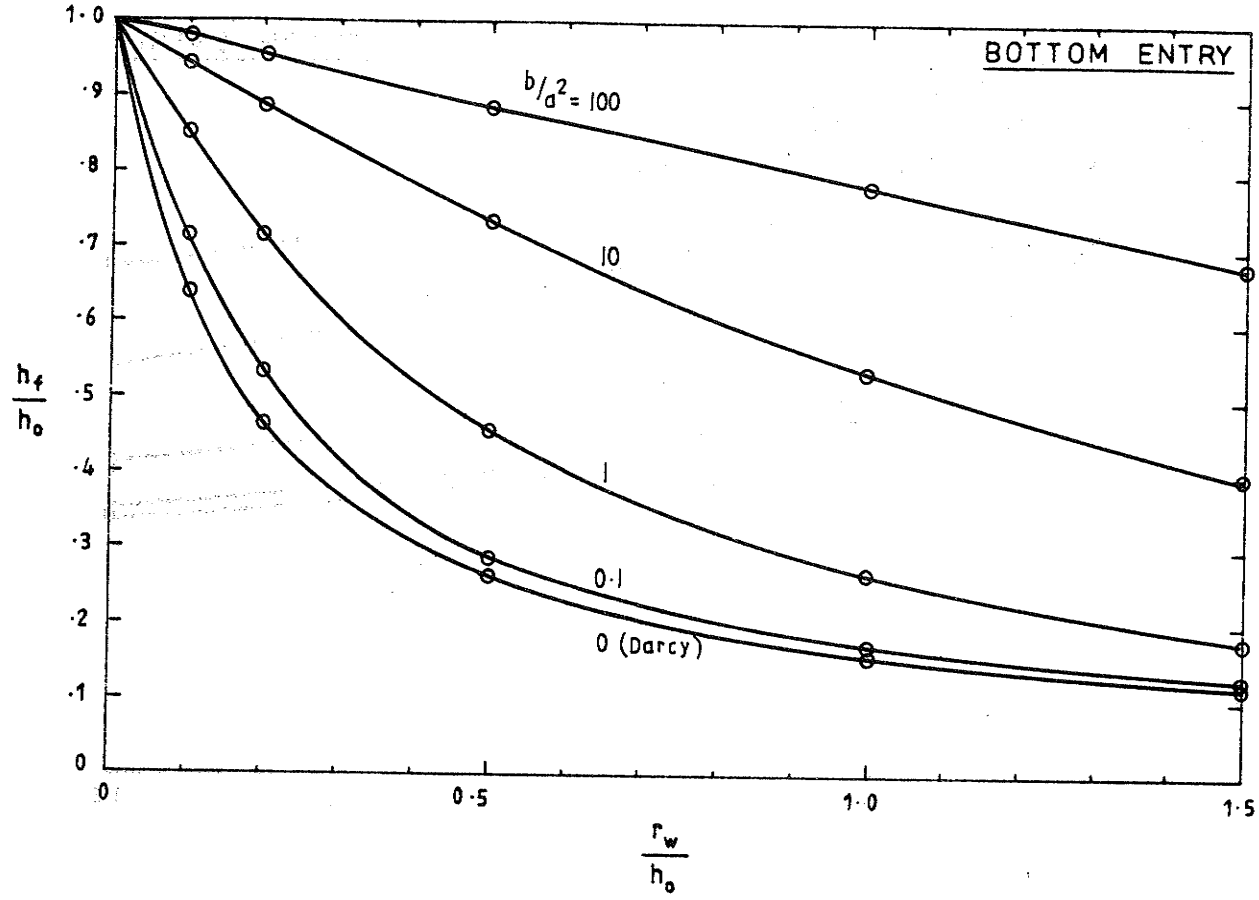

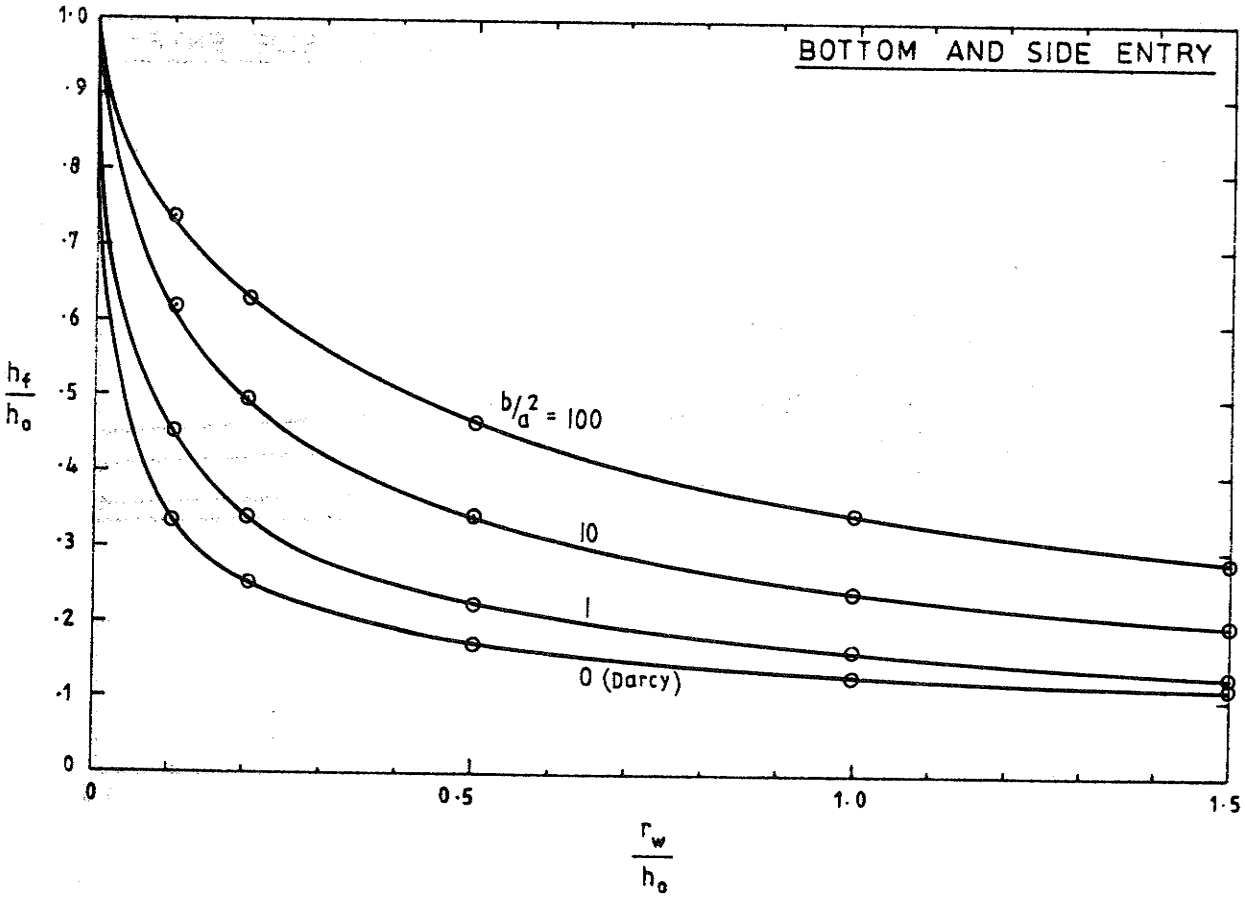

FIGURE 6·17: WATER LEVEL AT DE-WATERED CIRCULAR PIT IN UNCONFINED AQUIFER. $\frac{r_o}{h_o} = 100$ $\frac{h_b}{h_o} = 0{\cdot}1$

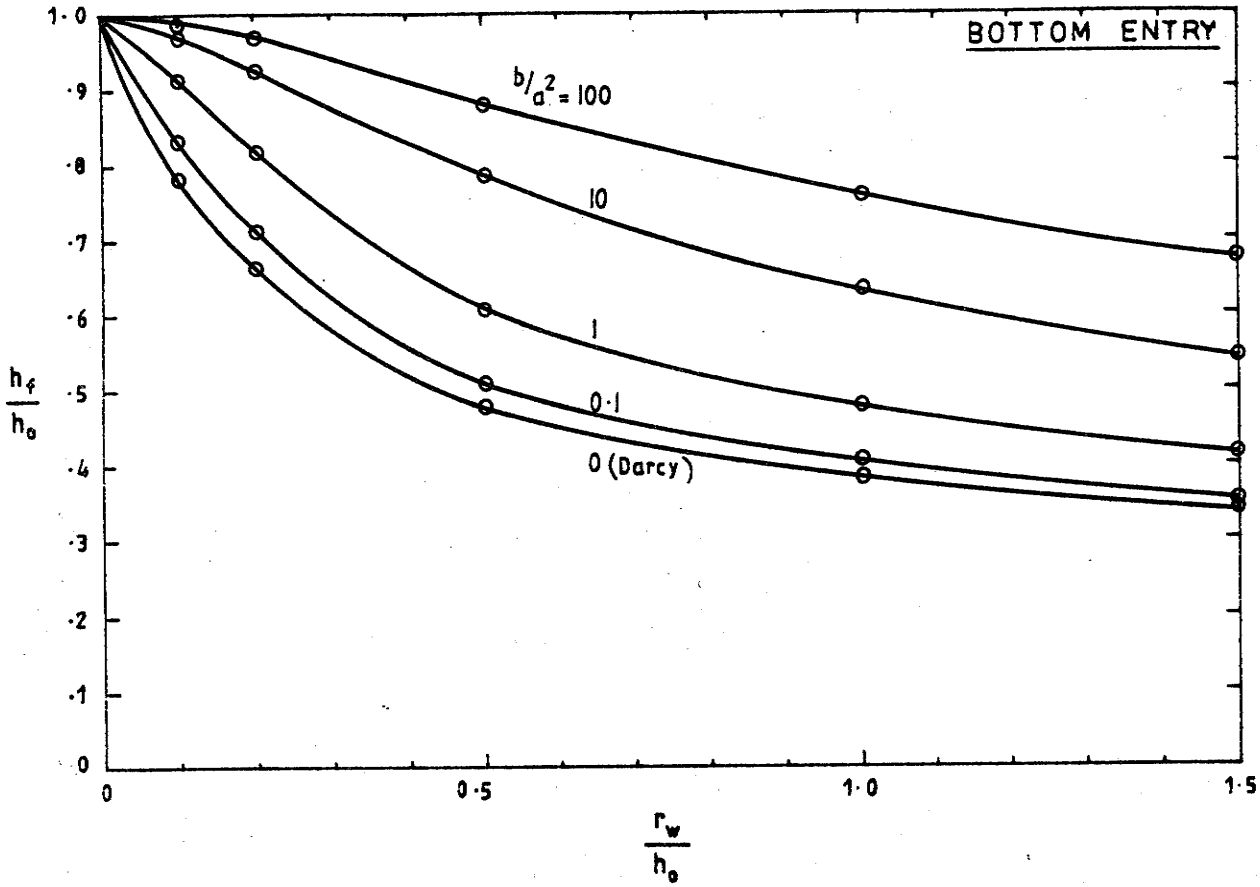

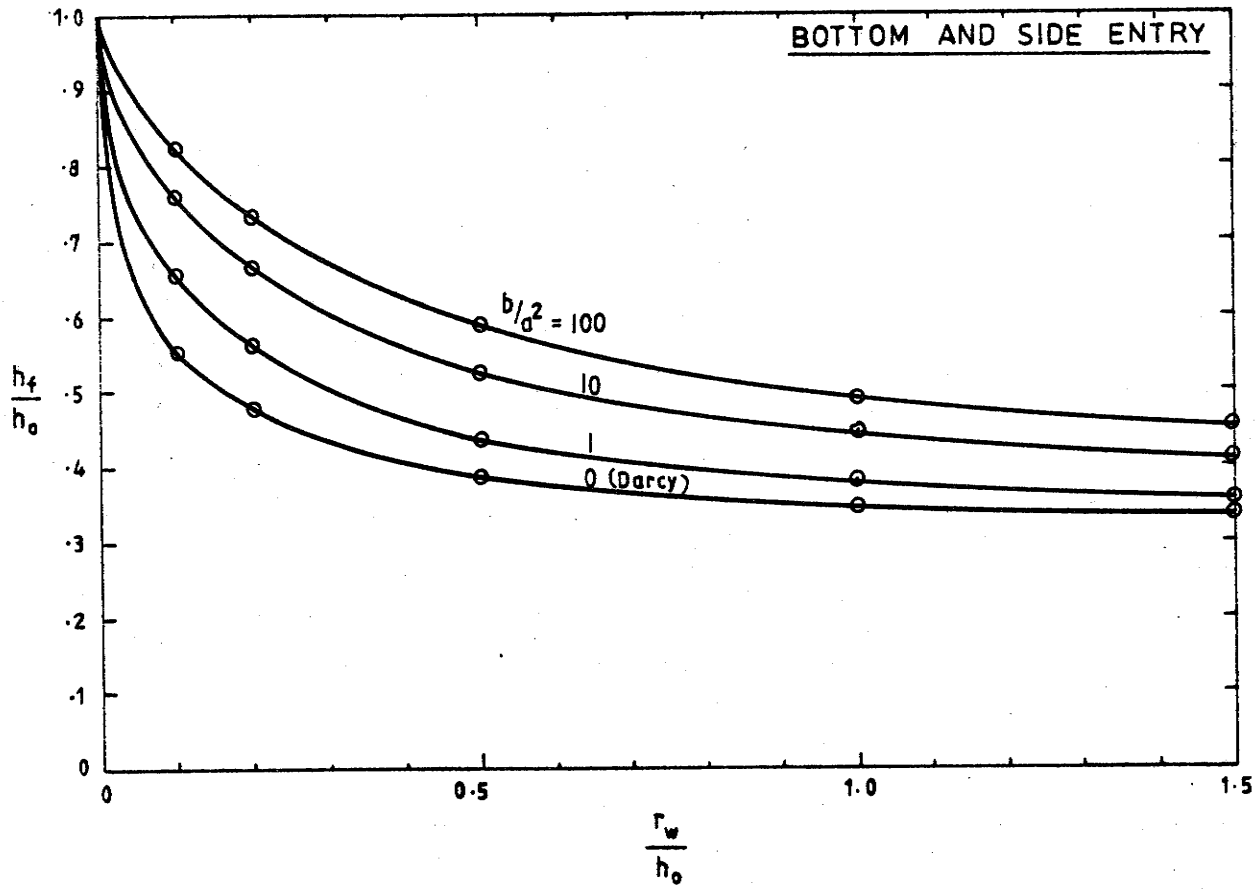

FIGURE 6·18: WATER LEVEL AT DE-WATERED CIRCULAR PIT IN UNCONFINED AQUIFER. $\frac{r_o}{h_o} = 8$ $\frac{h_b}{h_o} = 0{\cdot}3$

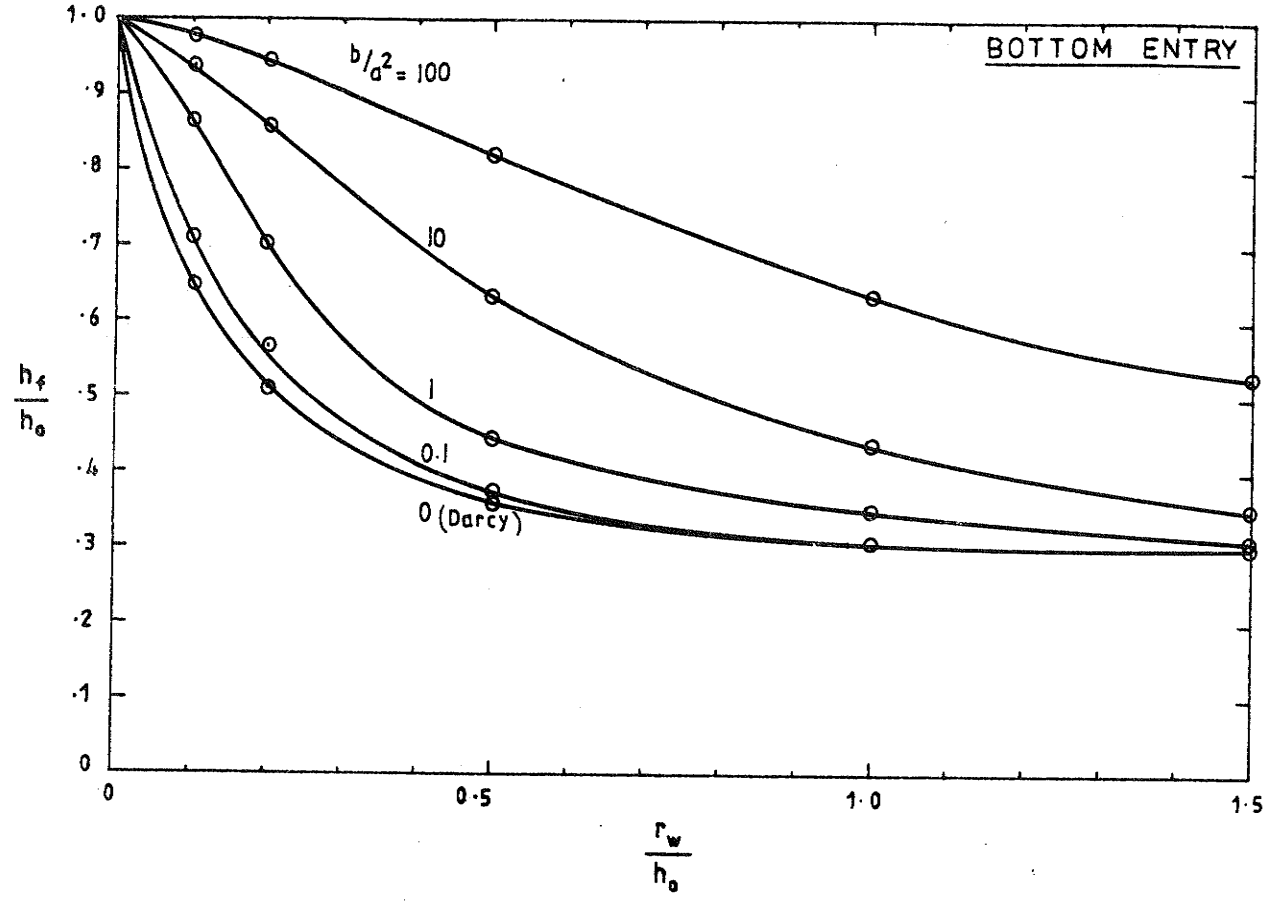

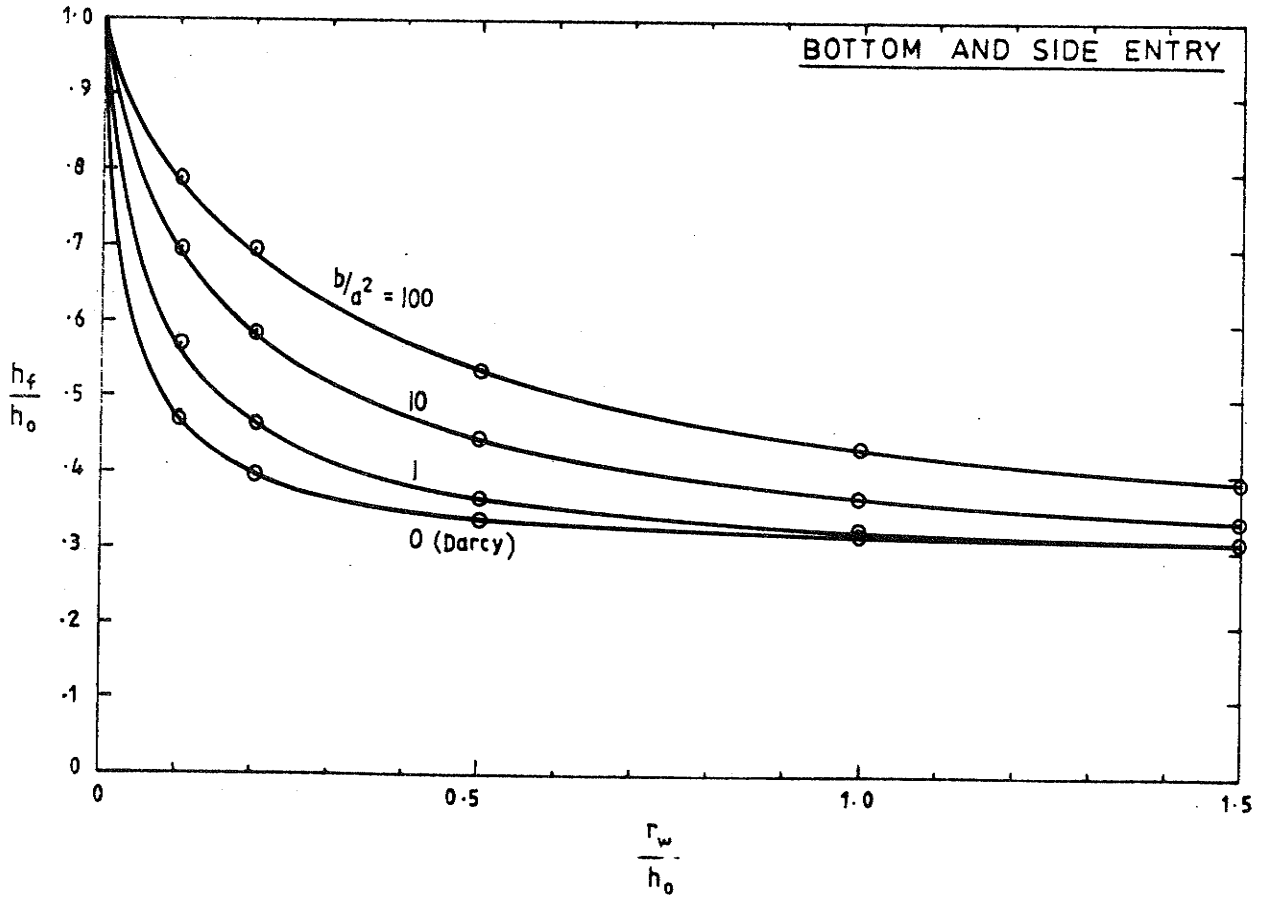

FIGURE 6·19: WATER LEVEL AT DE-WATERED CIRCULAR PIT IN UNCONFINED AQUIFER. $\frac{r_o}{h_o} = 100$ $\frac{h_b}{h_o} = 0{\cdot}3$

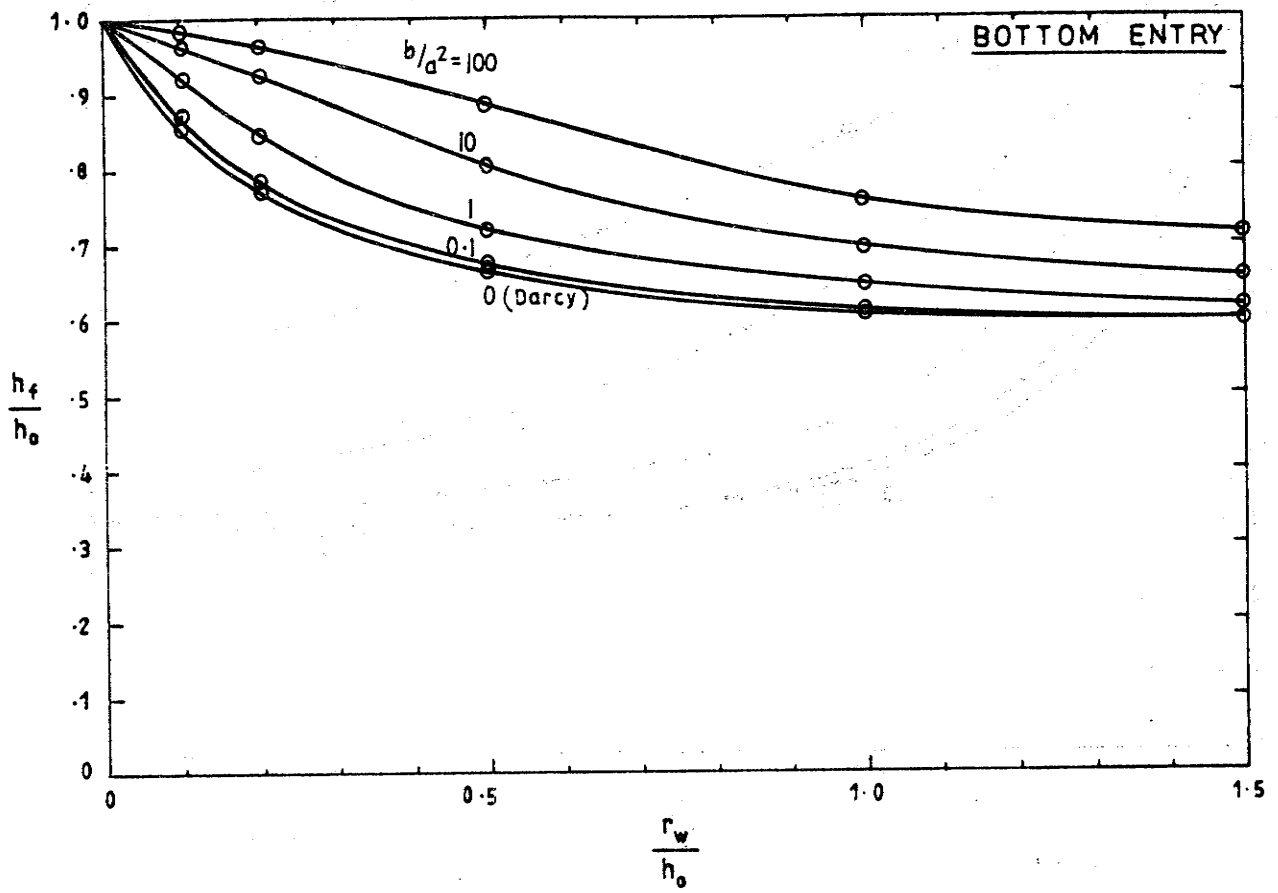

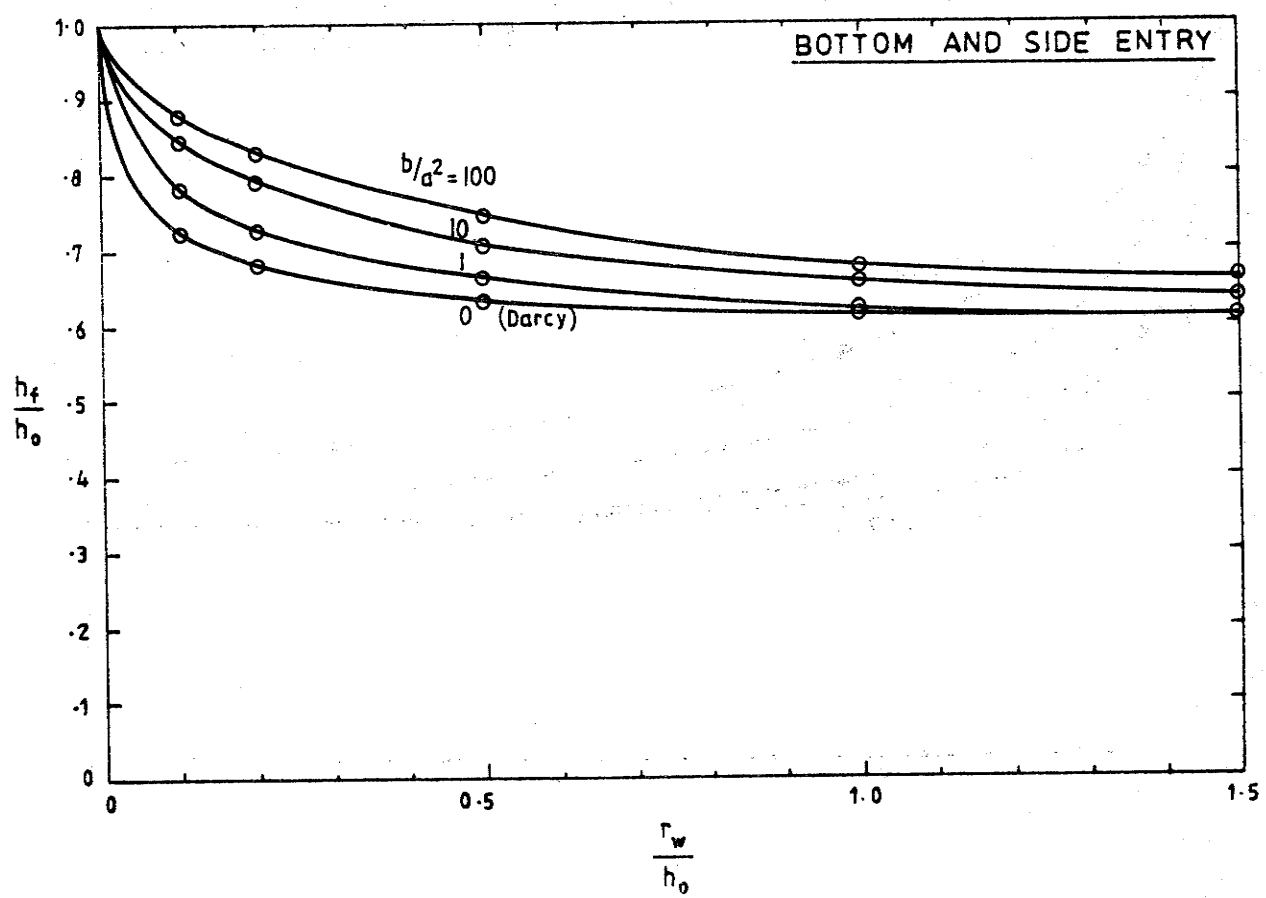

FIGURE 6·20: WATER LEVEL AT DE-WATERED CIRCULAR PIT IN UNCONFINED AQUIFER. $\frac{r_o}{h_o} = 8$ $\frac{h_b}{h_o} = 0{\cdot}6$

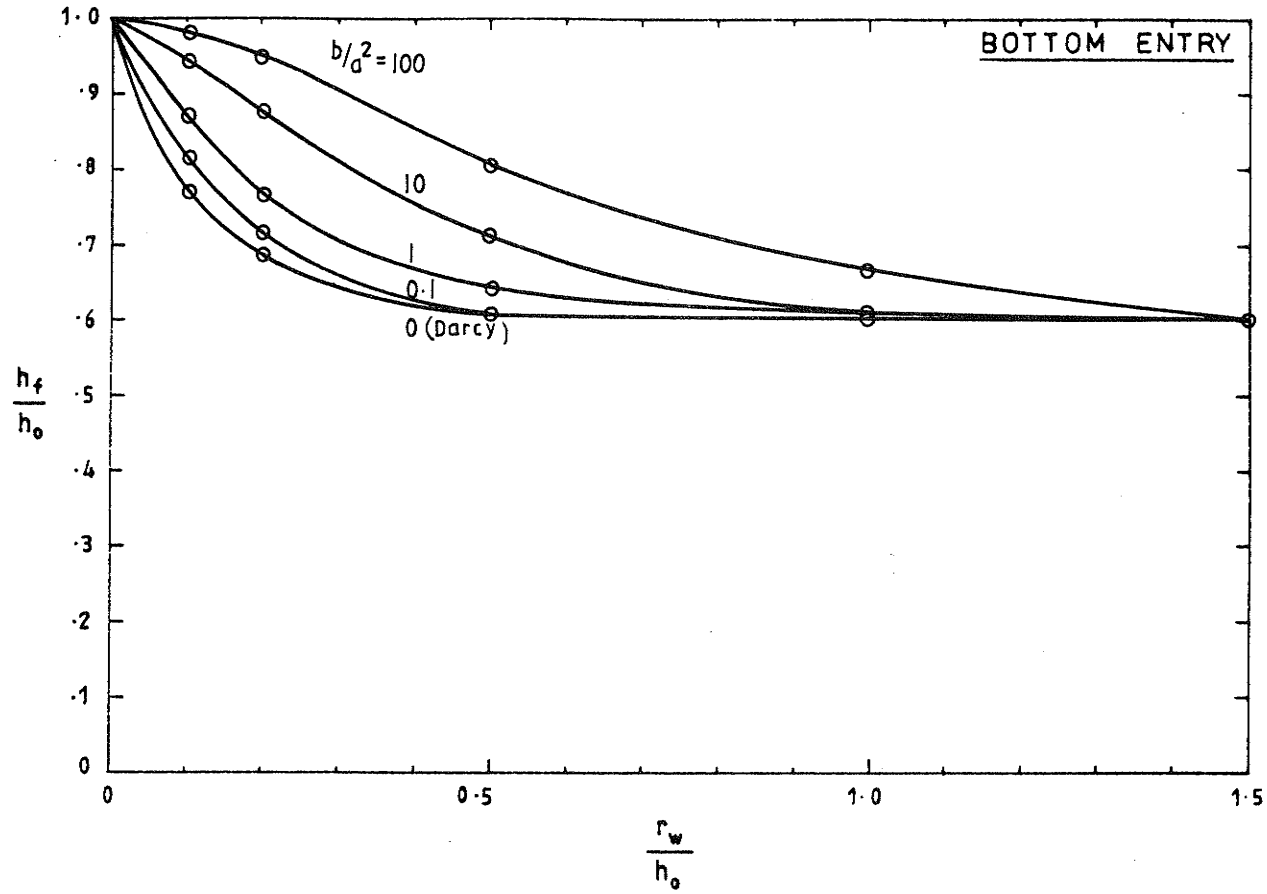

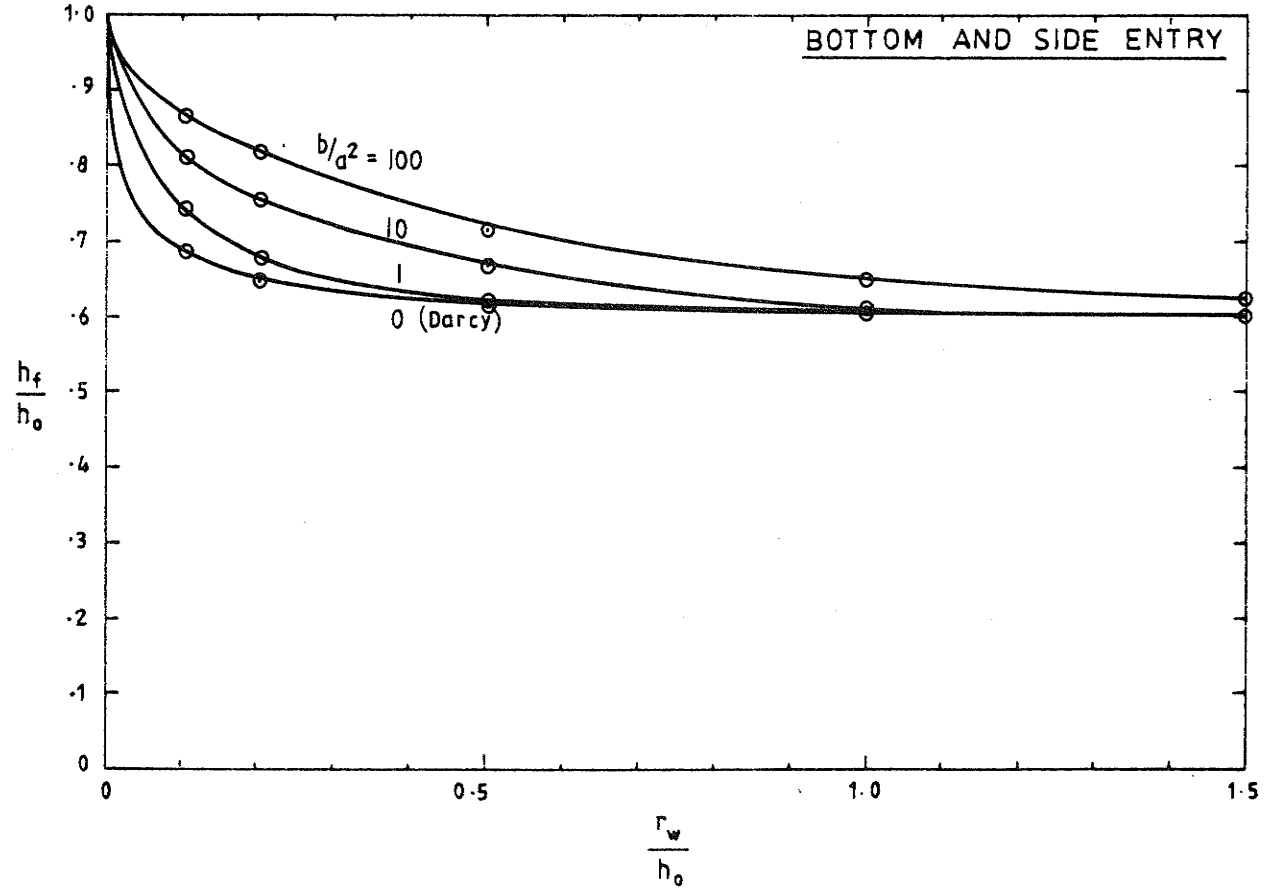

FIGURE 6·21: WATER LEVEL AT DE-WATERED CIRCULAR PIT IN UNCONFINED AQUIFER. $\frac{r_o}{h_o} = 100$ $\frac{h_b}{h_o} = 0{\cdot}6$

The figures again show the increased non-Darcy flow effect caused by restricting inflow to the bottom of the pit. There is, however, still a strong non-Darcy effect for the bottom and side entry case except for very large diameter shallow pits in all but the most permeable aquifers. As the pit becomes shallower and wider and the radius of influence increases, the difference between the bottom entry and bottom and side entry cases decreases since the water level at the de-watered pit approaches the level of the bottom of the pit in both cases.

6.3.3 Effect of Non-Darcy Flow On the Drawdown Cone Volume

Figures 6.22 to 6.27 show typical results of computation of the volume of de-watered aquifer material in the drawdown cone. The graphs have been extracted from Report No. 163. and the plotted points added to demonstrate the lack of scatter. Results for wholly Darcy flow ($b/a^2 = 0$) and non-Darcy flow in an aquifer with $b/a^2 = 10$ have been chosen for comparison.

The extent of the reduction of the de-watered cone volume caused by non-Darcy flow and restriction of inflow to the bottom of the pit can be seen from the figures. For wholly Darcy flow the difference between the results for the two entry conditions is significant only for small values of the ratio $\frac{r_w}{h_o}$ whereas for non-Darcy flow with $b/a^2 = 10$ the difference is significant over a much wider range of pit diameters and depths.

6.3.4 Variation Of Inflow Rate With Radius Of Influence

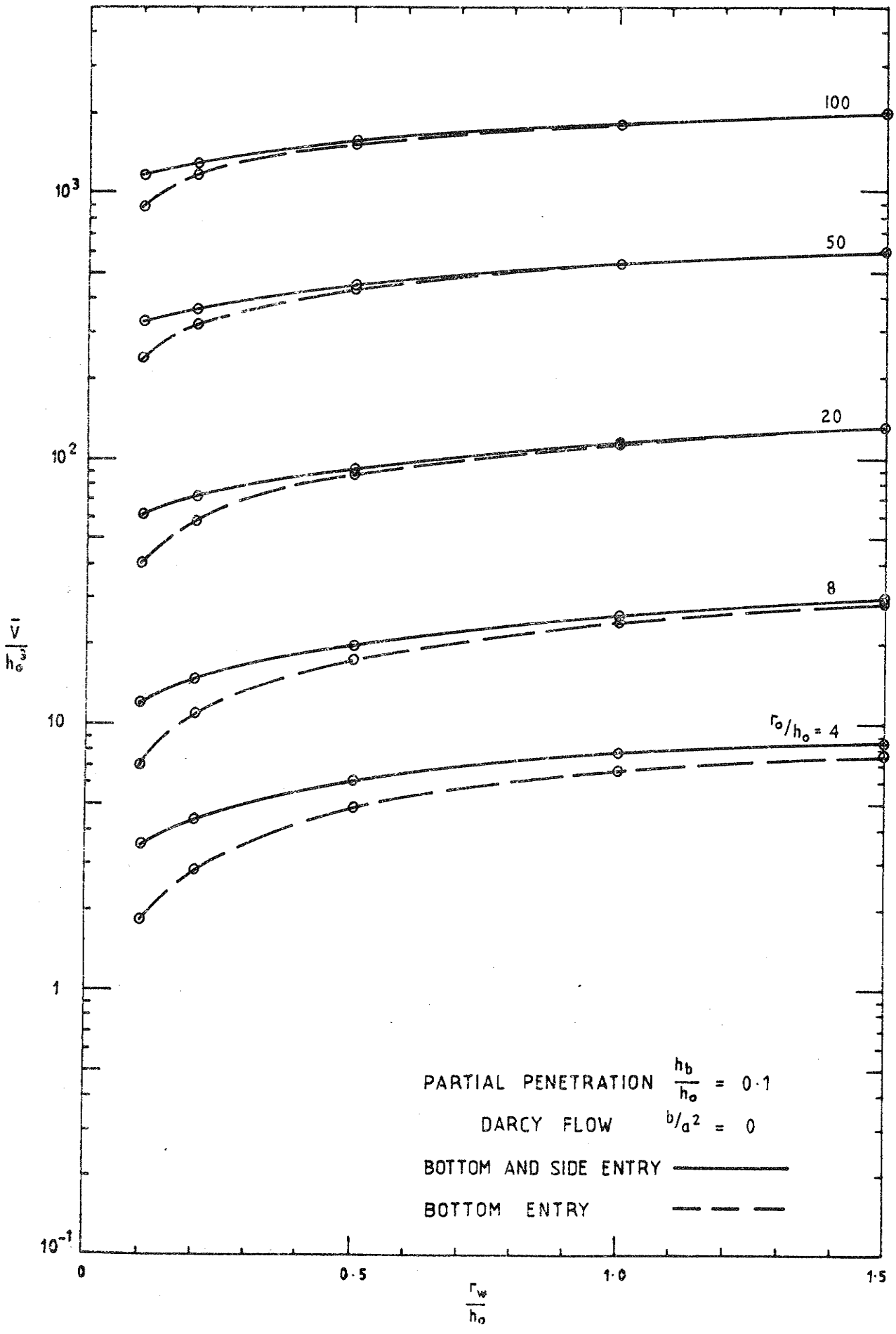

FIGURE 6·22: DIMENSIONLESS DRAWDOWN CONE VOLUME $\frac{\bar{V}}{h_o^3}$

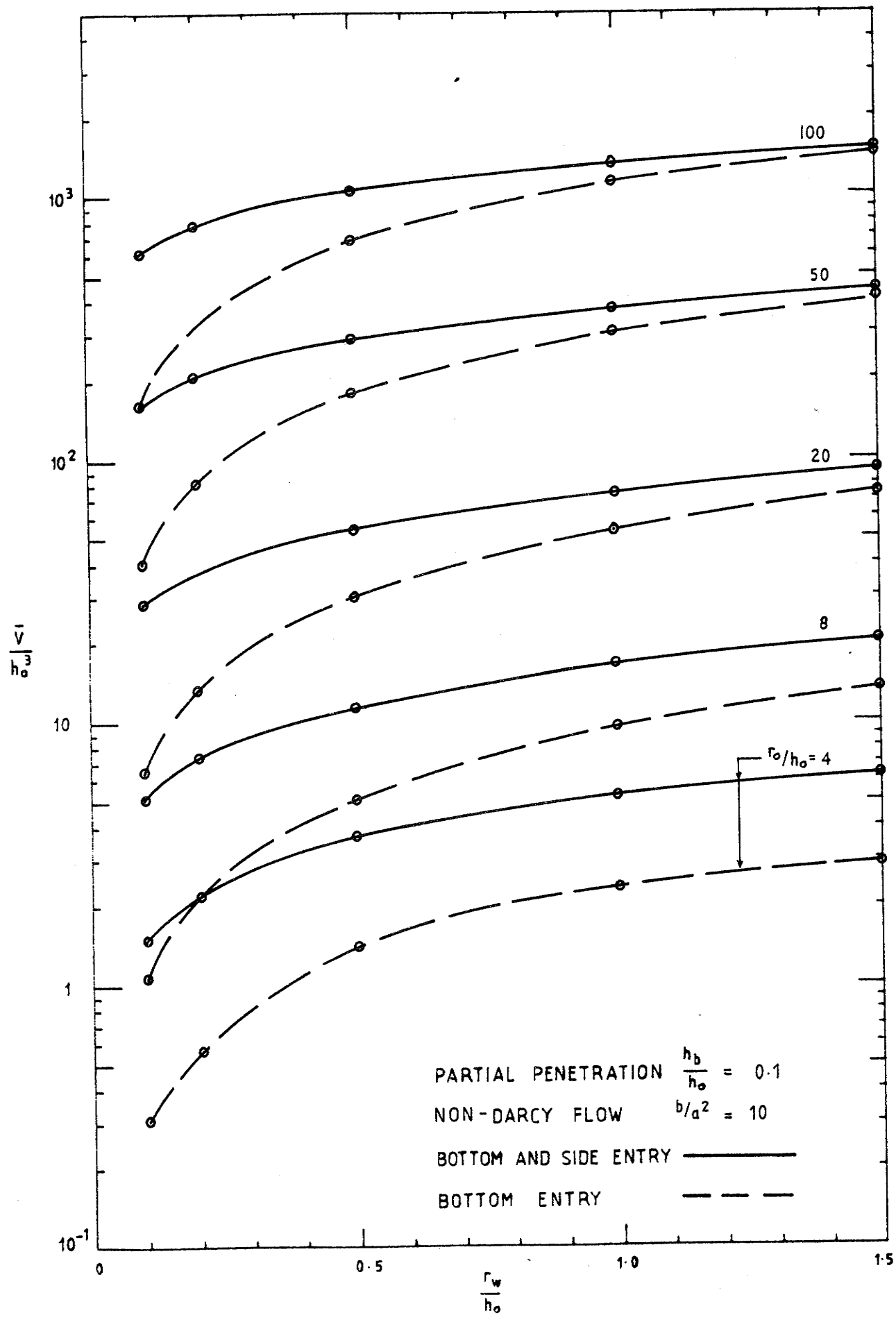

FIGURE 6·23: DIMENSIONLESS DRAWDOWN CONE VOLUME $\frac{\bar{V}}{h_o^3}$

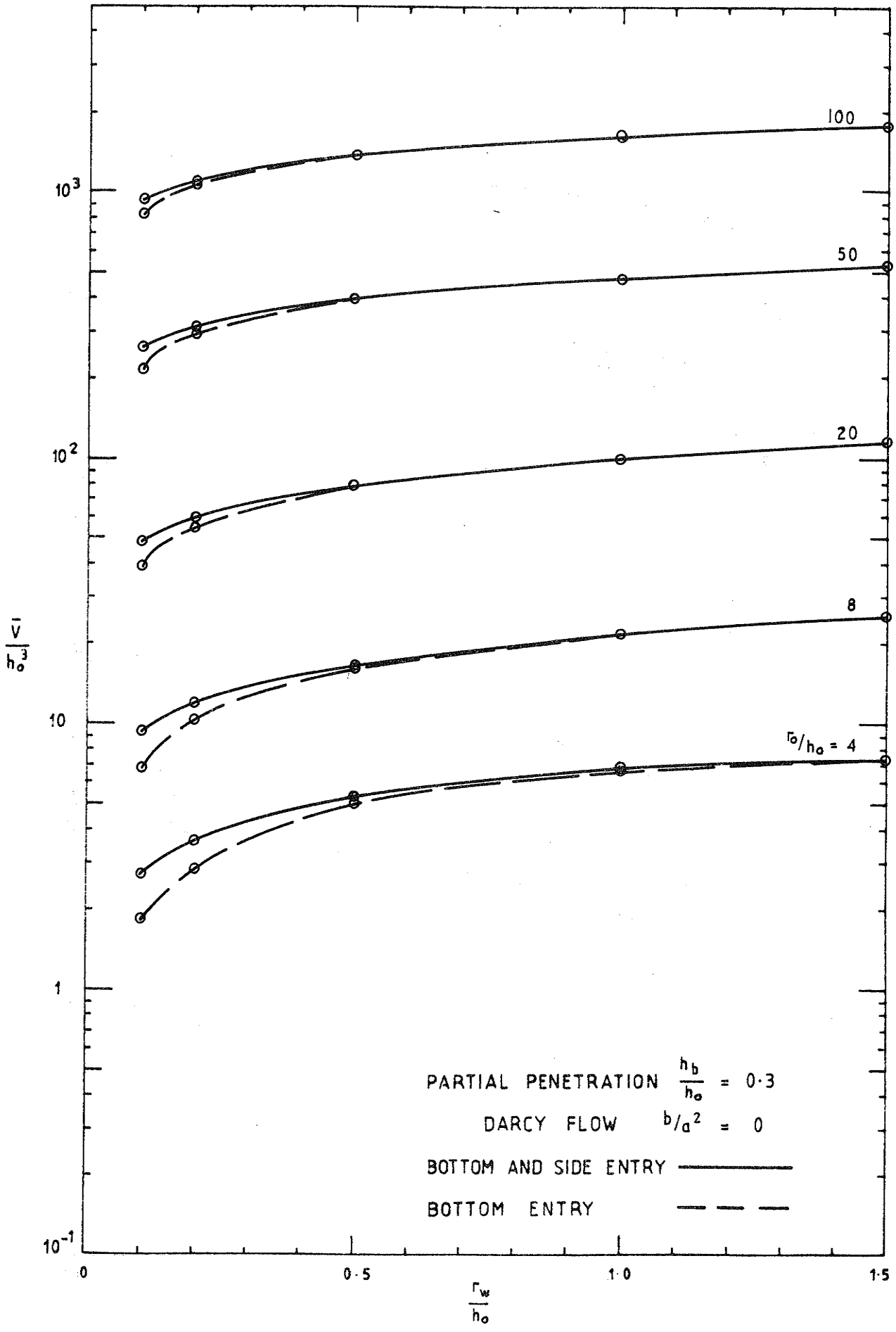

FIGURE 6·24: DIMENSIONLESS DRAWDOWN CONE VOLUME $\frac{\bar{V}}{h_o^3}$

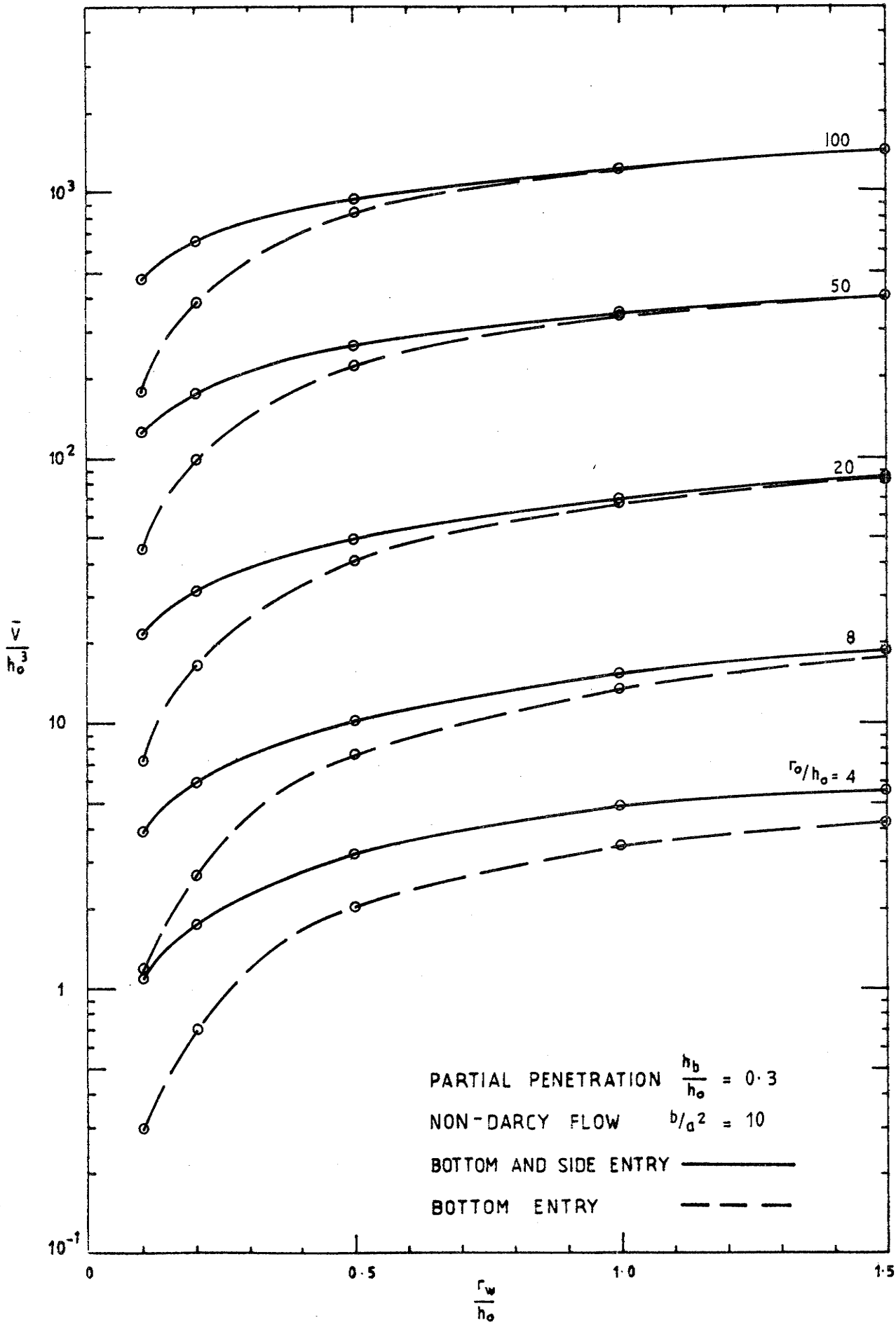

FIGURE 6·25: DIMENSIONLESS DRAWDOWN CONE VOLUME $\frac{\bar{V}}{h_o^3}$

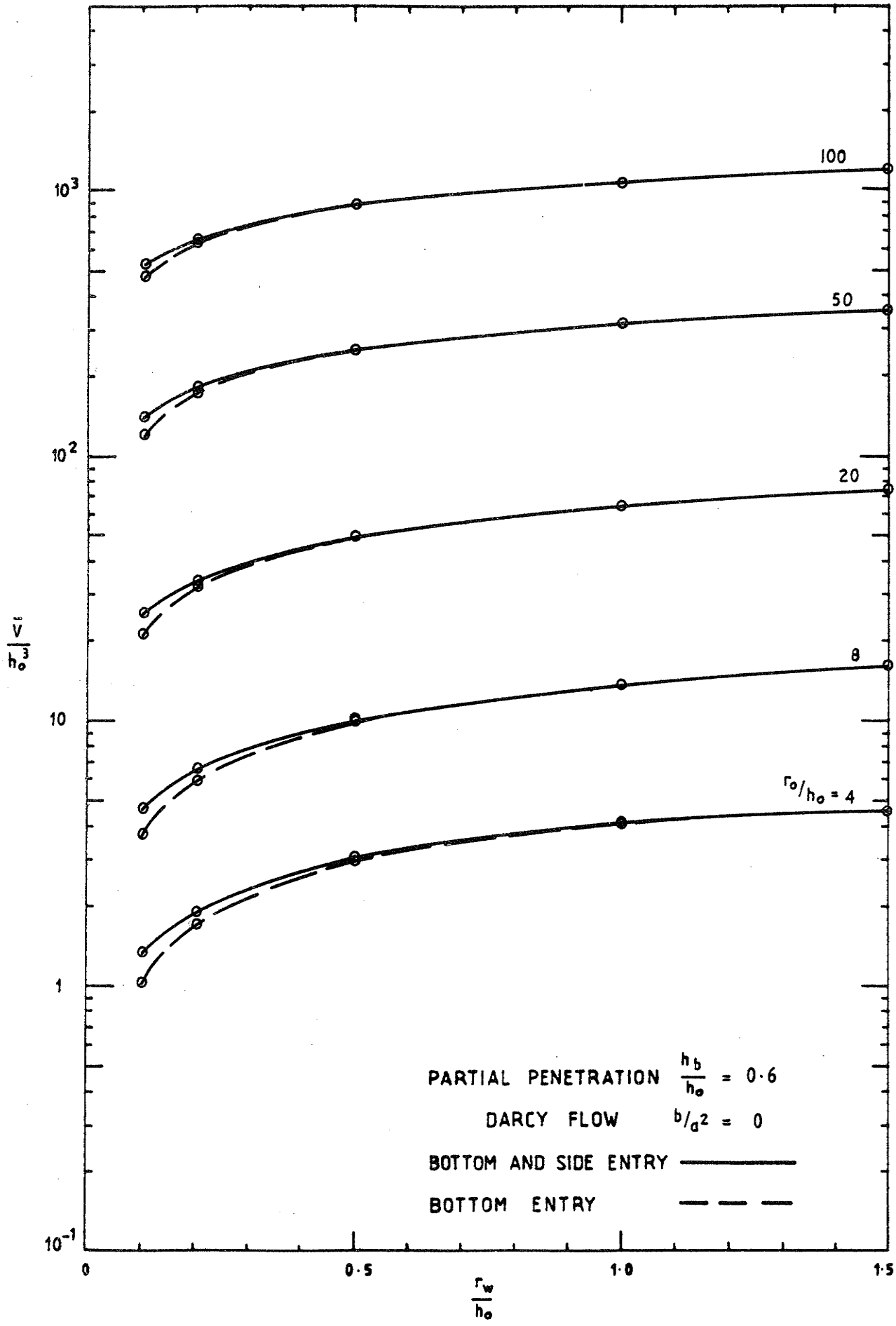

FIGURE 6·26: DIMENSIONLESS DRAWDOWN CONE VOLUME $\frac{\bar{V}}{h_o^3}$

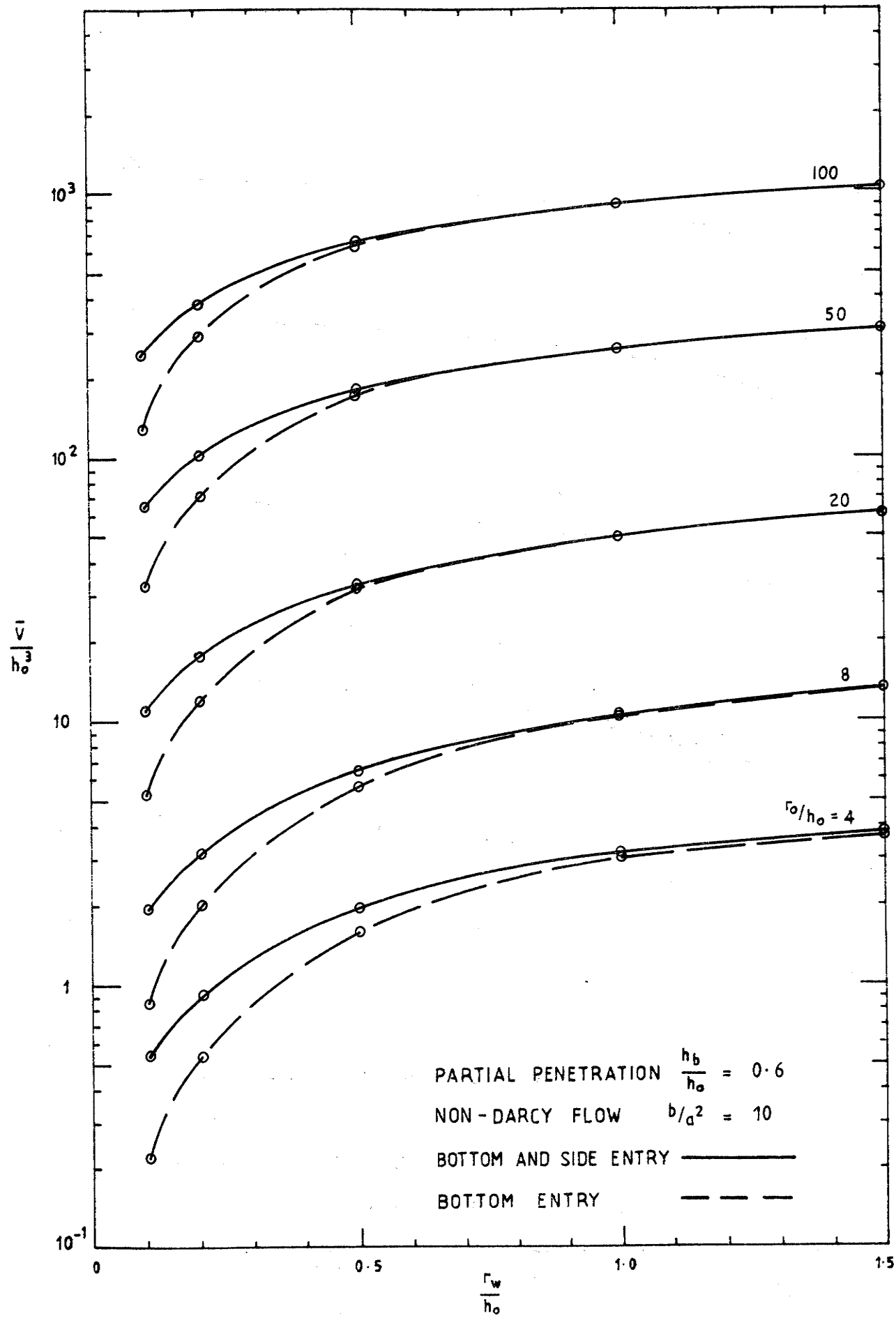

FIGURE 6·27: DIMENSIONLESS DRAWDOWN CONE VOLUME $\frac{\bar{V}}{h_o^3}$

The effect of the radius of influence on the inflow rate into a pit can be determined by selecting appropriate data from the relevant range of tables or figures in Report No. 163. The data can then be plotted to show the form of the relationship. Figures 6.28 to 6.31 have been produced from the data in Tables B.3, B.5, B.8 and B.12 in Report No. 163 to illustrate the difference between the effect of radius of influence for wholly Darcy flow and non-Darcy flow with $b/a^2 = 10$. For relatively small diameter pits non-Darcy flow acts to stabilise the inflow rate. For example, the $b/a^2 = 10$ line in Figure 6.29 is horizontal for $\frac{r_o}{h_o}$ values greater than 0.1. The sensitivity of the flow rate to change in the radius of influence increases with decreasing radius of influence and non-Darcy flow parameter b/a^2 until, for Darcy flow to a pit for which $\frac{r_w}{h_o} = 1.5$, the rate of change of inflow approaches infinity as $\frac{r_o}{h_o}$ approaches zero.

The effect of restricting inflow to the bottom of the pit in reducing the sensitivity of the flow rate to the radius of influence can be seen by comparison of Figures 6.28 and 6.29 and Figures 6.30 and 6.31. The effect of the restriction increases as the non-Darcy flow parameter b/a^2 increases.

During the excavation of an open cut mine in an extensive aquifer the effective radius of influence extends with time as pumping proceeds. At the same time the depth of penetration increases as the excavation is deepened. The two changes have opposing effects on the inflow rate and the net effect can be an overall reduction in the inflow rate over the life of the mine. If the rate at which the mine will be deepened is known, the net effect can be estimated by selecting data from Report No. 163 which allow for variation in both radius of influence and depth of

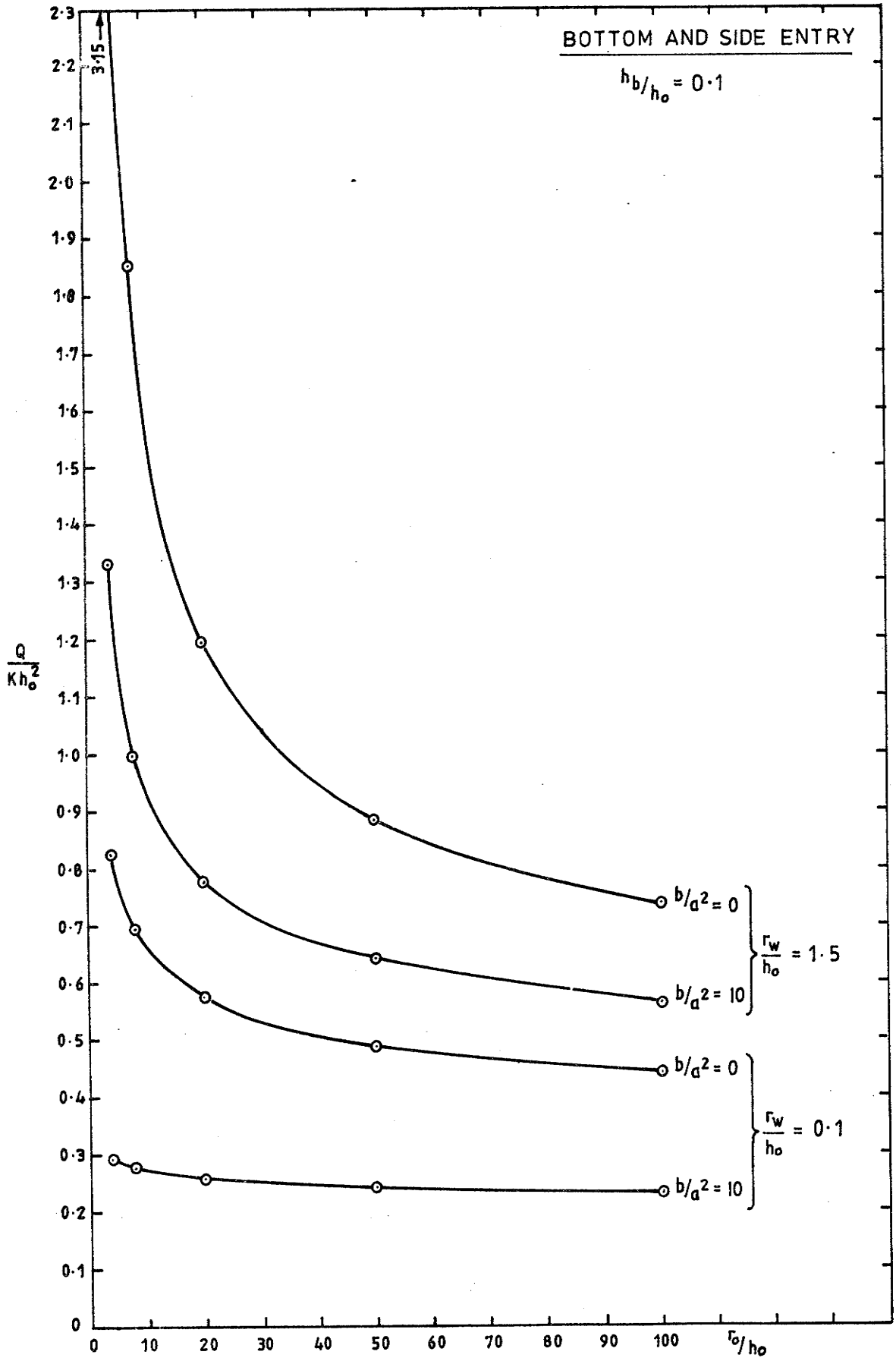

FIGURE 6·28: DE-WATERED CIRCULAR PIT IN UNCONFINED AQUIFER
VARIATION OF INFLOW RATE WITH
RADIUS OF INFLUENCE

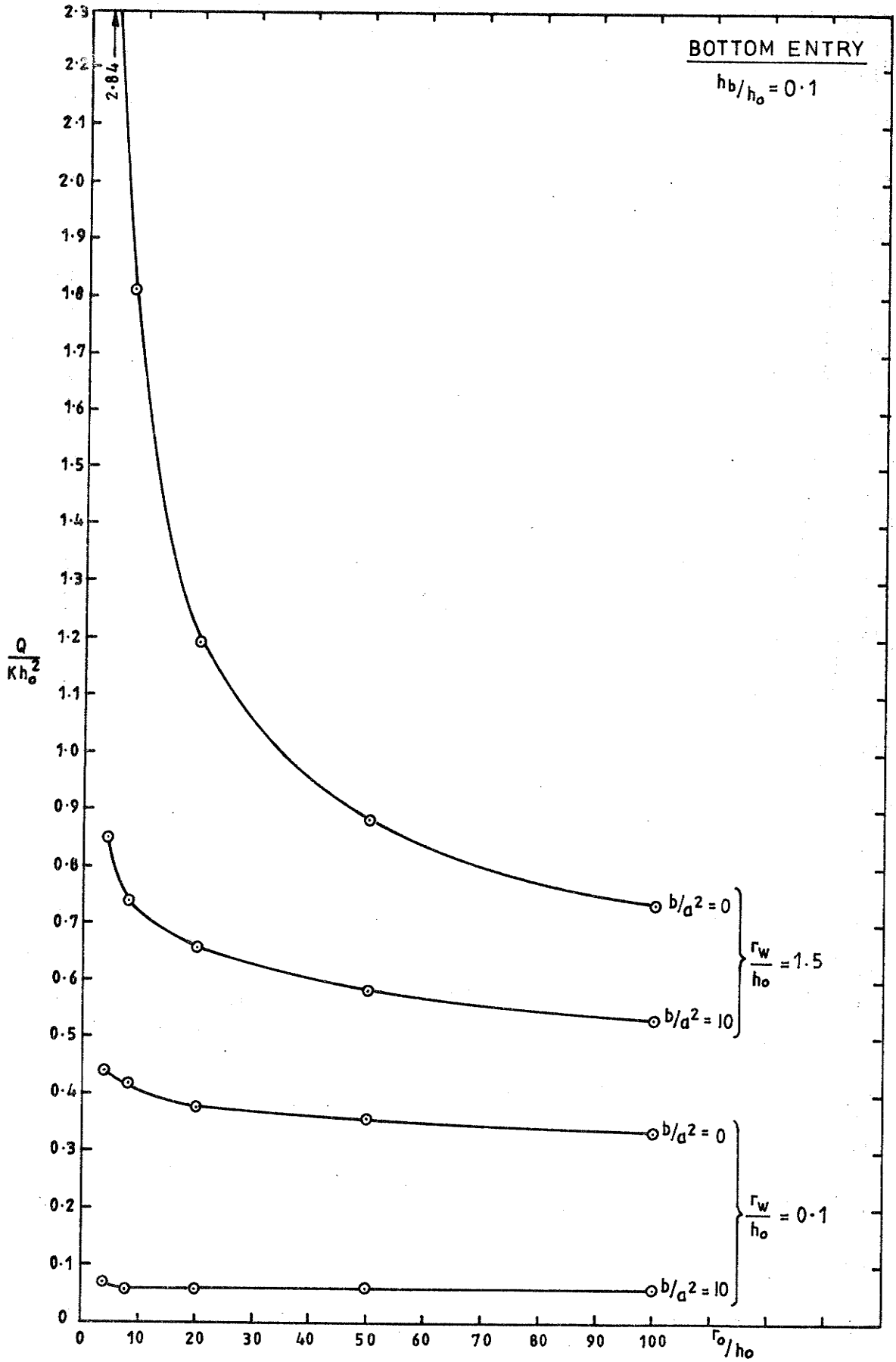

FIGURE 6·29: DE-WATERED CIRCULAR PIT IN UNCONFINED AQUIFER
VARIATION OF INFLOW RATE WITH
RADIUS OF INFLUENCE

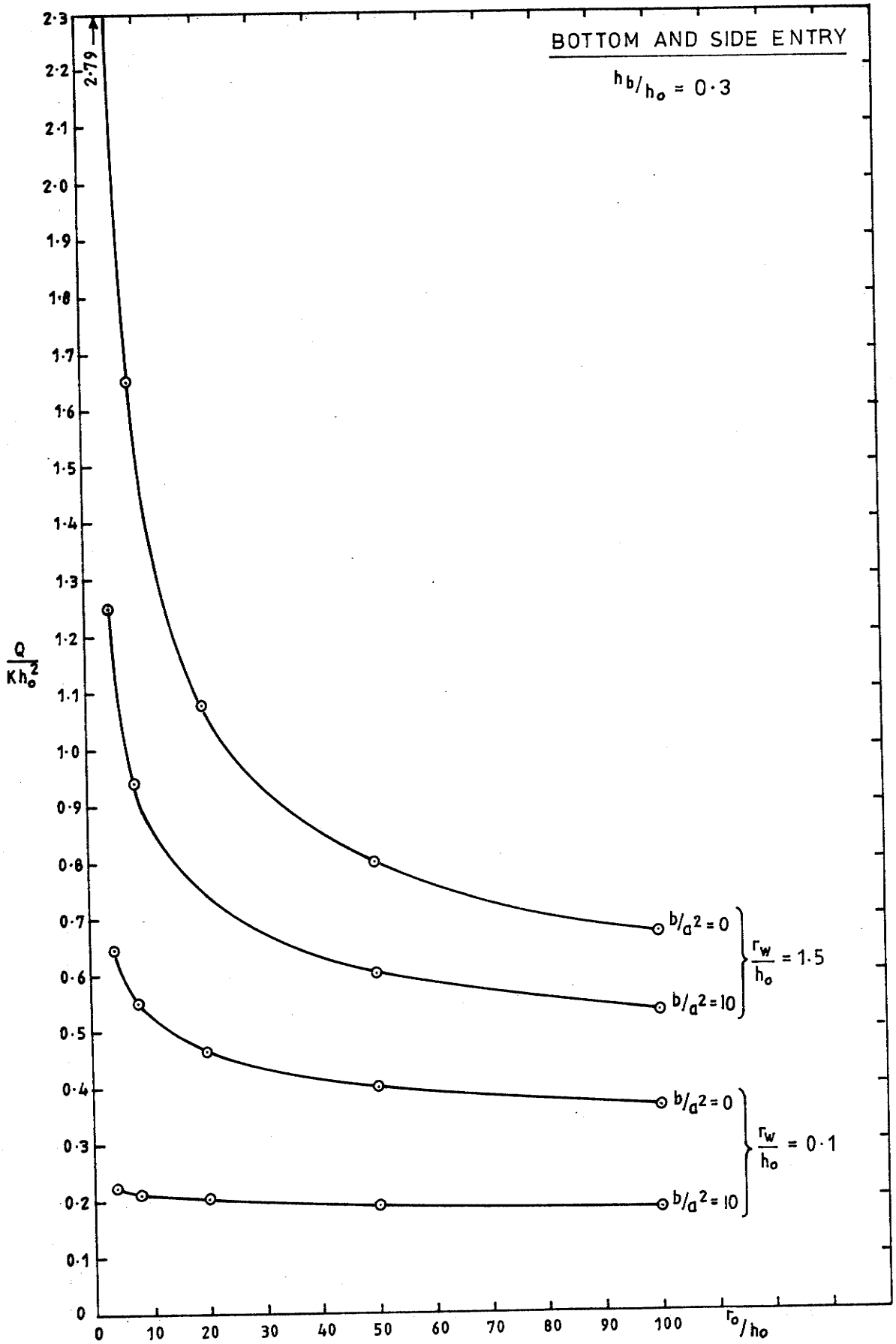

FIGURE 6·30: DE-WATERED CIRCULAR PIT IN UNCONFINED AQUIFER VARIATION OF INFLOW RATE WITH RADIUS OF INFLUENCE

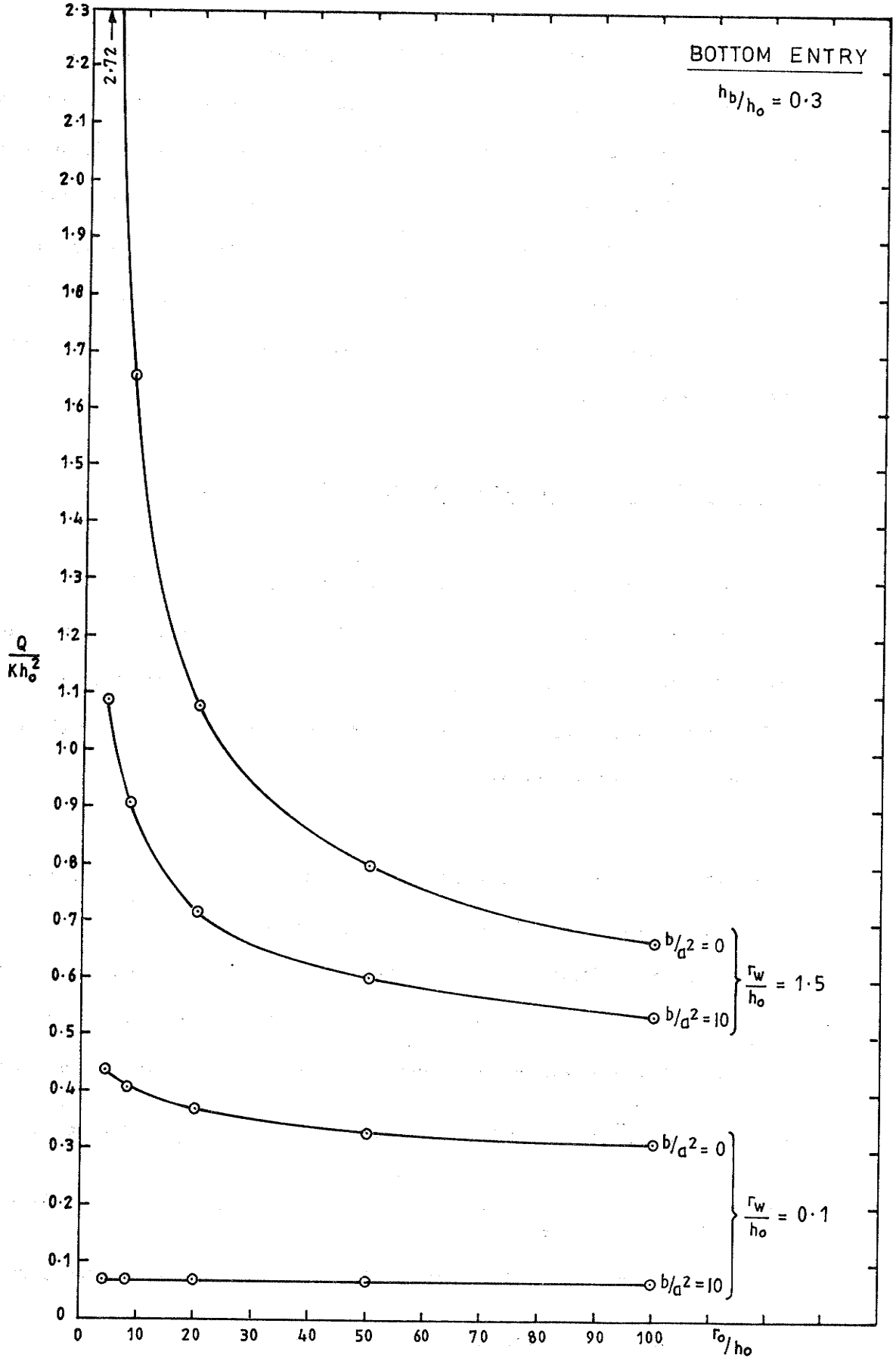

FIGURE 6·31: DE-WATERED CIRCULAR PIT IN UNCONFINED AQUIFER VARIATION OF INFLOW RATE WITH RADIUS OF INFLUENCE

penetration. Care should be exercised in estimating the effective diameter of the expanding pit. It will normally be the diameter inside the first bench above the bottom since the free surface near the pit will be less steep than the average pit wall slope. However, a high rate of excavation, low aquifer permeability, or the presence of aquitard layers may prevent the water surface at the pit falling to near the level of the base of the pit. This is, however, unlikely for aquifers in which non-Darcy flow is significant.

6.3.5 Variation Of Inflow Rate With Depth Of Penetration

Figures 6.32 to 6.34 have been plotted from data in Tables B.1 to B.14 in Report No. 163 to show the difference between the combined effects of depth of penetration and non-Darcy flow on the rate of flow into pits with bottom and side entry and those for which the inflow is restricted to the bottom of the pit.

For pits with only bottom entry the inflow rate reaches a maximum and then falls as the bottom of the pit approaches the base of the aquifer. Non-Darcy flow causes a shift in the degree of penetration for which the maximum inflow occurs. Figure 6.34 shows that the penetration ratio for which the maximum flow occurs changes from a value in excess of 90 per cent ($\frac{h_b}{h_o} = 0.1$) for Darcy flow to a ratio of approximately 70 per cent ($\frac{h_b}{h_o} = 0.3$) for $\frac{b}{a^2} = 10$ and $\frac{r_o}{h_o} = 8$ and 80 per cent for $\frac{b}{a^2} = 10$ and $\frac{r_o}{h_o} = 100$. Non-Darcy flow also flattens the peaks of the curves. This is particularly evident in Figure 6.32(b).

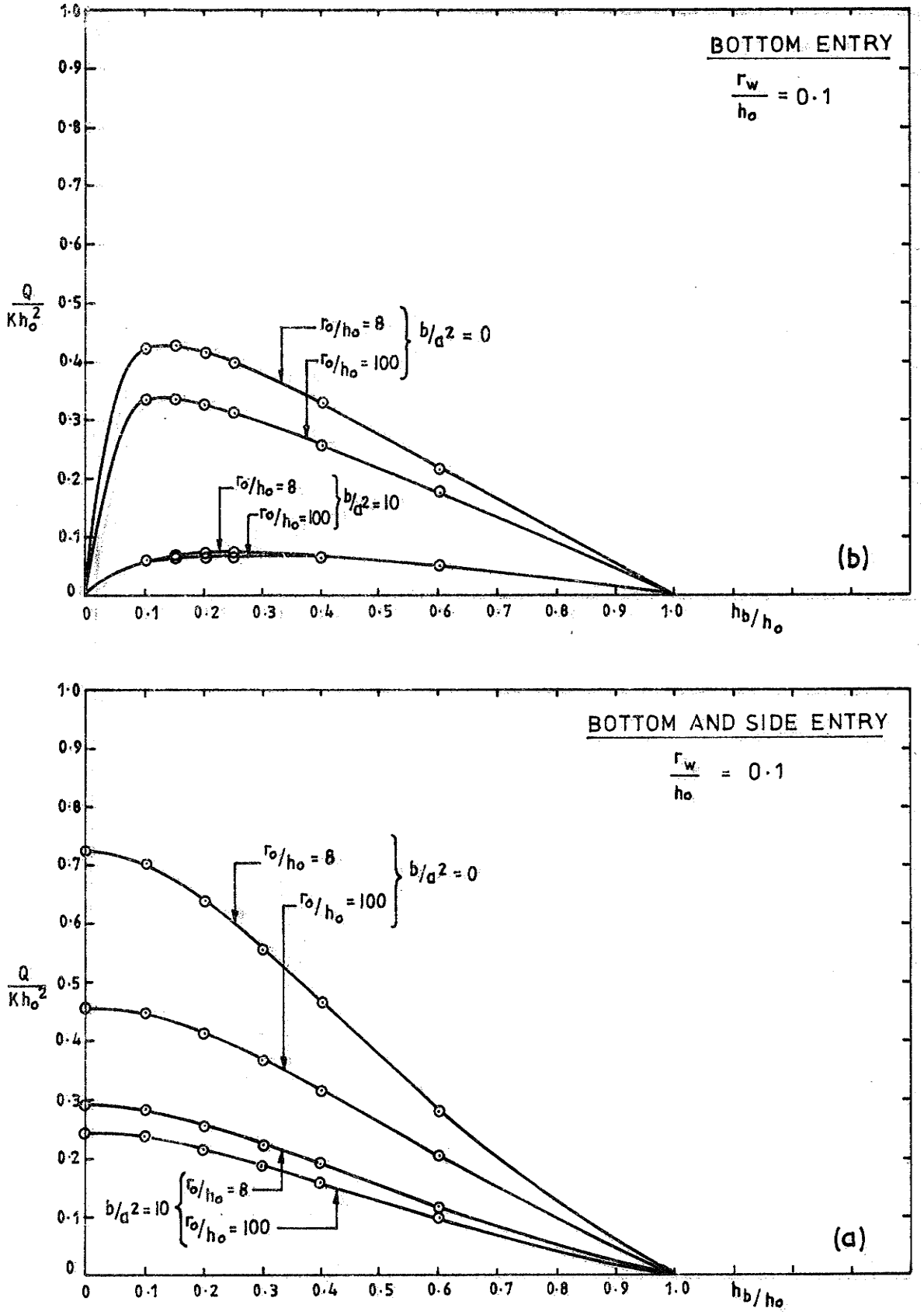

FIGURE 6·32: DE-WATERED CIRCULAR PIT IN UNCONFINED AQUIFER VARIATION OF INFLOW WITH DEPTH OF PENETRATION

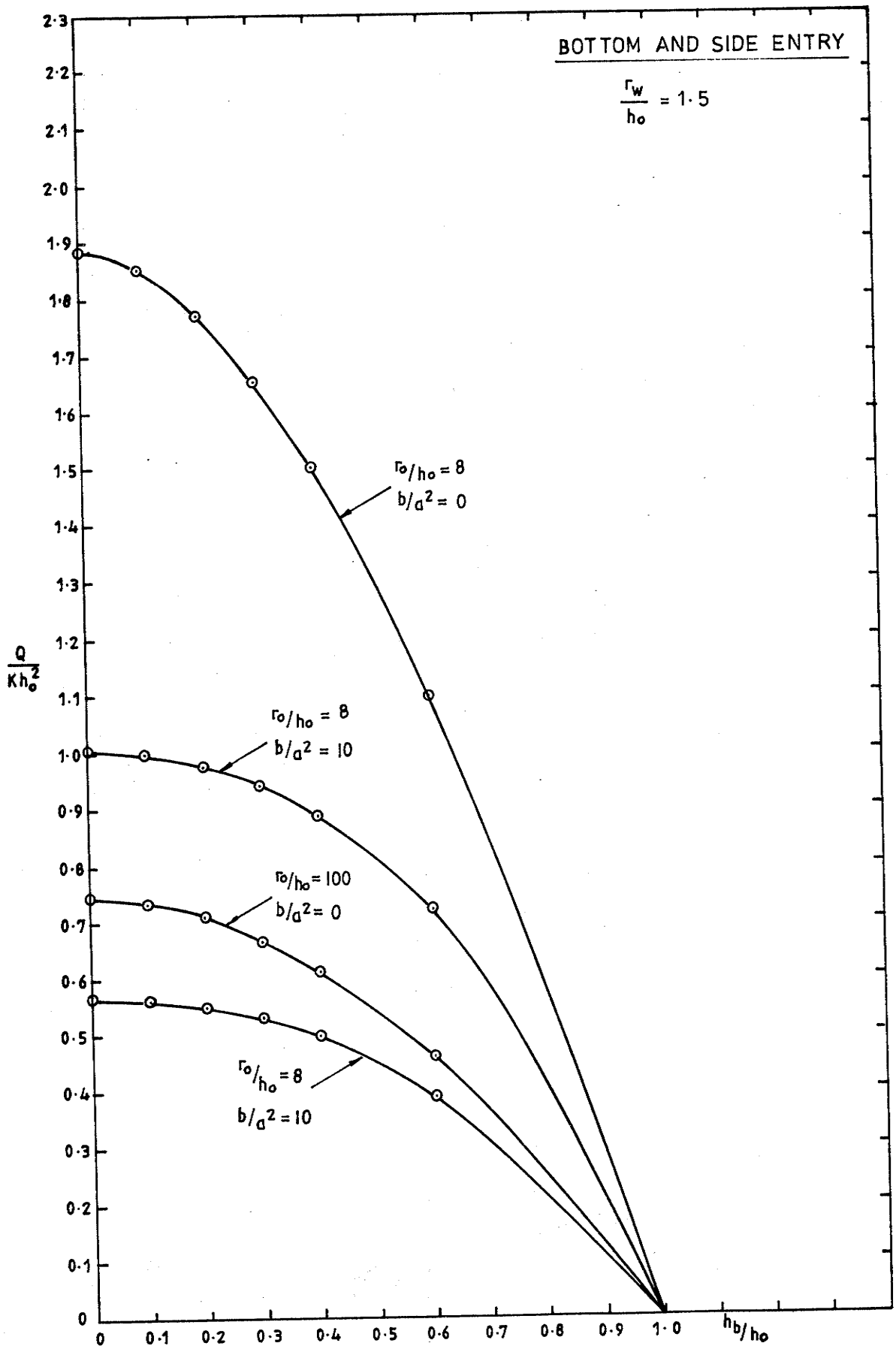

FIGURE 6·33: DE-WATERED CIRCULAR PIT IN UNCONFINED AQUIFER
VARIATION OF INFLOW RATE WITH
DEPTH OF PENETRATION

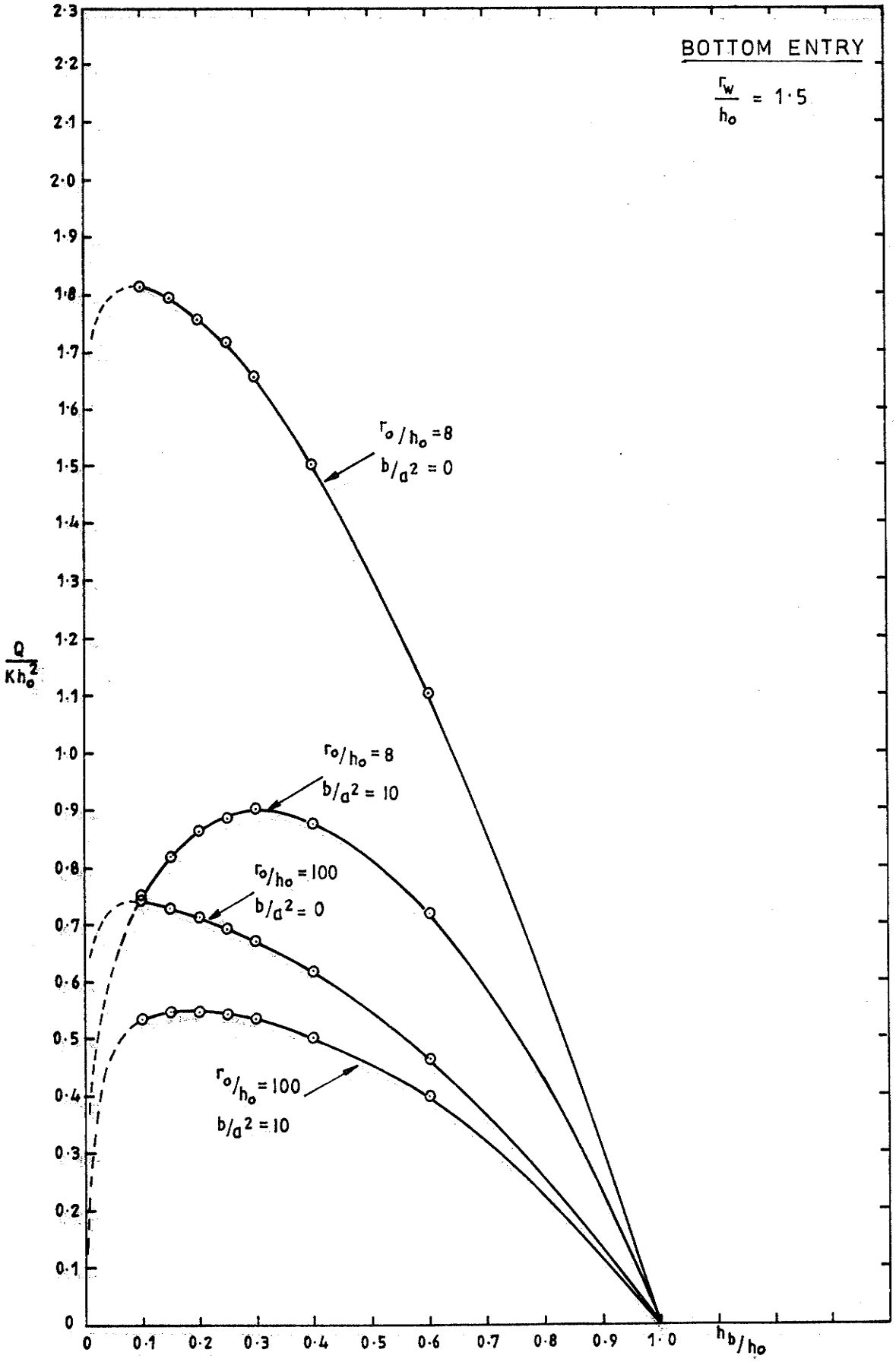

FIGURE 6·34: DE-WATERED CIRCULAR PIT IN UNCONFINED AQUIFER VARIATION OF INFLOW WITH DEPTH OF PENETRATION

Although non-Darcy head losses have the effect of throttling flow into a well and thus reducing the maximum flow rate, compensating effects occur. If non-Darcy flow occurs, bottom entry wells can penetrate less of the aquifer to achieve a near maximum inflow rate than if wholly Darcy flow occurs.

Similar compensations occur when side entry is allowed. Inflow into pits with both bottom and side entry, such as open cut mines, does not approach zero as full penetration is approached. However, the curves plotted in Figure 6.32 demonstrate that non-Darcy flow restricts the rate of increase in flow rate as the depth of penetration increases.

6.3.6 Variation of Water Level At A Pit With Radius Of Influence

Figures 6.35 and 6.36 plotted from data in Tables B.3, B.5, B.8 and B.12 in Report No. 163 show the effect of radius of influence on the water level at a de-watered pit. The effect is similar to, but less extreme than, the effect on the inflow rate discussed in Section 6.3.4. The water level is relatively insensitive to radius of influence for $\frac{r_o}{h_o}$ values greater than 20. Non-Darcy flow prevents the water level from falling as far as it does for the same pit and aquifer geometry and wholly Darcy flow. This is significant in aquifer de-watering operations. It also has the effect of restricting the regional impact of de-watering open cut mines and other excavations.

6.3.7 Variation Of Water Level At A Pit With Depth Of Penetration

The effect on the water level at a pit of varying the depth of penetration when non-Darcy flow occurs can be seen from Figures 6.37 and

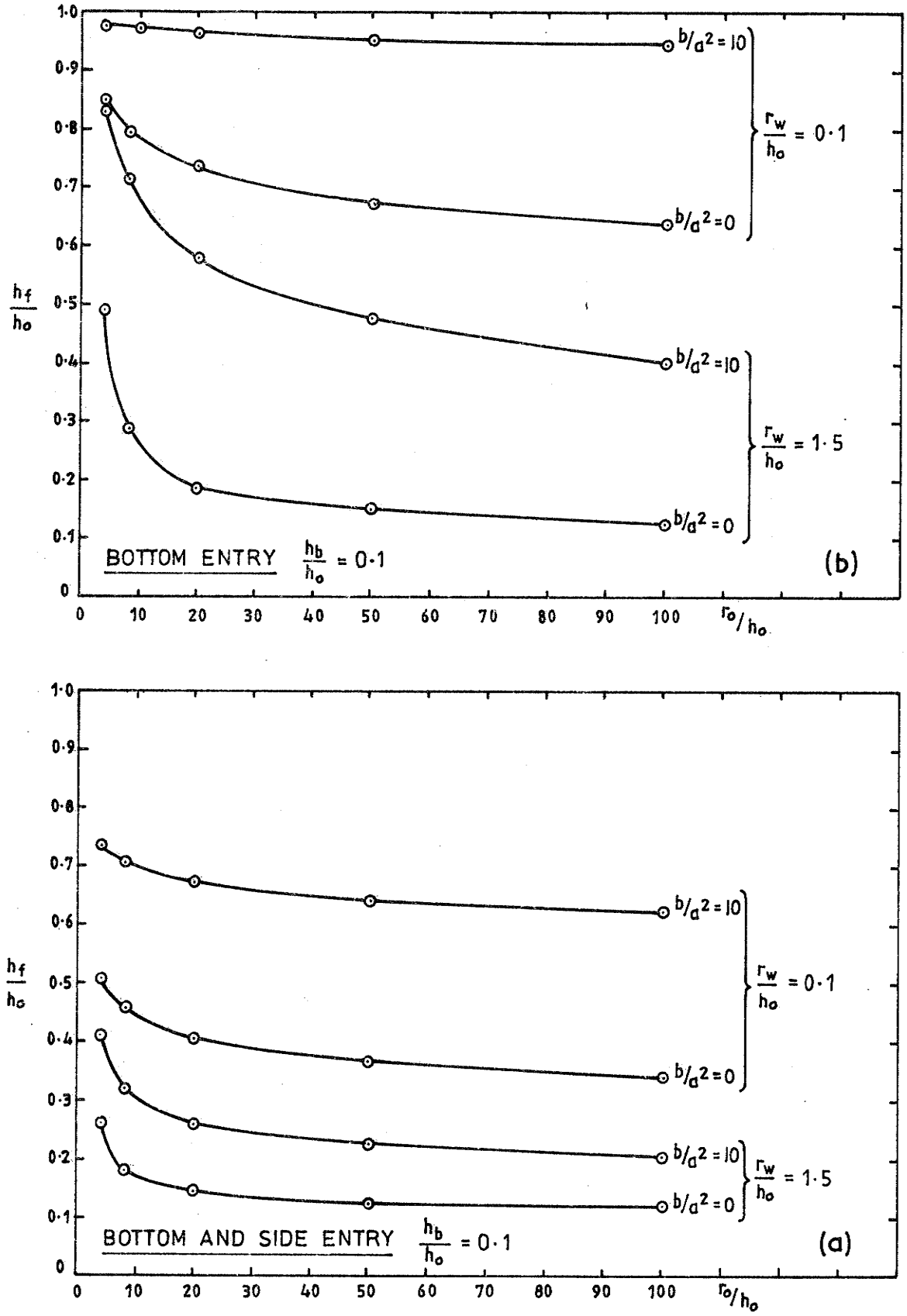

FIGURE 6·35: DE-WATERED CIRCULAR PIT IN UNCONFINED AQUIFER VARIATION OF WATER LEVEL AT PIT WITH RADIUS OF INFLUENCE

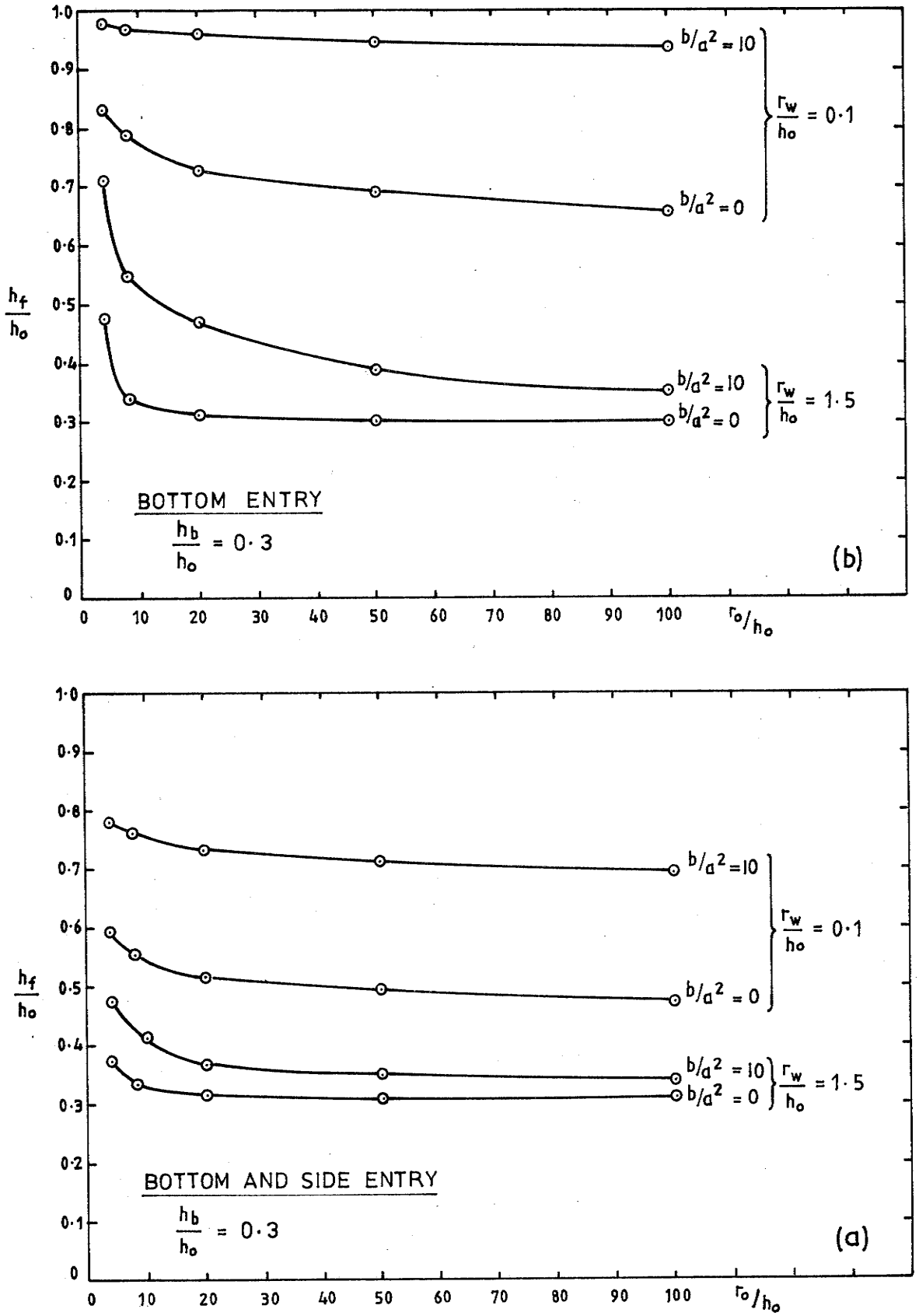

FIGURE 6·36: DE-WATERED CIRCULAR PIT IN UNCONFINED AQUIFER VARIATION OF WATER LEVEL AT PIT WITH RADIUS OF INFLUENCE

6.38 which have been plotted using data from Tables B.1 to B.14 in Report No. 163. For bottom entry pits with diameters near the upper end of the $\frac{r_w}{h_o}$ range covered by the computations a distinct minimum occurs in the computed water levels. For other cases the minimum is not as pronounced or does not occur in the range of $\frac{h_b}{h_o}$ covered by the results. A minimum must occur in all cases since h_f must equal h_o when $\frac{h_b}{h_o} = 0$ for bottom entry pits. Thus the minima must occur for $\frac{h_b}{h_o} < 1$ for those cases where a minimum value has not been reached. In these cases the subsequent rise in level must be very steep.

Non-Darcy flow reduces the influence of partial penetration on the water level, particularly for smaller pit diameters. Figure 6.37(b) shows that for $\frac{b}{a^2} = 10$ and $\frac{r_w}{h_o} = 0.1$ there is little fall in the water level at the pit after a penetration ratio of 40 per cent ($\frac{h_b}{h_o} = 0.6$) has been exceeded.

6.3.8 Distribution Of Inflow Into Pit

Examination of the computed inflow increments at nodes situated along the pit boundary shows that the inflow is concentrated to a large extent at the bottom "corner" of the pit. This is particularly so for the bottom entry case since the impermeable side boundary forces additional flow to the bottom boundary. The shortest path into the pit is via the "corner" so it is inevitable that flow will be concentrated at this point. A compensating effect is the additional head loss caused by the higher velocities, particularly when non-Darcy flow occurs.

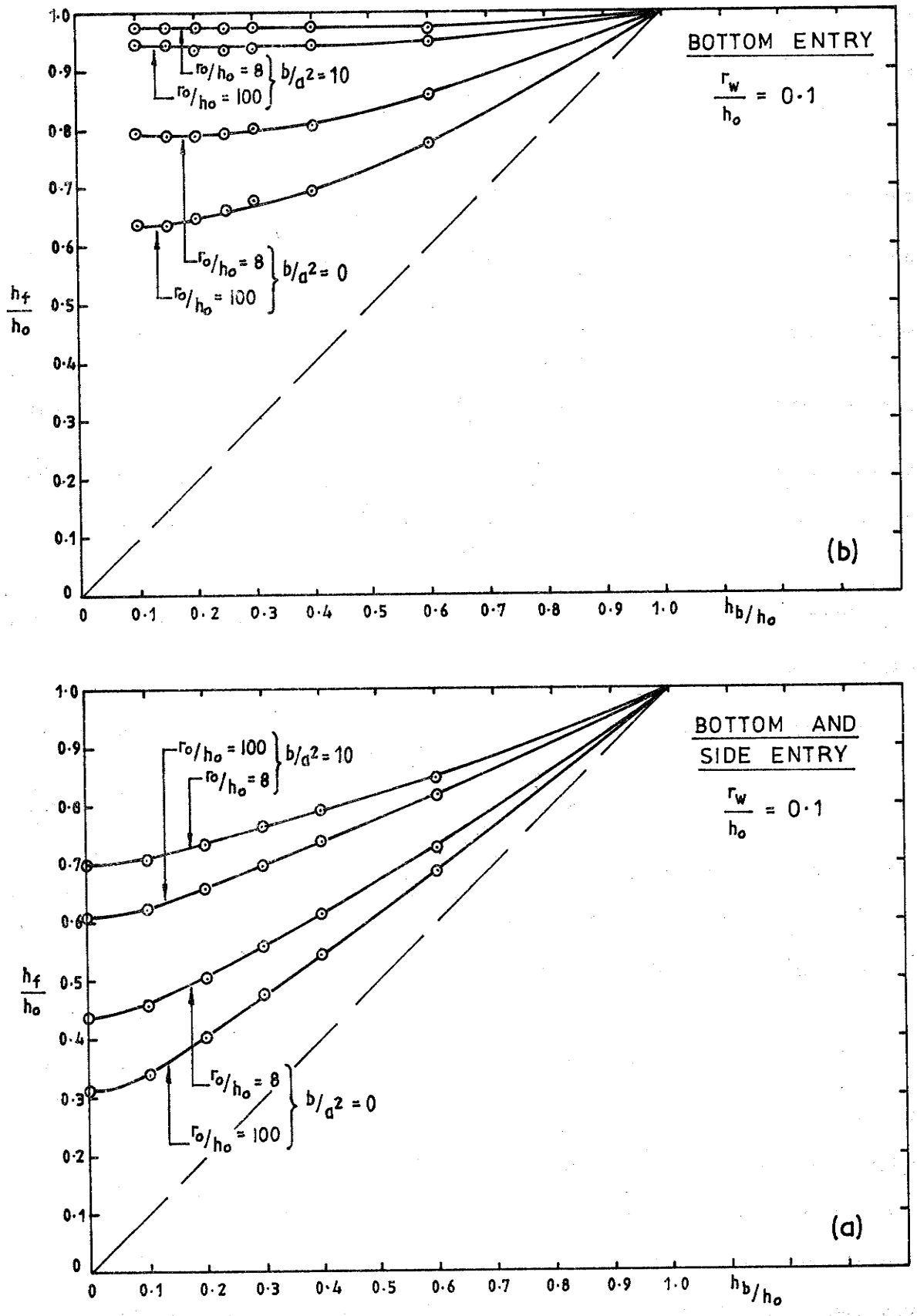

FIGURE 6·37: DE-WATERED CIRCULAR PIT IN UNCONFINED AQUIFER VARIATION OF WATER LEVEL AT PIT WITH DEPTH OF PENETRATION

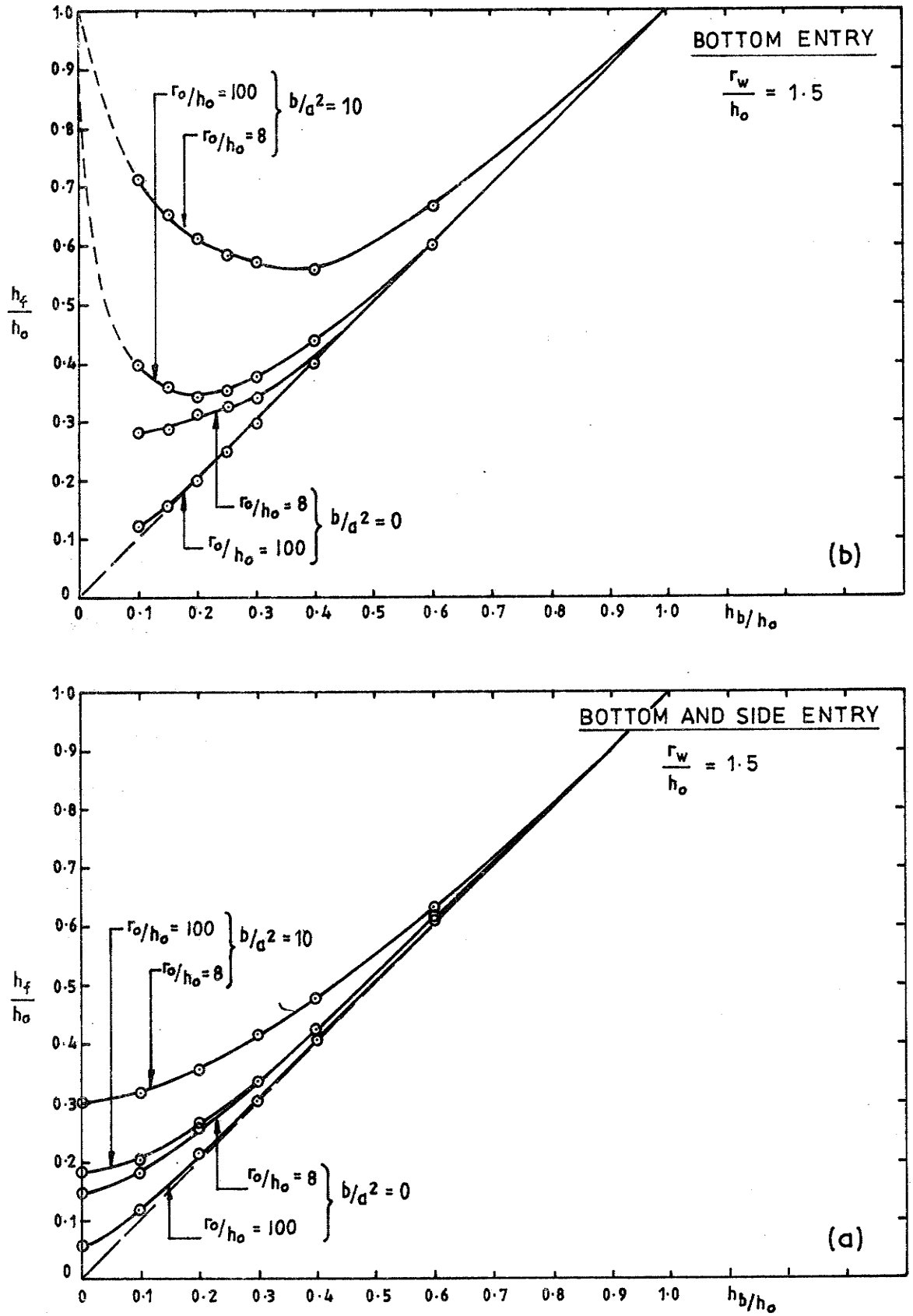

FIGURE 6·38: DE-WATERED CIRCULAR PIT IN UNCONFINED AQUIFER VARIATION OF WATER LEVEL AT PIT WITH DEPTH OF PENETRATION

Since it is impractical to include inflow distributions computed for all flow cases covered in the determination of the dimensionless relationships provided in Report No. 163. only typical distributions for extreme cases are given. These are shown in Figure 6.39. They show the effect of non-Darcy flow in modifying the inflow distribution.

6.4 Extension Of Results For Larger Values Of Radius Of Influence

Although the highest value of $\frac{r_o}{h_o}$ for which results are given should cover most of the practical applications it may be necessary to extrapolate to higher values. For cases in which the plotted curves are approximately straight at $\frac{r_o}{h_o} = 100$ it may be sufficient to extend the curves by eye or by fitting a polynomial equation with the aid of a calculator. For greater extensions, or where the curves have not approached straight lines, the basic flow rate and water level data can be extended by applying the Thiem equation (Equation (5.2)) between $r_o = 100\ h_o$ and the value of r_o required. since the flow in the added zone will be far enough from the well or pit for the effects of non-Darcy flow and partial penetration to be neglected, use of the Thiem equation is valid. Radius values measured from the centre of the pit will not be quite correct since the equation assumes flow to a hole of negligible radius. However, since $100\ h_o$ and the extended radius of influence will be large in comparison with the well or pit radius the resultant error will be small in comparison with other errors.

A problem which arises in the extrapolation using the Thiem equation is the necessity to use trial and error or a graphical procedure to determine the discharge and water level for a given set of data which includes a value of r_o greater than $1000\ h_o$. For instance, if a (and

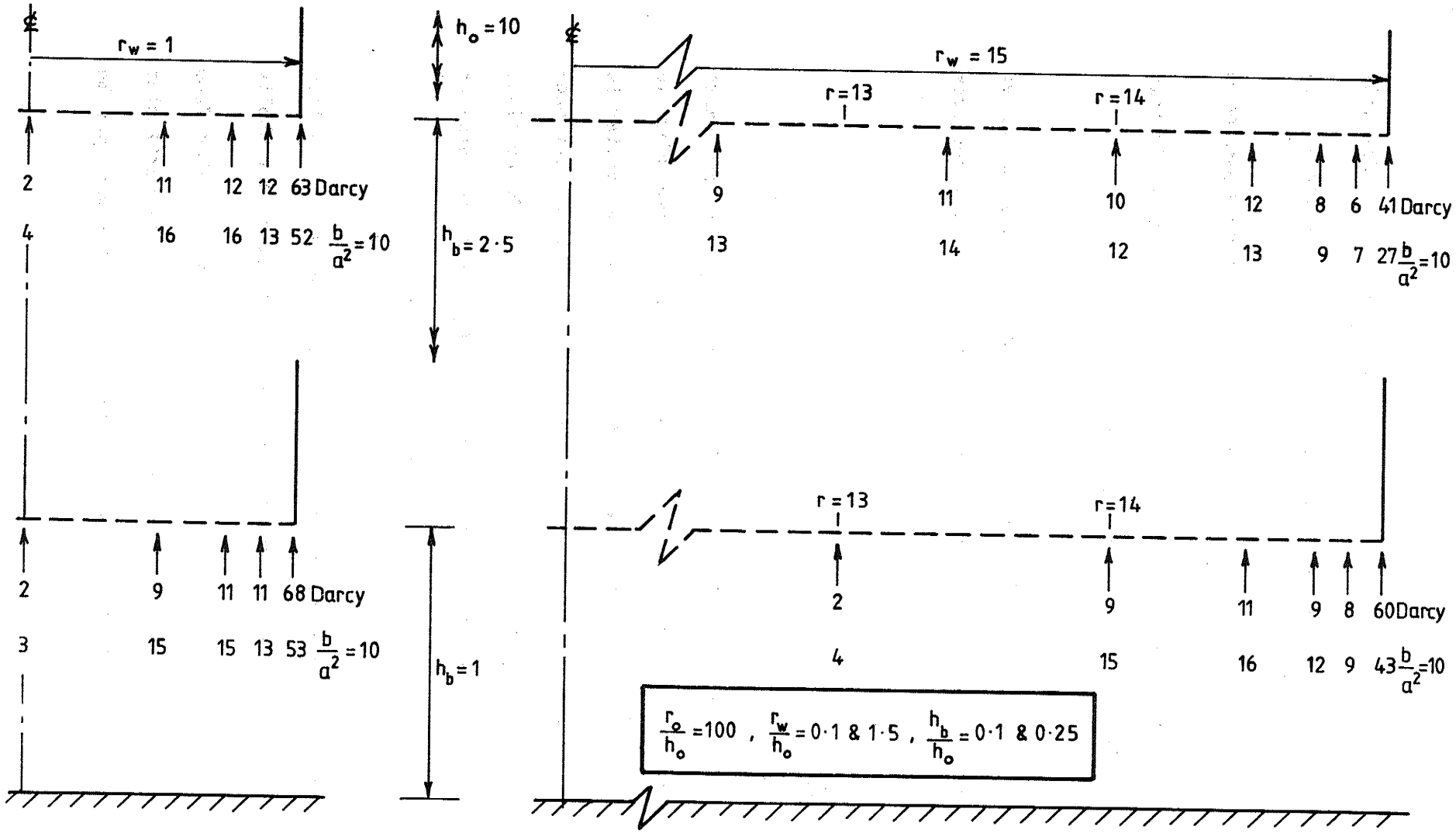

FIGURE 6·39 PERCENTAGE INFLOWS THROUGH CIRCULAR RING NODES AT BASE OF PIT

K), $\frac{b}{a^2}$, r_w, h_o and r_o are given, the curves plotted in Report No. 163. can be used to obtain $\frac{Q}{Kh_1^2}$ for a trial value of h_1 at $r_1 = 100\ h_1$. If the value of Q obtained from $\frac{Q}{Kh_1^2}$ is applied in the Thiem equation a value of h_o can be obtained for the actual radius of influence. If this is not equal to the given value the trial must be repeated.

When the correct values of h_o at the radius of influence and h_1 at $r = 100\ h_1$ have been achieved the values of h_f and $\overline{V}$ can be found from the curves in Report No. 163.

6.5 Conclusions

It has been demonstrated that post-linear non-Darcy flow can exert a very significant influence on inflows to de-watered open pits in unconfined aquifers and on water levels at such pits. If the aquifer is sufficiently permeable, inflow rates may be reduced to less than one-fifth of those predicted by an analysis which assumes wholly Darcy flow. Water levels at pits may be more than twice as high above the base of the aquifer as those which would occur for Darcy flow.

The changes in inflow rates and water levels caused by various values of the non-Darcy flow parameter $\frac{b}{a^2}$ relative to values for wholly Darcy flow for identical pit and aquifer geometries can be scaled from the figures in Report No. 163. Alternatively, data for the particular values of the dimensionless ratios used in the computations can be obtained from the associated tables.

Although the existence of non-Darcy flow near large diameter pits even in very permeable aquifers may cause surprise to some engineers and hydrologists familiar with the principles of groundwater flow, the reasons for its occurrence are quite clear. For partially penetrating bottom entry pits the water surface falls under the influence of gravity until the restricted entry causes hydraulic gradients near the pit to rise sufficiently to induce high Reynolds numbers and consequently non-Darcy flow. This will occur in aquifers with large pore dimensions regardless of the pit perimeter. The effect will, however, be magnified by the increased contraction of the flow in a horizontal plane which accompanies a reduction in pit diameter.

For fully penetrating pits and pits with side and bottom entry, gravitational force pulls the water level at the pit down until the seepage face height falls to such an extent that the restriction of the inflow area again induces high hydraulic gradients and non-Darcy flow. The effect is accentuated by, but not restricted to small pit diameters.

The range of the non-Darcy flow parameter b/a^2 used to compute the relationships given in Report No. 163 was chosen to cover the range of aquifers for which non-Darcy flow might have significant effects in groundwater extraction and de-watering operations. Although a value of b/a^2 as high as 100 is not likely to be met frequently, values in the range 1 to 10 are relatively common for aquifer materials such as unconsolidated gravels. There is little data available on non-Darcy flow characteristics of highly permeable consolidated aquifers with fracture permeability but non-Darcy flow can occur in these aquifers. An example quoted in Chapter 9 confirms this.

Values of $\frac{b}{a^2}$ which have been derived from permeameter tests on sands and gravels by Dudgeon (1964) and Kazemipour (1974) lie in the range given in Table 6.1.

Table 6.1: Approximate Range of b/a^2 For Clean Sands And Gravels

Material	Sand	Fine	Medium Gravel	Coarse Gravel	Boulders
b/a^2	10^{-3} to 10^{-1}	10^{-1} to 10	10 to 10^2	10^2 to 10^3	10^3 to 10^4

Inspection of this data or substitution of permeability coefficients into the equation:

$$\frac{b}{a^2} = 160\ K^{5/4} \qquad (6.18)$$

which is a modified version of an equation derived by Cox (1977) from the permeameter results and in which K is in metres per second should provide sufficient proof that post-linear regime non-Darcy flow in the vicinity of wells and pits in unconfined aquifers is a real possibility. The values of b/a^2 which have been found experimentally extend even higher than those used in the computations described in this chapter.

7. EXPERIMENTAL INVESTIGATION OF UNCONFINED NON-DARCY FLOW TO CIRCULAR PITS

A programme of large scale laboratory testing of flow to circular pits in unconfined aquifer material was undertaken to verify numerical solution methods and results described in Chapter 6. Tests on both fully and partially penetrating pits were included in the programme. For partially penetrating pits, both bottom entry and bottom and side entry conditions were examined.

7.1 Experimental Equipment And Procedures

7.1.1 Testing Tank

The experiments were carried out in a specially designed concrete tank 4.94 m × 4.94 m in area and 3.35 m deep. The planning, hydraulic design and supervision of construction of the facility were carried out by the author. Diagrams showing a plan view of the tank, a pipe layout and cross-sections are given in Figures 7.1 to 7.3. A general view of the complete facility is shown in Photograph 7.1(a).

The tank and ancillary equipment were designed to meet the need for a multi-purpose facility which would allow various aspects of groundwater flow to be studied. It is particularly suitable for examining the effects of partial penetration, entry conditions, non-Darcy flow and other factors on flow to boreholes, wells and civil and mining engineering excavations.

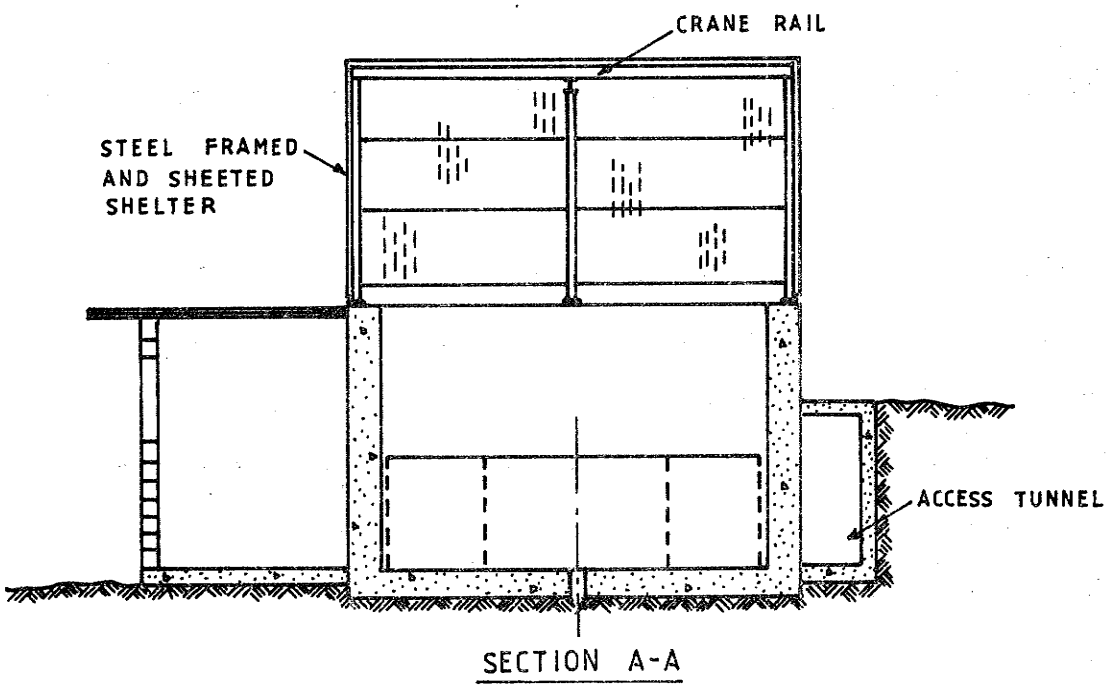

SECTION A-A

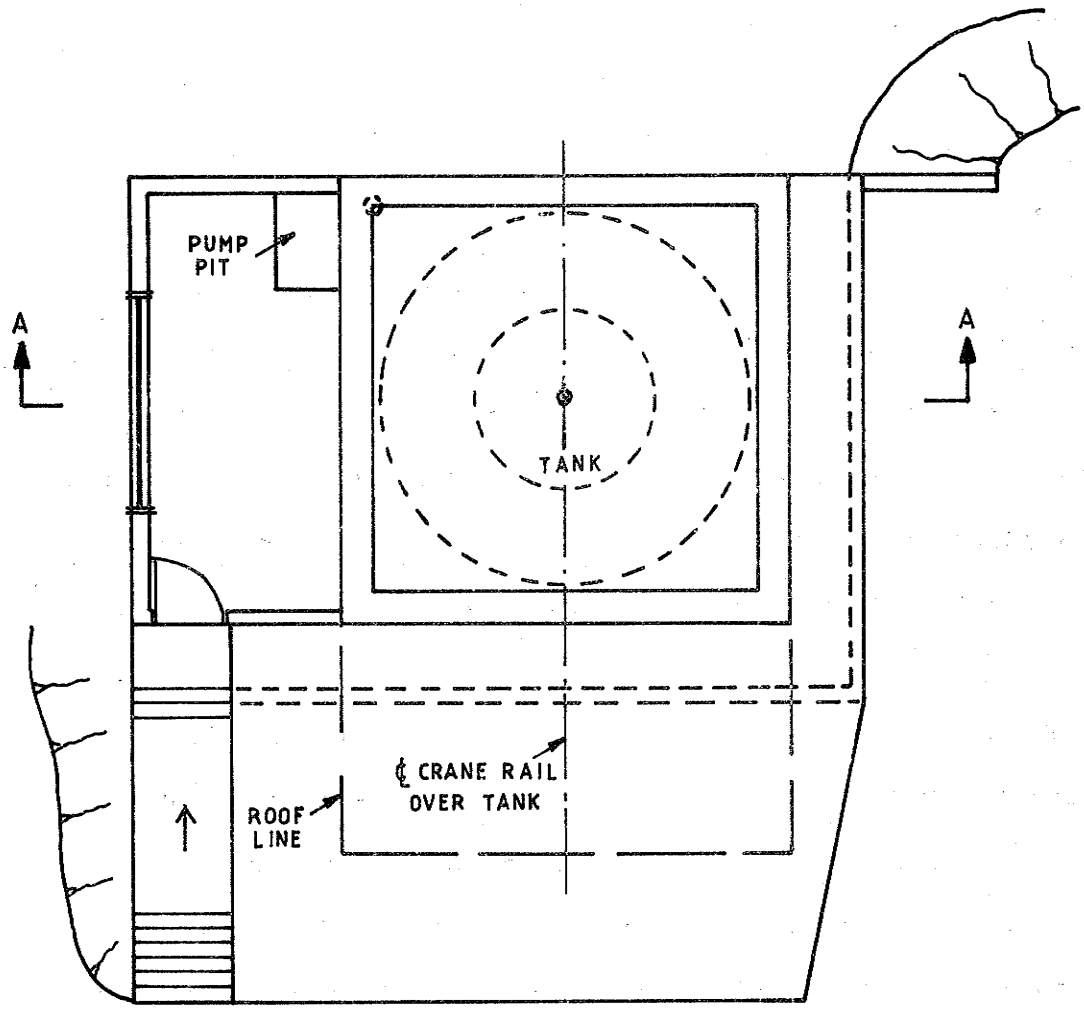

PLAN

FIGURE 7-1: GROUNDWATER FLOW TEST FACILITY

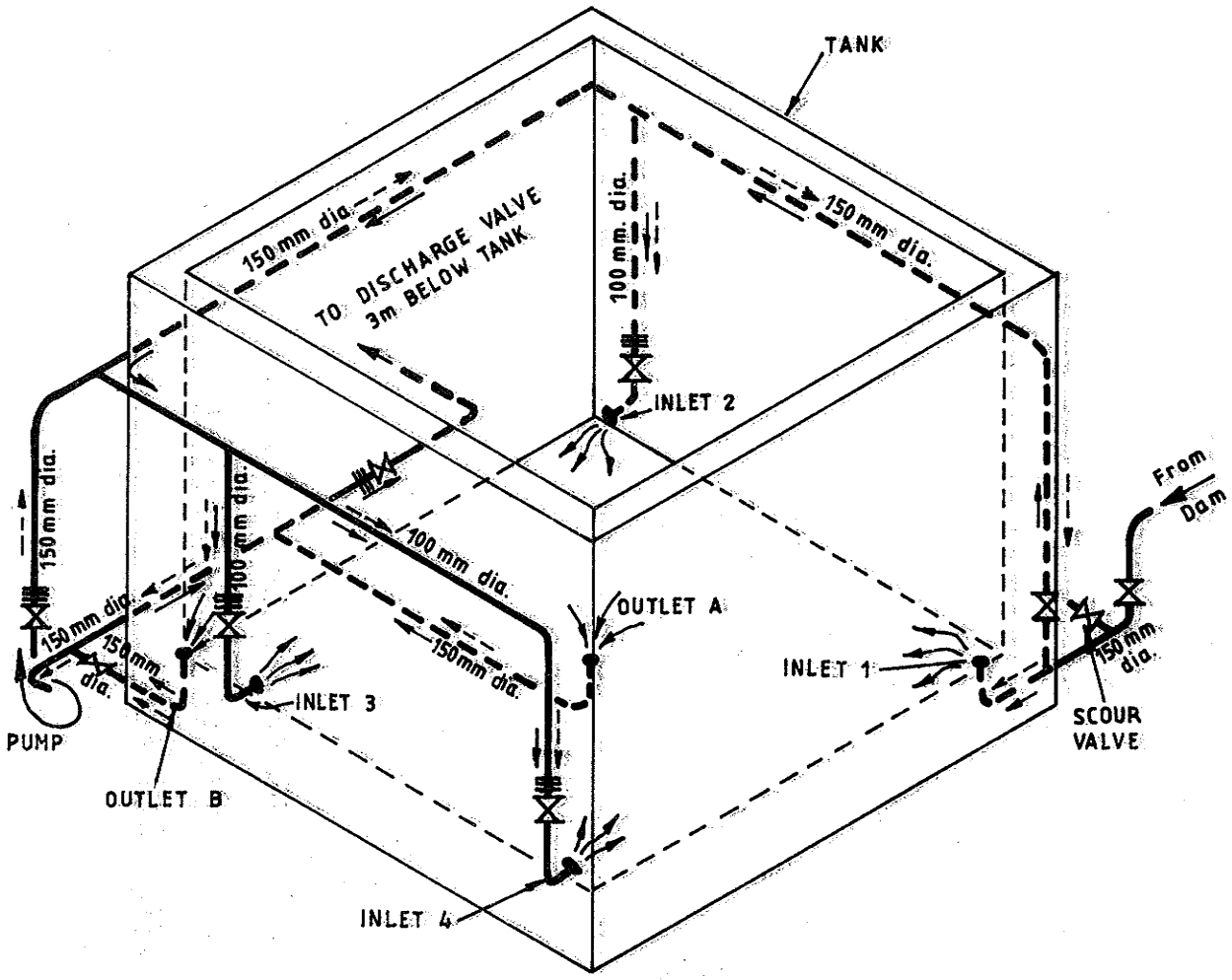

Legend:

- Orifice plate
- Gate valve
- Pumped flow
- Gravity flow

FIGURE 7·2: EXPERIMENTAL TANK PIPE LAYOUT AND FLOW DIAGRAM

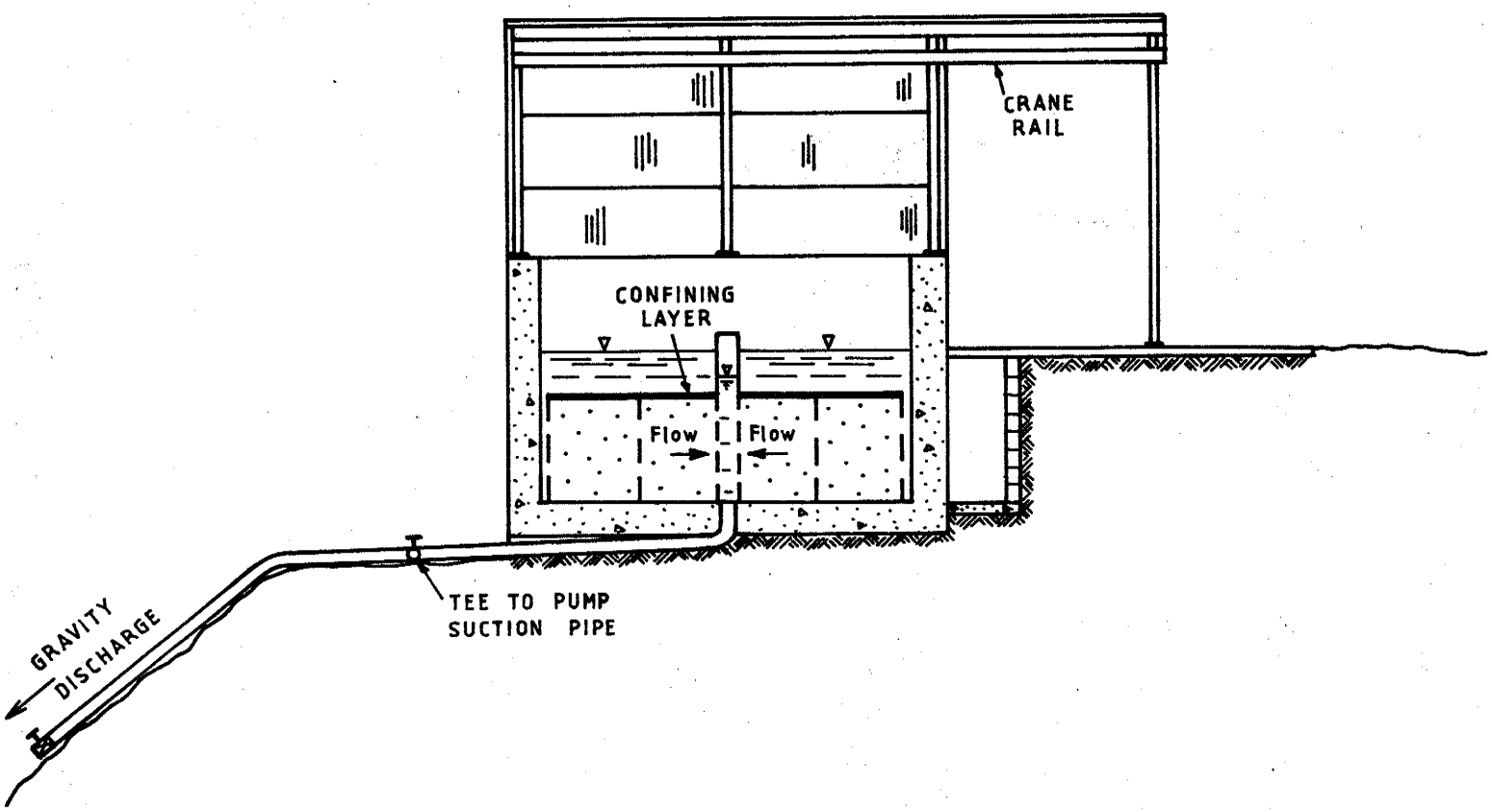

FIGURE 7·3: SECTION THROUGH GROUNDWATER FLOW TEST FACILITY WITH FULLY PENETRATING BOREHOLE SCREEN IN CONFINED AQUIFER

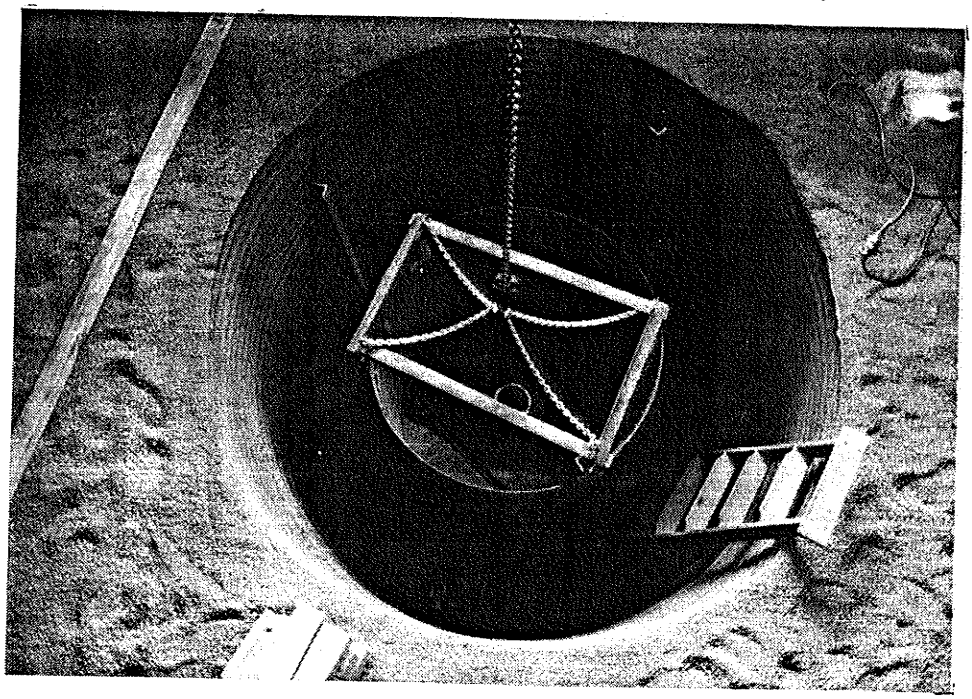

Photograph 7.1 (b) Pit Liner in Position Before Restoring Aquifer.

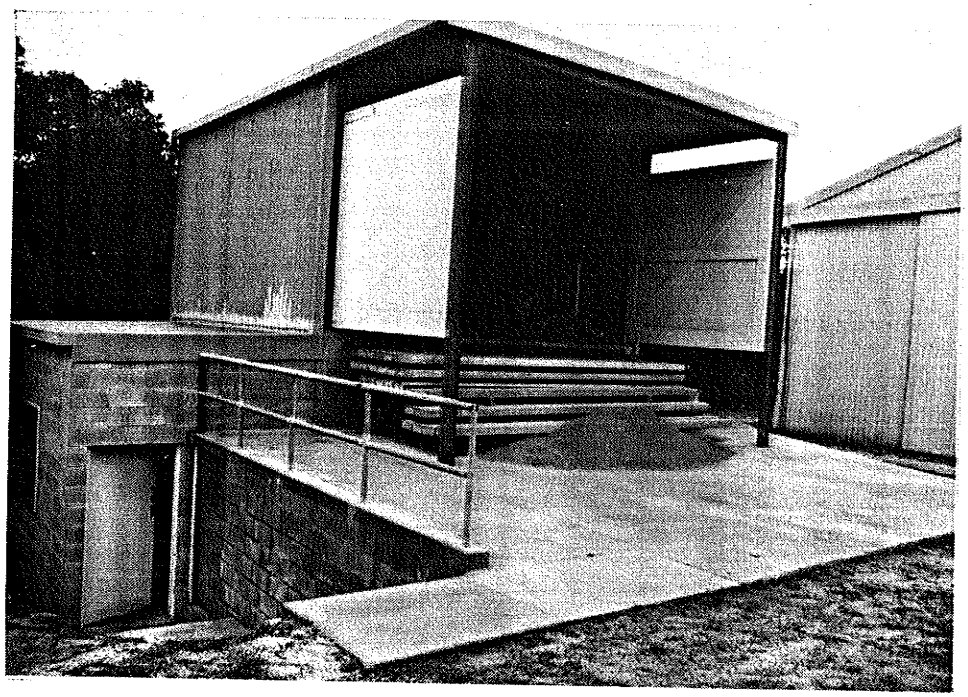

Photograph 7.1 (a) Groundwater Flow Test Facility

For axi-symmetric flow, either a full circle or quadrant aquifer can be used. In the former case the borehole or pit is located in the centre of the tank. A full circle retaining wall made up of perforated steel sheets attached to a steel framework is erected at a radius of influence of 2.4 m to retain aquifer material. In the latter case a fully or partially perforated cylinder with a cross-section equal to a quarter of the full section is formed in one corner of the tank and a perforated retaining wall is erected to form a quadrant aquifer with a radius of influence of 4.8 m.

7.1.2 Water Supply

Water is supplied to the tank from a pipeline connected to the laboratory's water supply dam. It can be gravitated to waste through outlets in the base of the tank. One 150 mm diameter outlet is located in the centre of the base and another in one corner. These allow water to be drawn from the bottoms of boreholes, wells and pits being tested. Water is discharged at a level approximately 3 m below the base of the tank to increase the maximum available outflow rate.

Alternatively, water can be re-circulated through a permanent pump and piping system capable of handling flows up to 50 L/s. The head and power characteristics of the pump are given in Figure 7.4 to give an indication of the magnitude of the experimental pumping operation. The head curve is also required for discussion later in this chapter.

In both modes of operation, the flow can be distributed as required to any one or all of the corners of the tank. A separate above-ground or submersible pump can be used to extract water from the top of a borehole or pit if this is considered necessary.

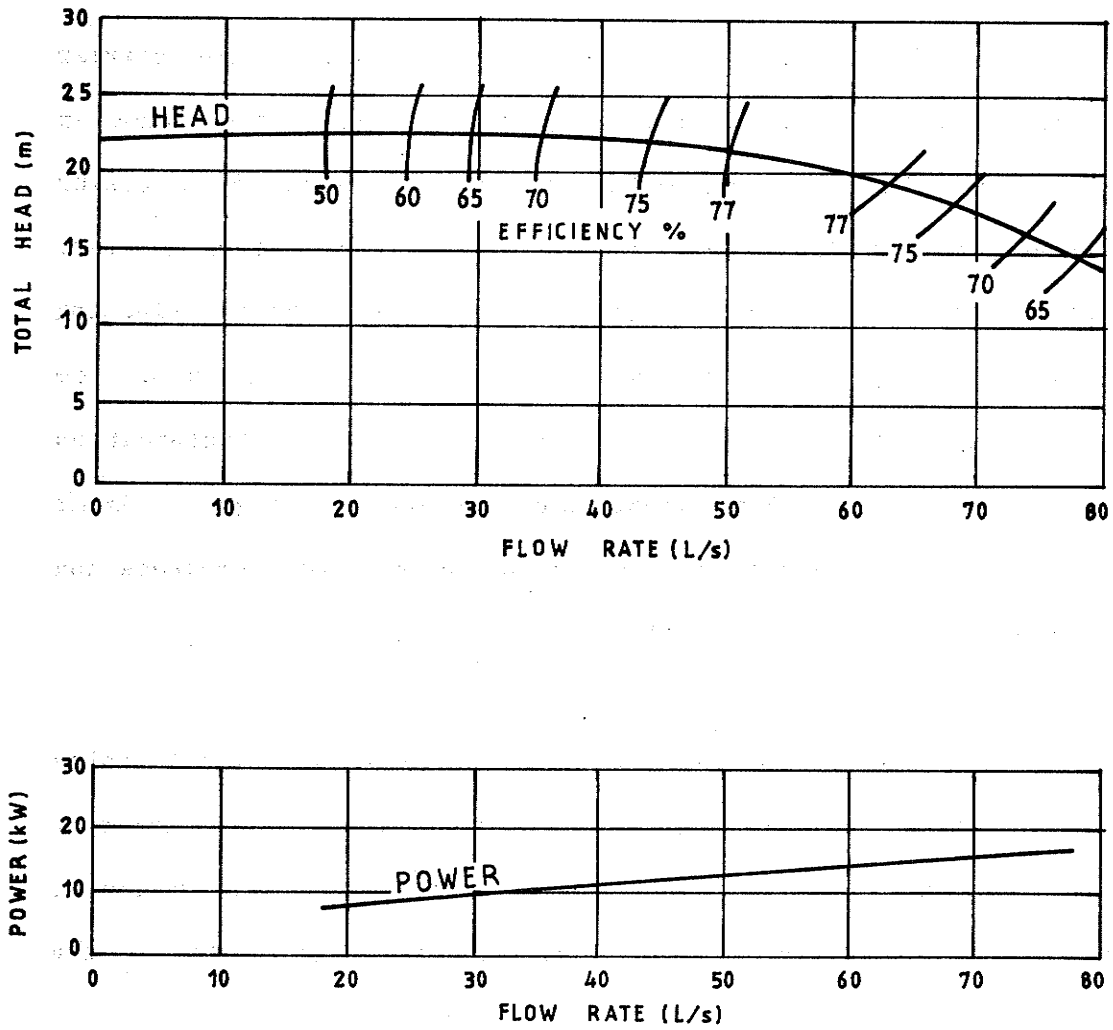

FIGURE 7·4: HEAD AND POWER VERSUS DISCHARGE CHARACTERISTICS OF PUMP USED FOR EXPERIMENTS

7.1.3 Aquifer Preparation

A circular screen 2.3 m in diameter and 1.5 m high was placed centrally in the tank to act as an intermediate barrier between the 4.8 m diameter, 1.5 m high perforated outer retaining wall and the pits to be constructed at the centre of the tank. The intermediate barrier extended the full height of the aquifer material subsequently placed in the tank. Its purpose was to allow excavation to be carried out during the construction of central pits without disturbing the entire aquifer. Since it was required to retain aquifer material without deflecting excessively or causing additional resistance to flow it was made from 1.9 mm thick perforated steel sheets corrugated to the same contour as galvanised roofing iron (76 mm pitch, 15 mm corrugation height). After being corrugated, the sheets were rolled to the required curvature and rivetted together to make a full circle.

For the first series of tests a 258 mm diameter wire-wound stainless steel borehole screen was positioned in the centre of the tank over the 150 mm diameter outlet. The open bottom of the screen was welded to a flange which was bolted to a recessed flange in the bottom of the tank.

After the outer and intermediate barriers and central screen were in position, fine gravel was placed in the tank to form a circular aquifer 4.8 m in diameter and 1.5 m deep. The gravel was distributed from a dump bucket suspended from a crane. Care was taken to deposit the material in a uniform manner so that the aquifer would be as homogeneous as practicable.

7.1.4 Piezometric Head Measurement

The testing tank was provided with a system of piezometer tubes to allow base pressure measurements to be taken. The tubes ran from manometer boards fixed to the walls of the tank to outlets located along one diagonal of the base of the tank. The outlets were flush with the bottom of the tank and covered with gauze. The water manometers were used to make direct measurements of piezometric pressure heads at the base of the aquifer during all tests.

Measurements of piezometric surface heights during the initial series of tests of unconfined flow to the fully penetrating 258 mm diameter borehole screen were also made in open piezometer tubes. These were fixed in position on sheets of 150 mm × 150 mm steel wire mesh reinforcement before the aquifer material was deposited. The piezometers were located along two radial lines separated in plan by an angle of 120^{o}. Openings in the piezometers were set to measure piezometric pressures at various levels.

For the tests of unconfined flow to large diameter pits, free surface water levels were measured in piezometers set to penetrate a short distance below the water table. The piezometers were located at the pit boundary and the intermediate barrier along three radial lines spaced in plan at 120^{o}.

All piezometers placed in the aquifer were made from 15 mm diameter PVC electrical conduit. Over the length of the tube to be open to the aquifer, four drilled holes were spaced at 90^{o} around the tube at 10 mm longitudinal intervals or two holes were drilled diametrically opposite and at 10 mm intervals to form a spiral pattern around the tube.

Perforated parts of the piezometers were wrapped with fine plastic gauze.

Water levels in open piezometer tubes were measured with a pair of electrical contacts at the end of wires taped to a thin PVC rod. Contact with the water surface was indicated by a light operated by a small battery powered circuit which sensed and amplified the flow of electricity between the contacts. Water levels in the pits and in the tank at the radius of influence were measured with the electrical probe or a graduated tape. In the latter case contact with the water surface was observed visually. The overall accuracy of measured water levels was estimated to be ± 3 mm.

7.1.5 Flow Measurement

Flow rates were determined from the readings of air-water manometers which indicated pressure head differences across orifice plates in the pumping and gravity flow lines. The orifice plates and pressure tappings were made to conform to the British Standard Code for Flow Measurement, B.S. 1042, 1964. Approach lengths did not conform with the specifications. Volumetric calibrations carried out for low to moderate flow rates using the empty tank as a calibrated volume tank had previously shown that differences between measured flow rates and those calculated using B.S. 1042 could be neglected. However, doubts about the accuracy of the orifice meter in the main pumping line arose during the course of the experiments so an "Annubar" was also installed in the pipeline. It was located in a straight length of pipe as far from the pump as practicable. Comparisons of flows indicated by the two meters are given in Section 7.4.1.

7.2 Determination of Aquifer Material Properties

7.2.1 Size Grading

The aquifer material used for all the flow tests described in this chapter was a fine sandy gravel fraction from the Nepean River near Sydney. It has been subjected to a number of sieve analyses which have yielded somewhat different results because the samples were taken at different times and places from the large volume of material required for tests in the tank. The inhomogeneity which is probably the main cause of the different size gradings will have decreased over the period of use of the material because of mixing. However, fines have probably been lost during flushing of aquifers in the tank and by segregation during handling.

Size gradings, including the most recent one by the author, of material taken from the aquifer in the tank, are shown in Figure 7.5.

7.2.2 Porosity Measurements

Porosity measurements were made by filling the tank slowly and measuring the volumes of water required to raise the water level by measured increments. Values of porosity P for the increments were then calculated using the equation:

$$P = \frac{\Delta \overline{V}_w - \Delta z \, (A_T - A_A)}{A_A \, \Delta z} \qquad (7.1)$$

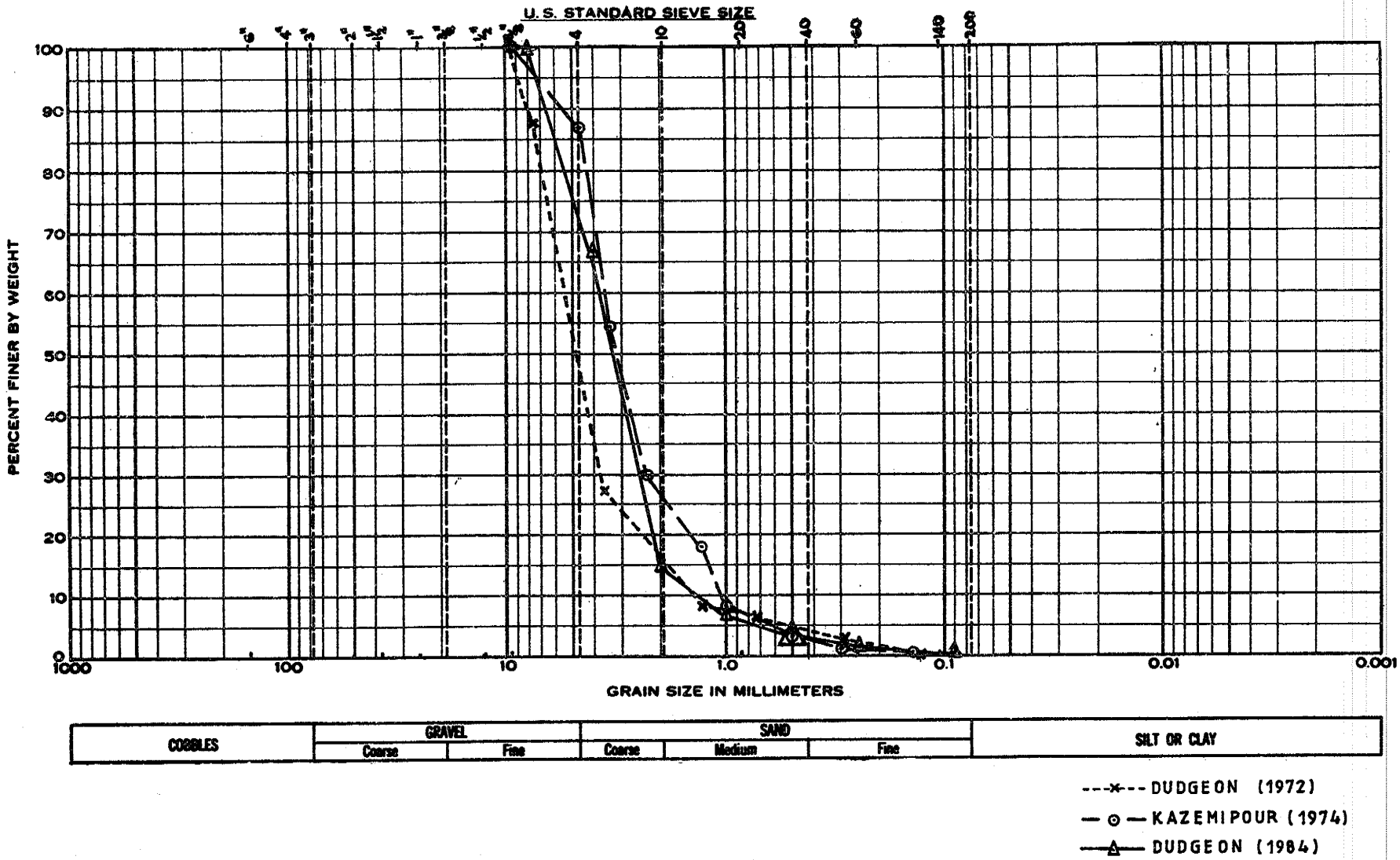

FIGURE 7·5: SIZE GRADINGS OF AQUIFER MATERIAL

where A_A = plan area of aquifer material

A_T = plan area of tank

ΔV_w = volume of water added to raise water level by Δz

Δz = height increment

The measured porosity variation is given in Table 7.1. A plot of the data is shown in Figure 7.6.

The average porosity of 35.3 per cent is slightly higher than the value of 33.1 per cent reported by Dudgeon et al. (1972) when the material was used in a quadrant aquifer of similar height. As suggested previously, fines could have been lost during the earlier use of the material. Alternatively, the material may have been compacted less during construction of the aquifer on this occasion.

Table 7.1: Vertical Variation of Porosity in Experimental Aquifer

Rest Level (m)	Height Increment (m)	Porosity (per cent)
1.242		
	0.148	36.3
1.094		
	0.184	33.5
0.914		
	0.146	37.4
0.768		
	0.149	35.7
0.619		
	0.151	34.7
0.468		
	0.156	32.2
0.312		
	0.144	38.4
0.168		
	0.153	34.3
0.015		
		———
Average		35.3
		———

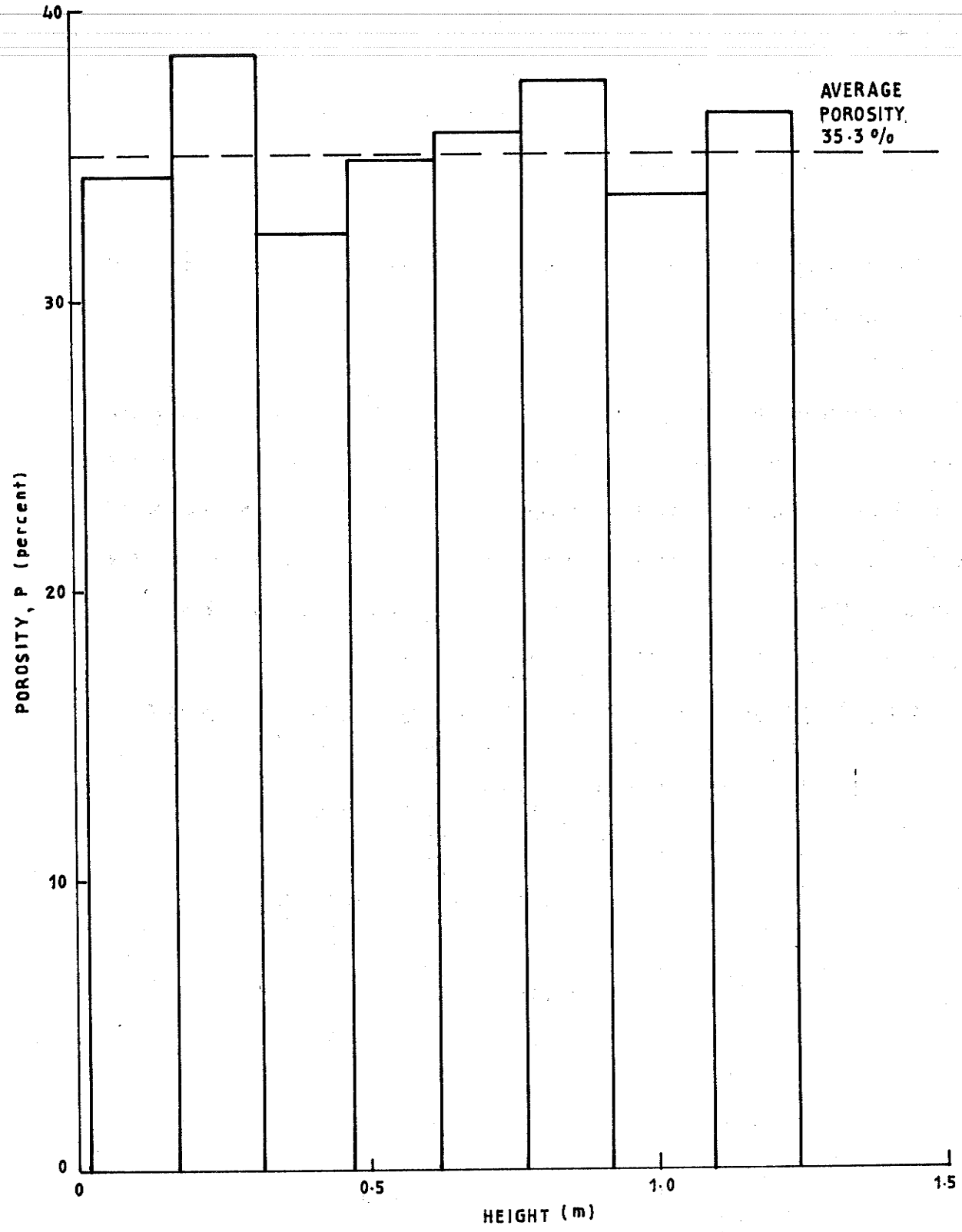

FIGURE 7·6: VERTICAL VARIATION OF POROSITY OF MODEL AQUIFER

7.2.3 Permeability Characteristics

The aquifer material was chosen because:

i. It was sufficiently permeable to allow the development of significant post-linear non-Darcy flow effects and yet be within the range which might occur in water supply or de-watering operations.

ii. Data from permeameter tests on the material were available for use in estimating Forchheimer coefficients of the aquifer.

iii. Previous tests in which the material was used in simulations of flow to boreholes had provided data on the in-situ permeability characteristics of a large sample.

Permeameter test data for a porosity of 39.4 per cent obtained by Kazemipour (1974) are plotted in Figure 7.7. A curve representing the Forchheimer equation with a single pair of coefficients ($a = 18\ s/m$, $b = 1450\ s^2/m^2$) is also plotted. This curve was fitted by selecting a value of the coefficient a which gave a match with the straight line (Darcy) part of the plot and then solving the equation for the value of the coefficient b which gave a good fit between the equation and the experimental points at high velocities. The curve does not give a good fit at intermediate velocities. It is suspected that the material in the permeameter consolidated during testing and that two curves should be fitted, one to the lower set of points and another to the higher set.

A second Forchheimer curve for a porosity of 35.3 per cent, the average value of Figure 7.6, is represented by the broken line in Figure 7.7. This curve has been plotted using coefficients ($a = 22\ s/m$,

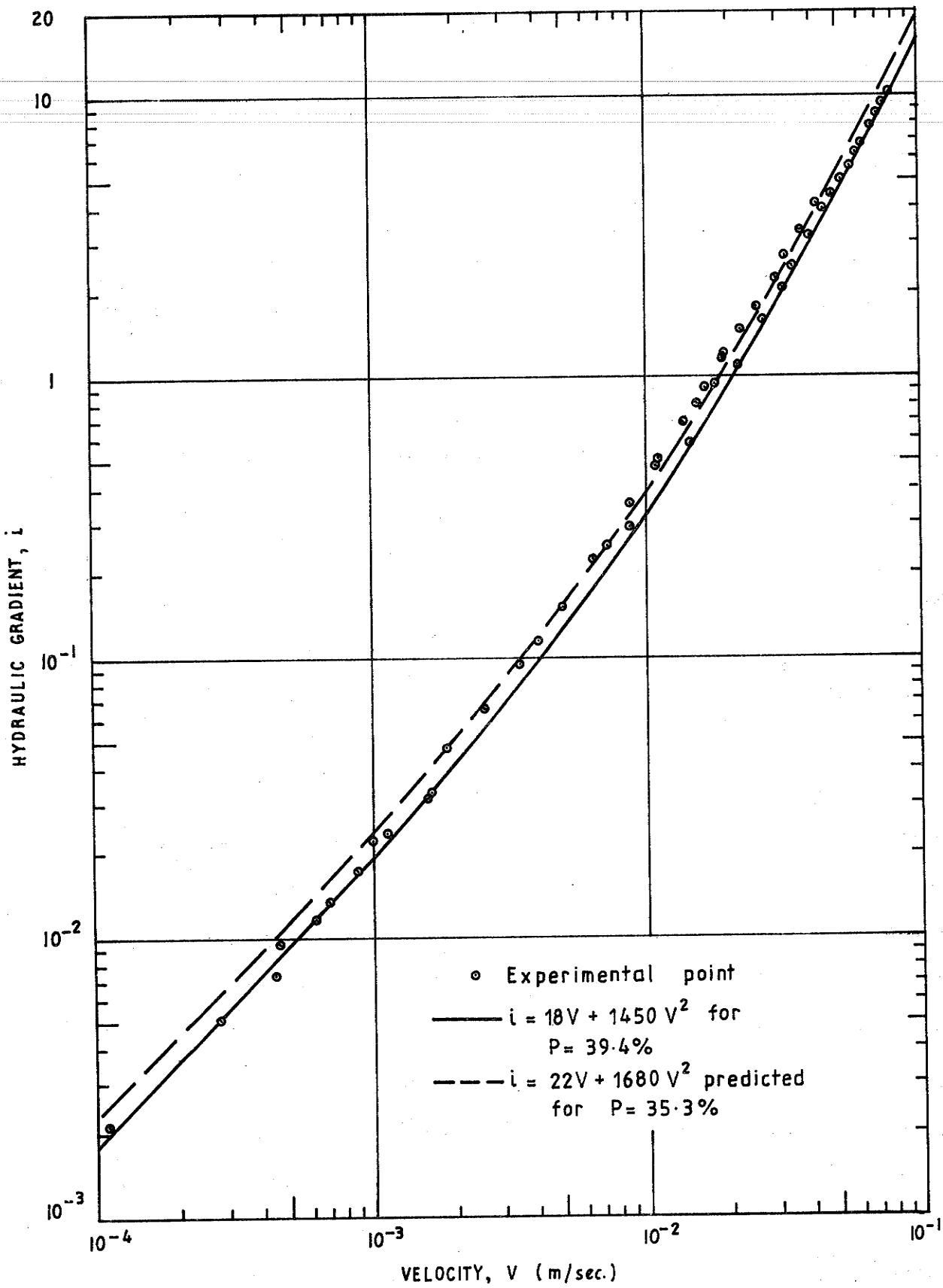

FIGURE 7·7: PERMEAMETER TEST DATA (Kazemipour (1974)) AND EXTRAPOLATION FOR POROSITY DIFFERENCE

$b = 1680\ s^2/m^2$) extrapolated from the values applying to the curve fitted to the permeameter date. The extrapolation has been carried out using relationships between the coefficients and a pore size based on a capillary model. The relationships were derived by Kazemipour from tests on a series of sands, gravels and gravel mixtures from the same source as the aquifer material. The test which produced the data plotted in Figure 7.7 formed part of the series.

The equations used for the extrapolation are:

$$e = d_{50} \sqrt{\left(\frac{P}{1 - P}\right)} \qquad (7.2)$$

$$a = 3.9\ e^{-2.55} \qquad (7.3)$$

$$b = 1.04\ e^{-1.80} \qquad (7.4)$$

where a = linear Forchheimer coefficient (s/m)

b = non-linear Forchheimer coefficient (s^2/m^2)

d_{50} = particle size (mm)

e = pore size (mm)

The Forchheimer equation

$$i = 22\ V + 1680\ V^2 \qquad (7.5)$$

obtained by this method fits the experimental points on Figure 7.7 better in the middle velocity range than does the curve fitted for a porosity of 39.4 per cent. This supports the argument that the porosity changed during the test.

Previous use of the material for tests of flow to screened boreholes in a quadrant aquifer (Dudgeon et al. (1972)) have provided data on the in-situ hydraulic characteristics at an average porosity of 33 per cent. However, the results have been interpreted by different methods to give different results.

The original interpretation was in terms of a two-regime flow with an outer Darcy flow region in which the macroscopic velocity was below a critical value V_{cr} and an inner post-linear non-Darcy flow region near the borehole. The Darcy region was represented by the Darcy equation and the non-Darcy region by the Forchheimer equation. An adaptation of the analytical solution given by Engelund (1953) for axi-symmetric flow to a borehole in a confined aquifer was used to obtain, from the results of confined flow tests:

$K = 0.060\,m/s$

$V_{cr} = 1.1 \times 10^{-3}\,m/s$

$a = 14.8\,s/m$

$b = 1860\,s^2/m^2$

Subsequently, Huyakorn (1973) determined a different set of values by using type curves to analyse the same confined flow data. The results reported are:

$K = 0.058\,m/s$

$V_{cr} = 2.5 \times 10^{-3}\,m/s$

$a = 11.8\,s/m$

$b = 1820\,s^2/m^2$

Cox (1977) also re-analysed the data but adopted the alternative approach discussed in Chapter 2 of using the Forchheimer equation with a single pair of coefficients for the relationship between velocity and hydraulic gradient over the entire flow region.

His results are:

$K = 0.056\,m/s$

$a = 18\,s/m$

$b = 270\,s^2/m^2$

The corresponding Forchheimer equation is:

$$i = 18\,V + 270\,V^2 \qquad (7.6)$$

It can be seen that the value of a is comparable with that of Equation (7.5) obtained by extrapolation from the permeameter test results. However, the b value is much smaller. The reason for the difference is not apparent. If a value of b were chosen to give the best fit between the Forchheimer equation and the permeameter data in the middle of the hydraulic gradient range, rather than at the top, it would be even greater than 1680. Thus the discrepancy can not be attributed to the method of selecting the b value from the permeameter results.

7.3 Flow Tests

7.3.1 Confined Flow To A Screened Borehole

The first series of tests was undertaken to allow the in-situ permeability characteristics of the aquifer material to be determined. Since confined flow is the simplest axi-symmetric flow which can be established in a circular aquifer it was chosen for the permeability determination. For these tests it was necessary to add a confining layer to the top of the aquifer described in Section 7.1.3.

The 258 mm diameter bore screen set up in the centre of the aquifer was extended vertically by adding a short length of 150 mm diameter PVC pipe. The aquifer was then covered with PVC sheeting weighted down with gravel. The central pipe and all piezometer tubes were taped to the sheeting to prevent leakage into the top of the aquifer.

Water was added slowly to the tank until the water surface was above the confining layer. A series of flow tests was then carried out using the pump to re-circulate water. The water level in the borehole was maintained above the top of the screen to prevent a free surface from developing in the aquifer. Measurements of flow rate, pressures at the base of the aquifer and water levels in the open borehole screen extension and at the aquifer boundary were made and checked for constancy during the tests.

The results are given in Section 7.4.1.

7.3.2 Unconfined Flow To A Screened Borehole

Without removing the confining layer or disturbing the aquifer, a series of fully unconfined flow tests was carried out after the water level in the tank was lowered beneath the confining layer. Measurements were taken as for the confined flow tests. Water levels were also

measured in the open piezometer tubes set in the aquifer.

The results are given in Section 7.4.2.

7.3.3 Unconfined Flow To A Large Diameter, Fully Penetrating Pit With Unrestricted Side Entry

The confining layer was removed and the aquifer material between the intermediate barrier and the borehole screen was excavated. The screen was removed leaving an open 150 mm diameter outlet in the tank floor. A 2.3 m diameter pit in a 4.8 m diameter aquifer was then available for testing.

An unconfined flow test with the water level in the pit drawn down as low as possible was then performed. Tests were subsequently carried out with higher water levels in the pit to simulate partial de-watering conditions.

Flow rates, base pressures and water levels inside the pit and outside the aquifer were measured.

The results of the tests are given in Section 7.4.3.

7.3.4 Unconfined Flow To A Large Diameter, Partially Penetrating Pit With Only Bottom Entry

A composite steel cylinder was constructed to serve as a pit liner for both bottom entry and bottom and side entry flow tests. Figure 7.8 shows a cross-section through the liner set up in the tank for a bottom

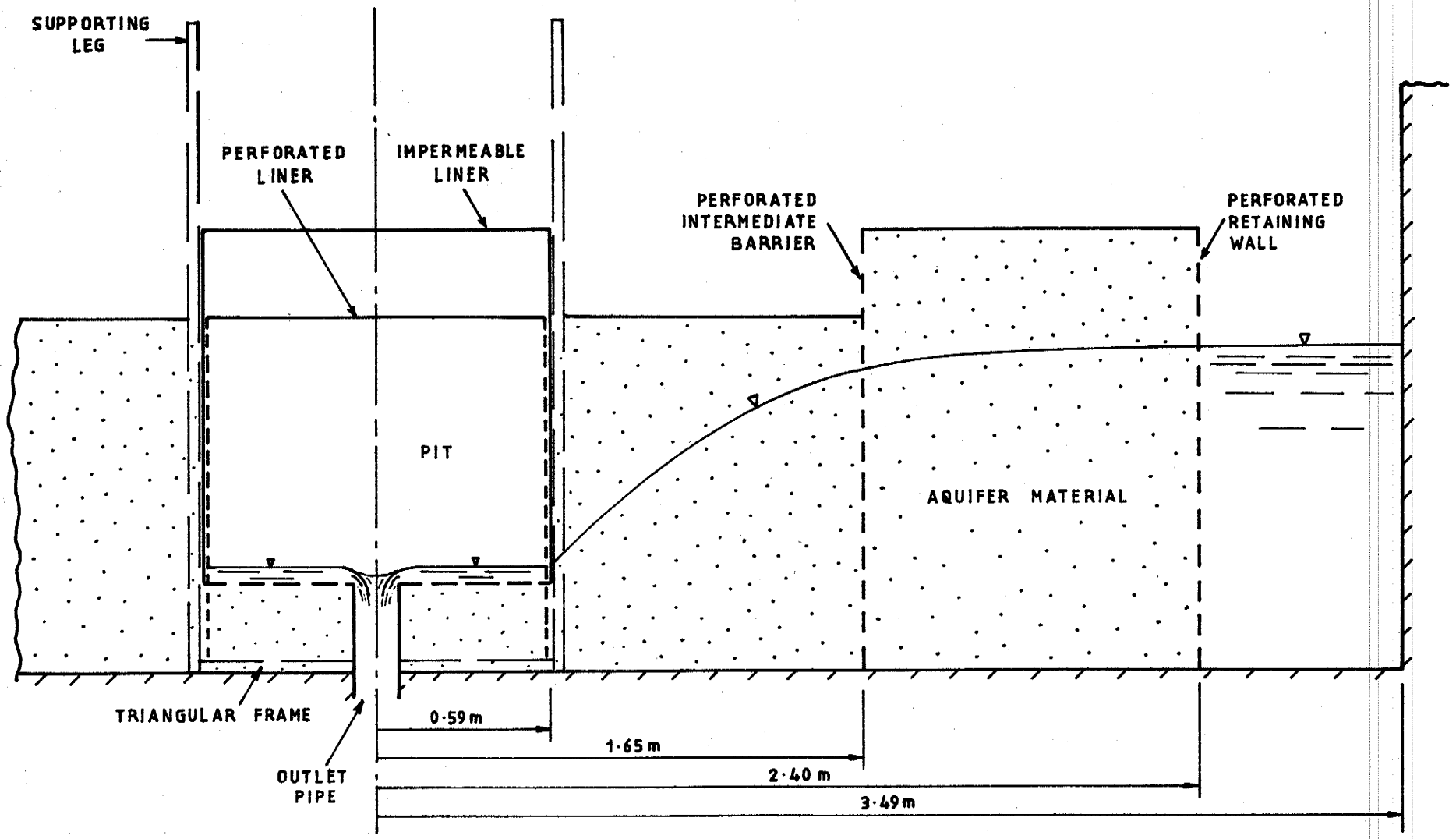

FIGURE 7·8: SECTION THROUGH PIT AND AQUIFER IN PLANE OF TANK DIAGONAL

entry flow.

An inner cylinder made from 1.9 mm thick corrugated perforated steel sheets was wrapped with 1.3 mm thick plain perforated steel sheets. The plain sheets were rivetted to the corrugated sheets to form a very rigid composite capable of resisting high external pressures without significant general or local deflection.

Triangular section PVC welding rods were then glued vertically at 100 mm intervals around the perforated outer sheeting. The rods were intended to act as separators and allow sliding between the perforated sheeting and an external cylinder of 1.6 mm thick galvanised steel which was used to form an impervious sheath.

A triangular steel frame made from steel angle and provided with legs welded to the vertices was bolted to the floor at the centre of the tank. The pit liner was then set up inside the legs with the perforated inner cylinder on the floor and the outer cover raised 150 mm off the floor. Three piezometer tubes spaced at 120^{o} around the outside of the pit liner were set to penetrate the anticipated free surface for the first test to be performed. The depth of penetration could be adjusted for other tests.

The annular space between the liner and the intermediate barrier was re-filled with aquifer material. An extension pipe was fitted to the outlet flange in the centre of the floor of the pit to raise the outlet to a level 150 mm above the floor. Aquifer material was then placed inside the pit up to this level. Perforated steel sheets were cut to fit the base of the pit to prevent movement of the aquifer material. The junction with the corrugated perforated inner cylinder

was filled with silicone sealant.

The construction represented a pit which had been sunk to within 150 mm of the base of the aquifer and lined with an impervious casing.

Flow tests were carried out with the pit de-watered to the maximum possible extent and with higher water levels. Flow rates, water levels and base pressures were measured as in previous tests. Water levels were also measured in the six open piezometer tubes located at the intermediate barrier and just outside the pit.

When the test series was complete, the perforated sheeting on the bottom of the pit was removed and the impervious outer liner was lifted 150 mm and re-fixed to the supporting legs. The outlet pipe was again extended and aquifer material added to the pit to raise the level 150 mm. The perforated base lining was replaced and sealed to the corrugated liner. Another series of tests with the water level in the pit drawn down as far as possible and at several higher levels was then carried out.

By repeating the procedure described, flow data was obtained for a total of five depths of penetration.

The results of the tests are given in Section 7.4.3.

7.3.5 Unconfined Flow To A Large Diameter Pit With Bottom And Side Entry

When the series of bottom entry tests was completed the impervious outer liner was lifted out of the tank leaving a partially penetrating pit with unrestricted side and bottom entry and the same depth of penetration as the final bottom entry test.

The series of tests performed on bottom entry pits was then repeated with side and bottom entry allowed. The depth of penetration was increased in 150 mm steps by removing aquifer material and pipe outlet extensions until, for the final configuration, only 150 mm depth of aquifer remained inside the perforated liner.

The results of the tests are given in Section 7.4.3.

7.3.6 Unconfined Flow To A Large Diameter Fully Penetrating Pit

A final series of tests was performed with all of the aquifer material removed from inside the pit liner. The fully penetrating pit with unrestricted side entry provided data for a smaller ratio of diameter to saturated thickness than that of the larger pit described in Section 7.3.3.

The results of the tests are given in Section 7.4.3.

7.4 Results of Tests

7.4.1 Confined Flow To A Screened Borehole

As previously indicated, the confined flow tests were carried out to provide the simplest possible flow conditions for determining Forchheimer coefficients for the aquifer. These were required for

subsequent comparisons of computed and measured inflows and free surface levels for more complex flow cases.

Base pressures measured during the confined flow tests were used to calculate drawdowns of the piezometric surface. The results for two tests used to determine the Forchheimer coefficients are given in Table 7.2. Locations of pressure tappings in relation to the borehole screen and perforated barriers are shown in Figure 7.9. The base pressure data are plotted in Figure 7.10.

The extent of the non-Darcy flow zone can be judged by the deviation from the straight lines drawn on Figure 7.10 to represent the Thiem equation. Fully Darcy flow should give a linear distribution of base pressure head as far as the borehole screen.

The linear portions of the two experimentally derived curves represent Darcy flow. Straight lines were drawn through the experimental points and extended to a conveniently small radius. The Thiem equation for steady, confined flow to a borehole, in the form:

$$Q = \frac{2\pi K m \Delta s}{\ell n \left(\frac{r_2}{r_1}\right)} \qquad (7.7)$$

allows the coefficient of permeability to be calculated for Darcy flow if piezometric heads are known at two radial distances from the borehole.

Radius values $r_2 = r_o = 2.40\,m$ and $r_1 = 0.197\,m$ were chosen.

The drawdown Δs for the extrapolated straight line between r_o and r_1 was

Table 7.2: Base Pressure Heads for Confined Flow Tests

Radial Distance (from centre) (m)	Pressure Heads at Base of Aquifer					
	Test No. 1			Test No. 2		
	Measured (m)	Computed for a=19.2s/m b=2100s^2/m^2 (m)	Computed for a=11.2s/m b=2790s^2/m^2 (m)	Measured (m)	Computed for a=19.2s/m b=2100s^2/m^2 (m)	Computed for a=11.2s/m b=2790s^2/m^2 (m)
0.197	1.842	1.838	1.868	0.984	0.966	0.967
0.273	1.905	1.906	1.940	1.123	1.116	1.138
0.349	1.952	1.949	1.983	1.221	1.208	1.239
0.425	1.989	1.979	2.013	1.296	1.271	1.306
0.502	2.018	2.003	2.035	1.355	1.319	1.355
0.578	2.036	2.021	2.052	1.394	1.357	1.392
0.730	2.070	2.050	2.077	1.459	1.413	1.446
0.883	2.090	2.071	2.095	1.494	1.454	1.484
1.035	2.103	2.088	2.108	1.521	1.486	1.513
1.340	2.125	2.114	2.128	1.559	1.533	1.553
1.797	2.146	2.141	2.149	1.597	1.583	1.593
2.102	2.159	2.155	2.159	1.612	1.608	1.613
2.407	2.167	2.167	2.167	1.628	1.628	1.628
2.711	2.169			1.628		
3.092	2.169			1.628		

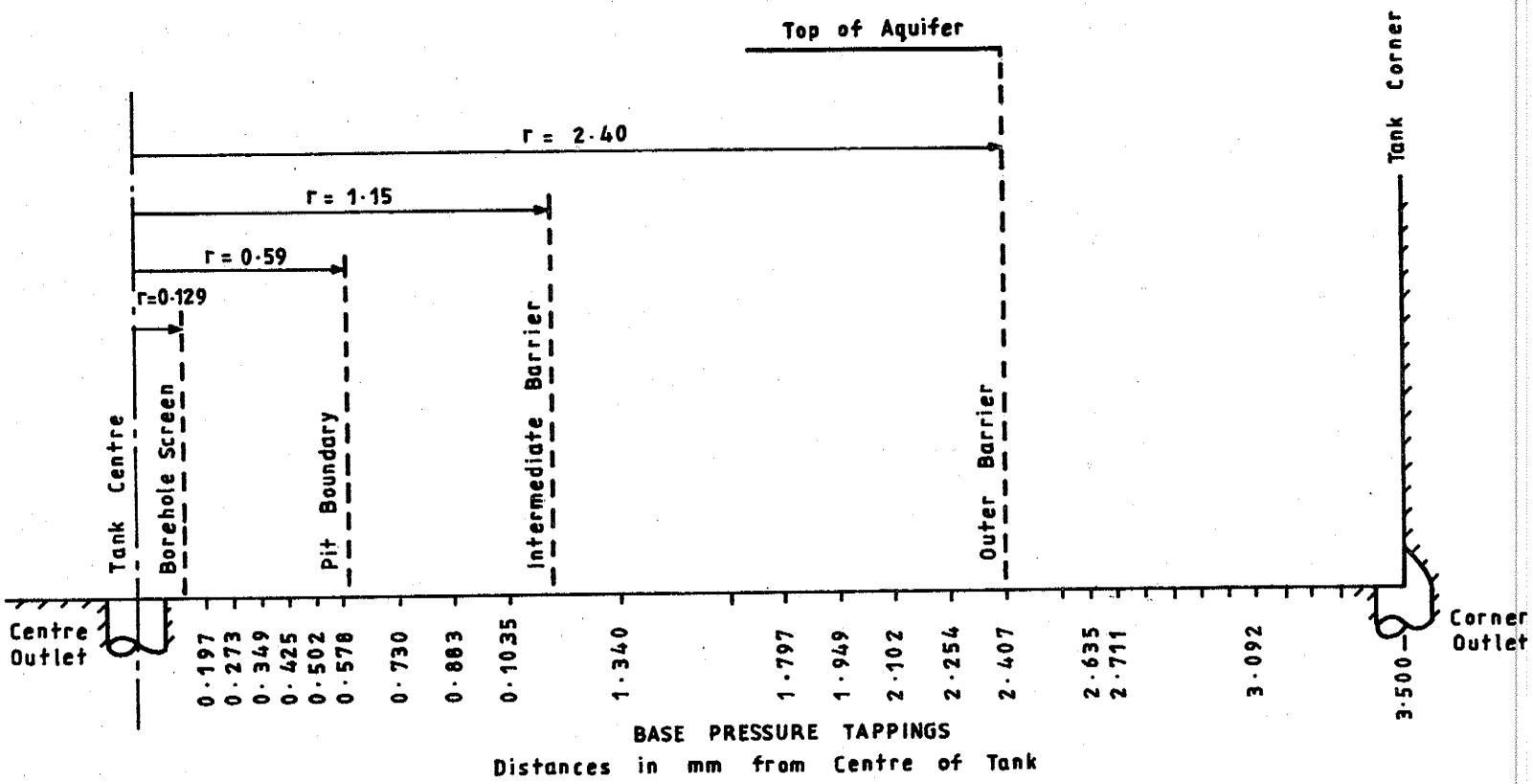

FIGURE 7·9: LOCATIONS OF PIEZOMETERS IN RELATION TO BOREHOLE, PITS AND AQUIFER BOUNDARY

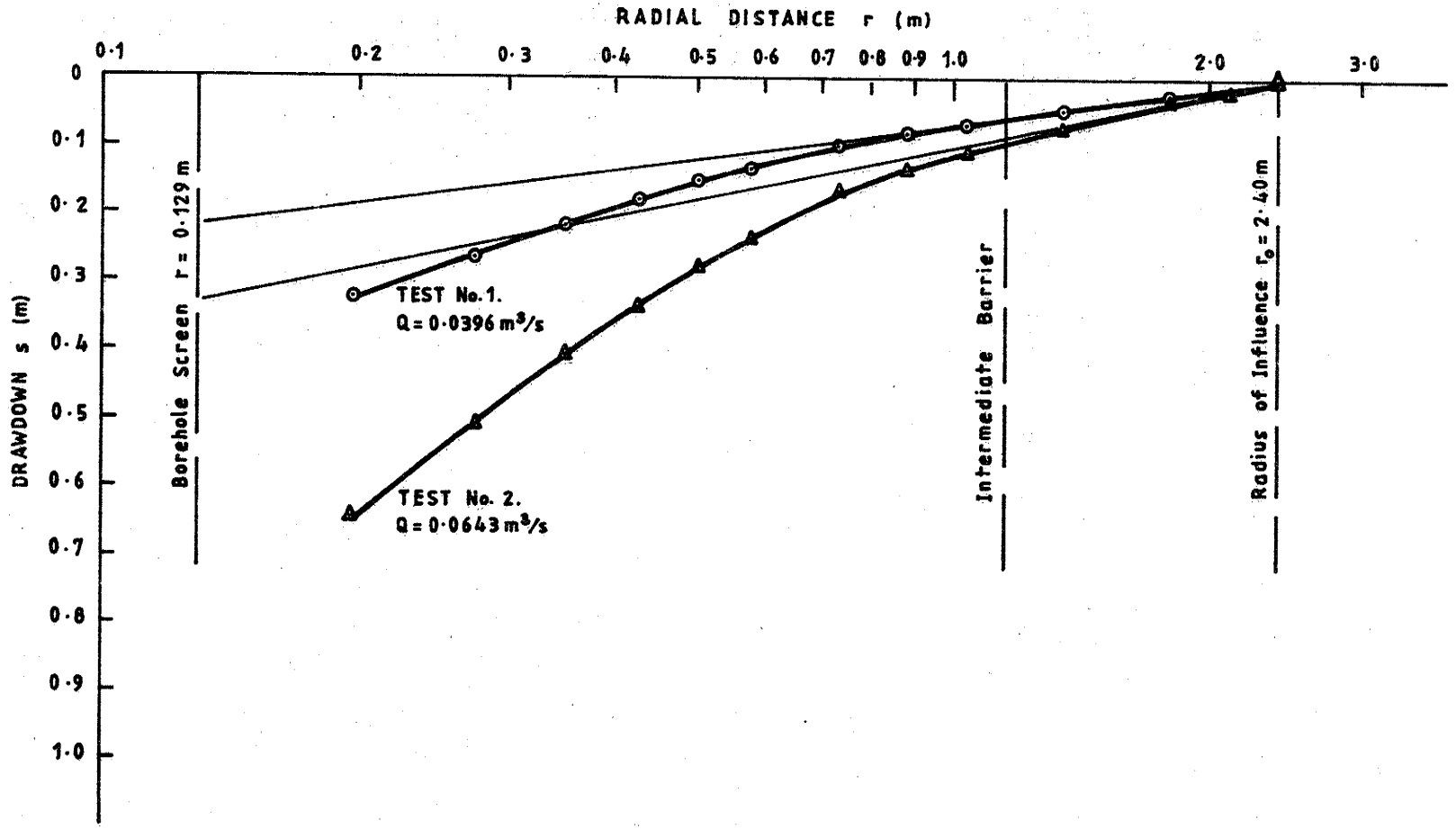

FIGURE 7·10: BASE PRESSURE HEAD DRAWDOWNS FOR CONFINED FLOW TESTS

scaled from the plot.

The aquifer thickness m was taken as 1.50 m.

The value of K was then calculated for each test. The linear Forchheimer coefficient a was calculated as the inverse of K.

Equation 5.6, the analytical solution for confined non-Darcy flow to a fully penetrating borehole, was used to calculate the non-linear coefficient b.

From Equation 5.6,

$$b = \left(\frac{r_2 r_1}{r_2 - r_1}\right) \left(\frac{2\pi m}{Q}\right)^2 \left(\Delta s - \frac{aQ}{2\pi m} \ln \left(\frac{r_2}{r_1}\right)\right) \qquad (7.8)$$

The original data and results of the calculations are given in Table 7.3.

Table 7.3: Forchheimer Coefficients From Confined Flow Tests

Test	Q	Δs		K	$a = \frac{1}{K}$	b	$\frac{b}{a^2}$
		Straight Line	Actual				
	(m^3/s)	(m)	(m)	(m/s)	(s/m)	(s^2/m^2)	
	Orifice						
1	0.0390	0.185	0.327	0.056	17.9	1830	5.7
2	0.0616	0.295	0.644	0.055	18.2	1800	5.4
	"Annubar"						
1	0.0362	0.185	0.327	0.052	19.2	2120	5.7
2	0.0578	0.295	0.644	0.052	19.2	2050	5.5

Some doubt exists concerning the measured flow rate Q. The orifice flowmeter referred to in Section 1.1.5 was situated in a vertical line directly above the pump and its accuracy may have been affected by distortion of the velocity distribution caused by the pump and by air entrained in the flow from the bottom outlet in the tank. As mentioned earlier the approach length between the pump and the meter was non-standard. The "Annubar" flowmeter, also referred to in Section 1.1.5, was installed in a horizontal line as far as practicable from the pump. Approach conditions were good so it should have given flow rates to within the rated tolerance of ± 1 per cent.

Comparisons of the "Annubar" and orifice plate flow measurements are given in Figures 7.11 and 7.12.

In Table 7.3 the flow rates originally measured by the orifice meter and the corresponding "Annubar" values taken from Figures 7.11 and 7.12 are both shown together with corresponding derived aquifer coefficients.

It can be seen from Table 7.3 that the a and b values are in good agreement with those determined during previous use of the aquifer material (see Section 7.2.3).

A comparison between the actual base pressure measurements for the confined flow tests and values computed from Equation 5.6 using the "Annubar" flow rates and Forchheimer coefficients a=19.2s/m and $b=2100 s^2/m^2$ can be made from the data in Table 7.2.

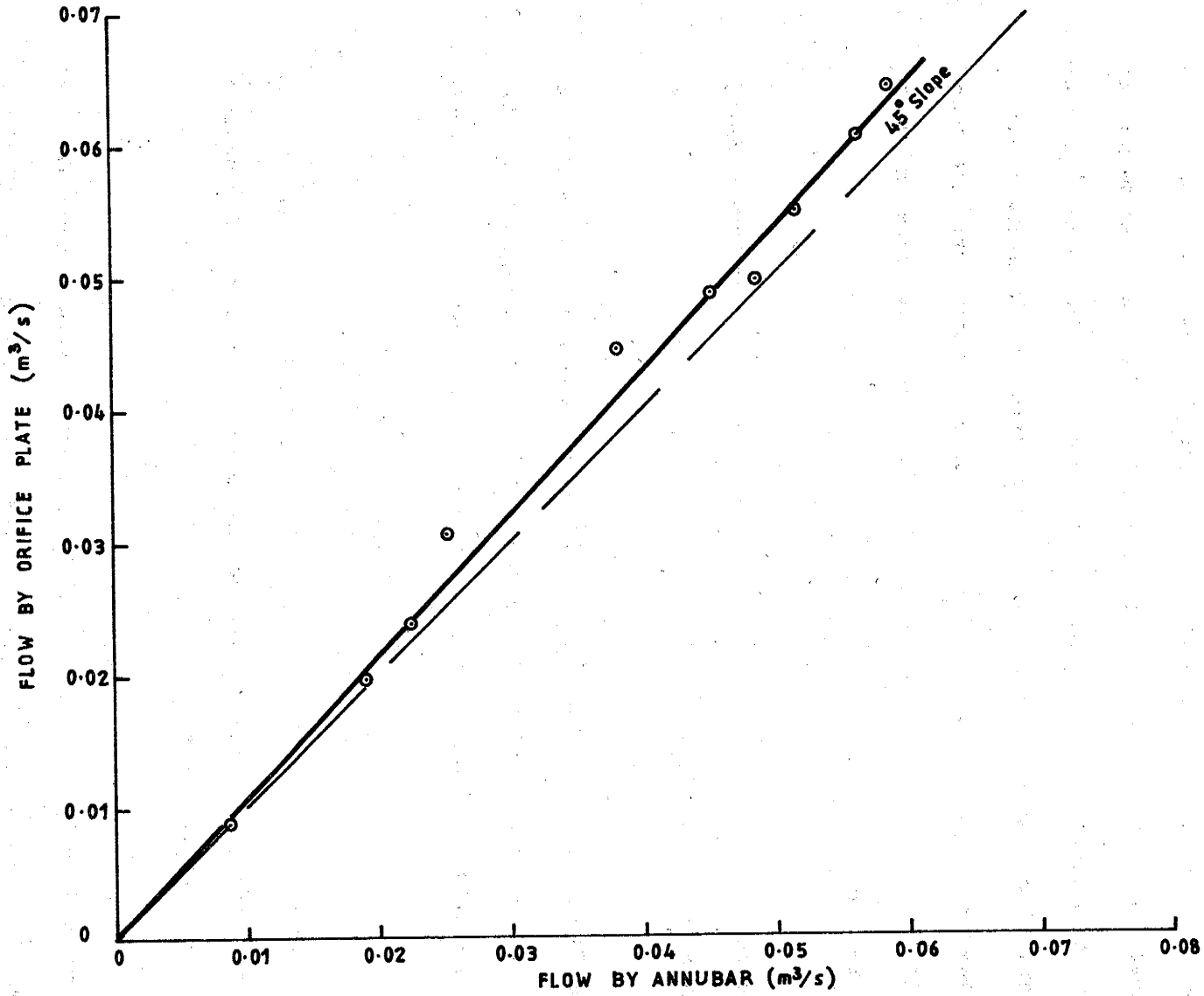

FIGURE 7·11: COMPARISON OF FLOW MEASURED BY "ANNUBAR" AND 121mm ORIFICE IN 157 mm PIPE

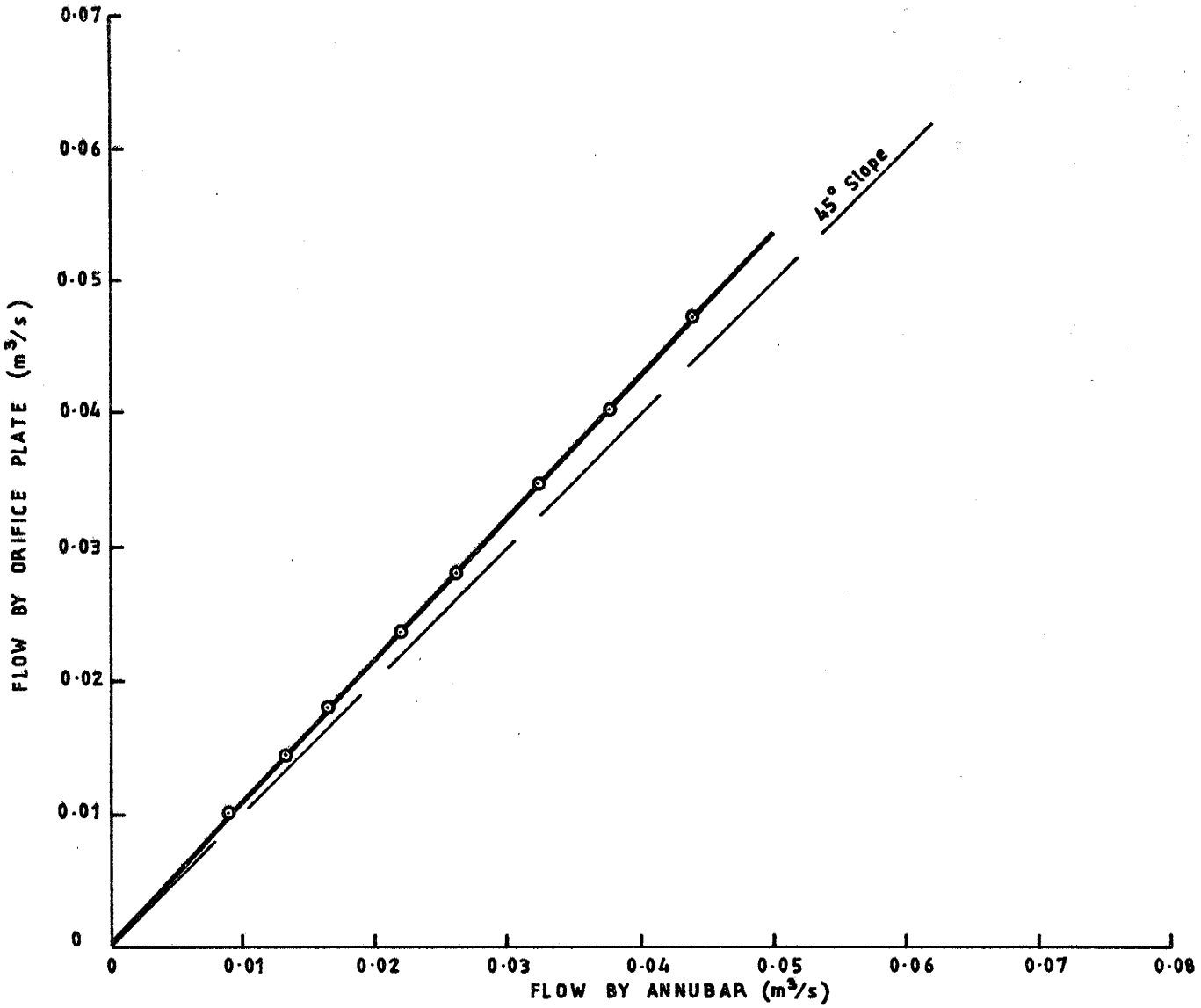

FIGURE 7·12: COMPARISON OF FLOW MEASURED BY "ANNUBAR" AND 102mm ORIFICE IN 157 mm PIPE

7.4.2 Unconfined Flow To A Fully Screened Borehole

The results of the unconfined flow tests with the borehole screen are given in Table 7.4. Computed values of flow rate and free surface height in the aquifer at the screen are also given. The sets of computed values are based on the pairs of Forchheimer coefficients shown.

Figure 7.13 shows the base pressure head distributions and an approximate free surface for one of the unconfined flows.

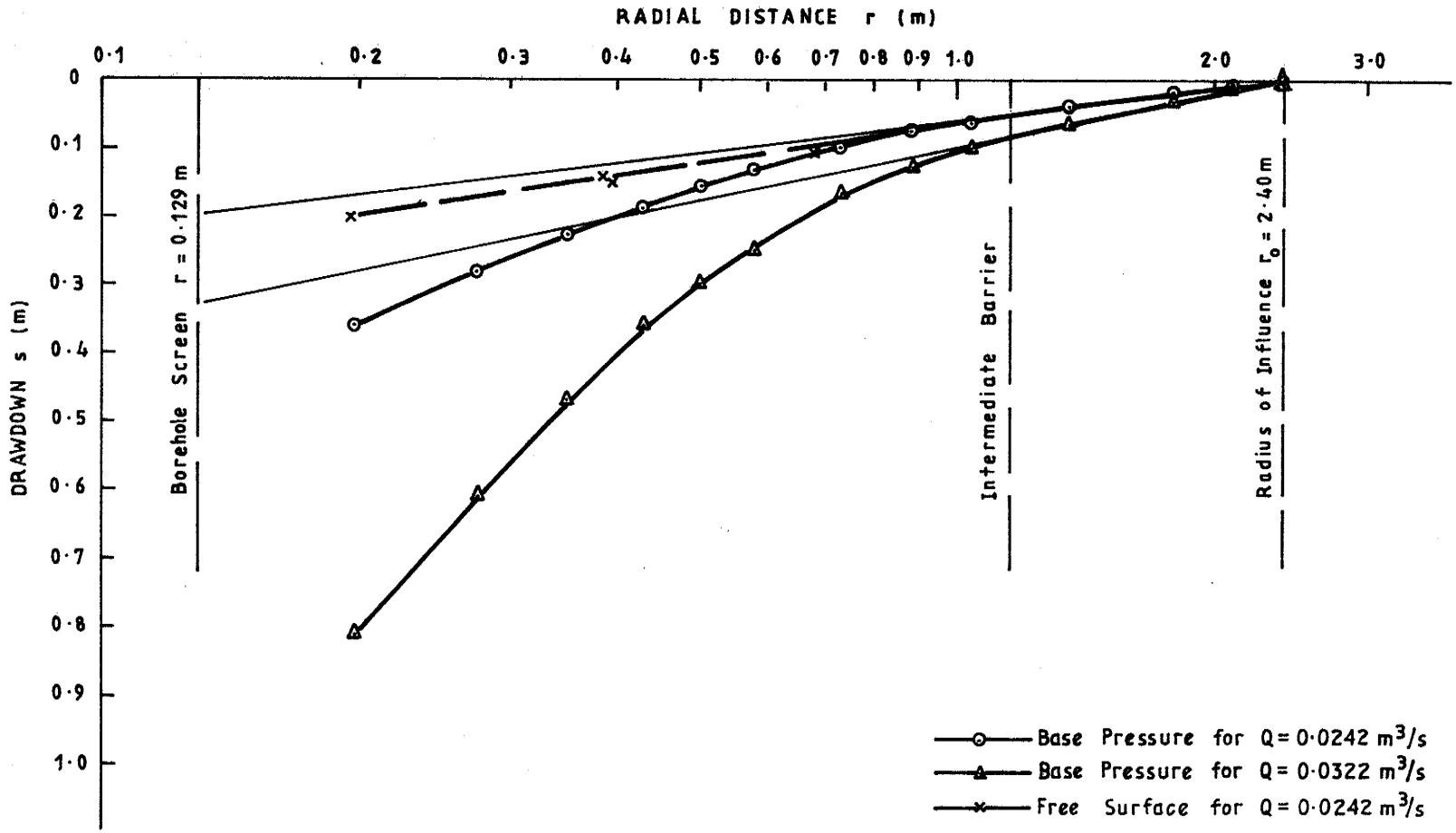

FIGURE 7·13: UNCONFINED FLOW TO BOREHOLE SCREEN

Table 7.4: Measured and Computed Unconfined Flows To Borehole Screen

$r_w = 0.129\,m \quad r_o = 2.40\,m$

Data		Trial	Computed		Experimental		
h_o (m)	h_w (m)	h_f (m)	h_f (m)	Q (m^3/s)	h_f (m)	Q (m^3/s)	
						Orifice	"Annubar"
a=17.5s/m $b=1700s^2/m^2$							
1.360	0.94	1.00	1.09	0.030	-	0.024	0.022
1.385	0.33	1.00	1.05	0.043	-	0.032	0.029
a=18s/m $b=1800s^2/m^2$							
1.360	0.94	1.00	1.07	0.029	-	0.024	0.022
1.385	0.33	1.00	1.08	0.036	-	0.032	0.029
a=19s/m $b=2000s^2/m^2$							
1.360	0.94	1.00	1.07	0.028	-	0.024	0.022
1.385	0.33	1.00	1.05	0.040	-	0.032	0.029
a=19.2s/m $b=2100s^2/m^2$							
1.360	0.94	1.00	1.08	0.027	-	0.024	0.022
1.385	0.33	1.00	1.05	0.039	-	0.032	0.029
a=11.2s/m $b=2790s^2/m^2$							
1.360	0.94	1.20	1.15	0.028	-	0.024	0.022
1.385	0.33	1.20	1.11	0.039	-	0.032	0.029

The comparison of computed and measured flow rates shows relatively poor agreement. This is accounted for by the difficulty of measuring the water level in the borehole with water cascading down from the high seepage face which resulted from the small radius of influence and the

permeable nature of the aquifer material. Since the unconfined flow measurements in the borehole screen were only incidental to the main experiments on flow into large diameter pits no attempt was made to refine the measuring techniques to give greater accuracy.

7.4.3 Unconfined Flow To Large Diameter Pits

The experimental results for flow into the pits described in Sections 7.3.3 to 7.3.5 are given in Tables 7.5 to 7.7. Measured values of flow rate and free surface heights at the pit are listed. Computed flow rates and water levels based on Forchheimer coefficients $a = 19.2 s/m$ and $b = 2100 s^2/m^2$ are also given to allow comparisons to be made.

It will be seen from the tables that the agreement between computed and experimental flow rates is within 10 per cent except for a few cases for which differences are of the order of 20 per cent. Possible reasons for the discrepancies are discussed later. Since one of the possibilities is too high a value of the coefficient a used in the computations, the finite element analysis was repeated for four other pairs of lower a and corresponding b coefficients. A comparison between the five sets of computed flow rates and the measured values is given in Tables 7.8 to 7.10.

Changes in the Forchheimer coefficients over the range shown in the tables resulted in only small differences in predicted free surface levels. This is accounted for by the small range of the ratio b/a^2. Figures B1 to B40 in Appendix B can be used to obtain a general picture of the small change in h_f caused by a small change in b/a^2. The values of $\frac{r_o}{h_o}$ in the figures do not, however, extend low enough to cover the exper-

Table 7.5: Experimental And Computed Results For Fully Penetrating Pits With Unrestricted Side Entry

$r_o = 2.40m$

Data			Trial	Computed for a = 19.2s/m b = $2100s^2/m^2$		Experimental	
r_w (m)	h_o (m)	h_w (m)	h_f (m)	h_f (m)	Q (m^3/s)	h_f (m)	Q (m^3/s)
1.15	0.715	0.310	0.50	0.48	0.0471	-	0.0555
	0.800	0.525	0.60	0.59	0.0465	-	0.0558
	0.915	0.700	0.75	0.74	0.0476	-	0.0563
	1.065	0.890	0.90	0.89	0.0496	-	0.0539
	1.430	1.320	1.00	1.32	0.0489	-	0.0538
0.59	1.075	0.570	0.70	0.69	0.0501	0.67	0.0555
	0.935	0.085	0.50	0.49	0.0470	0.50	0.0552

Table 7.6: Experimental And Computed Results For Partially Penetrating Pits With Bottom And Side Entry

r_w=0.59m r_o=2.40m

Data			Trial	Computed for a = 19.2s/m b = 2100s^2/m^2		Experimental	
h_o (m)	h_b (m)	h_w (m)	h_f (m)	h_f (m)	Q (m^3/s)	h_f (m)	Q (m^3/s)
1.090	0.750	0.835	0.90	0.88	0.0254	0.88	0.0264
1.090	0.750	0.825	0.90	0.88	0.0259	0.88	0.0266
1.090	0.750	0.920	0.95	0.93	0.0205	0.94	0.0195
1.085	0.750	1.030	1.00	1.03	0.0089	1.03	0.0085
1.140	0.600	0.700	0.80	0.83	0.0410	0.77	0.0391
1.090	0.600	0.680	0.80	0.79	0.0370	0.77	0.0340
1.085	0.600	0.830	0.85	0.86	0.0294	0.85	0.0261
1.085	0.600	1.020	1.00	1.02	0.0114	1.03	0.0089
1.085	0.600	0.900	0.90	0.92	0.0246	0.92	0.0220
1.085	0.450	0.595	0.75	0.73	0.0444	0.73	0.0510
1.090	0.450	0.675	0.75	0.76	0.0417	0.75	0.0471
1.095	0.450	0.895	0.90	0.90	0.0286	0.92	0.0285
1.095	0.450	1.020	1.00	1.02	0.0140	1.02	0.0138
1.100	0.300	0.650	0.75	0.74	0.0469	0.72	0.0571
1.095	0.300	0.765	0.80	0.80	0.0403	0.79	0.0446
1.060	0.300	0.930	0.95	0.93	0.0216	0.93	0.0226
1.095	0.300	0.950	0.95	0.96	0.0242	0.96	0.0250
1.080	0.150	0.620	0.70	0.70	0.0479	0.69	0.0479
1.055	0.150	0.760	0.80	0.79	0.0377	0.78	0.0377
1.085	0.150	0.805	0.85	0.84	0.0379	0.84	0.0377
1.060	0.150	0.905	0.90	0.92	0.0252	0.92	0.0247
1.085	0.150	0.935	0.95	0.94	0.0252	0.94	0.0247
1.085	0.150	1.005	1.00	1.01	0.0157	1.01	0.0144
0.900	0.150	0.240	0.50	0.49	0.0420	0.50	0.0477
1.090	0.300	0.420	0.65	0.65	0.0533	0.63	0.0436
1.085	0.300	0.570	0.70	0.69	0.0487	0.62	0.0394
1.090	0.300	0.705	0.75	0.75	0.0431	0.75	0.0338
1.085	0.300	0.845	0.90	0.89	0.0335	0.86	0.0265

Table 7.7: Experimental And Computed Results For Partially Penetrating Pits With Only Bottom Entry

r_w=0.59m r_o=2.40m

Data			Trial	Computed for a = 19.2s/m b = 2100s^2/m^2		Experimental	
h_o (m)	h_b (m)	h_w (m)	h_f (m)	h_f (m)	Q (m^3/s)	h_f (m)	Q (m^3/s)
1.075	0.750	1.000	1.00	1.04	0.0089	1.03	0.0098
1.085	0.750	0.930	1.00	1.02	0.0151	1.01	0.0167
1.100	0.750	0.830	1.00	1.00	0.0222	0.97	0.0258
1.080	0.600	1.020	1.00	1.06	0.0073	1.06	0.0079
1.075	0.600	0.915	1.00	1.02	0.0151	1.02	0.0153
1.085	0.600	0.770	1.00	0.99	0.0242	0.99	0.0244
1.090	0.600	0.680	1.00	0.97	0.0292	0.97	0.0312
1.085	0.450	0.965	1.00	1.05	0.0120	1.04	0.0110
1.080	0.450	0.860	1.00	1.02	0.0178	1.01	0.0167
1.090	0.450	0.715	1.00	1.00	0.0256	0.98	0.0244
1.095	0.450	0.525	1.00	0.97	0.0339	0.94	0.0345
1.080	0.300	0.955	1.00	1.05	0.0110	1.05	0.0121
1.080	0.300	0.835	1.00	1.03	0.0170	1.03	0.0191
1.055	0.300	0.815	1.00	1.01	0.0168	1.00	0.0193
1.075	0.300	0.675	1.00	1.00	0.0236	1.00	0.0269
1.100	0.300	0.395	1.00	0.98	0.0340	0.97	0.0378
1.090	0.300	0.455	1.00	0.98	0.0318	0.97	0.0351
1.085	0.150	0.805	1.00	1.05	0.0136	1.06	0.0129
1.085	0.150	0.685	1.00	1.04	0.0170	1.05	0.0160
1.090	0.150	0.425	1.00	1.02	0.0237	1.03	0.0223
1.090	0.150	0.185	1.00	1.00	0.0284	1.02	0.0266

Table 7.8: Inflow To Fully Penetrating Pits - Measured Flow Rates And Flow Rates Computed For A Range of Forchheimer Coefficients

h_b=0 r_o=2.40m

h_o (m)	h_w (m)	Inflow Rate, Q (m^3/s)					
		Measured	Computed for pairs of a(s/m), b(s^2/m^2) shown				
			a=17.5 b=1700	a=18.0 b=1800	a=19.0 b=2000	a=19.2 b=2100	a=11.2 b=2790
rw = 1.15m							
0.715	0.310	0.0555	0.0520	0.0506	0.0480	0.0471	0.0492
0.800	0.525	0.0558	0.0515	0.0500	0.0474	0.0465	0.0496
0.915	0.700	0.0563	0.0526	0.0511	0.0484	0.0476	0.0451
1.065	0.890	0.0539	0.0547	0.0532	0.0504	0.0496	0.0550
1.430	1.320	0.0538	0.0539	0.0524	0.0497	0.0489	0.0573
rw = 0.59m							
1.075	0.570	0.0555	0.0553	0.0538	0.0510	0.0501	0.0521
0.935	0.085	0.0522	0.0514	0.0500	0.0474	0.0470	0.0478

Table 7.9: Inflow To Partially Penetrating Pits With Bottom And Side Entry - Measured Flow Rates And Flow Rates Computed For A Range Of Forchheimer Coefficients

r_w=0.59m r_o=2.40m

h_o (m)	h_b (m)	h_w (m)	Inflow Rate, Q (m^3/s)					
			Measured	Computed for pairs of a(s/m), b(s^2/m^2) shown				
				a=17.5 b=1700	a=18.0 b=1800	a=19.0 b=2000	a=19.2 b=2100	a=11.2 b=2790
1.090	0.750	0.835	0.0264	0.0278	0.0272	0.0258	0.0254	0.0279
1.090	0.750	0.825	0.0266	0.0283	0.0278	0.0263	0.0259	0.0284
1.090	0.750	0.920	0.0195	0.0227	0.0220	0.0209	0.0205	0.0231
1.085	0.750	1.030	0.0085	0.0098	0.0095	0.0090	0.0089	0.0115
1.140	0.600	0.700	0.0391	0.0453	0.0440	0.0418	0.0410	0.0434
1.090	0.600	0.680	0.0340	0.0410	0.0398	0.0377	0.0370	0.0395
1.085	0.600	0.830	0.0261	0.0325	0.0316	0.0300	0.0294	0.0324
1.085	0.600	1.020	0.0089	0.0126	0.0122	0.0116	0.0114	0.0146
1.085	0.600	0.900	0.0220	0.0272	0.0264	0.0251	0.0246	0.0277
1.085	0.450	0.595	0.0510	0.0489	0.0478	0.0453	0.0444	0.0465
1.090	0.450	0.675	0.0471	0.0458	0.0448	0.0425	0.0417	0.0444
1.095	0.450	0.895	0.0285	0.0316	0.0307	0.0291	0.0286	0.0320
1.095	0.450	1.020	0.0138	0.0154	0.0150	0.0142	0.0140	0.0176
1.100	0.300	0.650	0.0571	0.0520	0.0505	0.0478	0.0469	0.0493
1.095	0.300	0.765	0.0446	0.0442	0.0433	0.0410	0.0403	0.0433
1.060	0.300	0.930	0.0226	0.0238	0.0232	0.0219	0.0216	0.0255
1.095	0.300	0.950	0.0250	0.0267	0.0260	0.0246	0.0242	0.0282
1.080	0.150	0.620	0.0479	0.0529	0.0515	0.0488	0.0479	0.0502
1.055	0.150	0.760	0.0377	0.0417	0.0405	0.0384	0.0377	0.0406
1.085	0.150	0.805	0.0377	0.0414	0.0407	0.0386	0.0379	0.0409
1.060	0.150	0.905	0.0247	0.0272	0.0270	0.0256	0.0252	0.0291
1.085	0.150	0.935	0.0247	0.0272	0.0271	0.0257	0.0252	0.0292
1.085	0.150	1.005	0.0144	0.0173	0.0169	0.0160	0.0157	0.0197
0.900	0.150	0.240	0.0477	0.0465	0.0452	0.0428	0.0420	0.0432

Table 7.10: Inflow To Partially Penetrating Pits With Bottom Entry Only - Measured Flow Rates And Flow Rates Computed For A Range Of Forchheimer Coefficients

r_w=0.59m r_o=2.40m

h_o (m)	h_b (m)	h_w (m)	Inflow Rate, Q (m^3/s)					
			Measured	Computed for pairs of a(s/m), b(s^2/m^2) shown				
				a=17.5 b=1700	a=18.0 b=1800	a=19.0 b=2000	a=19.2 b=2100	a=11.2 b=2790
1.075	0.750	1.000	0.0098	0.0098	0.0095	0.0090	0.0089	0.0105
1.085	0.750	0.930	0.0167	0.0167	0.0162	0.0153	0.0151	0.0168
1.100	0.750	0.830	0.0258	0.0246	0.0239	0.0226	0.0222	0.0235
1.080	0.600	1.020	0.0079	0.0081	0.0079	0.0075	0.0073	0.0089
1.075	0.600	0.915	0.0153	0.0164	0.0162	0.0154	0.0151	0.0168
1.085	0.600	0.770	0.0244	0.0268	0.0260	0.0247	0.0242	0.0252
1.090	0.600	0.680	0.0312	0.0323	0.0314	0.0298	0.0292	0.0296
1.085	0.450	0.965	0.0110	0.0132	0.0128	0.0122	0.0120	0.0132
1.080	0.450	0.860	0.0167	0.0197	0.0192	0.0182	0.0178	0.0192
1.090	0.450	0.715	0.0244	0.0281	0.0275	0.0261	0.0256	0.0263
1.095	0.450	0.525	0.0345	0.0373	0.0365	0.0346	0.0339	0.0336
1.080	0.300	0.955	0.0121	0.0121	0.0118	0.0112	0.0110	0.0119
1.080	0.300	0.835	0.0191	0.0185	0.0183	0.0173	0.0170	0.0180
1.055	0.300	0.815	0.0193	0.0183	0.0180	0.0171	0.0168	0.0177
1.075	0.300	0.675	0.0269	0.0259	0.0254	0.0241	0.0236	0.0240
1.100	0.300	0.395	0.0378	0.0375	0.0366	0.0347	0.0340	0.0332
1.090	0.300	0.455	0.0351	0.0351	0.0343	0.0325	0.0318	0.0313
1.085	0.150	0.805	0.0129	0.0148	0.0146	0.0138	0.0136	0.0139
1.085	0.150	0.685	0.0160	0.0187	0.0183	0.0174	0.0170	0.0171
1.090	0.150	0.425	0.0223	0.0261	0.0255	0.0242	0.0237	0.0227
1.090	0.150	0.185	0.0266	0.0314	0.0306	0.0291	0.0284	0.0269

imental values.

The computed values of h_f for the range of Forchheimer coefficients listed in Tables 7.8 to 7.10 were within 1 per cent of those shown in Tables 7.6 and 7.7 except for those computed for a=11.2s/m and b=2790s^2/m^2. For these coefficients the change in b/a^2 was sufficient to cause h_f to vary by up to 5 per cent from the values for a=19.2s/m and b=2100s^2/m^2.

7.5 Discussion of Test Results

The agreement between the computed and experimental results is generally within 10 per cent. This is considered to be quite good for large scale tests on an aquifer with a degree of uncontrolled permeability variation. Sources of error are discussed below.

7.5.1 Sources of Error

Computation Errors

The vertical and horizontal node spacings at the pit radius for the finite element solutions carried out for the experimental flow cases are listed in Table 7.11. An inspection of the data in Appendix B and some trial solutions with different node spacings indicated that the meshes used would give convergence to within 1 per cent of the ultimate solution. The close agreement between trial and computed values of h_f, the free surface height at the pit, for the final solutions adopted can be seen from Tables 7.5 to 7.7. The agreement demonstrates the absence of large errors caused by mesh distortion of the type described in Section 6.2.3.

Table 7.11: Finite Element Node Spacings For Analysis Of Experimental Flow Cases

Entry Condition	Node Spacing At Pit Radius
1. Full Penetration	1/8m for all cases
2. Partial Penetration	
(a) Bottom And Side Entry	1/8m for h_b=0.15m, 0.30m 1/4m for h_b=0.45m to 0.75m
(b) Bottom Entry	1/8m for h_b=0.15m 1/4m for h_b=0.30m to 0.75m

Flow Measurement Errors

The "Annubar" and orifice plate flow indications differed by approximately 7%. The "Annubar" measurements have been assumed correct because the installation was standard whereas the orifice plate location directly above the pump did not provide the necessary approach length.

The manufacturers of the "Annubar" claim an accuracy of ± 1%. Even if the error were twice this value it would not account for the discrepancies between measured and computed flow rates for some of the high flows.

Pressure Variation Inside The Pit

The computations assume a uniform hydrostatic pressure distribution along the base of the pit and along the side boundary below the water surface with atmospheric pressure above this level.

The actual free water surface within the pit fell towards the central outlet. Under the worst conditions of low water level and high flow the fall was of the order of 10 mm over a radial distance of 300 mm from the bottom corner of the pit with a further fall of 40 mm over the next 200 mm. The sloping water surface is the result of increasing velocity head and friction loss as the flow approaches the outlet. Since the inflow is concentrated at the bottom corner of the pit, the weighted error in assumed head at the base of the pit under the worst conditions would be of the order of 10 mm. This would not account for discrepancies of the order of 10% between measured and computed flow rates for partially penetrating pits. If this were the main source of the discrepancies there should also be significantly worse agreement for pits with only bottom entry than for pits with both bottom and side entry since the pressure on the base of the pit would affect a larger proportion of the inflow in the former case. The agreement is, in fact, worse for the bottom and side entry case. An additional argument against this source of error being large is that it does not occur for fully penetrating pits for which maximum discrepancies between measured and computed flow rates were also of the order of 20 per cent.

Velocity Head Of Water Entering Pit

It was argued in Section 6.2.3 that, except in cases of extremely permeable aquifers of small radius of influence, velocity head of water entering the pit can be neglected. If the inflow in the most severe bottom entry case were restricted to a 0.1 m wide strip in the corner of the pit the calculated microscopic velocity would not exceed 0.5m/s. The corresponding velocity head is 0.01m which is of the order of the overall error in measuring the total head difference of 0.7m. Since the assumptions are extreme, the actual error in total head loss through the

aquifer would not exceed 1 per cent.

Presence of Outlet Pipe

The outlet pipe required to extract water through the base of the aquifer slightly reduced the volume of aquifer material through which inflow could occur. Since the 150 mm diameter pipe took up only 2 per cent of the bottom area and it was situated at the centre of the pit where the discharge flux is least its effect can be neglected.

Air Entrainment

A problem encountered during pumping with low water levels in the pit was entrainment of air in the flow leaving the bottom of the pit. At times the amount of air entrained was sufficient to cause the pump to lose prime. The problem was overcome to a sufficient degree to keep the pump operating by placing a horizontal perforated steel sheet baffle over the outlet pipe. A wire mesh grid was used to space the baffle approximately 6 mm above the perforated bottom lining. De-watering of the pit was limited to the point at which there was a noticeable drop in the performance of the pump. Since the largest discrepancies between measured and computed flow rates occurred for the condition of low pit water level which was most conducive to air entrainment, the measured flow rates for these cases are suspect. Since the volume flow rates measured would have been for a mixture of air and water the water flow rate would be less than that of the mixture. This may account for a substantial part of the discrepancies.

Errors In Forchheimer Coefficients Used In Computations

A disadvantage of using the full circle pit located in the centre of the tank was that the radius of influence was half of that available for a quarter pit located at the corner outlet. The central pit was chosen because it would not have been possible to work inside a pit with a quadrant cross-section of 0.59 m radius.

The small radius of influence caused the zone of Darcy flow to be much smaller than that previously used by Dudgeon et al. (1972) for borehole flow tests. Figure 7.10 shows the short length of straight line plot available for fitting the Thiem equation. The a and b values are both in some doubt since the a value is used in the determination of b.

Tables 7.9 and 7.10 show that although the pair of coefficients $a = 17.5 s/m$ and $b = 1700 s^2/m^2$ significantly reduces the maximum discrepancy between computed and experimental values for high flow rates which occur for low pit water levels, the agreement for other values is worsened.

In an attempt to reduce the maximum percentage difference between computed and experimental inflow rates a curve fitting computer programme was used to determine a pair of a and b coefficients which spread the error over the whole range of velocities represented by the confined flow test data. The values obtained by calculation using the intercepts measured from Figure 7.10 gave more weight to the minimum and maximum velocity end of the range. The new values minimised the squares of differences between measured and calculated values.

For the tests numbered 1 and 2 for which data are given in Table 7.2 and Figure 7.9 the new pairs of a and b values determined were respectively 13.3s/m and $2990s^2/m^2$ and 11.2s/m and $2790s^2/m^2$. Since the larger drawdowns of Test No. 2 gave better measurement accuracy than the smaller values of Test No. 1 the values a=11.2s/m and $b=2790s^2/m^2$ were adopted for a further series of finite element computations of flow rates and water levels for the flow cases covered by the experiments.

Base pressure heads calculated from Equation 5.6 for the coefficients listed above can be found in Table 7.2. Flow rates computed for the fully and partially penetrating experimental flow cases are included in Tables 7.8, 7.9 and 7.10. Computed values of water levels at the experimental pits were up to 5 per cent higher than those calculated for a=19.2s/m and $b=2100s^2/m^2$. The two sets of values are given in Tables 7.12 and 7.13 for comparison. The tables reveal that the water levels for a=11.2s/m and $b=2790s^2/m^2$ do not match the experimental results better than those previously calculated.

Vertical and Radial Porosity Variation

The vertical variation of porosity shown in Figure 7.6 and the concentration of flow at a particular level because of restrictions on entry into the pit and the fall of the free surface towards the pit must affect the flow rate.

A more serious source of error caused by porosity variation is likely to be the natural "development" of the aquifer near the pit caused by flushing out of fines at the high flow rates. A considerable amount of fine material was observed to enter the pit at high inflow rates during the short series of tests which made use of the 1.15m

Table 7.12: Free Water Surface Levels At Partially Penetrating Pits With Bottom and Side Entry - Measured and Computed Values

r_w=0.59m r_o=2.40m

h_o (m)	h_b (m)	h_w (m)	Water Level At Pit, h_f (m)		
			Measured	Computed for pairs of a(s/m), b(s^2/m^2) shown	
				a=19.2 b=2100	a=11.2 b=2790
1.090	0.750	0.835	0.88	0.88	0.90
1.090	0.750	0.825	0.88	0.88	0.90
1.090	0.750	0.920	0.94	0.93	0.94
1.085	0.750	1.030	1.03	1.03	1.03
1.140	0.600	0.700	0.77	0.83	0.85
1.090	0.600	0.680	0.77	0.79	0.82
1.085	0.600	0.830	0.85	0.86	0.87
1.085	0.600	1.020	1.03	1.02	1.02
1.085	0.600	0.900	0.92	0.92	0.92
1.085	0.450	0.595	0.73	0.73	0.76
1.090	0.450	0.675	0.75	0.76	0.79
1.095	0.450	0.895	0.92	0.90	0.91
1.095	0.450	1.020	1.02	1.02	1.02
1.100	0.300	0.650	0.72	0.74	0.76
1.095	0.300	0.765	0.79	0.80	0.81
1.060	0.300	0.930	0.93	0.93	0.93
1.095	0.300	0.950	0.96	0.96	0.96
1.080	0.150	0.620	0.69	0.70	0.73
1.055	0.150	0.760	0.78	0.79	0.79
1.085	0.150	0.805	0.84	0.84	0.84
1.060	0.150	0.905	0.92	0.92	0.91
1.085	0.150	0.935	0.94	0.94	0.94
1.085	0.150	1.005	1.01	1.01	1.01
0.900	0.150	0.240	0.50	0.49	0.51
1.090	0.300	0.420	0.63	0.65	0.70
1.085	0.300	0.570	0.62	0.69	0.73
1.090	0.300	0.705	0.75	0.75	0.78
1.085	0.300	0.845	0.86	0.89	0.86

Table 7.13: Free Water Surface Levels At Partially Penetrating Pits With Bottom Entry Only - Measured and Computed Values

r_w=0.59m r_o=2.40m

h_o (m)	h_b (m)	h_w (m)	Water Level At Pit, h_f (m)		
			Measured	Computed for pairs of a(s/m), b(s^2/m^2) shown	
				a=19.2 b=2100	a=11.2 b=2790
1.075	0.750	1.000	1.03	1.04	1.05
1.085	0.750	0.930	1.01	1.02	1.03
1.100	0.750	0.830	0.97	1.00	1.02
1.080	0.600	1.020	1.06	1.06	1.06
1.075	0.600	0.915	1.02	1.02	1.03
1.085	0.600	0.770	0.99	0.99	1.01
1.090	0.600	0.680	0.97	0.97	1.00
1.085	0.450	0.965	1.04	1.05	1.06
1.080	0.450	0.860	1.01	1.02	1.04
1.090	0.450	0.715	0.98	1.00	1.02
1.095	0.450	0.525	0.94	0.97	1.00
1.080	0.300	0.955	1.05	1.05	1.06
1.080	0.300	0.835	1.03	1.03	1.04
1.055	0.300	0.815	1.00	1.01	1.02
1.075	0.300	0.675	1.00	1.00	1.02
1.100	0.300	0.395	0.97	0.98	1.01
1.090	0.300	0.455	0.97	0.98	1.01
1.085	0.150	0.805	1.06	1.05	1.06
1.085	0.150	0.685	1.05	1.04	1.05
1.090	0.150	0.425	1.03	1.02	1.04
1.090	0.150	0.185	1.02	1.00	1.03

radius intermediate barrier and the long series of tests on the 0.59 m radius pit. The increased permeability near the pit caused by removal of fines would have a disproportionate effect on high flow rates. The effect would be to increase measured flow rates relative to calculated values, particularly for high flow rates for which hydraulic gradients close to the pit become very large.

Flow Rate Sensitivity

Figures 6.28 to 6.31 indicate how sensitive the flow rate to a de-watered pit is to changes in saturated thickness h_o, pit radius r_w and non-linear parameter $\frac{b}{a^2}$ for a small radius of influence r_o. This is particularly true for flow cases involving both side and bottom entry. For the 0.59m radius pit in the 2.4m radius aquifer with a saturated thickness of 1.09m the ratios $\frac{r_o}{h_o}$ and $\frac{r_w}{h_o}$ were respectively 2.20 and 0.54. For $\frac{r_o}{h_o} = 2.20$, the operating points on the dimensionless discharge plots of Figures 6.28 to 6.31 are at the extreme left where the curves are almost vertical. It is apparent that any small change in the variables will have a marked effect on the rate of flow into the pit. Although the experimental pits could not be fully de-watered similar effects apply for low pit water levels.

For bottom entry pits no particular problem was encountered in stabilising the flow. This is reflected in the relatively good agreement shown by the experimentally derived and computed relationships between the dimensionless discharge and water level in the pit plotted in Figures 7.14 and 7.15.

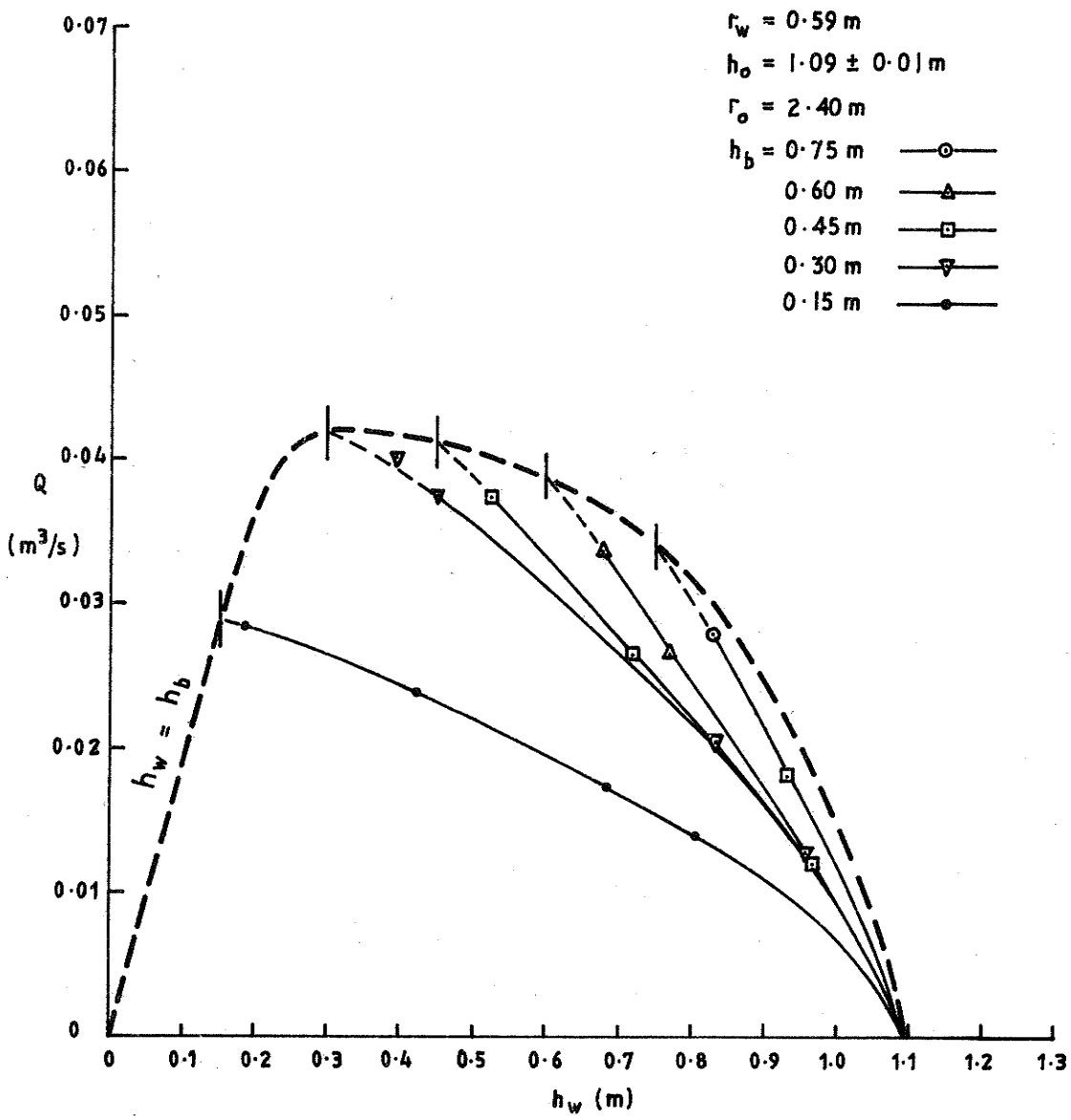

FIGURE 7·14: EXPERIMENTAL RESULTS SHOWING EFFECT OF VARIATION OF DEPTH OF PENETRATION AND WATER LEVEL ON FLOW INTO PIT WITH ONLY BOTTOM ENTRY.

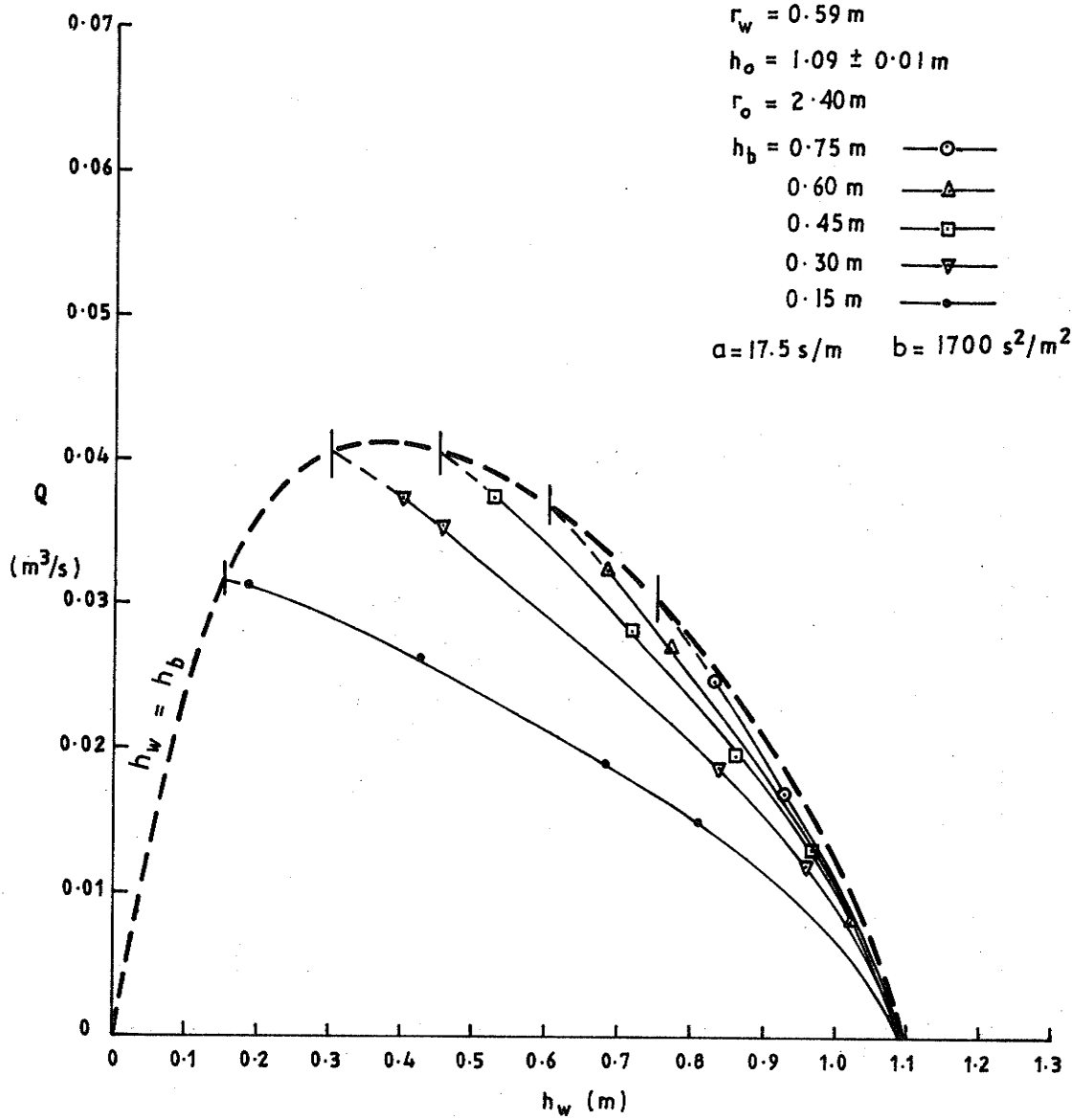

FIGURE 7·15: COMPUTED FLOW RATES FOR COMPARISON WITH EXPERIMENTAL VALUES PLOTTED IN FIGURE 7·14

However, for pits with both bottom and side entry it was found difficult at times to stabilise the flow with a low water level in the pit. Under some conditions it was possible to obtain the same inflow rate with different water levels in the pit and apparently the same saturated thickness at the radius of influence. The two flow configurations could be achieved by approaching the desired level in the pit from above and below. The effect was attributed to the lack of homogeneity of the aquifer material close to the pit boundary, the relatively flat head-discharge curve of the pump shown in Figure 7.4 and the variation in entrained air content with water level in the pit. These, combined with the very sensitive nature of the flow rate for the large pit diameter and small radius of influence, could cause the actual flow condition in the aquifer to differ sufficiently from those assumed in the computations to allow different stable phreatic surfaces to exist for a given flow rate.

The experimental results for pits with bottom and side entry are plotted in Figure 7.16. Flow rates computed for $a = 19.2 s/m$ and $b = 2100 s^2/m^2$ and the boundary conditions which applied during the experiments are plotted in Figure 7.17. It will be seen that although the experimental curves are of similar shape to the computed curves they do not form the same regular sequence as the latter. A feature of particular interest is the presence of two curves for the depth of penetration represented by $h_b = 0.30m$. The upper curve was the first obtained. The lower curve was plotted from data from repeat measurements made after tests for $h_b = 0.15m$ and $h_b = 0$ had been carried out and aquifer material was replaced in the pit to restore the $h_b = 0.30m$ condition.

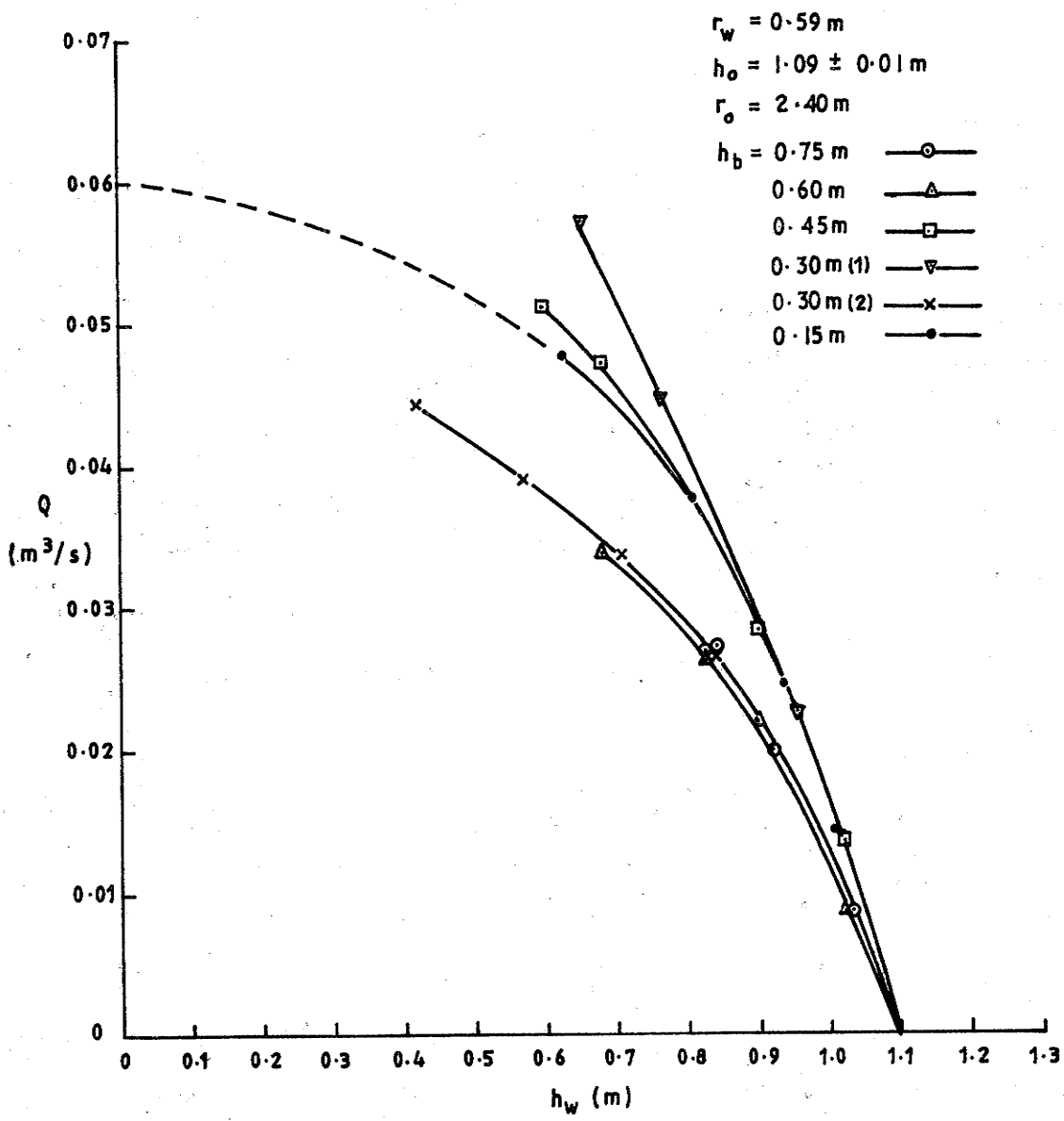

FIGURE 7·16: MEASURED FLOW RATES FOR PARTLY DE-WATERED CIRCULAR PIT WITH BOTTOM AND SIDE ENTRY

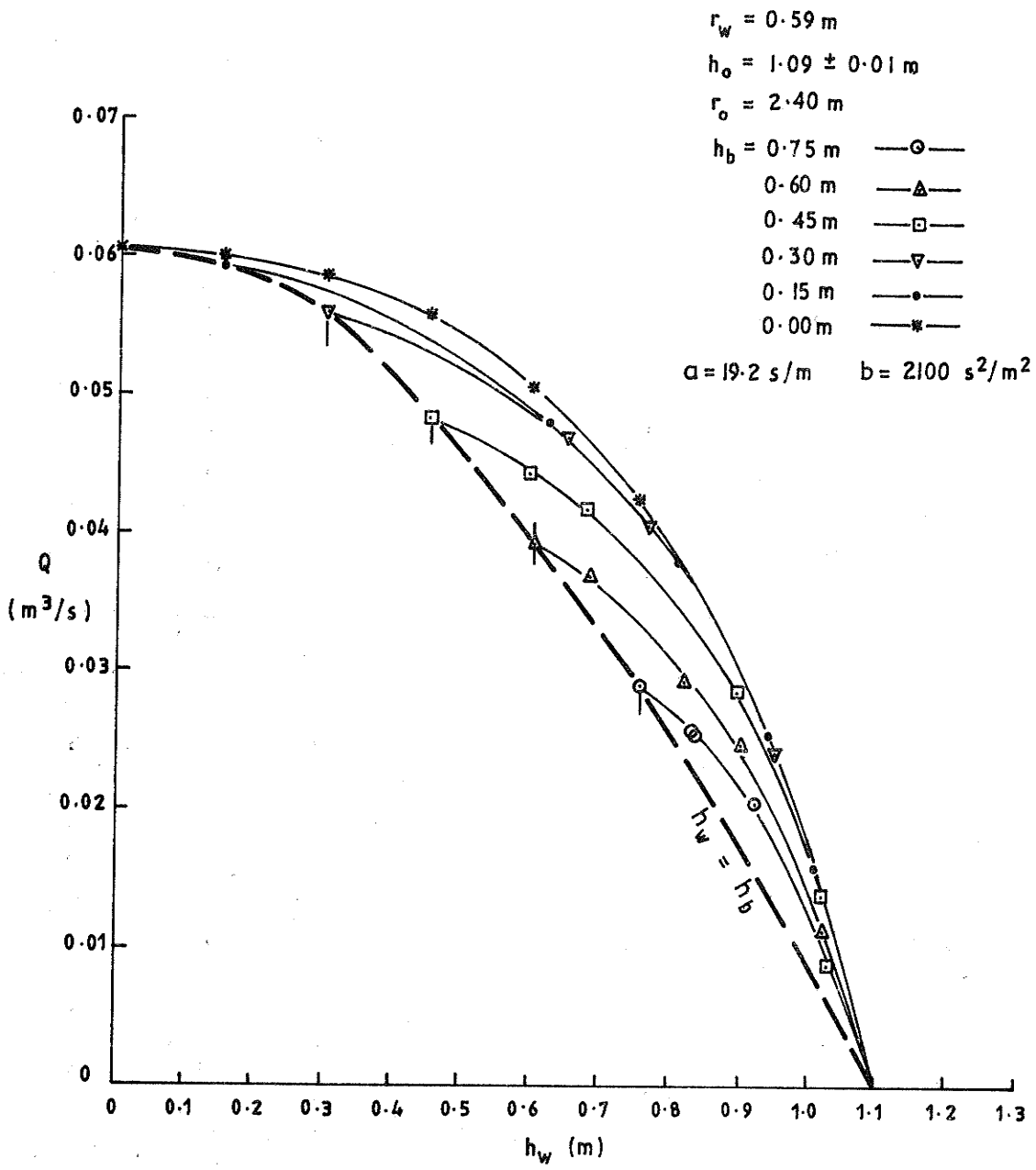

FIGURE 7·17: COMPUTED FLOW RATE FOR FULLY AND PARTLY DE-WATERED CIRCULAR PIT WITH BOTTOM AND SIDE ENTRY

Although the discrepancies between measured and computed values warrant further investigation in a controlled manner the problem is unlikely to be of importance in the de-watering of pits. The extremely small experimental ratio of radius of influence to saturated thickness is well outside the range of practical interest.

7.5.2 Conclusions

Appropriate choice of Forchheimer coefficients to match experimental and computed results can reduce the maximum discrepancy between measured and computed flow rates to approximately 20 per cent. Since most discrepancies are considerably less than 10 per cent it is concluded that the experiments have provided a satisfactory level of confirmation that the method used to compute flow rates to large diameter pits is valid. The problems caused by the small radius of influence, aquifer inhomogeneity and air entrainment with low water levels in the experimental pit are believed responsible for the few discrepancies which exceed 10 per cent.

The magnitude of the effect which post-linear regime non-Darcy flow can exert on the inflow into a pit is emphasized by data given in Table 7.14. Some of the results given in Tables 7.9 and 7.10 have been recomputed using values of a = 17.5s/m, 19.2s/m and 11.2s/m and disregarding non-Darcy flow effects by setting b = 0. The computed values of flow rate are up to three times those which allow for non-Darcy flow and which have been verified experimentally. Neglect of non-Darcy flow effects in wells and pits in highly permeable aquifers will result in gross errors if permeabilities are determined from relatively low velocity data and then used to estimate flow rates for cases for which high local velocities occur.

Table 7.14: Measured Flow Rates And Values Computed Without Allowing For Non-Darcy Flow

r_w=0.59m r_o=2.40m

h_o (m)	h_b (m)	h_w (m)	Inflow Rate, Q (m^3/s)			
			Measured	Computed for pairs of a(s/m), b(s^2/m^2) shown		
				a=17.5 b=0	b=19.2 b=0	a=11.2 b=0
Bottom And Side Entry						
1.090	0.750	0.835	0.0285	0.0465	0.0423	0.0724
1.140	0.600	0.700	0.0421	0.0855	0.0779	0.1331
1.085	0.450	0.595	0.0544	0.0940	0.0857	0.1464
1.100	0.300	0.650	0.0609	0.0972	0.0886	0.1507
1.080	0.150	0.620	0.0511	0.0999	0.0911	0.1550
Bottom Entry Only						
1.075	0.750	1.000	0.0106	0.0128	0.0117	0.0200
1.085	0.600	0.770	0.0263	0.0566	0.0516	0.0816
1.095	0.450	0.525	0.0372	0.1044	0.0952	0.1548
1.100	0.300	0.395	0.0403	0.1134	0.1034	0.1590
1.090	0.150	0.425	0.0261	0.0817	0.0745	0.1237

The less sensitive free surface water levels at the pit show very good agreement between experimental and computed values. It can therefore be concluded that the computation method satisfactorily predicts free surface water levels for unconfined flows to large diameter pits. Relative to its effect on inflow rates, post-linear regime non-Darcy flow has a smaller percentage effect on water levels adjacent to a well or pit. The data in Table 7.15 shows water levels computed assuming wholly Darcy flow for the same cases for which inflow data is given in Table 7.14. It can be seen that although the non-Darcy effect on water levels is substantial for the bottom entry condition it does not exceed 25 per cent for the cases examined. For the bottom and side entry condition the effect is negligible.

The effects of non-Darcy flow on inflows and water levels for a wider range of conditions can be seen by examining the graphs in Appendix B.

Table 7.15: Measured Water Levels Adjacent to Pits And Values Computed Without Allowing For Non-Darcy Flow

$r_w = 0.59m$ $r_o = 2.40m$

h_o (m)	h_b (m)	h_w (m)	Water Level at Pit, h_f (m)			
			Measured	Computed for pairs of a(s/m), b(s^2/m^2) shown		
				a=17.5 b=0	a=19.2 b=0	a=11.2 b=0
Bottom And Side Entry						
1.090	0.750	0.835	0.88	0.86	0.86	0.86
1.140	0.600	0.700	0.77	0.78	0.78	0.76
1.085	0.450	0.595	0.73	0.69	0.69	0.66
1.100	0.300	0.650	0.72	0.73	0.73	0.68
1.080	0.150	0.620	0.69	0.69	0.69	0.65
Bottom Entry Only						
1.075	0.750	1.000	1.03	1.03	1.03	1.03
1.085	0.600	0.770	0.99	0.90	0.90	0.92
1.095	0.450	0.525	0.94	0.70	0.70	0.82
1.100	0.300	0.395	0.97	0.76	0.76	0.82
1.090	0.150	0.425	1.03	0.89	0.89	0.89

8. APPLICATIONS OF POST-LINEAR NON-DARCY FLOW ANALYSIS IN GROUNDWATER ENGINEERING

Post-linear non-Darcy flow may occur at points of flow concentration in both groundwater supply and de-watering operations. The possibility of non-Darcy flow occurring should always be kept in mind when groundwater extraction facilities are designed, pumping tests are analysed and groundwater inflows to boreholes, wells, mines and other excavations are estimated.

8.1 Field Data Showing Evidence Of The Need For Non-Darcy Flow Analysis

Two sets of field data which provide evidence of the occurrence of non-Darcy flow near mines are shown in Figures 8.1 and 8.2 and Figures 8.3 to 8.5.

8.1.1 Excavation In Dolomite Aquifer

Figure 8.1 is a plot of water levels measured during long term pumping of a decline driven into an ore body in a fractured dolomite aquifer. Figure 8.2 shows the distribution of observation holes around the decline.

Pumping ceased after the water level measurements shown in Figure 8.1 were taken. This followed pumping for a period of approximately one month at an average discharge of 70 L/s. Analysis of the log-linear part of the plot of drawdown versus radial distance yielded a transmissivity value of 3,500 m^2/day.

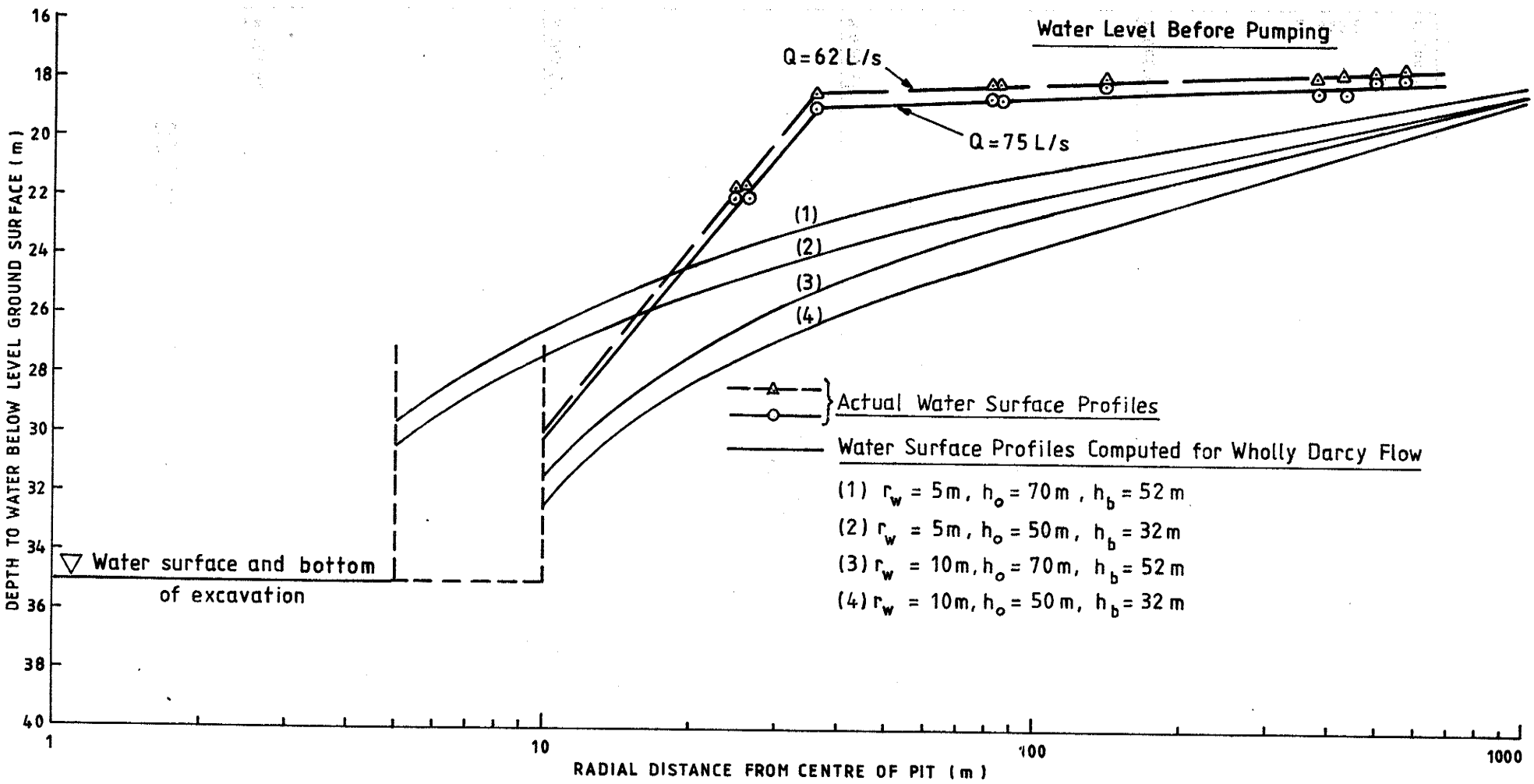

FIGURE 8·1 WATER SURFACE NEAR DE-WATERED EXCAVATION IN FRACTURED DOLOMITE

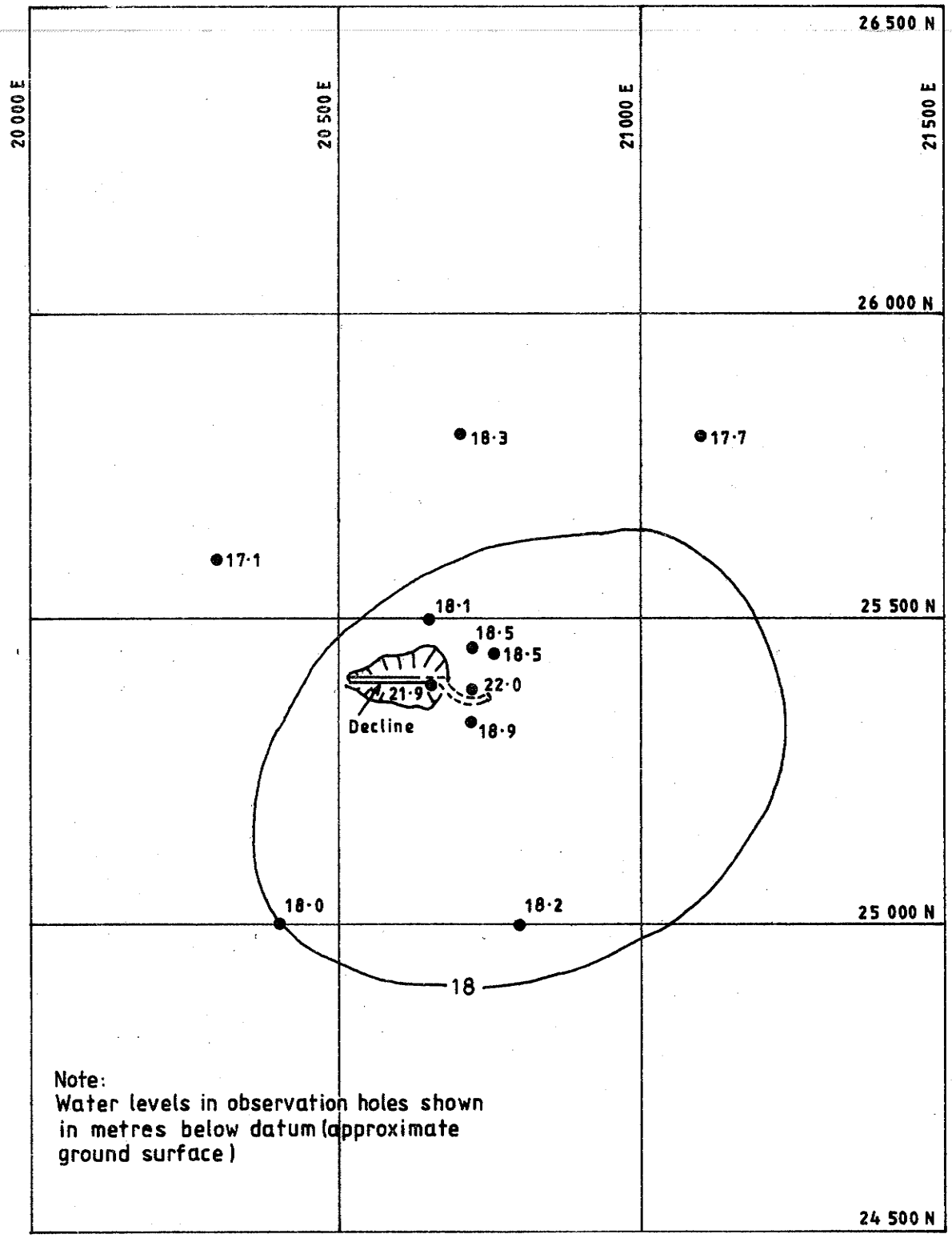

FIGURE 8·2: WATER LEVELS NEAR DE-WATERED EXCAVATION IN DOLOMITE

Since the excavation followed a sloping path through the aquifer the diameter of an equivalent vertical shaft was difficult to estimate but was assumed to be in the range 5 to 10 m.

Finite element computations were carried out for diameters of 5 m and 10 m and saturated aquifer thicknesses of 50 m and 70 m to obtain estimates of the free water surface profile. The computed free surfaces are plotted in Figure 8.1. A distinct difference between the shapes of the curves computed for wholly Darcy flow and the actual water surface profile is evident. The high measured water levels and steep gradient near the excavation is attributed to the occurrence of non-Darcy flow. The absence of observation holes closer to the excavation than those for which water levels are plotted has prevented the plotting of the true profile for small radii. The profile probably curved downwards towards an effective radius of about 10 m.

8.1.2 Open Cut Mine In Limestone Aquifer

Figure 8.3 shows the water surface profile measured at right angles to the major axis of an elongated drawdown cone around an open cut mine in a fractured limestone aquifer. Figure 8.4 shows piezometric surface contours before and during pumping. The aquifer is confined by clay to the south-east but is unconfined in other directions. Figure 8.5 shows details of part of the drawdown cone.

Finite element computations for an assumed saturated aquifer thickness h_o of 30 m were carried out to estimate the water surface profile for wholly Darcy flow. The results are shown in Figure 8.3. Since the convergence of the assumed radial flow is greater than that of the actual flow the computed gradients are exaggerated. Despite this, the

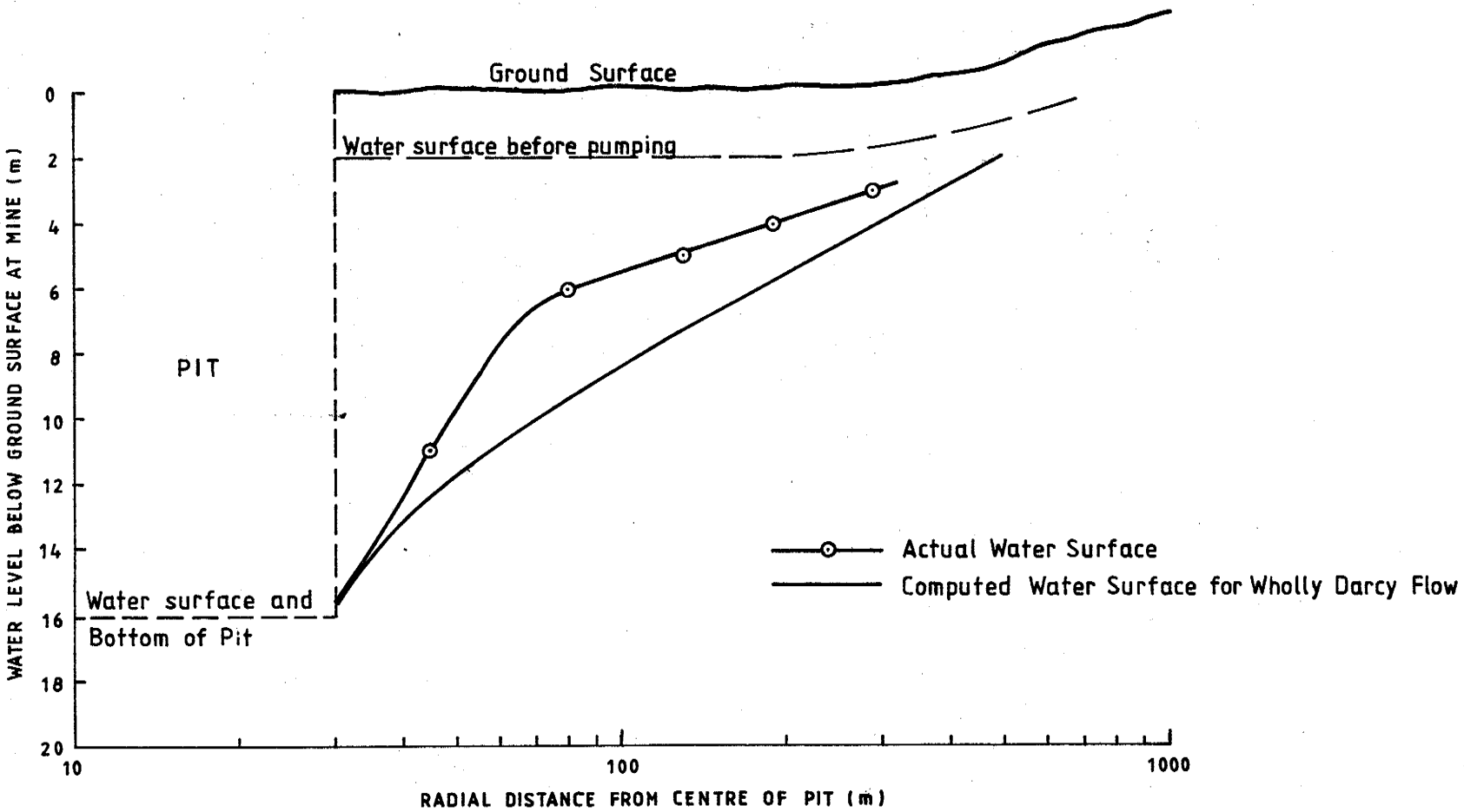

FIGURE 8·3 WATER SURFACE NEAR DE-WATERED PIT IN FRACTURED LIMESTONE

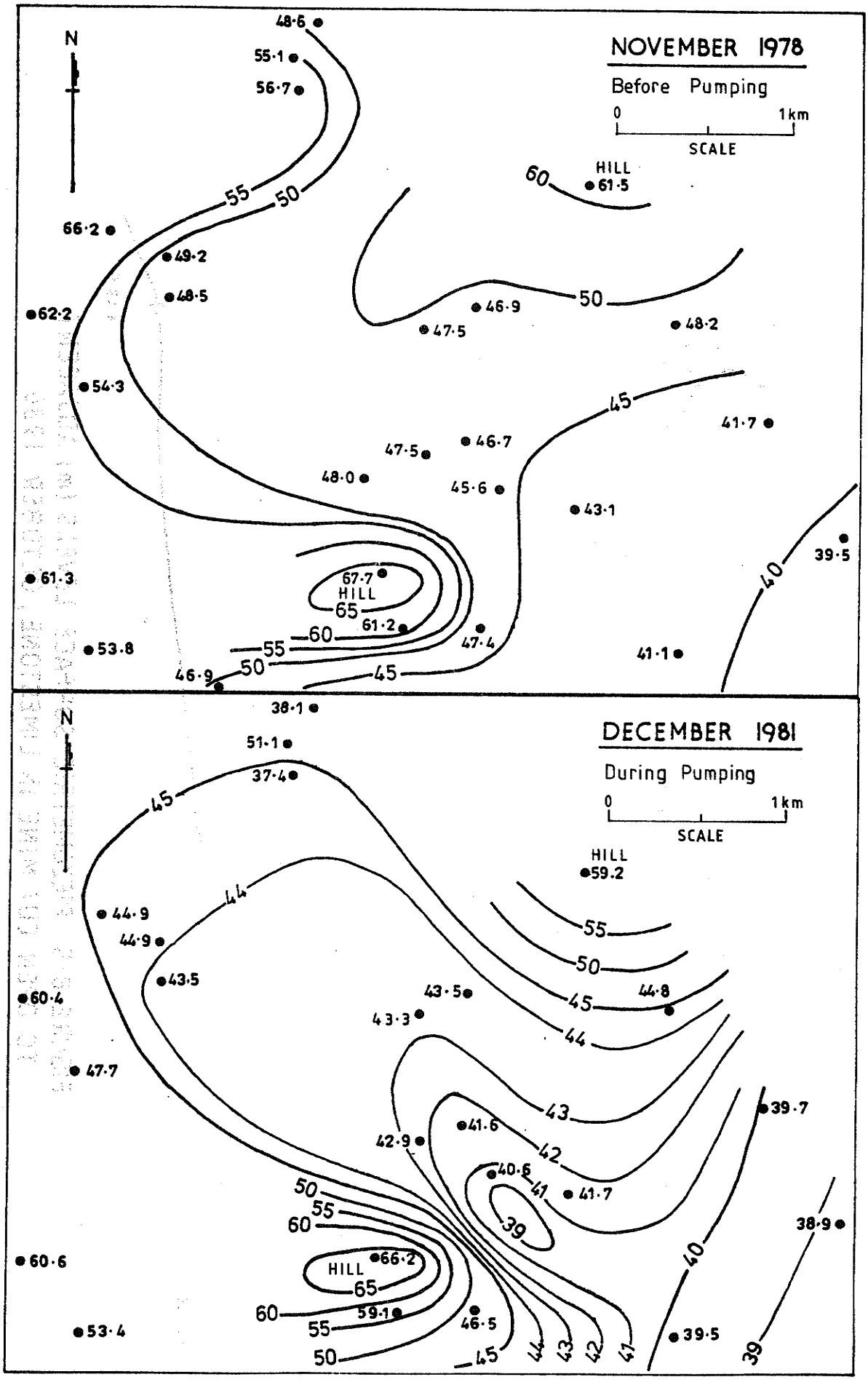

FIGURE 8·4 PIEZOMETRIC SURFACE LEVELS (m) AROUND OPEN CUT MINE IN LIMESTONE

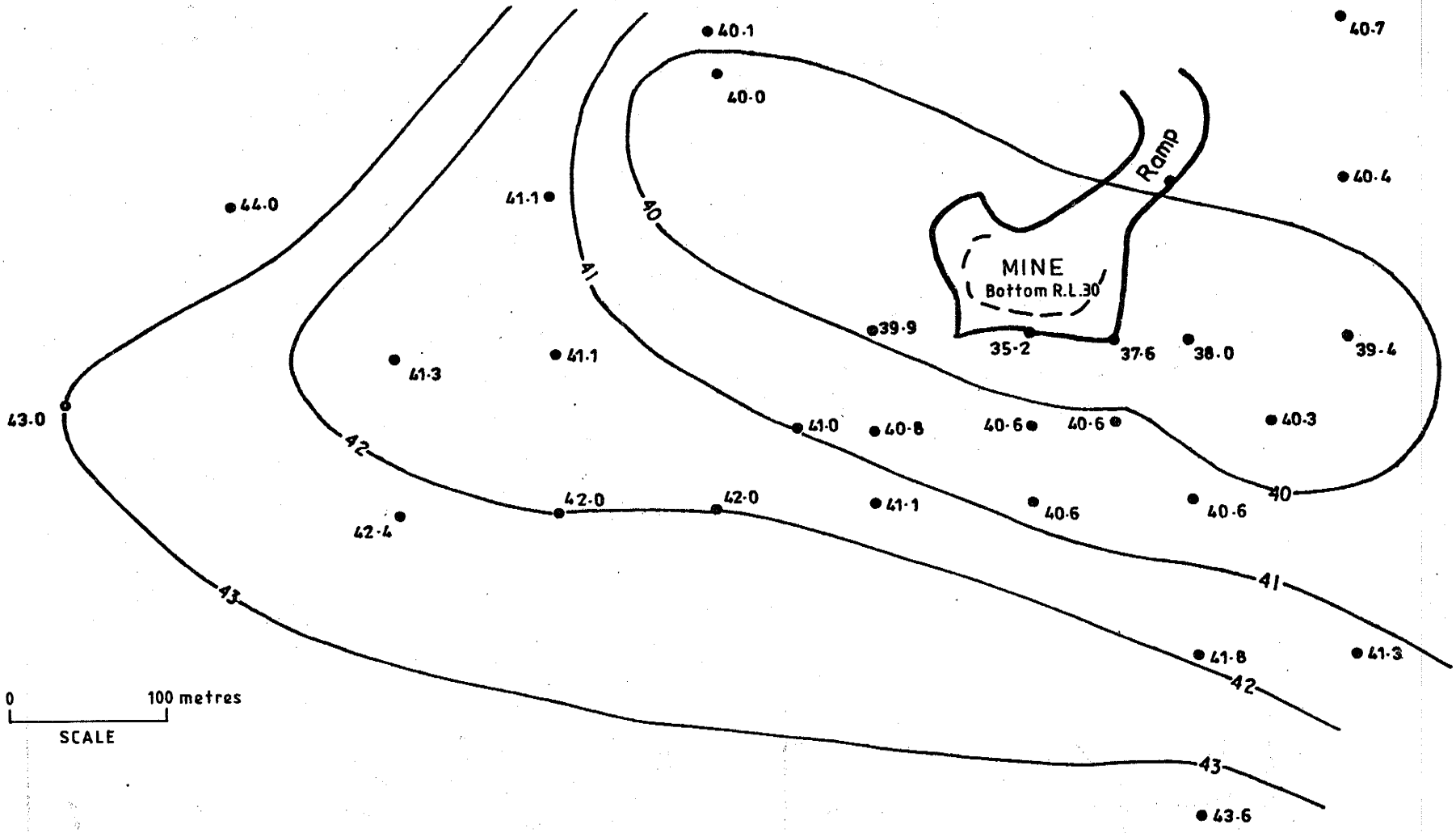

FIGURE 8·5 PIEZOMETRIC SURFACE LEVELS (m) ADJACENT TO OPEN CUT MINE IN LIMESTONE, OCTOBER 1980

computed curve is much less steep near the mine than the actual profile. The plot shows that actual head losses near the mine are much greater than those predicted by the Darcy flow analysis. The measured water surface shows the characteristics of a non-Darcy flow profile with high non-linear head losses near the mine. These result in a reduced rate of flow towards the mine and lower gradients at more distant points than those predicted by the Darcy flow analysis.

8.2 Use Of Dimensionless Relationships In Analysis And Design

The field equation which incorporates the Forchheimer equation cannot be solved easily for complex boundary conditions without the use of a large computer. Since many engineers and groundwater hydrologists throughout the world do not have ready access to such a computer, the numerical investigation described in Chapter 6 was undertaken to allow development of dimensionless relationships which would extend the range of conditions for which non-Darcy flow effects can be estimated. These relationships, given in Figures B and C of Water Research Laboratory Report No. 163 should be of assistance in solving many groundwater engineering problems. They cover the range of geometric and flow variables likely to be encountered in practice in the analysis and prediction of unconfined flows to fully and partially penetrating wells, mineshafts, open-cut mines and civil engineering excavations.

When the dimensionless relationships are used in the solution of particular groundwater problems the assumptions made in the numerical analysis described in Chapter 6 should be kept in mind. The aquifer was assumed to be homogeneous, isotropic and effectively of infinite extent. These conditions will never be met precisely but may be met to a sufficient extent in many practical problems to allow direct application of

the data provided in Figures B to D of Report No. 163. In other cases it may be possible to use the data in conjunction with equations such as those of Dupuit (Equation (5.4)), Theis (Equation (5.3)), and Boulton (1954) to extend the range of application.

The basic use, however, of the relationships provided is to allow the magnitude of the non-Darcy effect to be estimated for the range of pit and aquifer variables for flow which is steady or which is changing very slowly during the development of a drawdown cone.

The selection of the radius of influence pertinent to a given flow case deserves particular attention. Under some conditions, for example pumping from a pit in an island in a body of water such as a river, lake or ocean, there will be an actual external boundary meeting the conditions imposed on the numerical solutions. The conditions specified at the radius of influence were:

i. Constant water surface level.

ii. Hydrostatic pressure distribution.

iii. Flow through the boundary equals the discharge from the pit.

If the aquifer and pit geometry, aquifer permeability and flow rate are such that the drawdown cone cannot be distinguished from the pre-existing water surface at some radial distance from the pit a finite radius of influence less than the actual radius of the aquifer can be adopted. In such cases the aquifer is effectively infinite in extent at that time in the development of the drawdown cone. However, the drawdown cone may not be sufficiently steady to allow even approximate

application of the steady flow data. The degree of unsteadiness of the flow can be assessed by comparing the volume discharged from the pit in unit time with the change in storage in the drawdown cone which occurs in that time. If the contribution from storage is relatively small the condition of equality of discharge from the pit and inflow at the radius of influence is approximately satisfied and use of a steady flow analysis is justified.

Inspection of the graphs in the graphes in Report No. 163 will give an indication of the change in flow caused by changing the radius of influence. The radius at which the change becomes insignificant can be used as an approximation to the minimum size of the aquifer required to give steady flow conditions in the absence of a surrounding constant head recharge source. If the data in the graphes in Report No. 163 indicate that, for the given condition, drawdown will be significant beyond the maximum radius of influence covered by the data it will be necessary to add additional Darcy flow zones using the Dupuit equation until the effective limit of the drawdown cone is reached. The additional zones must be added beyond a radius which is large enough to ensure that non-Darcy flow effects have become negligible.

It should be possible to use the Theis or Boulton equation for unsteady flow to add an additional Darcy flow zone to one which includes non-Darcy flow to extend step calculations for gradually changing flow beyond the range of radius of influence covered by the data in Tables B to D of Report No. 163. Provided the water surface changes in the zone which includes non-Darcy flow are small enough for the water drawn from storage in this zone to be neglected in coparison with the total flow and the radius of the zone is large enough to extend beyond the influence of non-Darcy flow the superposition should satisfy both the

boundary conditions for the non-Darcy zone and the requirements of the Theis and Boulton equations. This procedure, which has not yet been tried, would provide a useful extension to the numerical investigation.

The preceding discussion should serve as a caution against indiscriminate use of the data given in Report No. 163. The relevance of the dimensionless relationships to the design and operation of particular groundwater extraction facilities and the de-watering of mines and other excavations is treated in the following sections.

8.2.1 Design Of Boreholes For Groundwater Supplies

In the design of boreholes for water supply it is normal practice to avoid high velocities at the inlet face to reduce the potential for encrustation and to prevent high head losses. Rational selection of appropriate diameters, depths of penetration, screen lengths and flow rates to achieve this aim requires computational methods and aids which will handle both Darcy and non-Darcy flow.

The procedures and dimensionless relationships published by Dudgeon and Cox (1977) provide sufficient information to allow optimal designs for boreholes to be determined for confined flow situations.

The data provided for unconfined flow are more restricted because the greater number of variables to be dealt with and the lack of resources available made it impractical to cover the complete range of interest. Optimisation of borehole design for unconfined flow using the data provided requires additional trial computations to be performed.

The procedures and data provided to optimise borehole design for both confined and unconfined flow cases assume that the screen will not be de-watered. Seepage faces in the boreholes are thus not allowed for in any of the data.

Boreholes in unconsolidated rocks are not normally cased and screened so seepage faces will generally be present during pumping. In practice, screened boreholes in unconsolidated aquifers may also be pumped hard enough to cause water levels to fall below the top of the screen. Dimensionless relationships which allow for seepage faces are required to analyse flow to boreholes of this type. Relationships which allow the prediction of the maximum inflow and corresponding seepage face height for such boreholes have been determined during the current investigation and are presented in Report No. 163, Figures B.1 to B.70.

8.2.2 Design Of Wells For Groundwater Supplies

In developed countries, including Australia, wells are now usually constructed by some rotary mechanical technique such as bucket augering. They are then lined with pre-cast concrete liners. Design questions which must be answered are:

i. Is it necessary or desirable to provide for side entry of water to supplement bottom entry?

ii. What is the optimal diameter and degree of penetration of the aquifer?

These questions can be answered only if a suitable means of assessing the combined effects of aquifer variables and well geometry is available. Optimal design of a well requires the determination of the discharge and water level at the well for a range of trial geometries. Since non-Darcy flow may occur in the zone of flow concentration near the well it is essential that the field equation used to calculate these values should allow for the possible occurrence of post-linear regime non-Darcy flow.

Flow concentration may also cause velocities at the well to become high enough to cause movement of unconsolidated aquifer material, possibly leading to collapse of the well. A knowledge of the distribution of inflow is therefore desirable to allow the likelihood of this occurrence to be assessed.

Since the construction of wells is limited to relatively shallow aquifers, flow will normally be unconfined when they are pumped at the maximum sustainable flow rate. A limited amount of data on the effect of non-Darcy flow on the performance of wells in unconfined aquifers is given in the design handbook by Dudgeon & Cox (1977) referred to in the previous section.

Rotary Drilled Wells With Only Bottom Entry

Only the bottom entry case for well diameters likely to be available with existing mechanical augering techniques is covered by the previously published data. The procedures described for using the data also require additional trial computations to be carried out before the performance of a well of given geometry can be predicted for a given radius of influence and saturated thickness. The necessity to spend

considerable time on the trials has detracted from the usefulness of the data. The need for these computations has been removed by the development in the course of the currently reported research of more comprehensive dimensionless relationships. These are given in Report No. 163, Figures B.6 to B.40 and B.71 to B.105.

Rotary Drilled Wells With Side And Bottom Entry

No data are given by Dudgeon and Cox for the side entry, seepage face case. For many sand and gravel aquifers in which properly constructed wells are likely to prove more economical than screened bores, the risk of collapse of bottom entry wells penetrating the aquifer to a depth which maximises the inflow is great. The maximum inflow velocity occurs under the bottom liner. Erosion of aquifer material at this point may cause a cavity to form behind the liner and the liner to sink. Progressive failure of the remainder of the well may follow. A more prudent procedure to follow when a risk of failure is perceived would be to drill to the base of the aquifer and to use permeable liners in the lower part of the well.

The maximum inflow rate will occur when the water level in the well is drawn down to the base of the well and the free surface level on the outside of the well is below the top of the permeable liners. Determination of maximum discharges and seepage face heights without direct use of a large computer requires dimensionless relationships for fully penetrating wells with unrestricted side entry. These relationships have been determined and are to be found in Report No. 163, Figures B.1 to B.5 and B.41 to B.45.

Comparisons between the performance of partially penetrating bottom entry wells, fully penetrating wells with unrestricted side entry and fully penetrating wells with restricted side entry (i.e partial screening) for diameters attainable by rotary drilling can be made using data from Report No. 163 and from the design handbook of Dudgeon and Cox (1977). The relative effects of partial penetration and non-Darcy flow can be assessed from the curves provided in both sources. The possible effect of blockage of the seepage face by encrustation can also be explored using the data. Comparison of inflows and water levels for bottom entry and bottom and side entry conditions for otherwise identical cases will allow the maximum effect of blockage of the seepage face to be assessed for fully de-watered wells.

Large Diameter Dug Wells

In developing countries, wells dug by hand frequently have diameters much larger than those of wells constructed by machine in developed countries. The large volume in the well provides useful storage. Side and bottom entry of water usually occurs since wells will be either unlined if in a stable formation or lined in a way which will allow entry of water if a lining is required to stabilise the well. Such wells are frequently pumped empty and allowed to recover overnight. If post-linear non-Darcy flow is to occur near such wells, the effect will be greatest when the well is emptied rapidly from an initially full condition with maximum water levels in the adjacent aquifer. When the water levels in the well and aquifer are allowed to recover, a point will be reached when non-Darcy effects will become insignificant because of the declining head difference across the inlet face of the well.

Selection of optimal well diameter and depth of penetration of the aquifer requires comparisons of inflows to partially penetrating wells with side and bottom entry for an extended range of well diameters. The data given in Report No. 163, Figures B.6 to B.40 and B.46 to B.70, for large diameter pits can be used directly for this purpose. The steady flow data may also prove useful for step calculations of the response of the well and aquifer to unsteady pumping.

8.2.3 Design of Boreholes and Wells for De-Watering Aquifers

Boreholes and wells used to de-water part or all of an aquifer for some engineering purpose must satisfy criteria which differ in many respects from those which water supply boreholes and wells should meet. The aim of de-watering is not to maximise the supply or minimise the cost of a given water requirement but to maximise the drawdown created by individual or groups of bores or wells or to achieve a required overall drawdown at minimum cost.

De-watering projects may have a long or short life. Progressive de-watering of aquifers in advance of open cut mining of coal deposits may proceed for many years. Other projects involving local de-watering of sand or gravel aquifers to stabilise them prior to excavating pipe-line trenches or foundation openings may require pumping for periods from hours to months. Thus the limitations on inflow velocities and de-watering of screens normally adopted for long life water supply boreholes and wells may or may not be appropriate. The shorter the expected period of pumping the less restrictive need be the limits on inflow velocities and drawdowns and thus the more likely are post-linear non-Darcy flow conditions to be met. Since non-Darcy flow results in decreased drawdowns in the aquifer, compromises must be adopted in the

design of an optimal de-watering system. The dimensionless curves provided in Report No. 163 and those previously published by Dudgeon and Cox (1977) will allow at least preliminary solutions to be obtained for most de-watering problems.

8.2.4 Estimation of Inflows And Water Levels For Excavations De-Watered From A Sump

Most open cut mineral civil engineering excavations are de-watered by pumping from within the excavation. The alternative of de-watering an aquifer within which excavation is to be carried out is usually too costly and can be justified only when some special condition, such as the ability to use cheaper explosives in dry holes, warrants de-watering in advance.

Comparisons Between Excavation De-Watering, Extraction Of Water Supplies And Aquifer De-Watering

The de-watering of mine shafts, open-cut mines and other excavations by pumping from a sump within the excavation presents a set of conditions which differ from those applying to the extraction of groundwater supplies from boreholes and wells and also differ from those associated with de-watering part or all of an aquifer. Ideally, water supply sources would provide maximum flow with negligible drawdown, boreholes used to de-water an aquifer would give maximum drawdown with negligible discharge and excavation de-watering would result in negligible inflow and drawdowns in the surrounding aquifer. It is clear that the additional head losses caused by non-Darcy flow will affect the attainment of these ideals in opposite ways.

Water supply facilities are normally designed to maximise the inflow whereas the primary aim in de-watering excavations is to minimise the inflow. In the former case, post-linear non-Darcy flow is a negative factor because it increases head losses near the borehole or well and reduces the inflow rate. In the latter case it is a positive factor since it reduces the inflow rate. An additional result of non-Darcy flow near de-watered excavations which may be desirable is the maintenance of higher water levels around the excavation than would exist if non-Darcy flow did not occur. Environmental problems caused by lowering of water levels around mines in highly permeable aquifers may thus be less serious than would be forecast by analyses which neglect non-Darcy flow.

A second difference between water supply wells and de-watered excavations is that the former are not usually completely de-watered for long periods whereas the latter will normally be fully drained to floor level for the useful life of the excavation. The piezometric surface at a water supply well will thus fluctuate more rapidly since there will be both variations in water level in the well and varying recharge to the aquifer. On the other hand, water levels around mines will continue to fall relatively slowly for a long period until there is a long term balance between inflow to the mine and recharge from a surface or boundary of sufficient extent. The fall in water level at the mine caused by expansion of the radius of influence and the consequential decrease in inflow rate have opposing influences on the occurrence of non-Darcy flow at entry as the former tends to increase velocity by decreasing inlet area and the latter tends to decrease the velocity. The relative effect of each factor can be assessed only by computation.

De-watering of an excavation by de-watering the surrounding aquifer through a system of pumped boreholes generally requires a higher rate of pumping than is required if pumping is carried out from within the excavation. Since the perimeter of the de-watered zone is larger, the restriction on flow caused by friction is less. The reduced concentration of flow also lowers the chance of non-Darcy flow and consequent flow reduction.

Unsteady Flow Predictions

Prediction of inflows and water levels which will occur during the progressive enlargement of an excavation requires unsteady flow analysis with varying boundary conditions. The analysis may be carried out on a digital computer using finite difference or finite element methods. This requires long execution times on a large computer. An alternative method is to perform a series of manual step calculations with the aid of pre-computed steady flow data to approximate the unsteady flow solution. In most cases the accuracy of such a technique will be adequate compared with the accuracy of available data on aquifer properties and estimates of the rate of enlargement of the de-watered excavation. In other cases the accuracy might be sufficient only for preliminary estimates of pumping rates required for feasibility studies with more specific numerical modelling demanded for final estimates.

Manual step calculation of unsteady flow for the full range of excavation geometries and aquifer properties met in practice would require the computation of an impractical number of dimensionless graphs from which flow rates and water levels could be calculated. In many cases the excavation will be a reasonable approximation to a pit of circular cross-section. Flow data covering the likely range of pit

diameters and depths and aquifer properties should thus be useful in making preliminary, and under favourable conditions final, estimates of inflows and water levels. If an equivalent pit diameter is chosen intelligently and the data are used to make sensitivity comparisons between the effects of change in diameter and change of aquifer properties over the respective probable ranges of error, the validity of the geometrical approximation should become apparent. If the errors introduced by assuming a circular cross-section are higher than, or are of comparable order to, those introduced by other variables and the overall error exceeds the desired limit, more refined computation techniques will be required.

Range Of Predictive Data Required

Excavations to be de-watered may allow only bottom inflow (e.g. caissons and sheet piled holes), or both side and bottom inflow (e.g. open-cut mines and other excavations with stable sides). Reliable prediction of inflow rates is important for predicting the feasibility of, and designing de-watering systems for all such excavation work. This is particularly so if excavation is to be carried out in a highly permeable aquifer. Since an aquifer with high permeability is one in which post-linear non-Darcy flow is most likely to occur, the predictive methods must be able to allow for non-Darcy flow.

Prediction of water levels adjacent to an excavation is required in the calculation of the stability of side-walls of pits and the determination of pressures which caissons and liners for shafts and wells must be designed to resist. Estimates of the effects of the excavation on groundwater levels at more remote points is also required for environmental impact assessments.

The range of dimensionless relationships determined during the numerical investigation described in Chapter 6 was designed to cover a range of pit diameter to aquifer thickness ratio which should be adequate to cover most mine shafts, open-cut mines and other excavations which can be approximated by a circular pit. The shapes of the plotted curves for large values of the dimensionless pit radius parameter are such that a reasonable degree of extrapolation may be done without introducing an unacceptable degree of error. Application of the data to typical mining situations is described in Chapter 9.

9. EXAMPLES OF THE USE OF NON-DARCY FLOW RELATIONSHIPS IN DE-WATERING AND WATER SUPPLY INVESTIGATIONS

The usefulness of the dimensionless flow relationships provided in Figures B to D of Water Research Laboratory Report No. 163 can be best demonstrated by applying them in the solution of actual groundwater engineering problems.

Several investigations which were carried out during the course of the research being reported proved the need for a set of data which could be used to give quick answers to questions involving high rate flows into wells and mines. Even if a large computer and the necessary programmes are available to solve the problems, the computer is not necessarily close at hand when the questions are posed.

Unfortunately the graphs to be found in Report No. 163 were not available when the investigations referred to were carried out. The actual mining and water supply investigations acted as a spur to the numerical investigation which produced the data given in that report and provided aquifer test data for subsequent analysis.

9.1 Open-Cut Mine In Dolomite Aquifer

A groundwater investigation aimed at assessing the feasibility of mining in a very permeable, well fractured dolomite aquifer yielded the following data from the results of long term pumping of a large diameter borehole:

Transmissivity $T = 12{,}000\,m^2/day$

Storage Coefficient $S = 10^{-3}$

Saturated Thickness $h_o = 100\,m$

The distance to surrounding, very permeable ancient river gravel deposits is 1,000 m.

The problem is to estimate the maximum possible groundwater inflow to an open-cut mine 100 m deep and 300 m in diameter at the base with an average side slope of 45^o.

The maximum possible inflow would occur if recharge from the river gravels could maintain the saturated thickness at the radius of influence for the proposed 3 year period of mining.

Assume a 300 m diameter pit with vertical sides.

$$\text{Calculate } K = \frac{T}{h_o} = \frac{12{,}000}{100} = 120\,m/day = 1.4 \times 10^{-3}\,m/s$$

In the absence of alternative information, and assuming the well fractured nature of the aquifer will cause it to behave in a similar manner to an unconsolidated aquifer, $\frac{b}{a^2}$ is estimated from Equation 6.18.

$$\frac{b}{a^2} = 160K^{5/4} \text{ (with K in m/s)} \qquad (9.1)$$

$$= 0.04$$

From the data, $\frac{r_o}{h_o} = \frac{1,000}{100} = 10$

and $\frac{r_w}{h_o} = \frac{150}{100} = 1.5.$

From Figure B.41,

for $\frac{r_o}{h_o} = 8$, $\frac{b}{a^2} = 0.04$ and $\frac{r_w}{h_o} = 1.5$, $\frac{Q}{Kh_o^2} = 1.85.$

From Figure B.42,

for $\frac{r_o}{h_o} = 20$, $\frac{b}{a^2} = 0.04$ and $\frac{r_w}{h_o} = 1.5$, $\frac{Q}{Kh_o^2} = 1.2.$

Interpolating,

for $\frac{r_o}{h_o} = 10$, adopt $\frac{Q}{Kh_o^2} = 1.7.$

Then $Q = 1.7 \times 120 \times 100^2 \, m^3/day$

$= 2 \times 10^6 \, m^3/day$

i.e. $Q = 24 \, m^3/s$

To check the seepage face height, $\frac{h_f}{h_o} = 0.14$ is estimated from Figures B.2 and B.3.

Then $h_f = 14 \, m.$

This indicates that if the 45^o pit slope were cut in 15 m deep benches, the last bench level above the final pit floor would be saturated and rock stability problems could occur.

Since the phreatic surface will be much flatter than 45^{o}, the assumption of a 150 m radius pit with vertical walls is satisfactory. The upper part of the pit will fall inside the de-watered drawdown cone and not affect the flow.

The predicted inflow is very large and would warrant a serious regional investigation of the capacity of the recharge area to maintain the flow.

The sensitivity of the discharge to variations in the estimated values of the radius of influence, aquifer depth and transmissivity could be checked rapidly from the data in Figures B of Water Research Laboratory Report No. 163 by entering the graphs with values of the variables extending over the range of uncertainty.

The volume in the de-watered drawdown cone is estimated from Figures C.1 and C.2 to be 30×10^{6} m^3. With a storage coefficient of 10^{-3}, only 30×10^{3} m^3 of water would come out of storage within the radius of influence during the three years of excavation. Since this represents only about 2 months inflow at the predicted maximum rate it is clear that the actual inflow will depend to a large extent on the rate of recharge of the dolomite from the surrounding gravels.

9.2 Maximum Inflow To A Bottom Entry Water Supply Well In A Shallow Gravel Aquifer

A thin gravel aquifer which extends over the whole area of a small island between two channels of a river is currently used to extract part of a town water supply. The water is drawn from a 300 mm diameter fully screened borehole which is operating with excessively high inflow

velocities and suffers problems of encrustation.

A comparison of potential inflows to the screened bore and the alternative of a large diameter bottom entry well is required. It is believed that the aquifer material, which is a mixture of very coarse and medium gravel, will not be unstable at the base of a well.

The following information is available:

Radius from well site to river channels r_o = 60 m

Saturated thickness of aquifer above impervious base h_o = 1.5 m

Transmissivity, from pumping test T = 1,200 m^2/day

Storage coefficient, from pumping test S = 0.04

$K = \frac{T}{h_o} = 800$ m/day

The predicted flow rates are computed in the following manner:

Fully Penetrating And Screened Borehole

$$\frac{r_w}{h_o} = \frac{0.15}{1.5} = 0.1$$

$$\frac{r_o}{h_o} = \frac{60}{1.5} = 40$$

From Equation (6.18), $\frac{b}{a^2} = 0.5$

From Figures B.44 and B.43,

$$\frac{Q}{Kh_o^2} = 0.45$$

$$\therefore Q = 0.45 \times 800 \times 1.5^2 \text{ m /day}$$

$$= 810 \text{ m}^3\text{/day}$$

$$= 9 \text{ L/s}$$

From Figures B.4 and B.3,

$$\frac{h_f}{h_o} = 0.45$$

$$\therefore h_f = 0.68 \text{ m}$$

The upper half of the screen would not be used and could be dispensed with to reduce costs.

Partially Penetrating 1.5 m Diameter Bottom Entry Well

$$\frac{r_w}{h_o} = \frac{0.75}{1.5} = 0.5$$

$$\frac{r_o}{h_o} = 40$$

$$\frac{b}{a^2} = 0.5$$

Inspection of Figures B.79, B.84 and B.89 shows that the value of $\frac{Q}{Kh_o^2}$ is almost identical for $\frac{h_b}{h_o} = 0.15$ and 0.2 and falls a little for $\frac{h_b}{h_o} = 0.25$. A penetration of 80 per cent of the aquifer thickness will thus yield maximum discharge.

$$\text{For } \frac{h_b}{h_o} = 0.2,$$

$$Q/Kh_o^2 = 0.6$$

$$\therefore Q = 0.6 \times 800 \times 1.5^2\ m^3/day$$

$$= 1{,}080\ m^3/day$$

$$= 13\ L/s$$

This represents an increase of approximately 30 per cent on the discharge which can be obtained from the screened borehole. Sensitivity calculations can again be performed quickly as in the previous example.

From Figures C.17 and C.18 the volume of the de-watered drawdown cone is estimated as $300\ m^3$. For the storage coefficient of 0.04, the volume of water extracted from the drawdown cone is $12\ m^3$. This represents the volume pumped from the well at the steady flow rate in one-quarter of an hour. It is evident that the well must draw water almost directly from the river. The supply is provided by the river flow and the well is simply a convenient extraction facility for filtered water.

10. CONCLUSIONS

Non-Darcy flow of groundwater falls into two distinct and independent categories.

The first type has been named pre-linear regime non-Darcy flow to indicate that it occurs only at velocities lower than that for which the linear Darcy law is valid within the accuracy of measurement of flow rates and hydraulic gradients. It has been observed in laboratory experiments with aquifer materials but does not appear to have been conclusively demonstrated in aquifers in the field. Its cause in flow through channels of the size important in aquifers appear to be the strength of molecular bonding in water under some conditions. Low shear rates, which result from a combination of relatively small microscopic flow channel cross-sections and low hydraulic gradients, are necessary for pre-linear non-Darcy flow to occur.

The second type has been named post-linear regime non-Darcy flow and occurs at velocities above the range of validity of Darcy's law. Its occurrence depends on the achievement of sufficiently high Reynolds numbers since it is caused by inertial and turbulent "loss" of energy at the microscopic level. Its occurrence has been observed in both laboratory and field investigations.

Since the two types of non-Darcy flow are independent, the conclusions drawn in relation to pre-linear and post-linear regime flows and their effects will be considered separately.

10.1 Pre-Linear Regime Non-Darcy Flow

i. Water of the purity obtainable by distillation in a high quality glass still behaves as a Newtonian fluid for all shear rates of practical interest in groundwater flow provided atmospheric gases are not carried in solution. This conclusion is drawn from a critical evaluation of the results of experiments in capillary tubes with diameters large enough (0.1 to 3 mm) to allow surface forces to be neglected. The experiments reported in this thesis, supported by experiments of Griffiths and Griffiths (1921), are considered to remove any doubt in this matter.

ii. One or more of the atmospheric gases in solution in otherwise pure distilled water causes water to behave as a non-Newtonian fluid at low rates of shear. The experimental results provided clearly demonstrate this fact. The effect is attributed to an increase in extent of molecular groupings in water caused by the tendency of water molecules to form "clathrates" or cages of bonded water molecules around non-polarised or weakly polarised solute molecules. The theoretical interpretation is based on a study of published experimental and theoretical investigations into the factors affecting the molecular structure of water.

iii. Water containing dissolved air has thixotropic properties which cause an increase in the effective viscosity with time during low shear rate flow. The effective viscosity can be returned to its normal high shear rate value by increasing the shear rate sufficiently. This can be achieved by increasing the hydraulic gradient. Return to the normal viscosity can also be achieved by adding energy to the water by applying shock or vibration. This

effect is attributed to either direct impulses applied to the molecular structure or to shearing on a microscopic scale caused by differential velocities generated by the shock and vibration.

iv. Evaluation of published theoretical and experimental work on the molecular structure of water leads to the conclusion that non-polar and ionic solutes other than those from dissolved air may also affect the structure of water sufficiently to affect the relationship between shear stress and shear rate at low shear rates. A great deal of additional research is required in this field. For this research to be more than an uncontrolled empirical examination of a minute number of the possible combinations of solutes which may be present in water, more basic theoretical and experimental information on water structure is required. Further experiments in capillary tubes and a co-axial viscometer on water containing solutes which have been shown to be capable of affecting the molecular structure of water should form the next stage of research into non-Newtonian flow of water at low shear rates.

v. Since groundwater is not pure water, but may contain dissolved atmospheric gases and other non-polar and ionic solutes, the conclusions (i) to (iv) are relevant to the study of groundwater flow at low shear rates. At this time it is not possible to apply the existing knowledge quantitatively. However, the qualitative effects of non-Newtonian flow at the microscopic level in aquifers can be deduced. The general effect in a given aquifer would be to reduce the macroscopic velocity for a given hydraulic gradient below that predicted by Darcy's law.

vi. In situations where dissolved atmospheric gases or other "structure-making" solutes are present in groundwater, the potential exists for pre-linear regime non-Darcy flow. A future step in the study of the effect of dissolved air should be directed towards determining whether the effects observed in the reported laboratory experiments can be detected in the field. A controlled field experiment should be set up to measure velocities and hydraulic gradients in a low shear rate flow of relatively pure groundwater containing dissolved air. A suitable site would be where rainwater percolates through a clean silica sand aquifer and then continues to flow under low hydraulic gradients in the saturated zone.

vii. Natural earth movements and vibrations generated from within the earth and by lunar and solar attraction may provide a sufficient level of vibrational or shear energy input to groundwater to prevent molecular structure from becoming sufficiently strong to cause non-Newtonian flow on the microscopic scale and thus pre-linear non-Darcy flow on the macroscopic scale. The effects of impact, vibration and atmospheric pressure fluctuations on flow at low shear rates in a capillary tube reported in this thesis suggest this possibility. Any controlled field experiment such as that recommended in (vi), or future laboratory experiments, should closely monitor shock and vibration levels and atmospheric pressure and earth tide effects.

10.2 Post-Linear Regime Non-Darcy Flow

i. An evaluation of previous investigations into the upper limit of Darcy's law provides conclusive evidence of the occurrence of post-linear regime non-Darcy flow through aquifer materials. The

evidence includes numerical solutions of the Navier-Stokes equations for two-dimensional arrays of particles of regular geometry and results from experiments in permeameters and axi-symmetric flow tanks. Macroscopic velocities predicted by Darcy's law become increasingly erroneous the more the velocity exceeds some critical value. Above this value, actual velocities are always less than those given by Darcy's law.

A Reynolds number which combines the influence of velocity, flow channel dimensions and fluid viscosity should be used as the criterion for the upper limit of the Darcy regime in groundwater flow. However, experimental evidence clearly indicates that no single limiting value of Reynolds number applies to all aquifer materials. This is the result of the impracticality of measuring a sufficient number of geometric variables to define families of geometrically similar aquifer materials to which a common limiting value of Reynolds number would apply.

ii. The velocities for which non-Darcy flow occurs are within the range of velocities which may occur near points of groundwater flow concentration such as pumped boreholes and wells and de-watered open pits.

iii. For the practical purpose of predicting the characteristics of both Darcy and non-Darcy groundwater flow, the Forchheimer equation with a single pair of coefficients provides a sufficiently accurate fit to the relationship between macroscopic velocity and hydraulic gradient for a given aquifer material.

iv. The numerical and experimental investigations reported in this thesis have demonstrated that significant non-Darcy flow effects can exist near large diameter wells, open-cut mines and other excavations in highly permeable aquifers.

v. The finite element procedures used to compute inflow rates and water levels for unconfined flows to circular pits in homogeneous isotropic aquifers have been verified by comparison with the results of large scale tests in a specially designed testing facility.

vi. A set of dimensionless relationships has been determined by numerical analysis to allow the prediction of inflows and water levels for circular pits in unconfined aquifers. The relationships cover the range of pit and aquifer dimensions likely to be met in groundwater engineering practice. Full penetration, partial penetration with bottom entry and partial penetration with bottom and side entry conditions are covered.

vii. The usefulness of the dimensionless relationships in making rapid estimates of maximum inflows to wells and open-cut mines has been demonstrated. The ease of use is such that it is feasible to carry out a sensitivity analysis for a considerable range of uncertainty of the variables without an uneconomic level of effort.

viii. The dimensionless flow rate, water level and drawdown cone data can be used in conjunction to perform step computations of unsteady flows if the boundary conditions approximately satisfy those assumed in the derivation of the data.

ix. Although the numerical analysis and dimensionless results apply only to circular pits in homogeneous isotropic aquifers, intelligent application should allow at least preliminary estimates to be made of non-Darcy flow effects for more complex pit geometries and aquifer conditions. If preliminary estimates indicate that non-Darcy flow effects will be insignificant, the more detailed analysis required to predict flow rates and water levels for more complex conditions can be simplified by setting the non-linear coefficient in the Forchheimer equation equal to zero. Alternatively, equations based directly on Darcy's law instead of the Forchheimer equation can be used.

11. LIST OF REFERENCES

[1] Ahmed, N. and Sunada, D.K. (1969). "Non-linear flow in porous media." A.S.C.E., Jour., 95, HY6, 1847-1857.

[2] Barends, F.B.J. (1976). "SEEP, a finite element code for groundwater flow." Delft (Netherlands) Soil Mech. Lab. Rept. 74 - 680215.

[3] Bear, J. (1979). "Hydraulics of groundwater." McGraw-Hill, New York.

[4] Ben-Naim, A. (1980). "Hydrophobic interactions." Plenum, New York.

[5] Bondarenko, N.P. (1968). "Bingham flow in capillary-porous media." Int. Socy. of Soil Science, Congress, Adelaide, Australia, 205-212.

[6] Bondarenko, N.P. and Nerpin, S. (1965). "Rheological properties of water in porous media." RILEM, Bulletin 29, 13-16.

[7] Boulton, N.S. (1951). "The flow pattern near a gravity well in a uniform water bearing medium." Inst. Civil Engrs. (U.K.), Jour., 36, 534-550.

[8] Boulton, N.S. (1954). "The drawdown of the water-table under non-steady conditions near a pumped well in an unconfined formation." Inst. Civil Engrs. (U.K.), Proc., 3, Part 3, 564-579.

[9] Boulton, N.S. and Streltsova, T.D. (1975). "The drawdown near an abstraction well of large diameter under non-steady conditions in an unconfined aquifer." J. Hydrology, 30, 29-46.

[10] Bouwer, H. (1978). "Groundwater hydrology." McGraw-Hill, New York.

[11] Chauveteau, G. and Thirriot, C.I. (1967). "Regimes d'ecoulement en milieu poreux et limite de la loi' de Darcy." La Houille Blanche, n. 2, 141-148.

[12] Childs, E.C. and Tzimas, (1971). "Darcy's law at small potential gradients." Jour. Soil Sci., 22, 319-327.

[13] Cox, R.J. (1977). "A study of near well groundwater flow and its implications in well design." Univ. of New South Wales, Water Research Lab., Rept. No. 148.

[14] Darcy, H. (1856). "Les fontaines publiques de la ville de Dijon." Victor Dalmont, Paris.

[15] De Wiest, R.J.M. (1965). "Geohydrology". Wiley, New York.

[16] Drost-Hansen, W. (1976). "The nature and role of interfacial water in porous media." Am. Chem. Soc., Div. Pet. Chem., Prepr., 21,2, 278-280.

[17] Dudgeon, C.R. (1964). "Flow of water through coarse granular materials." Univ. of New South Wales, Water Research Lab., Rept. No. 76.

[18] Dudgeon, C.R. and Cox, R.J. (1977). "Hydraulic design data for water wells in unconsolidated sediments." Australian Water Resources Council, Technical Paper No. 22.

[19] Dudgeon, C.R. et al. (1972). "Hydraulics of flow near wells in unconsolidated sediments." Univ. of New South Wales, Water Research Lab., Rept. No. 126, 1972.

[20] Duff, A.W. (1905). "Poiseuille's law at very low rates of shear." Philosophical Magazine, 9, 53, 685-692.

[21] Engelund, F. (1953). "On the laminar and turbulent flows of groundwater through homogeneous sand." Dan. Acad. Tech. Sci., Trans., n. 3; Univ. of Denmark, Bull. No. 4.

[22] Forchheimer, P. (1901). "Wasserbewegung durch boden." Zeit. Ver. Deutsch. Ing., 45, 1782-1788.

[23] Franks, F. (1981). "Polywater." MIT Press, Cambridge, Mass. (U.S.A.) and London (England).

[24] Gallagher, R.H. et al. (Ed.) (1975). "Finite elements in fluids." (Conference series), v. 1 et seq.

[25] Greenkorn, R.A. (1983). "Flow phenomena in porous media." Marcel Dekker, New York.

[26] Griffiths, A. and Griffiths, C.H. (1921). "Viscosity of water at low shear rates." Physical Soc. of London, Proc., 33, 231-242.

[27] Griffiths, A. and Knowles, C.H. (1912). "The resistance to flow of water along a capillary soda-glass tube at low rates of shear." Physical Soc. of London, 24, 350-357.

[28] Gurney, L.E. (1908(a)). "The viscosity of water at very low rates of shear." Physical Review, 26, 98-120.

[29] Gurney, L.E. (1908(b)). "Some observations on the surface rigidity of water." Physical Review, 26, 121-122.

[30] Gurney, L.E. (1908(c)). "Effects of the soluble constituents of glass upon the viscosity of water at very low rates of shear." Physical Review, 26, 123-124.

[31] Hannoura, A.A. and Barends, F.B.J. (1981). "Non-darcy flow; a state of the art." Euromech 143, Delft (Netherlands), Proc., 37-51.

[32] Hedstrom, B.O.A. (1952). "Flow of plastics materials in pipes." Industr. Eng. Chem., 44, 3, 651-656.

[33] Herbert, R. and Kitching, R. (1981). "Determination of aquifer parameters from large-diameter dug well pumping tests." Ground Water, 19, 6, 593-599.

[34] Huyakorn, P.S. (1973). "Finite element solution of two-regime flow towards wells." Univ. of New South Wales, Water Research Lab., Rept. No. 137, 1973.

[35] Huyakorn, P.S. and Pinder, G. (1983). "Computational methods in subsurface flow." Academic Press, New York.

[36] Kazemipour, A.K. (1974). "Prediction of hydraulic characteristics of aquifer materials." Univ. of New South Wales, M.Eng.Sci. Thesis.

[37] Klassen, V.I. et al. (1969). "Structural features of water." Inst. Georyuch. Iskop., Moscow, Trans., 25, 2, 121-9, 1969.

[38] Kovacs, G. (1969(a)). "Seepage law for microseepage." I.A.H.R., 13th Congress (Kyoto, Japan), Proc., 4, 1-7.

[39] Kovacs, G. (1969(b)). "General characterization of different types of seepage." I.A.H.R., 13th Congress (Kyoto, Japan), Proc., 4, 205-214.

[40] Kutilek, M. (1969). "Non-darcian flow of water in soils (laminar region)." I.A.H.R., 1st Symp. on Fundamentals of Transport Phenomena in Porous Media, Haifa (Israel), (Publ. Elsevier, 1972), 327-340.

[41] Kyle, C.R. and Perrine, R.L. (1971). "An experimental model for visual studies of turbulent flow in porous materials." Canadian Jour. of Chem. Eng., 49, 19-24.

[42] McCorquodale, J.A. (1970). "Variational approach to non-Darcy flow." A.S.C.E., Jour., 96, HY11, 2265-2278.

[43] McCorquodale, J.A. et al. (1978). "Hydraulic conductivity of rockfill." Jour. of Hydraul. Res., 16, 2, 123-137.

[44] Nilssen, L.Y. (1966). "Short-time variation of the ground water and its reasons." Ground Water Problems, Proc. Int. Symp., Stockholm (Ed. Eriksson, E. et al.), Pergamon Press, 57-69.

[45] Papadopulos, I.S. (1967). "Drawdown distribution around a large diameter well." American Water Resources Assoc., Proc., n. 4, (Proc. Symp. on Groundwater Hydrology, San Francisco), 157-168.

[46] Papadopulos, I.S. and Cooper (H.H.) (1967). "Drawdown in a well of large diameter." Water Resources Research, 3, 1, 241-244.

[47] Poiseuille, J.L.M. (1840, 1841). "Recherches experimentales sur le mouvement des liquides dans les tubes de tres petits diametres." Academie des Sciences, Paris, Comptes Rendus, 961-967, 1041-1048 (1840); 112-115 (1841).

[48] Rushton, K.R. and Holt, S.M. (1981). "Estimating aquifer parameters for large-diameter wells." Ground Water, 19, 5, 505-509.

[49] Rushton, K.R. and Singh, V.S. (1983). "Drawdowns in large-diameter wells due to decreasing abstraction rates." Ground Water, 21, 6, 670-677.

[50] Schneebeli, G.P. (1955). "Experiences sur la limite de validite de la loi de Darcy et l'apparition de la turbulence dans un ecoulement de filtration." La Houille Blanche, n. 2, 141-148.

[51] Skawinski, R. and Lasowska, A. (1974(a)). "Nonlinear flow of water solutions in capillaries." Polish Academy of Sciences, Bull., 22, 5, 239-242.

[52] Skawinski, R. and Lasowska, A. (1974(b)). "Non-Darcian flow of water solutions in artificial porous medium with grain sizes of several millimetres." Polish Academy of Sciences, 22, 5, 235-238.

[53] Slepicka, F. (1961). "The laws of filtration and limits of their validity." I.A.H.R., Proc. 9th Convention, Belgrade, 2, 383-394.

[54] Stark, K.P. and Volker, R.E. (1967). "Non-linear flow through porous materials. Some theoretical aspects." Univ. College of Townsville (Australia), Research Bull. No. 1.

[55] Stillinger, F.H. (1980). "Water revisited." Science, 209, 4455, 451-457.

[56] Swartzendruber, D. (1966). "Soil-water behaviour as described by transport coefficients and functions." Advances in Agronomy, 18, 327-370.

[57] Van der Kamp, G. and Gale, J.E. (1983). "Theory of earth tide and barometric effects in porous formations with compressible grains." Water Resources Research, 19, 2, 538-544.

[58] Volker, R.E. (1969). "Non-linear flow in porous media by finite elements." A.S.C.E., Jour., 95, HY6, 2093-2111.

[59] Walton, K.C. (1970). "Groundwater resource evaluation." McGraw-Hill, New York.

[60] Ward, J.C. (1964). "Turbulent flow in porous media." A.S.C.E., Jour., 90, HY5, 1-12.

[61] Wright, D.E. (1968). "Non-linear flow through granular media." A.S.C.E., Jour., 94, HY3, 851-872.

APPENDIX A

LOW SHEAR RATE FLOW IN CAPILLARY TUBE

A1. Listing and Sample of Data and Output for Weighing Adjustment Programme

A2. Tables of Results of Flow Tests

Table A1.1: Listing of FORTRAN Weighing Adjustment Programme

```
      PROGRAM TUBPRG(OUTPUT,TAPE1,TAPE3)
C     LOW SHEAR RATE FLOW TESTS
C     PROGRAMME TO ADJUST WEIGHINGS OF DOWNSTREAM CONTAINER FOR
C        ATMOSPHERIC BUOYANCY EFFECTS AND CALCULATE FLOW RATES
C     SEE HANDBOOK OF CHEMISTRY AND PHYSICS (45TH EDN.) AND SMITHSONIAN
C        METEOROLOGICAL TABLES FOR RELEVANT TABULATED DATA
C     WEIGHINGS ARE DONE ON A SINGLE PAN BALANCE.UNLESS STATED OTHERWISE
C        THE CONTAINER IS OPEN TO THE ATMOSPHERE JUST BEFORE WEIGHING
C        AND SEALED FOR WEIGHING
C     INPUT DATA ARE
C          WD=DENSITY OF BALANCE WEIGHTS (GRAMS/CC) (OR DENSITY ASSUMED
C                IN STANDARDISATION OF WEIGHTS WHERE APPROPRIATE)
C        CONT=CONTAINER IDENTIFICATION CODE (NOT TO EXCEED FOUR
C                                            CHARACTERS AND/OR SPACES)
C        VEXT=EXTERNAL VOLUME OF CONTAINER (CC)
C        VINT=INTERNAL VOLUME OF CONTAINER (CC)
C       WTDRY=WEIGHT OF EMPTY CONTAINER (GRAMS)
C        NDAY=DAY   )
C       MONTH=MONTH) OF DATE OF WEIGHING
C       NYEAR=YEAR )
C       NHOUR=HOUR    )
C        MINS=MINUTES) OF TIME OF WEIGHING
C        SECS=SECONDS)
C       DAPPM=APPARENT MASS OF CONTAINER AND CONTENTS (GRAMS)
C       BAROM=BAROMETER READING AT BALANCE AT TIME OF WEIGHING (INS.HG)
C        TDRY=DRY BULB TEMPERATURE (DEG.C)
C        TWET=WET BULB TEMPERATURE (DEG.C)
C      ISTART=CODE TO SHOW DATA APPLIES TO START OF A TEST ) 0=NO,1=YES
C        IEND=CODE TO SHOW DATA APPLIES TO END OF A TEST    )
C     DELTAH=DIFFERENCE BETWEEN WATER SURFACE LEVELS  IN UPSTREAM AND
C                DOWNSTREAM CONTAINERS
C      VAPRES=A VECTOR OF 510 VALUES OF WATER VAPOUR PRESSURE(MM.HG) FOR
C                TEMPERATURES BETWEEN 0 AND 50.9DEG.C LISTED 10 PER CARD
C      RELDEN=A VECTOR OF 50 VALUES OF RELATIVE DENSITY OF WATER BETWEEN
C              0 AND 49DEG.C LISTED 10 PER CARD
C     LAYOUT OF INPUT DATA ON CARDS MUST BE
C        VAPRES (51 CARDS WITH 10 VALUES PER CARD IN FORMAT F8.5)
C        RELDEN (5 CARDS WITH 10 VALUES PER CARD IN FORMAT F8.5)
C        WD (FORMAT F5.2)
C        CONT,VEXT,VINT,WTDRY (FORMAT A4,3F10.5) FOR D/S CONTAINER USED
C        THEN ONE CARD FOR EACH WEIGHING WITH THE FOLLOWING INFORMATION
C        NDAY(I2) STARTING IN COLUMN 1
C        MONTH(I2)                    4
C        NYEAR(I2)                    7
C        NHOUR(I2)                   12
C        MINS(I2)                    15
C        SECS(F4.1)                  18
C        DAPPM(F9.5)                 25
C        BAROM(F6.3)                 37
C        TDRY(F4.1)                  46
C        TWET(F4.1)                  53
C        ISTART(I1)                  60
C        IEND(I1)                    64
C        DELTAH(F8.4)                68
C        CONT(A2)                    78(FOR IDENTIFICATION ONLY.NOT READ)
C***  DATA CARDS FOR WEIGHINGS MUST BE STACKED TO READ IN ORDER STARTING
C***     FROM THE LEAST RECENT DATE
C     IF WD,VEXT,VINT OR WTDRY ALTER,INSERT CARD FULL OF 1'S INTO DATA.
C        THEN NEW CARDS FOR WD AND CONT,VEXT,VINT,WTDRY FOLLOWED BY
C        DATA CARDS FOR SUBSEQUENT TESTS
C     LAST DATA CARD TO BE A CARD FULL OF ZEROS TO SIGNAL END OF DATA
C     OTHER SYMBOLS ARE
C        VAIR=VOLUME OF AIR INSIDE CONTAINER (CC)
C        AIRD=DENSITY OF AIR IN CONTAINER (EXCLUSIVE OF WATER VAPOUR)
C                (GRAMS/CC)
C        AIRM=MASS OF AIR IN CONTAINER (GRAMS)
C                (EXCLUSIVE OF WATER VAPOUR)
C      DTRUM=CORRECTED MASS OF CONTAINER AND CONTENTS (GRAMS)
C      DXAIRM=CORRECTED MASS LESS MASS OF CONTAINED AIR (GRAMS)
C        EDRY=WATER VAPOUR PRESSURE AT DRY BULB TEMPERATURE (MM.HG)
C        EWET=WATER VAPOUR PRESSURE AT WET BULB TEMPERATURE (MM.HG)
```

Table A1.1 (Continued)

```
C       WATDEN=WATER DENSITY (GRAMS/CC)
C         BINS=CORRECTED BAROMETRIC PRESSURE (INS.HG)
C        DTIME=DATE AND TIME OF WEIGHING EXPRESSED IN DAYS AND DECIMALS
C      DELTIME=TIME DIFFERENCE (HOURS) FROM START OF TEST TO FINISH
C      DELMAS=INCREASE IN TRUE MASS OF CONTAINER AND CONTENTS FROM START
C                TO FINISH OF TEST
C      DELEXM=INCREASE IN TRUE MASS OF CONTAINER AND CONTENTS EXCLUDING
C                CONTAINED AIR
C       QTRUM=FLOW RATE DURING TEST BASED ON INCREASE IN TRUE MASS
C                (GRAMS/HOUR)
C      QXAIRM=FLOW RATE DURING TEST BASED ON INCREASE IN TRUE MASS
C                EXCLUDING MASS OF CONTAINED AIR (GRAMS/HOUR)
C      PROGRAMME REQUIRES FUNCTION SUBPROGRAMME DECDYS
       DIMENSION VAPRES(510),RELDEN(50)
       DATA NREAD,NPRINT,NPUNCH /1,3,2/
       READ (NREAD,1000) VAPRES
 1000  FORMAT (10F8.5)
       WRITE (NPRINT,2000) VAPRES
 2000  FORMAT (*1*,*WATER VAPOUR PRESSURES FROM 0 TO 50.9DEG.C (MM.HG)*/(
      1* *,10F11.5))
       READ (NREAD,2500) RELDEN
 2500  FORMAT (10F8.5)
       WRITE (NPRINT,2600) RELDEN
 2600  FORMAT (*0*,*RELATIVE DENSITIES OF WATER FROM 0 TO 49DEG.C*/(* *,1
      10F11.5))
 2700  READ (NREAD,2800) WD
 2800  FORMAT (F5.2)
       WRITE (NPRINT,3000) WD
 3000  FORMAT (*1*,*DENSITY OF BALANCE WEIGHTS=*,F5.2,*GRAMS/CC*)
       READ (NREAD,3100) CONT,VEXT,VINT,WTDRY
 3100  FORMAT (A4,3F10.5)
       WRITE (NPRINT,4000) CONT,VEXT,VINT,WTDRY
 4000  FORMAT (* CONTAINER *,A4,*.EXTERNAL VOLUME=*,F8.3,*CC*/* *,15X,*IN
      1TERNAL VOLUME=*,F8.3,*CC*/* WEIGHT OF EMPTY CONTAINER=*,F9.4,*GRAM
      2S*)
       WRITE (NPRINT,5000)
 5000  FORMAT (*0*,3X,*DATE*,9X,*TIME*,6X,*APPARENT MASS*,4X,*BAROMETER*,
      14X,*CORRECTED*,4X,*DRY BULB*,4X,*WET BULB*,4X,*TRUE MASS*,5X,*TRUE
      2 MASS*,9X,*HEAD*/* *,T58,*BAROMETER*,T107,*LESS AIR MASS*,4X,*DIFF
      3ERENCE*/* *,T16,*H  M  S.*,7X,*(GRAMS)*,8X,*(INS.HG)*,5X,*(INS.HG
      4)*,5X,*(DEG.C)*,5X,*(DEG.C)*,5X,*(GRAMS)*,7X,*(GRAMS)*,10X,*(INS)*
      5)
C      PROGRAMME RETURNS TO THIS POINT AFTER EACH WEIGHING IS CORRECTED.
C         UNLESS NEW VALUES OF WD,VEXT,VINT OR WTDRY ARE REQUIRED IN
C         WHICH CASE RETURN IS TO 2700.
C      PROGRAMME IS STOPPED BY READING IN A CARD FULL OF ZEROS
 5100  ICOUNT=0
       LIGHT=0
 5150  READ (NREAD,5200) NDAY,MONTH,NYEAR,NHOUR,MINS,SECS,DAPPM,BAROM,TDR
      1Y,TWET,ISTART,IEND,DELTAH
 5200  FORMAT (I2,1X,I2,1X,I2,3X,I2,1X,I2,1X,F4.1,3X,F9.5,3X,F6.3,3X,F4.1
      1,3X,F4.1,3X,I1,3X,I1,3X,F9.5)
       IF(DAPPM.LT.0.00000001) GO TO 5300
       GO TO 5500
 5300  WRITE (NPRINT,5900)
       WRITE (NPRINT,5400)
 5400  FORMAT (*1END OF DATA.STOP EXECUTION.*)
       STOP
 5500  BINS=0.9955*BAROM-0.002
C      TDRY GREATER THAN 100.0 SIGNALS NEW CONTAINER OR BALANCE WEIGHTS
C         DATA TO BE READ
       IF(TDRY.GT.100.0) GO TO 5600
       IF(TDRY.GE.49.0.OR.TDRY.LE.0.0) GO TO 5800
       IF(TWET.GE.49.0.OR.TWET.LE.0.0) GO TO 5800
       GO TO 6200
 5600  WRITE (NPRINT,5900)
       WRITE (NPRINT,5700)
 5700  FORMAT (*1NEXT SET OF DATA REQUIRES NEW VALUES FOR DENSITY OF BALA
      1NCE WEIGHTS OR CONTAINER WEIGHT OR VOLUMES.*)
       GO TO 2700
 5800  WRITE (NPRINT,5900)
```

Table A1.1 (Continued)

```
5900 FORMAT (*0----------
     1----------
     2----------*)
      DTRUM=0.0
      DXAIRM=0.0
      WRITE (NPRINT,6000) NDAY,MONTH,NYEAR,NHOUR,MINS,SECS,DAPPM,BAROM,B
     1INS,TDRY,TWET,DTRUM,DXAIRM,DELTAH
6000 FORMAT (*0*,3I3,3X,2I3,F5.1,4X,F10.5,7X,F7.3,6X,F7.3,6X,F5.1,7X,F5
     1.1,T94,F10.5,4X,F10.5,T124,F10.5)
      IF(LIGHT.NE.0) GO TO 6120
      WRITE (NPRINT,6100)
6100 FORMAT (*0DRY BULB OR WET BULB TEMPERATURE OUTSIDE RANGE OF 0.1 TO
     148.9DEG.C.READ NEXT SET OF DATA.*)
      GO TO 5100
6120 WRITE (NPRINT,6150)
6150 FORMAT (*0FUNCTION DECDYS ARGUMENT OUTSIDE ALLOWABLE RANGE.READ NE
     1XT SET OF DATA.*)
      GO TO 5100
6200 IDRY=1+IFIX(10.0*TDRY)
      IWET=1+IFIX(10.0*TWET)
      EDRY=VAPRES(IDRY)
      EWET=VAPRES(IWET)
      X=0.35313/(273.13+TDRY)
      B=25.40*BINS
      Y=B-0.3783*(EWET-0.00066*B*(TDRY-TWET)*(1.0+0.00115*TWET))
      Z=VEXT/SNGL(DAPPM)-1.0/WD
      C=X*Y*Z/760.0
      DTRUM=DAPPM+DBLE(C)*DAPPM
      AIRD=X*(B-EDRY)/760.0
      JDRY=1+INT(TDRY)
      WATDEN=0.999973*(RELDEN(JDRY)-((TDRY-AINT(TDRY))*(RELDEN(JDRY)-REL
     1DEN(JDRY+1))))
      VAIR=VINT-(SNGL(DAPPM)-WTDRY)/WATDEN
      AIRM=AIRD*VAIR
      DXAIRM=DTRUM-DBLE(AIRM)
      CALL SLITE(0)
      DTIME=DECDYS(NDAY,MONTH,NYEAR,NHOUR,MINS,SECS)
      CALL SLITET(1,J)
      GO TO (6300,6400),J
6300 LIGHT=1
      GO TO 5800
6400 IF(ICOUNT.EQ.0) GO TO 6500
      IF(IEND.EQ.0) GO TO 6500
      GO TO 6900
6500 WRITE (NPRINT,5900)
      IF(ISTART.EQ.0) GO TO 6700
6600 DSTORT=DTIME
      DSTORM=DTRUM
      DSTORX=DXAIRM
      STDRY=TDRY
      DELHST=DELTAH
      ICOUNT=1
6700 WRITE (NPRINT,6000) NDAY,MONTH,NYEAR,NHOUR,MINS,SECS,DAPPM,BAROM,B
     1INS,TDRY,TWET,DTRUM,DXAIRM,DELTAH
      GO TO 5150
6900 DELTIM=24.0*(DTIME-DSTORT)
      DELMAS=DTRUM-DSTORM
      DELEXM=DXAIRM-DSTORX
      TDRYMN=(TDRY+STDRY)/2.0
      DELHMN=(DELTAH+DELHST)/2.0
      QTRUM=SNGL(DELMAS/DELTIM)
      QXAIRM=SNGL(DELEXM/DELTIM)
      WRITE (NPRINT,7000) DELMAS,DELEXM,DELTIM,TDRYMN,DELHMN
7000 FORMAT (*0*,T83,*DIFFERENCES*,F10.5,4X,F10.5/* TIME DIFF=*,F10.4,*
     1HRS*,T67,*MEAN=*,F5.1,T119,*MEAN=*,F10.5)
      WRITE (NPRINT,7100) QTRUM,QXAIRM
7100 FORMAT (* *,T83,*RATES GM/HR*,F12.7,2X,F12.7)
      IF(ISTART.EQ.1) GO TO 6600
      ICOUNT=0
      GO TO 6700
      END
```

Table A1.1 (Continued)

```
      FUNCTION DECDYS(NDAY,MONTH,NYEAR,NHOUR,MINS,SECS)
C     FUNCTION SUBPROGRAMME TO CONVERT DATES AND TIMES TO DECIMAL DAYS
C     DUMMY ARGUMENTS ARE... NDAY=DAY OF MONTH (4 BYTE INTEGER)
C                            MONTH=MONTH OF YEAR (4 BYTE INTEGER)
C                            NYEAR=YEAR (4 BYTE INTEGER)
C                                      (PROGRAMME VALID FOR YEARS 1901)
C                                      (TO 1999 INCLUSIVE,LAST TWO     )
C                                      (DIGITS ONLY TO BE USED,FOR     )
C                                      (EXAMPLE,WRITE 1969 AS 69       )
C                            NHOUR=HOUR OF DAY(01 TO 23) (4 BYTE INTEGER)
C                             MINS=MINUTES (4 BYTE INTEGER)
C                             SECS=SECONDS (4 BYTE REAL NUMBER)
C**** IF ONE OR MORE ARGUMENTS ARE OUTSIDE VALID RANGE,DECDYS IS SET
C        EQUAL TO 0.0 AND SENSE LIGHT(1) IS SWITCHED ON
C     SWITCH OFF SENSE LIGHTS BY INSERTING STATEMENT  *CALL SLITE(0)*
C        JUST BEFORE CALLING STATEMENT OR AT SOME OTHER APPROPRIATE
C        POINT
      IF((NDAY.LE.0).OR.(MONTH.LE.0).OR.(MONTH.GT.12).OR.(NYEAR.LE.0).OR
     1.(NYEAR.GT.99)) GO TO 6000
      IF((NHOUR.LT.0).OR.(NHOUR.GT.23).OR.(MINS.LT.0).OR.(MINS.GT.59).OR
     1.(SECS.LT.0.0).OR.(SECS.GE.60.0)) GO TO 6000
      GO TO (1010,1020,1030,1040,1050,1060,1070,1080,1090,1100,1110,1120
     1),MONTH
 1010 IF(NDAY.GT.31) GO TO 6000
      MDAYS=0
      GO TO 2000
 1020 IF((NDAY.GT.29).OR.((NDAY.EQ.29).AND.((NYEAR/4)*4.NE.NYEAR))) GO T
     1O 6000
      MDAYS=31
      GO TO 2000
 1030 IF(NDAY.GT.31) GO TO 6000
      MDAYS=59
      GO TO 2000
 1040 IF(NDAY.GT.30) GO TO 6000
      MDAYS=90
      GO TO 2000
 1050 IF(NDAY.GT.31) GO TO 6000
      MDAYS=120
      GO TO 2000
 1060 IF(NDAY.GT.30) GO TO 6000
      MDAYS=151
      GO TO 2000
 1070 IF(NDAY.GT.31) GO TO 6000
      MDAYS=181
      GO TO 2000
 1080 IF(NDAY.GT.31) GO TO 6000
      MDAYS=212
      GO TO 2000
 1090 IF(NDAY.GT.30) GO TO 6000
      MDAYS=243
      GO TO 2000
 1100 IF(NDAY.GT.31) GO TO 6000
      MDAYS=273
      GO TO 2000
 1110 IF(NDAY.GT.30) GO TO 6000
      MDAYS=304
      GO TO 2000
 1120 IF(NDAY.GT.31) GO TO 6000
      MDAYS=334
 2000 IF(MONTH.LE.2) GO TO 3000
      IF((NYEAR/4)*4.EQ.NYEAR) GO TO 4000
 3000 LEAPDY=0
      GO TO 5000
 4000 LEAPDY=1
 5000 MNDAYS=365*(NYEAR-1)+(NYEAR-1)/4+MDAYS+LEAPDY+NDAY-1
      DECDYS=FLOAT(MNDAYS)+FLOAT(NHOUR)/24.0+FLOAT(MINS)/1440.0+SECS/
     186400.0
      RETURN
 6000 DECDYS=0.0D0
      CALL SLITE(1)
      RETURN
      END
```

Table A1.2: Sample Data For Weighing Adjustment Programme

```
04.5790 04.6130 04.6470 04.6810 04.7150 04.7500 04.7850 04.8200 04.8550 04.8905
04.9260 04.9620 04.9980 05.0340 05.0700 05.1070 05.1440 05.1815 05.2190 05.2565
05.2940 05.3320 05.3700 05.4085 05.4470 05.4860 05.5250 05.5650 05.6050 05.6450
05.6850 05.7255 05.7660 05.8070 05.8480 05.8895 05.9310 05.9730 06.0150 06.0580
06.1010 06.1440 06.1870 06.2305 06.2740 06.3185 06.3630 06.4080 06.4530 06.4980
06.5430 06.5890 06.6350 06.6815 06.7280 06.7750 06.8220 06.8695 06.9170 06.9650
07.0130 07.0620 07.1110 07.1600 07.2090 07.2590 07.3090 07.3600 07.4110 07.4620
07.5130 07.5650 07.6170 07.6695 07.7220 07.7750 07.8280 07.8820 07.9360 07.9905
08.0450 08.1000 08.1550 08.2110 08.2670 08.3235 08.3800 08.4370 08.4940 08.5515
08.6090 08.6680 08.7270 08.7860 08.8450 08.9050 08.9650 09.0255 09.0860 09.1475
09.2090 09.2710 09.3330 09.3955 09.4580 09.5215 09.5850 09.6495 09.7140 09.7790
09.8440 09.9100 09.9760 10.0425 10.1090 10.1765 10.2440 10.3120 10.3800 10.4490
10.5180 10.5880 10.6580 10.7285 10.7990 10.8700 10.9410 11.0130 11.0850 11.1580
11.2310 11.3050 11.3790 11.4535 11.5280 11.5668 11.6800 11.6999 11.8330 11.8435
11.9870 11.9938 12.1440 12.1479 12.3020 12.3050 12.4620 12.4645 12.6240 12.6263
12.7880 12.8705 12.9530 13.0370 13.1210 13.2055 13.2900 13.3755 13.4610 13.5475
13.6340 13.7215 13.8090 13.8980 13.9870 14.0765 14.1660 14.2565 14.3470 14.4385
14.5300 14.6225 14.7150 14.8090 14.9030 14.9975 15.0920 15.1880 15.2840 15.3805
15.4770 15.5750 15.6730 15.7720 15.8710 15.9710 16.0710 16.1715 16.2720 16.3745
16.4770 16.5810 16.6850 16.7895 16.8940 16.9995 17.1050 17.2120 17.3190 17.4270
17.5350 17.6440 17.7530 17.8635 17.9740 18.0855 18.1970 18.3095 18.4220 18.5360
18.6500 18.7650 18.8800 18.9965 19.1130 19.2310 19.3490 19.4680 19.5870 19.7070
19.8270 19.9485 20.0700 20.1930 20.3160 20.4405 20.5650 20.6900 20.8150 20.9415
21.0680 21.1960 21.3240 21.4535 21.5830 21.7140 21.8450 21.9775 22.1100 22.2435
22.3770 22.5125 22.6480 22.7850 22.9220 23.0600 23.1980 23.3370 23.4760 23.6160
23.7560 23.8975 24.0390 24.1825 24.3260 24.4715 24.6170 24.7645 24.9120 25.0605
25.2090 25.3590 25.5090 25.6605 25.8120 25.9645 26.1170 26.2715 26.4260 26.5825
26.7390 26.8970 27.0550 27.2145 27.3740 27.5350 27.6960 27.8585 28.0210 28.1850
28.3490 28.5145 28.6800 28.8475 29.0150 29.1845 29.3540 29.5255 29.6970 29.8610
30.0430 30.2175 30.3920 30.5685 30.7450 30.9235 31.1020 31.2815 31.4610 31.6425
31.8240 32.0075 32.1910 32.3760 32.5610 32.7475 32.9340 33.1230 33.3120 33.5035
33.6950 33.8885 34.0820 34.2765 34.4710 34.6675 34.8640 35.0625 35.2610 35.4620
35.6630 35.8655 36.0680 36.2725 36.4770 36.6840 36.8910 37.0995 37.3080 37.5185
37.7290 37.9420 38.1550 38.3695 38.5840 38.8010 39.0180 39.2375 39.4570 39.6775
39.8980 40.1210 40.3440 40.5700 40.7960 41.0235 41.2510 41.4805 41.7100 41.9425
42.1750 42.4095 42.6440 42.8805 43.1170 43.3560 43.5950 43.8365 44.0780 44.3205
44.5630 44.8085 45.0540 45.3015 45.5490 45.7995 46.0500 46.3030 46.5560 46.8115
47.0670 47.3245 47.5820 47.8420 48.1020 48.3645 48.6270 48.8920 49.1570 49.4245
49.6920 49.9615 50.2310 50.5025 50.7740 51.0485 51.3230 51.6010 51.8790 52.1605
52.4420 52.7255 53.0090 53.2945 53.5800 53.8680 54.1560 54.4465 54.7370 55.0305
55.3240 55.6170 55.9100 56.2100 56.5100 56.8100 57.1100 57.4150 57.7200 58.0300
58.3400 58.6500 58.9600 59.2700 59.5800 59.9000 60.2200 60.5400 60.8600 61.1800
61.5000 61.8200 62.1400 62.4700 62.8000 63.1300 63.4600 63.7900 64.1200 64.4600
64.8000 65.1400 65.4800 65.8200 66.1600 66.5100 66.8600 67.2100 67.5600 67.9100
68.2600 68.6150 68.9700 69.3300 69.6900 70.0500 70.4100 70.7750 71.1400 71.5100
71.8800 72.2500 72.6200 72.9900 73.3600 73.7400 74.1200 74.5000 74.8800 75.2650
75.6500 76.0400 76.4300 76.8200 77.2100 77.6050 78.0000 78.4000 78.8000 79.2000
79.6000 80.0050 80.4100 80.8200 81.2300 81.6400 82.0500 82.4600 82.8700 83.2900
83.7100 84.1350 84.5600 84.9900 85.4200 85.8500 86.2800 86.7100 87.1400 87.5800
88.0200 88.4600 88.9000 89.3450 89.7900 90.2400 90.6900 91.1400 91.5900 92.0500
92.5100 93.0050 93.5000 93.9500 94.4000 94.8500 95.3000 95.8000 96.3000 96.7500
 0.99987 0.99993 0.99997 0.99999 1.00000 0.99999 0.99997 0.99993 0.99988 0.99981
 0.99973 0.99963 0.99952 0.99940 0.99927 0.99913 0.99897 0.99880 0.99862 0.99843
 0.99823 0.99802 0.99780 0.99756 0.99732 0.99707 0.99681 0.99654 0.99626 0.99597
 0.99567 0.99537 0.99505 0.99473 0.99440 0.99406 0.99371 0.99336 0.99299 0.99262
 0,99224 0.99186 0.99147 0.99107 0.99066 0.99025 0.98982 0.98940 0.98896 0.98852
 8.00
 'G'  133.482    102.105     73.603
10 04 73    09 11 00.0    146.50090    30.438    20.1    15.9    1    0    0.89    G
11 04 73    08 58 00.0    146.50770    30.446    20.1    15.9    0    1    0.89    G
11 04 73    09 00 00.0    146.50770    30.446    20.1    15.9    1    0    0.89    G
12 04 73    07 16 00.0    146.51340    30.423    19.9    16.0    0    1    0.89    G
12 04 73    07 17 00.0    146.51340    30.423    19.9    16.0    1    0    0.89    G
13 04 73    09 13 00.0    146.52000    30.366    19.9    16.0    0    1    0.89    G
13 04 73    09 14 00.0    146.52000    30.366    19.9    16.0    1    0    0.89    G
15 04 73    09 38 00.0    146.53150    30.064    20.0    15.9    0    1    0.89    G
15 04 73    09 40 00.0    146.53150    30.064    20.0    15.9    1    0    0.89    G
16 04 73    10 55 00.0    146.53650    29.990    20.1    16.1    0    1    0.89    G
16 04 73    10 57 00.0    146.53650    29.990    20.1    16.1    1    0    0.89    G
17 04 73    09 42 00.0    146.54110    30.012    20.0    16.0    0    1    0.89    G
1111111111111111111111111111111111111111111111111111111111111111111111111111111111
```

DENSITY OF BALANCE WEIGHTS= 8.00GRAMS/CC
CONTAINER 'G' .EXTERNAL VOLUME= 133.482CC
INTERNAL VOLUME= 102.105CC
WEIGHT OF EMPTY CONTAINER= 73.6030GRAMS

Table A1.3: Sample Output From Weighing Adjustment Programme

DATE	TIME H M S.	APPARENT MASS (GRAMS)	BAROMETER (INS.HG)	CORRECTED BAROMETER (INS.HG)	DRY BULB (DEG.C)	WET BULB (DEG.C)	TRUE MASS (GRAMS)	TRUE MASS LESS AIR MASS (GRAMS)	HEAD DIFFERENCE (INS)
10 4 73	9 11 0.0	146.50090	30.438	30.299	20.1	15.9	146.64057	146.60592	.89000
						DIFFERENCES	.00684	.00683	
TIME DIFF= 23.7833HRS					MEAN= 20.1			MEAN=	.89000
						RATES GM/HR	.0002874	.0002874	
11 4 73	8 58 0.0	146.50770	30.446	30.307	20.1	15.9	146.64740	146.61276	.89000
11 4 73	9 0 0.0	146.50770	30.446	30.307	20.1	15.9	146.64740	146.61276	.89000
						DIFFERENCES	.00567	.00566	
TIME DIFF= 22.2667HRS					MEAN= 20.0			MEAN=	.89000
						RATES GM/HR	.0002544	.0002541	
12 4 73	7 16 0.0	146.51340	30.423	30.284	19.9	16.0	146.65307	146.61842	.89000
12 4 73	7 17 0.0	146.51340	30.423	30.284	19.9	16.0	146.65307	146.61842	.89000
						DIFFERENCES	.00634	.00641	
TIME DIFF= 25.9333HRS					MEAN= 19.9			MEAN=	.89000
						RATES GM/HR	.0002443	.0002472	
13 4 73	9 13 0.0	146.52000	30.366	30.227	19.9	16.0	146.65940	146.62483	.89000
13 4 73	9 14 0.0	146.52000	30.366	30.227	19.9	16.0	146.65940	146.62483	.89000
						DIFFERENCES	.01007	.01046	
TIME DIFF= 48.4000HRS					MEAN= 20.0			MEAN=	.89000
						RATES GM/HR	.0002081	.0002162	
15 4 73	9 38 0.0	146.53150	30.064	29.927	20.0	15.9	146.66948	146.63529	.89000
15 4 73	9 40 0.0	146.53150	30.064	29.927	20.0	15.9	146.66948	146.63529	.89000
						DIFFERENCES	.00459	.00470	
TIME DIFF= 25.2500HRS					MEAN= 20.1			MEAN=	.89000
						RATES GM/HR	.0001817	.0001861	
16 4 73	10 55 0.0	146.53650	29.990	29.853	20.1	16.1	146.67407	146.63999	.89000
16 4 73	10 57 0.0	146.53650	29.990	29.853	20.1	16.1	146.67407	146.63999	.89000
						DIFFERENCES	.00475	.00472	
TIME DIFF= 22.7500HRS					MEAN= 20.1			MEAN=	.89000
						RATES GM/HR	.0002090	.0002073	
17 4 73	9 42 0.0	146.54110	30.012	29.875	20.0	16.0	146.67882	146.64470	.89000

Table A2.1: Flow Rates In Capillary Tube - Test Series 1(a)

Day	Head Difference mm	Mass Flow Rate (grams/hour)		
		Measured	Predicted by Poiseuille's Equation d=0.29mm	d=0.297mm
13-14	252	0.0194	0.0333	0.0367
14-15	"	0.0178	"	"
15-18	"	0.0168	"	"
18-19	"	0.0158	"	"
19-20	"	0.0152	"	"
20-21	"	0.0147	"	"
21-22	"	0.0134	"	"
22-23	"	0.0128	"	"
23-24	"	0.0126	"	"
24-25	"	0.0125	"	"
25-26	"	0.0120	"	"
26-27	"	0.0119	"	"
27-28	"	0.0108	"	"
28-29	"	0.0109	"	"
29-30	"	0.0109	"	"
30-31	"	0.0106	"	"
31-32	"	0.0103	"	"
32-33	"	0.0099	"	"
33-34	"	0.0096	"	"
34-35	"	0.0100	"	"
35-36	"	0.0100	"	"
36-37	"	0.0095	"	"
37-38	"	0.0091	"	"
38-39	"	0.0088	"	"
39-40	"	0.0086	"	"
40-41	"	0.0081	"	"
41-42	"	0.0079	"	"
42-43	"	0.0075	"	"
43-44	"	0.0073	"	"
44-45	"	0.0071	"	"
45-46	"	0.0070	"	"
46-47	"	0.0069	"	"
47-48	"	0.0067	"	"
48-49	"	0.0065	"	"
49-50	"	0.0063	"	"
50-53	"	0.0061	"	"
53-54	"	0.0060	"	"
54-55	"	0.0056	"	"
55-56	"	0.0054	"	"
56-57	"	0.0053	"	"

Table A2.2: Flow Rates In Capillary Tube - Test Series 1(b)

Day	Head Difference mm	Mass Flow Rate (grams/hour)		
		Measured	Predicted by Poiseuille's Equation d=0.29mm	d=0.297mm
57	1344	0.0846	0.1774	0.1956
57	"	0.0851	"	"
57	"	0.0852	"	"
57-59	"	0.0716	"	"
59-60	"	0.0467	"	"
60	"	0.0345	"	"
60	"	0.0337	"	"
60-61	"	0.0335	"	"
61-62	"	0.0281	"	"
62	"	0.0276	"	"
62	"	0.0259	"	"
62-63	"	0.0260	"	"
63-64	"	0.0161	"	"
64	"	0.0183	"	"
64-65	1345	0.0285	0.1775	0.1957
65-66	"	0.0434	"	"
66-67	"	0.0371	"	"
67	"	0.0338	"	"
67-68	"	0.0308	"	"
68-69	"	0.0280	"	"
69-70	"	0.0261	"	"
70-71	"	0.0233	"	"
71-72	"	0.0209	"	"
72-73	"	0.0169	"	"
73-74	"	0.0171	"	"
74-75	"	0.0174	"	"
75-76	"	0.0170	"	"
76-77	"	0.0154	"	"
77-78	"	0.0124	"	"
78-81	"	0.0102	"	"
81-82	"	0.0118	"	"
82-83	"	0.0113	"	"
83-84	"	0.0105	"	"
84-85	"	0.0098	"	"
85-88	"	0.0092	"	"
88-89	"	0.0082	"	"
89-90	"	0.0078	"	"
90-91	"	0.0079	"	"
91-92	"	0.0077	"	"

Table A2.3: Flow Rates In Capillary Tube - Test Series 2

Day	Head Difference mm	Mass Flow Rate (grams/hour)		
		Measured	Predicted by Poiseuille's Equation d=0.29mm	d=0.297mm
1	250	0.0206	0.0330	0.0364
1	"	0.0233	"	"
1	"	0.0215	"	"
1- 2	"	0.0264	"	"
2	"	0.0281	"	"
2	"	0.0275	"	"
2- 3	"	0.0209	"	"
3- 4	"	0.0172	"	"
4- 5	"	0.0171	"	"
5- 8	"	0.0166	"	"
8- 9	"	0.0160	"	"
9-10	"	0.0158	"	"
10-11	"	0.0159	"	"
11-12	"	0.0161	"	"
12-15	"	0.0160	"	"
15-17	"	0.1059	"	"
17-18	"	0.0159	"	"
18-19	"	0.0167	"	"
19-20	"	0.0169	"	"
20-22	"	0.0168	"	"
22-23	"	0.0168	"	"
23-24	"	0.0181	"	"
24-25	"	0.0179	"	"
25-26	"	0.0204	"	"
26-27	"	0.0296	"	"
27-28	"	0.0295	"	"
28-29	"	0.0293	"	"
29-30	"	0.0296	"	"
30-31	"	0.0298	"	"
31-32	"	0.0298	"	"

Table A2.4: Flow Rates In Capillary Tube - Test Series 3

Day	Head Difference mm	Mass Flow Rate (grams/hour)		
		Measured	Predicted by Poiseuille's Equation d=0.29mm	d=0.297mm
45	1342	0.159	0.1771	0.1953
45	"	0.158	"	"
45	"	0.158	"	"
45-46	"	0.1538	"	"
46-47	"	0.1513	"	"
47-51	"	0.1487	"	"
51-52	"	0.1414	"	"
52	"	0.144	"	"
52-53	"	0.1413	"	"
53	"	0.153	"	"
53-54	"	0.1489	"	"
54-55	"	0.1437	"	"
55-57	"	0.1356	"	"
57-58	"	0.1263	"	"
58-59	"	0.1219	"	"
59-60	"	0.1318	"	"
60-61	1340	0.1253	0.1769	0.1950
61-64	1344	0.1235	0.1774	0.1956
64-65	1342	0.1991	0.1771	0.1953
65-66	"	0.1159	"	"
66-67	"	0.1136	"	"
67-68	"	0.1112	"	"
68-69	"	0.1106	"	"
69-71	"	0.1071	"	"
71-72	"	0.1045	"	"
72-73	"	0.1020	"	"
73	"	0.098	"	"
73-74	"	0.1011	"	"
74-75	"	0.0997	"	"
75-78	"	0.0977	"	"
78-79	"	0.0945	"	"
79-80	"	0.0931	"	"
80-82	"	0.0923	"	"
82-83	"	0.0911	"	"
83-84	"	0.0898	"	"
84-85	"	0.0881	"	"
85-86	"	0.1196	"	"
86	"	0.1150	"	"
86-87	"	0.1114	"	"
87-88	"	0.1053	"	"
88	"	0.1033	"	"
88-89	"	0.1010	"	"
89-90	"	0.0999	"	"
90-92	"	0.0931	"	"
92-93	"	0.0877	"	"
93	"	0.086	"	"
93-94	"	0.0872	"	"
94	"	0.0856	"	"

Table A2.4: Flow Rates In Capillary Tube - Test Series 3 (Cont'd)

Day	Head Difference mm	Mass Flow Rate (grams/hour)		
		Measured	Predicted by Poiseuille's Equation d=0.29mm	d=0.297mm
94-95	1342	0.0793	0.1771	0.1953
95-96	"	0.0843	"	"
96-99	1344	0.0788	0.1774	0.1956
99-100	"	0.0754	"	"
100-101	"	0.0712	"	"
101-102	"	0.0708	"	"
102-107	"	0.0602	"	"
107-108	"	0.0509	"	"
108-109	"	0.0453	"	"
109-110	"	0.0436	"	"
110-113	"	0.0476	"	"
113-114	"	0.0474	"	"
114-115	"	0.0472	"	"
115	"	0.0477	"	"
115	"	0.0776	"	"
115-116	"	0.0723	"	"
116	"	0.0674	"	"
116	"	0.124	"	"
116	"	0.148	"	"
116	"	0.142	"	"
116-117	"	0.1303	"	"
117-118	"	0.1108	"	"
118-120	"	0.0876	"	"
120-121	"	0.0684	"	"
121-122	"	0.0610	"	"
122-123	1337	0.0662	0.1765	0.1945
123-124	1344	0.0632	0.1774	0.1956
124-125	"	0.0592	"	"
125-127	"	0.0508	"	"
127-128	"	0.0412	"	"
128	"	0.0375	"	"
128-130	"	0.0334	"	"
130-131	"	0.0278	"	"
131-134	"	0.0236	"	"
134-136	"	0.0207	"	"
136	"	0.0223	"	"
136	"	0.0283	"	"
136-137	"	0.0203	"	"
137	"	0.0200	"	"
137	"	0.0192	"	"
137-138	"	0.0188	"	"
138-141	"	0.0148	"	"
141	1346	0.0075	0.1777	0.1958
141-142	"	0.0091	"	"
142-143	"	0.0086	"	"
143-144	"	0.0082	"	"

Table A2.4: Flow Rates In Capillary Tube - Test Series 3 (Cont'd)

Day	Head Difference mm	Mass Flow Rate (grams/hour)		
		Measured	Predicted by Poiseuille's Equation d=0.29mm	d=0.297mm
144	1346	0.0272	0.1777	0.1958
144	"	0.0271	"	"
144	"	0.052	"	"
144	"	0.0912	"	"
144	"	0.0898	"	"
144-145	"	0.0399	"	"
145	"	0.0274	"	"
145-146	"	0.0203	"	"
146-148	"	0.0142	"	"
148-149	"	0.0136	"	"
149-150	"	0.0118	"	"
150-151	"	0.0110	"	"
151-152	"	0.0100	"	"
152-153	"	0.0099	"	"
153-154	"	0.0095	"	"
154-155	"	0.0092	"	"
155-156	"	0.0089	"	"
156-157	"	0.0079	"	"
157-158	"	0.0076	"	"
158-159	"	0.0072	"	"
159-160	"	0.0071	"	"
160-162	"	0.0068	"	"
162-163	"	0.0065	"	"
163-165	"	0.0059	"	"
165-166	"	0.0057	"	"
166-169	"	0.0056	"	"
169-173	"	0.0047	"	"
173-181	"	0.0034	"	"
181-184	"	0.0019	"	"
184-191	"	0.0013	"	"
191-198	"	0.0004	"	"
198-199	"	0.0000	"	"

Table A2.5: Flow Rates In Capillary Tube - Test Series 4 and 5

Day	Head Difference mm	Mass Flow Rate (grams/hour)		
		Measured	Predicted by Poiseuille's Equation d=0.29mm	d=0.297mm
1	1352	0.1976	0.1785	0.1967
1	1352	0.1976	0.1785	0.1967
1- 2	1352	0.1970	0.1785	0.1967
2- 3	1352	0.1975	0.1785	0.1967
3- 5	1352	0.2070	0.1785	0.1967
5- 7	1346	0.1985	0.1777	0.1958
7- 8	1352	0.1930	0.1785	0.1967
8- 9	1349	0.1889	0.1781	0.1963
9-10	1349	0.1878	0.1781	0.1963
10-11	1349	0.1869	0.1781	0.1963
11-12	1349	0.1857	0.1781	0.1963
12-13	1351	0.1839	0.1783	0.1966
13-15	1345	0.1807	0.1775	0.1957
15-16	1345	0.1813	0.1775	0.1957
16-17	1345	0.1821	0.1775	0.1957
17-20	1345	0.1795	0.1775	0.1957
20-21	1345	0.1834	0.1775	0.1957
21-22	1354	0.1823	0.1787	0.1970
22-23	1354	0.1824	0.1787	0.1970
23-25	1355	0.1825	0.1789	0.1972
25-28	1353	0.1828	0.1786	0.1969
28	21.1	0.0029	0.0028	0.0031
28	21.1	0.0030	0.0028	0.0031
28-29	21.1	0.0030	0.0028	0.0031
29-30	21.1	0.0031	0.0028	0.0031
30-33	21.1	0.0031	0.0028	0.0031
33-34	21.1	0.0030	0.0028	0.0031
40-41	21.3	0.0030	0.0028	0.0031
69-71	2.40	0.00042	0.00032	0.00035
71-72	2.40	0.00040	0.00032	0.00035
72-87	2.40	0.00037	0.00032	0.00035
106-107	0.199	0.00005	0.00003	0.00003
107-110	0.171	0.00003	0.00002	0.00002
119-125	-0.034	0.00000	0.00000	0.00000
142-146	0.648	0.00014	0.00009	0.00009
153-159	0.572	0.00008	0.00008	0.00008
181-184	0.410	0.00003	0.00005	0.00006
457-460	0.643	0.00008	0.00008	0.00009

Table A2.5 (Cont'd): Flow Rates In Capillary Tube - Test Series 4 and 5

Day	Head Difference mm	Mass Flow Rate (grams/hour)		
		Measured	Predicted by Poiseuille's Equation d=0.29mm	d=0.297mm
517-527	0.572	0.000078	0.00008	0.00008
527-531	0.511	0.000068	0.00007	0.00007
531-539	0.696	0.000099	0.00009	0.00010
539-545	0.253	0.000036	0.00003	0.00004
546-555	0.099	0.000010	0.00001	0.00001
567-576	0.069	0.000020	0.00001	0.00001
626-627	242	0.0332	0.0319	0.0352
627-628	575	0.0786	0.0759	0.8366
628-629	242	0.0319	0.0319	0.3521
757-763	1.422	0.00004	0.00019	0.00021
763-776	0.343	0.00001	0.00005	0.00005
779	583	0.0679	0.07696	0.0848
779	583	0.0687	0.07696	0.0848
780-789	0.297	0.000002	0.00004	0.00004
791-822	0.010	-0.00001	0.00001	0.00002
838-839	0.152	0.000006	0.00002	0.00002
852-853	249	0.0159	0.0328	0.0362
853-854	582	0.0588	0.0768	0.0847
854-855	582	0.0579	0.0768	0.0847
855-856	582	0.0538	0.0768	0.0847
856-859	582	0.0519	0.0768	0.0847
859	582	0.0532	0.0768	0.0847
859	13460	1.855	1.777	1.958
859	10210	1.328	1.348	1.486
859	7090	0.936	0.936	1.032
859	3450	0.454	0.455	0.502
859-860	584	0.0516	0.0770	0.0850
860-861	252	0.0203	0.0332	0.0367
861	252	0.0203	0.0332	0.0367
861-862	252	0.0205	0.0332	0.0367
862-863	252	0.0199	0.0332	0.0367
863-866	33.1	0.00146	0.00437	0.00482
866-869	33.1	0.00098	0.00437	0.00482
869-873	33.1	0.00096	0.00437	0.00482
873-876	33.1	0.00079	0.00437	0.00482
876-884	33.1	0.00061	0.00437	0.00482
884-891	33.1	0.00035	0.00437	0.00482
891-897	33.1	0.00033	0.00437	0.00482
897-898	33.1	0.00033	0.00437	0.00482
898-905	33.1	0.00033	0.00437	0.00482
905-912	33.1	0.00032	0.00437	0.00482
928-938	33.2	0.00049	0.00438	0.00483
938-940	33.2	0.00059	0.00438	0.00483
940-954	33.0	0.00060	0.00436	0.00480

Table A2.5 (Cont'd): Flow Rates In Capillary Tube - Test Series 4 and 5

Day	Head Difference mm	Mass Flow Rate (grams/hour)		
		Measured	Predicted by Poiseuille's Equation d=0.29mm	d=0.297mm
954- 959	32.8	0.00081	0.00433	0.00477
959- 964	32.7	0.00118	0.00432	0.00476
964- 965	32.6	0.00113	0.00430	0.00474
975- 978	32.4	0.00129	0.00428	0.00471
978- 990	32.3	0.00145	0.00426	0.00470
990- 995	32.2	0.00163	0.00425	0.00469
995- 997	32.2	0.00175	0.00425	0.00469
997-1002	32.1	0.00177	0.00424	0.00467
1002-1004	32.1	0.00181	0.00424	0.00467
1004-1011	32.0	0.00187	0.00422	0.00466
1011-1017	31.9	0.00191	0.00421	0.00464
1017-1038	31.4	0.00218	0.00414	0.00457
1038-1046	31.0	0.00222	0.00409	0.00451
1046-1052	30.9	0.00219	0.00408	0.00450
1052-1060	30.8	0.00225	0.00407	0.00448
1060-1073	30.6	0.00222	0.00404	0.00445
1073-1081	30.2	0.00198	0.00399	0.00439
1081-1087	30.0	0.00192	0.00396	0.00437
1087-1094	29.8	0.00190	0.00393	0.00434
1094-1095	29.8	0.00229	0.00393	0.00434
1095-1099	29.8	0.00228	0.00393	0.00434
1099-1101	29.7	0.00227	0.00392	0.00432
1101-1108	29.7	0.00228	0.00392	0.00432
1108-1115	29.7	0.00219	0.00392	0.00432
1115-1122	29.6	0.00212	0.00391	0.00431
1122-1129	29.6	0.00209	0.00391	0.00431
1129-1136	29.6	0.00173	0.00391	0.00431
1143-1147	29.3	0.00145	0.00387	0.00426
1147-1149	29.2	0.00154	0.00385	0.00425
1149-1171	28.4	0.00151	0.00375	0.00413
1171-1189	28.3	0.00128	0.00374	0.00412
1189-1196	28.3	0.00127	0.00374	0.00412
1196-1199	28.3	0.00124	0.00374	0.00412
1199-1202	28.3	0.00125	0.00374	0.00412

Table A2.5 (Cont'd): Flow Rates In Capillary Tube - Test Series 4 and 5

Day	Head Difference mm	Mass Flow Rate (grams/hour)		
		Measured	Predicted by Poiseuille's Equation d=0.29mm	d=0.297mm
1202-1203	28.6	0.00095	0.00378	0.00416
1203-1205	28.6	0.00131	0.00378	0.00416
1205-1206	28.6	0.00131	0.00378	0.00416
1206-1209	28.5	0.00130	0.00376	0.00415
1209	578	0.04589	0.0763	0.0841
1209-1210	578	0.04734	0.0763	0.0841
1210-1211	578	0.04769	0.0763	0.0841
1211-1212	578	0.04319	0.0763	0.0841
1212-1213	29.0	0.00080	0.00383	0.00422
1213-1214	28.9	0.00079	0.00381	0.00421
1214-1216	28.8	0.00073	0.00380	0.00419
1216-1218	28.7	0.00084	0.00379	0.00418
1218-1220	28.6	0.00075	0.00378	0.00416
1220	28.5	0.00072	0.00376	0.00415
1220-1223	28.7	0.00069	0.00379	0.00418
1223-1224	28.7	0.00066	0.00379	0.00418
1224-1225	28.7	0.00061	0.00379	0.00418
1225-1227	28.6	0.00056	0.00378	0.00416
1227-1228	28.6	0.00064	0.00378	0.00416
1228-1230	28.6	0.00069	0.00378	0.00416
1230-1231	28.6	0.00062	0.00378	0.00416
1231-1233	28.6	0.00058	0.00378	0.00416
1233-1234	28.5	0.00051	0.00376	0.00415
1234-1237	28.5	0.00058	0.00376	0.00415
1237-1239	28.5	0.00056	0.00376	0.00415
1239-1241	28.4	0.00068	0.00375	0.00413
1241-1244	28.4	0.00062	0.00375	0.00413
1244-1245	28.4	0.00065	0.00375	0.00413
1245	28.4	0.00102	0.00375	0.00413
1245-1246	28.3	0.00094	0.00374	0.00412
1246-1248	28.3	0.00070	0.00374	0.00412
1248-1251	28.2	0.00056	0.00372	0.00410
1251-1254	28.1	0.00049	0.00371	0.00409
1254-1259	28.0	0.00038	0.00370	0.00407
1259-1260	27.8	0.00032	0.00367	0.00404
1260-1262	27.7	0.00036	0.00366	0.00403
1262-1265	27.6	0.00038	0.00364	0.00402
1265-1266	27.5	0.00038	0.00363	0.00400
1266-1267	27.5	0.00036	0.00363	0.00400
1267-1269	27.5	0.00042	0.00363	0.00400
1269-1276	27.5	0.00040	0.00363	0.00400
1276-1283	27.4	0.00038	0.00362	0.00400
1283-1286	27.3	0.00027	0.00360	0.00399
1286	27.3	0.00103	0.00360	0.00399
1286-1287	27.3	0.00081	0.00360	0.00399
1287-1288	27.2	0.00063	0.00359	0.00396
1288-1289	27.2	0.00087	0.00359	0.00396
1289-1300	27.0	0.00074	0.00356	0.00393

Table A2.5 (Cont'd): Flow Rates In Capillary Tube - Test Series 4 and 5

Day	Head Difference mm	Mass Flow Rate (grams/hour)		
		Measured	Predicted by Poiseuille's Equation d=0.29mm	d=0.297mm
1300-1307	27.0	0.00087	0.00356	0.00393
1307-1309	26.9	0.00075	0.00355	0.00391
1309-1311	26.9	0.00063	0.00355	0.00391
1311-1314	26.9	0.00062	0.00355	0.00391
1314-1322	26.9	0.00058	0.00355	0.00391
1322-1324	26.8	0.00061	0.00354	0.00390
1324-1333	26.8	0.00063	0.00354	0.00390
1333-1342	26.4	0.00070	0.00348	0.00384
1342-1347	26.4	0.00047	0.00348	0.00384
1381-1384	2.21	-0.00005	0.00029	0.00032
1384-1386	2.17	-0.00007	0.00029	0.00032
1386-1396	2.14	0.00002	0.00028	0.00031
1396-1402	2.13	0.00002	0.00028	0.00031
1415-1429	2.01	0.00002	0.00027	0.00029
1431-1437	5.79	0.00003	0.00076	0.00084
1437-1442	5.77	0.00003	0.00076	0.00084
1442-1448	25.5	0.00011	0.00337	0.00371
1448-1450	25.5	0.00020	0.00337	0.00371
1450-1454	25.5	0.00034	0.00337	0.00371
1454-1455	25.5	0.00186	0.00337	0.00371
1455-1456	25.5	0.00156	0.00337	0.00371
1456-1458	25.5	0.00132	0.00337	0.00371
1458-1460	25.5	0.00118	0.00337	0.00371
1460-1462	25.4	0.00108	0.00335	0.00370
1462-1465	25.4	0.00104	0.00335	0.00370
1465-1468	25.4	0.00095	0.00335	0.00370
1468-1470	25.4	0.00090	0.00335	0.00370
1470-1472	25.4	0.00089	0.00335	0.00370
1472-1475	25.4	0.00088	0.00335	0.00370
1475-1477	25.4	0.00090	0.00335	0.00370
1477-1479	25.4	0.00091	0.00335	0.00370
1479-1486	25.4	0.00084	0.00335	0.00370
1486-1493	25.4	0.00083	0.00335	0.00370
1493-1500	25.4	0.00085	0.00335	0.00370
1500-1505	25.4	0.00079	0.00335	0.00370
1505-1920	24.2	0.00036	0.00319	0.00352
1920-1923	23.0	0.00034	0.00304	0.00335
1923-1926	23.0	0.00048	0.00304	0.00335

Table A2.5 (Cont'd): Flow Rates in Capillary Tube - Test Series 4 and 5

Day	Head Difference mm	Mass Flow Rate (grams/hour)		
		Measured	Predicted by Poiseuille's Equation d=0.29mm	d=0.297mm
1961-1962	22.5	0.00002	0.00279	0.00327
1962-1965	"	0.00007	"	"
1965-1967	"	0.00008	"	"
1967	"	0.00108	"	"
1967-1968	"	0.00058	"	"
1968-1969	"	0.00036	"	"
1969-1970	"	0.00033	"	"
1970-1972	"	0.00026	"	"
1972-1973	"	0.00020	"	"
1973-1974	"	0.00017	"	"
1974-1976	"	0.00012	"	"
1976-1979	"	0.00009	"	"
1979-1980	"	0.00008	"	"
1980-1981	"	0.00008	"	"
1981-1983	"	0.00008	"	"
1983-1985	"	0.00008	"	"
1985-1986	"	0.00008	"	"
1986	"	0.00002	"	"
1986	"	0.00067	"	"
1986-1987	"	0.00043	"	"
1987-1988	"	0.00031	"	"
1988-1989	"	0.00028	"	"
1989-1990	"	0.00027	"	"
1990-1992	"	0.00024	"	"
1992-1993	"	0.00021	"	"
2037-2046	22.7	0.00009	0.00300	0.00330
2046-2050	22.7	0.00009	0.00300	0.00330
2050-2051	246	0.00202	0.0325	0.0358
2051	246	0.00200	"	"
2051-2052	"	0.00202	"	"
2052	"	0.00206	"	"
2052-2053	"	0.00214	"	"
2053	"	0.00224	"	"
2053-2056	"	0.00249	"	"
2056-2057	"	0.00275	"	"
2057	581	0.00900	0.0767	0.0845
2057-2058	582	0.00946	0.0768	0.0847
2058	"	0.00939	"	"
2058-2059	"	0.00981	"	"
2059	"	0.01008	"	"
2059-2060	"	0.01064	"	"
2060	"	0.01080	"	"
2060-2063	"	0.01122	"	"
2063	"	0.01150	"	"
2063-2064	"	0.01162	"	"
2064-2065	"	0.01223	"	"
2065-2066	"	0.01235	"	"
2066-2067	"	0.01265	"	"
2067-2070	"	0.01319	"	"

Table A2.5 (Cont'd): Flow Rates In Capillary Tube - Test Series 4 and 5

Day	Head Difference mm	Mass Flow Rate (grams/hour)		
		Measured	Predicted by Poiseuille's Equation d=0.29mm	d=0.297mm
2070-2071	581	0.01366	0.0767	0.0845
2071	"	0.03922	"	"
2071	"	0.04005	"	"
2071	"	0.03976	"	"
2071	"	0.04000	"	"
2071	"	0.04133	"	"
2071	"	0.04182	"	"
2071	"	0.04009	"	"
2071	"	0.04035	"	"
2071	"	0.03970	"	"
2071-2072	"	0.03847	"	"
2072	"	0.03853	"	"
2072	"	0.03926	"	"
2072	"	0.03889	"	"
2072-2073	"	0.03816	"	"
2073	"	0.03731	"	"
2073-2074	"	0.03707	"	"
2074	"	0.03752	"	"
2074-2076	"	0.03595	"	"
2076-2077	"	0.03435	"	"
2077	"	0.03505	"	"
2077-2078	"	0.03363	"	"
2078-2079	"	0.03312	"	"
2079-2080	"	0.03079	"	"
2080-2081	"	0.03272	"	"
2081	23.5	0.00058	0.00310	0.00342
2081	22.7	0.00073	0.00300	0.00330
2081-2082	"	0.00069	"	"
2082-2083	"	0.00060	"	"
2083-2084	"	0.00057	"	"
2084-2091	"	0.00043	"	"
2091-2093	"	0.00039	"	"
2093-2095	"	0.00041	"	"
2095-2098	"	0.00040	"	"
2098-2100	"	0.00038	"	"
2100-2102	"	0.00034	"	"
2102-2105	"	0.00035	"	"
2105-2107	"	0.00032	"	"
2107-2109	"	0.00024	"	"
2109-2112	"	0.00018	"	"
2112-2114	"	0.00022	"	"
2114-2116	"	0.00008	"	"
2116-2119	"	0.00008	"	"
2119-2121	"	0.00006	"	"
2121-2128	"	0.00006	"	"
2128-2135	"	0.00004	"	"
2135-2142	"	0.00004	"	"
2142-2149	"	0.00003	"	"

Table A2.5 (Cont'd): Flow Rates In Capillary Tube - Test Series 4 and 5

Day	Head Difference mm	Mass Flow Rate (grams/hour)		
		Measured	Predicted by Poiseuille's Equation d=0.29mm	d=0.297mm
2149-2156	22.7	0.00003	0.00300	0.00330
2156-2163	"	0.00003	"	"
2163-2168	"	0.00002	"	"
2168	246	0.00028	0.0325	0.0358
2168-2169	"	0.00143	"	"
2169	"	0.00167	"	"
2169-2170	"	0.00120	"	"
2170	"	0.00097	"	"
2170-2171	"	0.00091	"	"
2171-2173	"	0.00083	"	"
2173-2175	"	0.00072	"	"
2175-2176	"	0.00064	"	"
2176-2177	"	0.00059	"	"
2177-2179	"	0.00054	"	"
2179-2182	"	0.00047	"	"
2182-2184	"	0.00044	"	"
2184-2186	"	0.00042	"	"
2186-2189	"	0.00041	"	"
2189-2191	"	0.00041	"	"
2191-2193	"	0.00040	"	"
2193-2196	"	0.00038	"	"
2196-2198	"	0.00039	"	"
2198-2200	"	0.00039	"	"
2200-2203	"	0.00037	"	"
2203-2205	"	0.00036	"	"
2205-2207	"	0.00037	"	"
2207-2210	"	0.00036	"	"
2210-2212	"	0.00034	"	"
2212-2214	"	0.00035	"	"
2214-2217	"	0.00033	"	"
2217-2219	"	0.00032	"	"
2219-2224	"	0.00031	"	"
2224-2226	"	0.00032	"	"